De slimme contactlens: van een artificiële iris tot een contactlensbeeldscherm

The Smart Contact Lens: from an Artificial Iris to a Contact Lens Display

Jelle De Smet

Promotoren: prof. dr. ir. H. De Smet, dr. ir. D. Cuypers
Proefschrift ingediend tot het behalen van de graad van
Doctor in de Ingenieurswetenschappen

Vakgroep Elektronica en Informatiesystemen
Voorzitter: prof. dr. ir. J. Van Campenhout
Faculteit Ingenieurswetenschappen en Architectuur
Academiejaar 2013 - 2014

UNIVERSITEIT
GENT

ISBN 978-90-8578-663-4
NUR 950, 954
Wettelijk depot: D/2014/10.500/9

Ghent University
Faculty of Engineering and Architecture

Promoters:

Prof. dr. ir. Herbert De Smet
Department of Electronics and Information Systems,
Ghent University

Dr. ir. Dieter Cuypers (*)
Department of Electronics and Information Systems,
Ghent University

Other members of the examination committee:

Prof. dr. ir. Luc Taerwe (Chairman)
Department of Structural Engineering,
Ghent University

Prof. dr. ir. Jeroen Beeckman (Secretary)
Department of Electronics and Information Systems,
Ghent University

Prof. dr. ir. Wim Bogaerts (*)
Department of Information Technology,
Ghent University

Prof. dr. ir. Chris Van Hoof (*)
Department of Electrical Engineering,
Katholieke Universiteit Leuven

Prof. dr. ir. ing. Michael Vervaeke (*)
Brussels Photonics Team,
Vrije Universiteit Brussel

Dr. ir. Rik Verplancke
Department of Electronics and Information Systems,
Ghent University

(*) Reading committee.

A dissertation submitted in partial fulfillment of the requirements for the degree of Doctor in Engineering

Academic year 2013-2014

Dankwoord - Word of Thanks

Vijf jaar begint al te tellen in een mensenleven, en nu deze bijzonder leerrijke periode tot een einde komt, is een terugblik en een bedanking van alle betrokken personen onontbeerlijk.

Een idee hebben is gemakkelijk, maar er de juiste ondersteuning voor vinden is de eerste uitdaging. Gelukkig was Herbert bereid een niet onaanzienlijk risico te nemen en de promotor te worden van dit werk. Zelfs bij het falen van de eerste beursaanvraag zag hij toch voldoende potentieel in het idee en zorgde hij voor de ondersteuning die ik nodig had. De vele discussies die we gehad hebben, hebben niet alleen tot de praktische realisatie van dit werk geleid, maar zorgden er ook voor dat het brede plaatje nu veel duidelijker is. We hebben nog maar een kleine stap gezet, maar ik denk dat we er samen voor gezorgd hebben dat slimme contactlenzen op de kaart staan als een boeiend en veelbelovend onderzoeksdomein.

Voor veel van de praktische aspecten van dit werk en in het bijzonder betreffende LCD-technologie, heb ik beroep kunnen doen op mijn co-promotor Dieter. Hij heeft mij hierover veel bijgeleerd en het is mede daardoor dat ik er in geslaagd ben de resultaten van dit werk te verwezelijken. Op mijn eerste buitenlandse conferentie heeft hij me geïntroduceerd tot de Japanse cultuur, dewelke ik ook ben beginnen appreciëren.

Tijdens mijn onderzoek heb ik ook technologisch ondersteuning gekregen van verscheidene mensen binnen CMST. Steven, bedankt voor het vele laserwerk, ook al was ik niet altijd even goed met de planning. Het is in ieder geval een belangrijk deel van mijn doctoraat geworden. Kristof, bedankt voor de lithografie op de SET, het fabriceren van de koperbaantjes en het geven van andere 'tips & tricks' in de cleanroom. Filip T, bedankt voor het maken van de substraathouders en andere benodigdheden. Bjorn, bedankt voor je hulp bij alles omtrent dispensing. Nadine, bedankt voor het professionele management van de cleanroom.

Voorts wil ik ook de andere leden van het support team, Sheila, Filip V, Peter en Bart, bedanken voor hun ondersteuning tijdens dit werk. Ik vermeld ook graag Lothar, wiens filmpjes mij echt geholpen hebben bij het publiek verspreiden van mijn werk.

Alle andere leden van CMST verdienen ook een bedanking, aangezien ik over de jaren heen wel met iedereen interessante conversaties heb gevoerd, waarvan ik altijd iets heb van meegenomen. Mijn thesisstudenten Jan-Willem, Sampo, Pieter, Esma en Mathieu bedank ik voor hun inzet, hopelijk heb ik ook naar jullie toe voldoende ondersteuning geboden.

De sfeer in mijn bureau werd tijdens dit doctoraat verzorgd door toffe collega's zoals Iaci, Roel, Aykut, Kristof, Swarna, Pankaj, Xiaobing en Esma (en de facto Kamal). We hebben zowel in het bureau als in Gent vele leuke momenten beleefd (kajakken met de collega's is een aanrader) en hebben belangrijke momenten in elkaars leven gedeeld. Alhoewel sommmigen niet meer voor CMST werken, zal ik ze niet snel vergeten.

Werk vormt uiteraard slechts een deel van het leven, en vrienden en familie hebben die naast je staan is minstens even belangrijk.

Fre, bedankt om er onvoorwaardelijk te zijn. Je bent het archetype van het gezegde 'Je hebt niet veel vrienden nodig, enkel de juiste'. Je hebt me 15 jaar geleden uit mijn kot gehaald en daar pluk ik nog elke dag de vruchten van. Simon, we zien elkaar niet zo veel maar ik hou er aan om, zolang we nog kunnen, samen de jeanettenstoet te lopen. Kjo, bedankt voor de Westmalles in de Hotsy Totsy. De jaren tijdens mijn doctoraat waren heel woelig voor jou, maar hopelijk vind je nu de rust die je verdient.

Verder bedank ik iedereen op de korfbal en in het bijzonder de mensen van de kern. Er werkt niets zo bevrijdend en ontspannend voor mij als na een drukke werkdag te trainen en nadien iets te drinken.

Aangezien een goed huis rust op een solide fundering, wil ik ook mijn ouders bedanken. Ze hebben me altijd gesteund en er voor gezorgd dat ik alle kansen heb gekregen. Ik bouw nu verder aan mijn eigen leven, maar de deur zal altijd openstaan. Voorts bedank ik mijn zus en mijn familie uit Aalst en Halle voor de steun en warmte die ik zowel vroeger als nu heb gekregen. Ook mijn hele schoonfamilie verdient een vermelding voor hun hartelijke ontvangst, hun frikandon en de leuke momenten die we al gehad hebben.

De grootste en meest oprechte bedanking moet ik richten aan Dorien. We hebben dit doctoraat samen meegemaakt en alle hoogtes en laagtes gedeeld. Het laatste jaar was zwaar en je hebt speciaal voor mij opofferingen moeten maken. Het boek ligt er nu eindelijk en dat had niet gekund zonder je vertrouwen en steun. Je zegt altijd dat ik zo veel weet, maar ik heb de voorbije zes jaar nog veel meer geleerd van jou. Hopelijk kan ik je bij jouw doctoraat net zo goed ondersteunen als jij bij mij hebt gedaan.

Jelle.
Aalst, februari 2014

Table of Contents

List of Figures

List of Tables

List of Acronyms

A

AR	Augmented reality
AZ 4562	Photoresist by AZ Electronic Materials

B

BCB	Benzocyclobutene
BOZD	Back optic zone diameter
BOZR	Back optic zone radius
BPZD	Back peripheral zone diameters
BVP	Back vertex power

C

CAB	Cellulose acetate butyrate
CMOS	Complementary metal–oxide–semiconductor
CMST	Centre for Microsystems Technology
CNC	Computer numerically controlled
CR	Contrast ratio

D

DC	Direct current
Dk	Oxygen permeability
Dk/t	Oxygen transmissibility

E

ECD	Electrochromic displays
EKD	Electrokinetic displays
EWD	Electrowetting displays

F

FCA	Flexible conductive adhesive
FWHM	Full width at half maximum

H

HEMA	Hydroxyethylmethacrylate
HTP	Helical twisting power

I

IOP	Intraocular pressure
ISO	International Organization for Standardization
ITO	Indium Tin Oxide

L

LC-resonance	Resonance in an electrical circuit containing an inductor and a capacitor
LC	Liquid crystal
LCD	Liquid crystal display
LCOS	Liquid crystal on silicon
LED	Light emitting diode

M

MW80	Mounting Wax 80, a wax by Electron Microscopy Sciences

N

Nd:YAG	Neodymium-doped yttrium aluminum garnet

P

PECVD	Plasma enhanced chemical vapour deposition
PEDOT:PSS	Poly(3,4-ethylene-dioxy-thiophene):poly(styrene-sulfonate)
PET	Polyethylene terephthalate
PDMS	Polydimethyl siloxane
PMMA	Poly methyl methacrylate
PVA	Polyvinyl alcohol

R

RF	Radio frequency

RPM	Revolutions per minute

S

SEM	Scanning electron microscope
SU8 3010	Photoresist by MicroChem

T

TIC	Translationally invariant configuration
TFT	Thin film transistors
T_g	Glass transition temperature
TN	Twisted nematic

U

US	United States
UV	Ultraviolet

V

V_{pp}	Peak-to-peak voltage

Summary

Regular, passive contact lenses are ophthalmic devices used to correct vision disorders such as myopia and hyperopia. From their inception in 1888, research efforts were focused on increasing their comfort, performance and ease of manufacturing, but their purpose rarely diverted to other applications than vision correction. However, after World War II, a new use found its way into the lab when one sought to extend their function by integrating electronic components. Unfortunately, none of the initial efforts resulted in a successful implementation beyond research prototyping. In retrospect, it seems the major limiting factor was a lack of adequate microfabrication technologies for constructing the micro-electronic components themselves and for successfully embedding them in a contact lens. However, around 2000 these technologies appeared to have caught up with the ideas and designs of several researchers and a new upsurge in electronic contact lens studies has since been seen.

The application domains of these so-called 'smart' contact lenses have up till now been mainly limited to biomedical sensing and augmented reality. While the added value of augmented reality is less clear at this point and certainly needs much more research, the opportunities for biomedical sensing are more obvious and are likely to expand in the coming years. Strangely, it appears one large application domain has not been investigated yet, namely vision correction. Conventional contact lenses were specifically developed to correct ophthalmic disorders such as myopia and hyperopia, but the question emerges whether smart contact lenses can outperform them in terms of vision correction. After an initial round-up of existing research and the identification of potential future applications in the domain of active vision correction, a clear starting point was found: the development of a basic non-emitting electro-optic technology which could be integrated into a contact lens.

After an initial survey of existing display technologies, we found that LCD technology provides the best fit with the desired properties for integration into a

contact lens. However, it was recognized from early on that conventional polarizers are generally too thick for contact lens embedding, suggesting a polarizer-free LCD technology should be investigated first. For this purpose, guest-host liquid crystal displays were deemed to be the best choice.

The focus of this work thus became the design and fabrication of a spherically conformed LC cell. Since this a is special kind of flexible display, existing manufacturing techniques for flexible displays were explored, resulting in a first prototype. This revealed a straightforward implementation is not possible, as application specific issues such as poor optical uniformity, lack of precise control of the dimensions and the appearance of wrinkles impede a successful integration into a contact lens. Furthermore, the yield of our process was low due to the initially used processing techniques.

Therefore, new processing techniques were created to improve the yield and manufacturability while the inclusion of an additional photolithograpic layer allowed us to address other pending issues such as the optical uniformity and the need for a precisely dimensioned glue joint. A finger pattern in this layer reinforced the filling entrance while an in-depth study exposed the relationship between the thickness of the used PET-films and the formation of wrinkles. A smooth cell with a thickness of 135 µm was established by using an asymmetric configuration with a thin layer at the convex side and a thicker but threshold dependent layer at the concave side, thereby reaching our target thickness of below 140 µm. This smooth 50 µm convex – 75 µm concave configuration was therefore used as the standard configuration in the remainder of this work.

To create an active LC cell, both an alignment and a transparent conductive layer was integrated in the cell. An obliquely evaporated SiO_2-layer was selected and used as a contact-free, low-temperature alignment layer. Due to the delicate nature of the SiO_2-layer, it was applied after deposition and patterning of the photolithographic spacers, which resulted in small transient alignment zones near to the spacers. Since ITO proved to be too brittle for the molding process, the transparent conductive polymer PEDOT:PSS was chosen as an alternative. This required the addition of a barrier layer in between PEDOT:PSS and the photolithographic layer, as the development process of the photolithographic layer was disturbed by the presence of the PEDOT:PSS.

With the electro-optic effect established, the quality of the mold was found to be important to achieve a good uniformity across the cell while a sufficiently high spacer density also proved to be necessary. Different patterning techniques for the PEDOT:PSS layer were investigated and were mainly based on laser ablation. Even after optimization, minor damage to the underlying PET-films could not be

avoided, apparently affecting the alignment of the LC molecules. The isolation technique, having the smallest footprint, led to good patterned cells and was thus deemed as a viable technique for PEDOT:PSS patterning.

To investigate the performance boundaries of the guest-host technology, an in-depth study was performed on the influence of the twist and the dye concentration on the electro-optical response of the LC cell. This revealed a 180° twist results in the best contrast while still being practically implementable. Although increasing the dye concentration does indeed lead to an improved contrast, this also increases the threshold voltage and the saturation voltage and a trade-off should thus be considered.

With an optimized mixture, the LC cell was fully characterized, giving special attention to the transition between glass test cells and the LC cell. Transmission-voltage measurements and switching speed measurements indicated the cell gap of the LC cell was lower than intended, which was confirmed by cell gap measurements. This indicated the height of the photolithographic spacer should be carefully monitored during fabrication. Even then, contrast and switching speed were only moderate, which might hamper use of the LC cell for some applications. An initial study concerning the integration of polarizers revealed PVA based polarizers are too thermally unstable to be integrated into contact lenses. Thin film polarizers seem to be a good alternative and should be the subject of future research.

With the basic technology established and characterized, the first applications could be explored. For use as an artificial iris, the LC cell was adapted and new features such as a central hole for increased biocompatibility were added. Alignment markers were added as the high number of pixels - up to nine in our prototypes - required careful alignment. A new flexible connector based on commercial copper clad laminates was developed to drive the different pixels. By consecutively switching on and off the concentric pixels, iris constriction and dilation could be successfully mimicked. A crossover was also implemented as this allows to bring all necessary connections to one side of the substrates. The deposition process of the flexible conductive glue was, however, not well controlled and could lead to unwanted connections deteriorating the contrast of the pixels. Although further work should address this problem, the artificial iris seems well suited as a first application for this newly developed technology.

Another application in the vision correction domain is a smart contact lens for presbyopia. Therefore, its use in a smart contact lens with multifocal functionality was studied, but since this is currently the subject of a patent application, no more information can be disclosed here.

For the final application, a contact lens display for augmented reality, it was quickly realized that pixels residing just in front of the cornea cannot be seen clearly as they are beyond the eye's minimal focussing limit. Exploratory simulations indicate that even under ideal circumstances a classical approach using integrated microlenses could likely lead to projected spot sizes as large as 0.4 mm. This would mean only about 4 by 4 pixels could be projected in the region with highest acuity, allowing the projection of only very simple patterns. Therefore, it seems before any display technology should be further investigated for application as a contact lens display, a more in-depth study is needed on how a highly detailed image can be projected onto the fovea. It remains to be seen whether LCD technology can be used for this purpose as it is the proven optical concept which will probably dictate which technology one should opt for.

To conclude, we have shown for the first time it is possible to create a non-emitting electro-optic technology that can be integrated into a contact lens. This milestone brings us one step closer to a new generation of contact lenses, potentially leading to breakthrough applications in biomedical and augmented reality fields.

Samenvatting

Gewone, passieve contactlenzen zijn ophtalmologische hulpmiddelen die worden gebruikt om visuele aandoeningen zoals myopie en hyperopie te corrigeren. Vanaf hun totstandkoming in 1888, richtte aangaand onderzoek zich voornamelijk op het verhogen van comfort, performantie en gemak van fabricatie, maar hun gebruiksdoeleinde week zelden af naar toepassingen buiten visuele correctie. Echter, na Wereldoorlog II, vonden nieuwe gebruiken hun weg naar het labo wanneer men trachtte hun functie uit te breiden door elektronische componenten te integreren. Helaas leidde geen enkel van deze initiële betrachtingen tot een succesvolle implementatie buiten het onderzoekslabo. Achteraf bekeken lijkt het ernaar dat de grootste limiterende factor het gebrek was aan afdoende microfabricatietechnieken om de micro-elektronische componenten zelf te construeren en om deze succesvol in een contactlens in te bedden. Echter, rond het jaar 2000 bleken deze technologieën zich bijgebeend te hebben met de ideeën en ontwerpen van verscheidene onderzoekers en een nieuwe opleving van studies betreffende elektronische contactlenzen werd sindsdien geobserveerd.

De toepassingsgebieden van deze zogenaamde 'slimme' contactlenzen worden tot nu toe uitgemaakt door biomedische detectie en verhoogde realiteit. Hoewel de toegevoegde waarde van verhoogde realiteit minder duidelijk is en zeker nog verder onderzoek nodig heeft, zijn de opportuniteiten voor biomedische detectie duidelijker en zullen deze de komende jaren toenemen. Vreemd genoeg blijkt één groot toepoassingsgebied nog niet onderzicht te zijn, namelijk visuele correctie. Conventionele contactlenzen werden specifiek ontwikkeld om ophthalmologische aandoeningen to corrigeren zoals myopie en hyperopie, maar de vraag rijst waar slimme contactlenzen gewone contactlenzen kunnen overtreffen op het gebied van visuele correctie. Na een intiële prospectie van bestaand onderzoek en de identificatie van potentiële toekomstige toepassingen op het gebied van actieve visuele correctie, werd er een duidelijk startpunt gevonden: de ontwikkeling van een nietemitterde elektro-optische basistechnologie dewelke in een contactlens

geïntegreerd kan worden.

Na een initiële studie van bestaande beeldschermtechnologieën, vonden we dat vloeibaarkristalbeeldscherm-technologie het best overeenkomt met de gewenste eigenschappen voor integratie in een contactlens. Echter, het werd al snel erkend dat conventionele polarisatoren over het algemeen te dik zijn voor inbedding in een contactlens, wat suggereert dat een polarisatorvrije vloeibaarkristalbeeldscherm-technologie eerst onderzocht moest worden. Hiervoor werd het gast-gastheer-vloeibaarkristalbeeldscherm als het meest geschikt bevonden.

Dit werk was dus hoofdzakelijk gericht op het ontwerp en de fabricage van een sferisch gevormde vloeibaarkristalcel. Aangezien deze cel een bijzondere vorm van flexibel beeldscherm is, werden bestaande technieken om flexibele beeldschermen te vervaardigen onderzocht, hetgeen heeft geleid tot een eerste prototype. Hierbij werd snel duidelijk dat een rechtlijnige implementatie niet mogelijk is omdat toepassingsgebonden problemen zoals een zwakke optische uniformiteit, een gebrek aan nauwkeurige controle van de verschillende dimensies en het verschijnen van rimpels succesvolle integratie in een contactlens verhinderen. Bovendien was het rendement van het proces laag omwille van de initieel gebruikte productietechnieken.

Om die redenen werden nieuwe productietechnieken opgezocht om het rendement en de maakbaarheid te verbeteren, terwijl het gebruik van een bijkomende fotolithografische laag toeliet andere problemen aan te pakken, zoals de optische uniformiteit en de nood om de lijmnaad nauwkeurig te dimensioneren. Een vingervormig patroon in deze laag versterkte de vulingang terwijl een diepgaand onderzoek de relatie naar voor bracht tussen de dikte van de gebruikte PET-films en het ontstaan van rimpels. Door het gebruik van een asymmetrische samenstelling bestaande uit een dunne laag aan de convexe zijde en een dikkere maar drempelafhankelijke laag aan de concave zijde, werd een gladde cel gecreëerd met een dikte van 135 µm. Hiermee werd ons doel bereikt om een dikte beneden de 140 µm te verkrijgen. Bijgevolg werd deze gladde 50 µm convexe – 75 µm concave configuratie gebruikt als de basisconfiguratie voor de rest van dit werk.

Om een actieve vloeibaarkristalcel te creëren, werd er een aligneringslaag en transparante, geleidende laag geïntegreerd in de cel. Een schuinopgedampte SiO_2-laag werd geselecteerd en gebruikt als een contactloze, lagetemperatuur aligneringslaag. Door de delicate aard van de SiO_2-laag werd deze pas na de depositie en de patronering van de fotolithografische afstandshouders aangebracht, hetgeen leidde tot een kleine transientzone rond de afstandshouders. Aangezien ITO te bros bleek voor het vervormingsproces, werd het transparante geleidende

polymeer PEDOT:PSS gekozen als alternatief. Dit leidde tot het gebruik van een additionele barrièrelaag tussen het PEDOT:PSS en de fotolithografische laag, omdat de ontwikkelingsproces van de fotolithografische laag verstoord werd door het PEDOT:PSS.

Na de verwezenlijking van het elektro-optische effect werd er gevonden dat de kwaliteit van de mal erg belangrijk was om een goede uniformiteit te verkrijgen over de hele cel, terwijl de voldoende hoge afstandshoudersdensiteit ook belangrijk bleek. Verscheidene patroneringstechnieken voor het PEDOT:PSS werden onderzocht en waren voornamelijk gebaseerd op laserablatie. Zelfs na optimalisatie kon lichte schade aan de onderliggende PET-films niet vermeden worden, hetgeen blijbaar de alignering van de vloeibaarkristalmoleculen beïnvloedde. De isolatietechniek, dewelke ook de kleinste voetafdruk bezat, leidde tot goed gepatroneerde cellen en werd dus als een afdoende techniek voor de patronering van PEDOT:PSS geacht.

Om het performantiebereik van de gast-gastheertechnologie te onderzoeken, werd er een diepgaande studie uitgevoerd naar de invloed van de draaiing en de kleurstofconcentratie op de elektro-optische respons van de vloeibaarkristalcel. Deze onthulde dat een draaiing van 180 graden resulteerde in het beste contrast terwijl deze ook nog praktisch implmenteerbaar was. Alhoewel het verhogen van de kleurstofconcentratie inderdaad leidt tot een verbeterd contrast, leidt dit ook tot het verhogen van de drempelspanning en de saturatiespanning en dient een afweging gemaakt te worden.

Met een geoptimaliseerd mengsel werd de cel volledig gekarakteriseerd, waarbij specifieke aandacht ging naar de overgang van glazen testcellen naar de vloeibaarkristalcellen. Transmissiespanning-metingen en schakelsnelheidmetingen gaven aan de dat celhoogte lager dan voorzien was, hetgeen bevestigd werd door celhoogtemetingen. Deze wezen aan dat de hoogte van de fotolithografische afstandshouders oplettend in het oog moet gehouden worden tijdens het fabricageproces. Zelfs dan nog bleek het contrast en de schakelsnelheid slechts een matige waarde te hebben, hetgeen het gebruik van de vloeibaarkristalcel voor sommige toepassingen kan verhinderen. Een intiële studie van de integratie van polarisatoren toonde aan dat PVA-gebaseerde polarisatoren waarschijnlijk thermisch te onstabiel waren om geïntegreerd te worden in contactlenzen. Dunnefilmpolarisatoren lijken een goed alternatief te zijn en zouden in de toekomst onderzocht moeten worden.

Na de verwezelijking en de karakterisatie van de basistechnologie, konden de eerste toepassingen verkend worden. De vloeibaarkristalcel werd aangepast voor het gebruik als een artificiële iris en nieuwe kenmerken zoals een centrale holte

voor verhoogde biocompatibiliteit werden toegevoegd. Aligneringsmarkeringen werden toegevoegd omdat het hoge aantal pixels - tot en met negen in onze prototypes - speciale aandacht vereiste. Een nieuwe, flexibele connector gebaseerd op met koper bekleden laminaten werd ontwikkeld om de verscheidene pixels aan te sturen. Door de concentrische pixels opeenvolgend aan en af te zetten, kon de irisconstrictie en -dilatatie nagebootst worden. Een elektrische overbrugging werd ook geïmplementeerd omdat dit toeliet om alle nodige verbindingen aan één kant van de substraten te brengen. Het depositieproces van de flexibele, geleidende lijm was echter weinig controleerbaar kon leiden tot ongewenste verbindingen, hetgeen nadelig was voor het contrast van de pixels. Alhoewel toekomstig werk dit probleem zou moeten aanpakken, lijkt de artifiële iris goed geschikt te zijn als eerste toepassing van deze nieuw ontwikkelde technologie.

Een andere toepassing in het gebied van visuele correctie is een slimme contactlens voor presbyopie. Hiervoor werd het gebruik in een slimme contactlens met multifocale functionaliteit bestudeerd, maar aangezien dit op dit moment het onderwerp is van een patentaanvraag, kan hierover geen verdere informatie verstrekt worden.

Voor de finale toepassing, een contactlensbeeldscherm voor verhoogde realiteit, werd er algauw gerealiseerd dat pixels die zich net voor de cornea bevinden, niet scherp waargenomen kunnen worden aangezien zij dichter dan de minimale focusafstand van het oog gelocaliseerd zijn. Verkennende simulaties geven aan dat zelfs onder ideale omstandigheden, een klassieke aanpak die gebruik maakt van geïntegreerde microlenzen waarschijnlijk leidt tot een geprojecteerde spotgrootte van 0.4 mm. Dit wil zeggen dat er slechts 4 bij 4 pixels geprojecteerd kunnen worden in het gebied met de grootste visuele acuïteit, wat enkel de projectie van eenvoudige patronen toelaat. Daarom lijkt het aangewezen dat, vooraleer beeldschermtechnologieën verder onderzocht worden als toepassingen in een contactlensbeeldscherm, er een diepgaande studie nodig is over hoe een gedetaileerd beeld op de fovea geprojecteerd kan worden. Het valt af te wachten of vloeibaarkristalbeeldscherm-technologie gebruikt kan worden voor dit doel, aangezien het bewezen optische principe waarschijnlijk zal dicteren welke technologie het meest geschikt is.

Om te concluderen, hebben we voor het eerst aangetoond dat het mogelijk is om een nietemitterende, elektro-optische technologie te creëren die geïntegreerd kan worden in een contactlens. Deze mijlpaal brengt ons één stap dichter tot een nieuwe generatie contactlenzen, dewelke potentieel kan leiden tot doorbraaktoepassingen in biomedische- en verhoogderealiteit-domeinen.

Research Dissemination

Papers in journals with Web of Science indexation

1. **J. De Smet**, A. Avci, P. Joshi, D. Schaubroeck, D. Cuypers, and H. De Smet, 2013, Progress toward a liquid crystal contact lens display. *Journal of the Society for Information Display,* doi: 10.1002/jsid.188, (available online)

2. A. Avci, J. De Cock, **J. De Smet**, Y. Meuret, P. Lambert, and H. De Smet, 2012, "Reduced-complexity Multiview Prediction Scheme with Content-adaptive Disparity Vector Estimation," *Journal of Electronic Imaging*, 21 (3): 1–7.

3. A. Avci, J. De Cock, P. Lambert, R. Beernaert, **J. De Smet**, L. Bogaert, Y. Meuret, H. Thienpont, and H. De Smet, 2012, "Efficient Disparity Vector Prediction Schemes with Modified P Frame for 2D Camera Arrays," *Journal of Visual Communication and Image Representation*, 23 (2): 287–292.

4. **J. De Smet**, A. Avci, R. Beernaert, D. Cuypers, and H. De Smet, 2012, "Design and Wrinkling Behavior of a Contact Lens with an Integrated Liquid Crystal Light Modulator," *Journal of Display Technology*, 8 (5): 299–305.

5. R. Beernaert, T. Podprocky, J. De Coster, A. Witvrouw, L. Haspeslagh, A. Avci, **J. De Smet**, and H. De Smet, 2010, "Novel Micromirror Design with Variable Pull-in Voltage," *Microelectronic Engineering*, 87 (5-8): 1248–1252.

6. R. Beernaert, A. Avci, **J. De Smet**, H. De Smet, J. De Coster, S. Severi, and A. Witvrouw, 2010, "Novel Analog Pulse-width-modulated 15-μm SiGe Micromirrors," *Journal of the Society for Information Display*, 18 (10): 855–861.

Proceedings of conferences, with Web of Science indexation

1. A. Avci, J. De Cock, **J. De Smet**, Y. Meuret, P. Lambert, and H. De Smet, 2012, "A Content-adaptive Scheme for Reduced-complexity, Multi-view Video Coding," In *Proceedings of SPIE, the International Society for Optical Engineering*, ed. Atilla M Baskurt and Robert Sitnik. Vol. 8290. Bellingham, WA, USA: SPIE, the International Society for Optical Engineering.

2. A. Avci, J. De Cock, R. Beernaert, **J. De Smet**, L. Bogaert, Y. Meuret, H. Thienpont, P. Lambert, and H. De Smet, 2011, "Reduced Complexity Multi-view Video Coding Scheme for 2D Camera Arrays," In *3DTV-conference: the True Vision: Capture, Transmission and Display of 3D Video* New York, NY, USA: IEEE.

3. R. Beernaert, J. De Coster, T. Podprocky, A. Witvrouw, S. Severi, A. Avci, **J. De Smet**, and H. De Smet, 2010, "SiGe Micromirrors for Optical Applications," In *Proceedings of SPIE, the International Society for Optical Engineering*, ed. Henry P Schriemer and Rafael N Kleiman. Vol. 7750. Bellingham, WA, USA: SPIE, the International Society for Optical Engineering.

4. A. Avci, L. Bogaert, R. Beernaert, **J. De Smet**, Y. Meuret, H. Thienpont, and H. De Smet, 2010, "Efficient Disparity Vector Coding for Multi-view 3-D Displays," *In Proceedings of the Society of Photo-optical Instrumentation Engineers*, ed. Atilla M Baskurt. Vol. 7526. Bellingham, WA, USA: SPIE, the International Society for Optical Engineering.

5. R. Beernaert, T. Podprocky, A. Avci, **J. De Smet**, and H. De Smet, 2009, "Micromirror with Electromechanical Pulse Width Modulation," In *Conference Record of the International Display Research Conference*, ed. Norbert Fruehauf, 428–431. Society for Information Display (SID).

6. **J. De Smet**, R. Van Holen, S. Staelens, S. Vandenberghe, and I. Lemahieu, 2009, "Slat Collimated Multipinhole Human Brain SPECT," In *Ieee Nuclear Science Symposium - Conference Record*, 3309–3310. New York, NY, USA: IEEE.

Proceedings of conferences, without Web of Science indexation

1. **J. De Smet**, P. De Backer, E. Islamaj, D. Cuypers, and H. De Smet, 2013, "A Spherically Shaped Display for Use as an Artificial Iris," In *EuroDisplay 2013, Proceedings*, 61–63. Wiley.

2. **J. De Smet**, P. Joshi, D. Cuypers, and H. De Smet, 2013, "Spherically Curved Guest-host Liquid Crystal Light Modulator for Use in Contact Lens Applications," In *SID Mid-Europe Spring Meeting 2013 Book of Extended Abstracts*, ed. Herbert De Smet, 34–37, SID Mid-Europe Chapter.

3. H. De Smet, **J. De Smet**, D. Cuypers, C.P. Weng, and J. Pankaj, 2013, "A Contact Lens with Built-in Display: Science Fiction or Not?" In *Proceedings of the 33rd International Display Research Conference*, ed. Ian Sage, Graham Weaver, and Alasdair Campbell, 8–11. London, UK: Society for Information Display (SID).

4. P. Joshi, **J. De Smet**, X. Shang, D. Cuypers, G. Van Steenberge, S. Van Vlierberghe, P. Dubruel, and H. De Smet, 2013, "A Single Step Method for Characterizing Blue Phase LCs at Various Temperatures," In *IDW'13: Proceedings of the International Display Workshops*, 20:243–246, Tokyo, Japan: Institute of Image Information and Television Engineers, Society for Information Display.

5. S. Valyukh, **J. De Smet**, O. Slobodyanyuk, and H. De Smet, 2012, "A Liquid Crystal Lens Array-based Projection System for Near Eye Displays," In *Proceedings of the International Display Workshops*, 1305–1308. Society for Information Display.

6. **J. De Smet**, A. Avci, P. Joshi, D. Cuypers, and H. De Smet, 2012, "A Liquid Crystal Based Contact Lens Display Using PEDOT: PSS and Obliquely Evaporated SiO2," In *SID Symposium Digest of Technical Papers*, 43:1375–1378. Wiley.

7. **J. De Smet**, A. Avci, R. Beernaert, D. Cuypers, and H. De Smet, 2011, "Wrinkle Formation in Conformable Liquid Crystal Cells for Use in a Contact Lens Display," In *IDW'11: Proceedings of the International Display Workshops*, 1203–1206. Society for Information Display (SID).

8. **J. De Smet**, A. Avci, R. Beernaert, D. Cuypers, and H. De Smet, 2010, "Spherically Curved Guest-host Display for Use in a Contact Lens," In *Proceedings of the International Display Workshops*, 17:1585–1586. Society for Information Display (SID).

Other conferences, without proceedings

1. R. Beernaert, T. Podprocky, A. Witvrouw, L. Haspeslagh, A. Avci, **J. De Smet**, and H. De Smet, 2009, "Novel Micromirror Design with Variable Pull-in Voltage," In *International Conference on Micro- and Nano-Engineering*, 35th, Abstracts.

2. **J. De Smet**, R. Van Holen, S. Staelens, S. Vandenberghe, and I. Lemahieu, 2008, "Multipinhole Brain SPECT: Feasibility Study," In *Liège Image Days*, 1st, Abstracts.

Patents

The patent 'Active multifocal lens' has been filed on 19/9/2013, but has currently not been published yet.

Public Dissemination

This work was extensively covered in public media, of which only a selected overview will be given here.

News Broadcasts

1. News item on 'Het Journaal' on 5/12/2013, VRT (Dutch Belgian National Television)

2. News item on 'Het Journaal' on 5/12/2013, RTL-TV1 (Fench Belgian National Television)

3. News item on 'Z-nieuws' on 11/12/2013, Kanaal Z (Belgian Business Television)

4. News item on 8/1/2013, Inter TV (Ukranian Television)

5. News item on 'News Today' on 11/1/2013, CNC World (Chinese Global News Channel)

6. News item on 12/12/2012 on NBC News (US Television), published as 'Contact lens displays LCD images' on http://www.nbcnews.com

Newspapers

1. Article 'De zonnecontactlens komt er aan', in Belgian newspaper De Standaard on 6/12/2012

2. Article 'Eye that does not need a screen', in English newspaper Telegraph on 10/12/2012

3. Article 'Augmented reality LCD contact lens', in Indian newspaper Ahmedabad Mirror on 11/12/2012

Online Articles

1. Article 'imec demonstreert lcd op contactlens', published on 5/12/2012 on http://www.bits-chips.nl

2. Article 'Screw Google Glass, I want my augmented-reality heads-up-display contact lenses', published on 5/12/2012 on http://www.venturebeat.com

3. Article 'Breakthrough in Augmented Reality Contact Lens', published on 5/12/2012 on http://www.sciencedaily.com

4. Article 'Belgian team develops "LCD" contact-lens display', published on 5/12/2012 on http://www.optics.org

5. Article 'THE END OF SMARTPHONES: Here's A Computer Screen On A Contact Lens', published on 10/12/2012 on http://www.businessinsider.com

6. Article 'Researcher Eyes Display on Contact Lens', published on 8/10/2013 on http://www.eetimes.com

Other Activities

1. Interview on popular science program 'Scheire en de Schepping' on 14/2/2013

2. Talk 'The smart contact lens' on TEDxGhent on 22/6/2013

3. A prototype was shown on 'Gadget Man' (Episode: Smaller is Better), a show on Channel 4 (British television)

Prizes and Nominations

1. SID-Mid Europe Chapter Student Award 2012, awarded for an outstanding scientific/technical achievements and contributions to research in the field of information display.

2. Nominated for 'Strafste Gentenaar 2012' (Outstanding citizen of Ghent) in the category Academia. This award is organized by Het Nieuwsblad, a Flemish newspaper.

3. Nominated for 'De Gouden Pipet' (The Golden Pipette), awarded to the most promising young scientist in 2013. This award is organized by Eos, a Flemish science magazine. The work was also featured in the issue of November 2013.

Prelude

"One's mind, once stretched by a new idea, never regains its original dimensions."

—Oliver Wendell Holmes Sr.

Although science and technology tend to progress step by step, sometimes a new idea seemingly pops out of nowhere, grasping the creator's attention and keeping a stubborn grip on him. In this case, the seed of the idea came out of two mundane or less mundane facts. For the last 15 years, my morning ritual comprises cleaning and inserting contact lenses in my eyes, since like many people I need some corrective optics for my nearsightedness. Next to this, I have taken a keen interest in display technology during my education as an engineer, as I find it a wonderful combination of physics, optics and electronics. Since this morning ritual is also a short moment of contemplation, it thus seemed inevitable that at some point in time the question would arise what it would be like if we could integrate a display in a contact lens. Although I cannot remember anymore on what day this new idea emerged, it kept such a firm grasp on me that it prompted me to find support to perform a thorough study on this matter.

This support was provided to me by Prof. Herbert De Smet and the people at the Centre for Microsystems Technology (CMST) at Ghent University and the result of this study is presented in this book. At this point, I can already disclose that a fully autonomous electronic contact lens providing an additional view on top of your normal view is far beyond the scope of this work. Such a lens would require a tremendous research effort combining skills in biocompatiblity, optics, microelectronics, wireless communication, energy harvesting, microbatteries and stretchable integration technology. Instead, we decided to look at the integration of existing Liquid Crystal Display (LCD) technology in contact lenses to initiate an exploratory research effort on the idea of a contact lens display. Furthermore, this work broadened our vision on the new exciting domain of smart contact lenses as we quickly realized the integration of display technology in a contact

lens could lead to significant advances in more medically oriented applications, but this will be elucidated in the following chapters.

A brief overview of the structure of this book is presented hereafter. In Chapter 1, an introduction is given to contact lenses and their history, explaining many terms that are used throughout this work. After introducing conventional contact lenses, Chapter 2 explores the new domain of smart contact lenses, a developing field aiming to add functionality to contact lenses by the integration of microelectronic components. Next to this, liquid crystals and LCD technology are introduced, ending with the formulation of the objectives of this work. Chapter 3 outlines the design and fabrication process of a spherically deformed LC cell, which is the main mechanical component of this work. In contrast to existing LCD technology, which is hard and flat, the spherical and flexible shape posed some severe challenges which prompted the creation and use of new fabrication methods and materials. The electro-optic activation of this spherical LC cell is presented in Chapter 4, describing the different cell layers needed for this activation and the additional techniques that were developed to create a uniformly switching cell. Since any real display technology needs the ability to show patterns, we also zoom in to some patterning methods that were used to effectively create a patterned modulation. In Chapter 5, we characterize the main parameters of the technology and explore the possibilities to further improve these through the integration of polarizers. With the basic technology established, Chapter 6 explores some first applications, such as for instance the artificial iris. Finally, we draw our conclusions and present our vision for future work in Chapter 7.

1 An Introduction to Contact Lenses

"Competence, like truth, beauty, and contact lenses, is in the eye of the beholder."

—Laurence J. Peter

1.1 The human visual system

1.1.1 Evolution of the human eye

Sight is one of the most important senses of humans. Our visual perception is basically the result of light signals that are detected with our eyes and then interpreted by the visual cortex of our brain. Although the processing of visual stimuli is an interesting field of study, we will focus our attention on the 'measurement tool' itself, the eye. To understand its working principle, it is helpful to look at how scientists believe the eye has evolved. The most profound theory about the evolution of the human eye was developed by Nilsson and Pelger [1] and is illustrated in Figure 1.1.

The first step is the development of light-sensitive cells at the skin's surface which are just able to detect the overall brightness of the surroundings. Such a

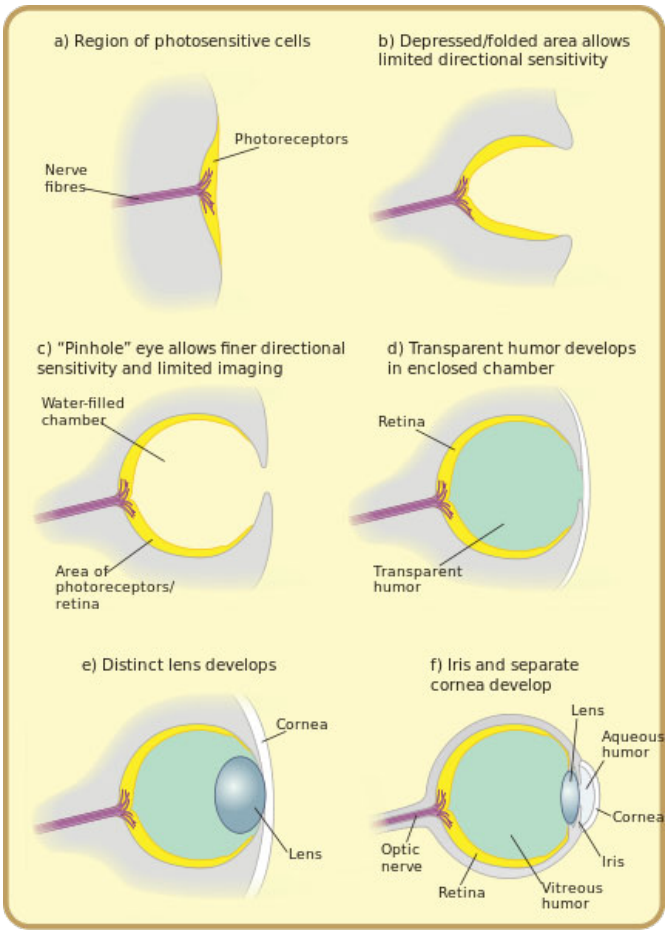

Figure 1.1: Evolution of the human eye.

light sensitive area can sag into a depression, giving it the ability to distinguish where the light is approximately coming from. This ability will increase with the depth of the depression, but when the depth equals the width it becomes more efficient to constrict the aperture. Such a structure will start resembling a pinhole camera and the visual acuity will start increasing with decreasing aperture size at the expense of image brightness. To protect this primitive eye, the inner volume is filled with a vitreous body, thus forming an enclosed chamber. In order to increase the brightness of the image, a lens can be introduced near to the aperture.

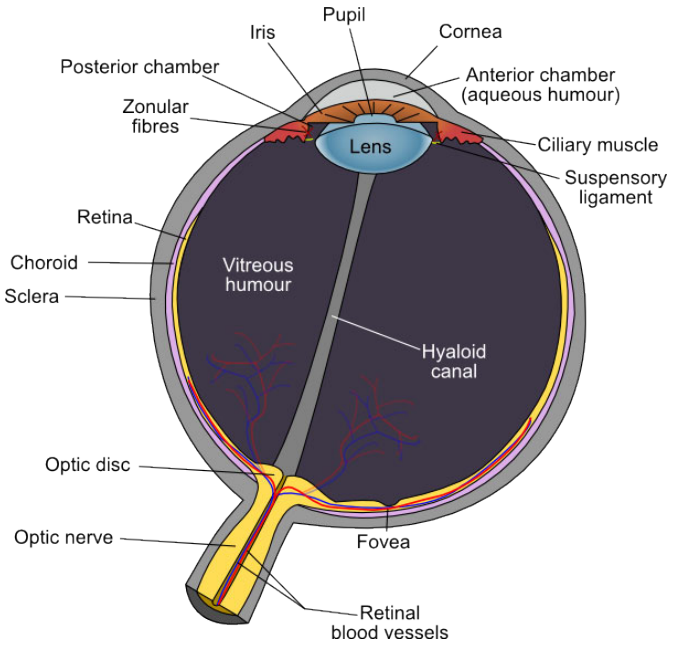

Figure 1.2: Anatomy of the human eye. Image from [2].

Moreover, such a lens will increase the resolution of the system, when the image brightness is kept constant. Note that the introduction of the lens itself is already beneficial to the overall performance of the system and the focal plane of the lens does not need to be coinciding with the retinal surface. Of course, as the focal strength of the lens increases, a sharper image will be formed leading to a better visual acuity. This drive for improved acuity prompts the formation of the cornea, a transparent semi-spherical object in front of the aperture that increases the refractive power of the system. Eventually focused images will be formed on the retina, while additional features such as an adaptable lens, allowing for multiple focal planes, and an iris, allowing to adapt to a broad range of dynamic lighting conditions, further improve the eye's performance.

1.1.2 Anatomy of modern human eyes

Although some anatomic features have already been described in the previous section, for completion we will give a full description of the most important parts of a human eye, complemented by the illustration in Figure 1.2. The eye is a soft

organ with a spherical shape, having a mean diameter of about 24 mm [3]. It is however, not completely round, as a small hemispherical protrusion is located at the front of the eye, having a mean radius of 7.8 mm [4]. This protrusion is the cornea and acts as the main refractive component of the eye, constituting 2/3 of the refractive power of the eye [5]. A peculiar, but very important anatomical feature about the cornea is that, because of its need of being transparent, no capillaries are present and oxygenation of the corneal cells happens through diffusion of oxygen molecules from the surrounding air.

Apart from the cornea, the outer tissue of the eye is called the sclera, also known as the white of the eye. Behind the cornea one can see the iris, having a colourful appearance that is genetically determined and in which an opening is foreseen. This opening is called the pupil and by adjusting the size of the iris, more or less light is entering the eye through the pupil. The ability to control the amount of light entering the eye allows it to adapt to different lighting conditions: the brighter the surroundings, the smaller the pupil size. Additionally, a sharper image will be created, similar to the characteristics of a pinhole camera. Directly behind the iris is the intraocular lens, attached to the ciliary muscles by zonular fibres. The main function of the lens is to allow the eye to accommodate and bring objects into focus located at different distances, but this process will be more thoroughly described in section 1.1.3.

Behind the lens one can find the vitreous humour, a jelly-like transparent substance giving the eye consistency and keeping other parts in their place. One of the most important of these parts is the retina, the top layer at the inner side of the eye. In this layer, light sensitive receptors are located that convert incoming photons into electrical pulses. When inspecting these photoreceptors more closely, one can distinguish two types: rods and cones (see Figure 1.3). Both have distinctly different properties and, as can be seen in Figure 1.4, have a different distribution across the retina. Cones are mainly found in the fovea, an area near the optical axis of the eye with a small pit in the center, where they reach a maximum density. Here the eye reaches its maximum visual acuity and the fovea is thus primarily aimed at objects that have our immediate attention. Moreover, since there are three different cones having an absorption maximum at either the red, green and blue part of the visual spectrum, they allow us to discriminate different colors. In contrast, rods can mainly be found away from the fovea and exist only in one kind, therefore having only a grey-level output. However, rods are very sensitive and can even detect a single photon [6], and are thus used in low light conditions.

This increased light sensitivity comes at the expense of a slower response time

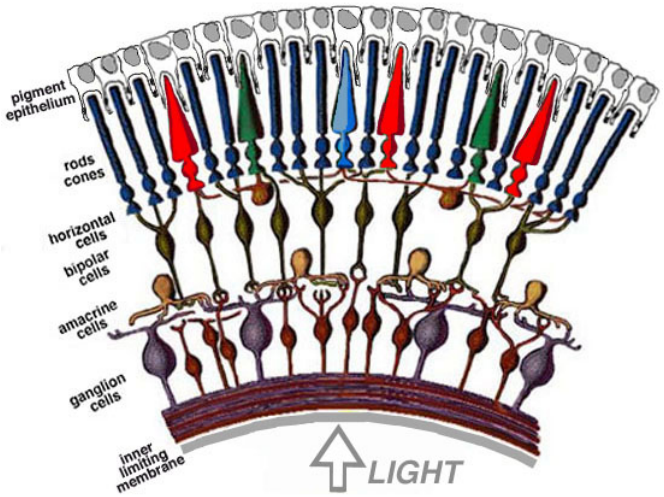

Figure 1.3: Schematic overview of the retina comprising cone and rod cells. Image from [7].

when compared to cones. One should also bear in mind that although the density of cones and rods roughly reach the same maximum in some areas, this does not lead to an equal resolution and can be attributed to the innervation of the photoreceptors. As illustrated in Figure 1.3, the photoreceptors are connected to ganglion cells, neurons which are responsible for transmitting the visual information to the visual cortex of the brain. However, to limit the needed bandwidth for sending this information, multiple photoreceptors are connected to only one ganglion cell. Furthermore, the ratio depends both on the type of photoreceptor as the location on the retina. For instance, in the fovea one ganglion cell is connected with as little as one to three cones, while at the periphery of the retina a ganglion cell can be connected with over thousands of rods. Somewhat counterintuitively, the ganglion cells are actually located above the photoreceptors, meaning that light has to pass through them before being absorbed. As a result, the nerves coming from all ganglion cells have to penetrate the retina at some point, which is happening at one central location called the optic disc. From this optic disc the optic nerve transports all visual signals to the brain. However, as there is no room for photoreceptors at the optic disc, this is also a blind spot for the human eye.

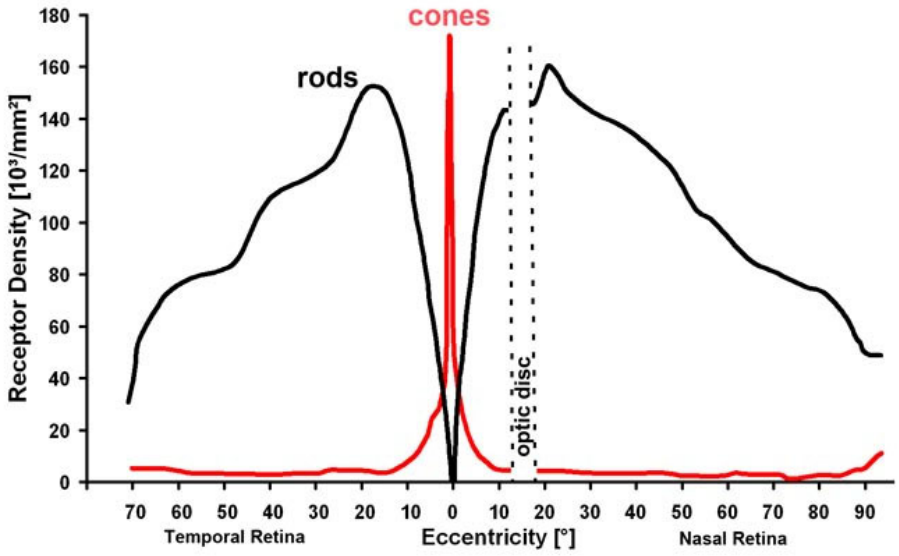

Figure 1.4: Distribution of cones and rods across the retina. Image from [8].

1.1.3 Accommodation

The accommodation process

Although the main refractive power of the eye is coming from the cornea, its focal point is fixed. Nevertheless, the eye has the ability to change this focal point by a process which is called accommodation (see Figure 1.5). According to the classical Helmholtz theory [9], accommodation is the result of the reshaping of the intraocular lens by contraction of the ciliary muscles. Counterintuitively, the contraction of the muscles actually results in a more convex lens, while their relaxation results in a flatter lens with a larger focal distance. This is because the lens is put under tension through the zonular fibres and the suspensory ligaments. The contraction of the ciliary muscles counteracts this tension and thus allows the lens to elastically regain its original, more convex shape.

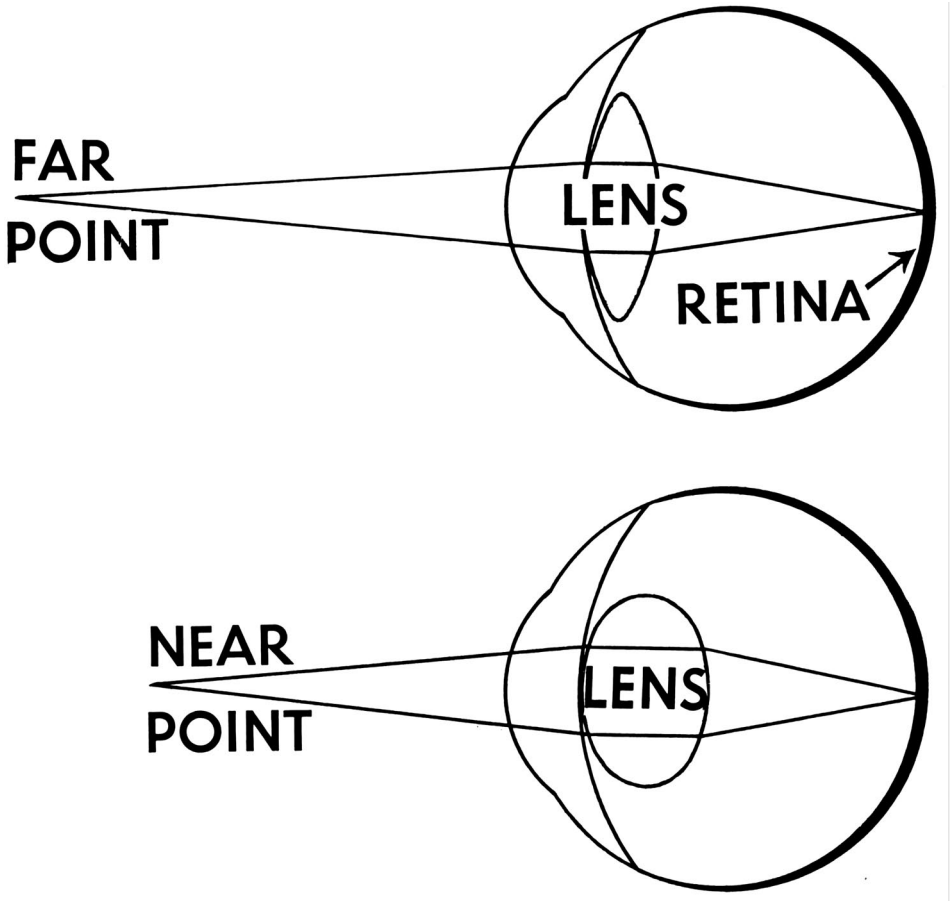

Figure 1.5: The accommodation process: the eye changes its focal distance by reshaping the intraocular lens.

Accommodation disorders

As every organ, the human eye is prone to malfunction. Although there is a plethora of ophthalmic disorders with different prevalences and impact, the most well-known and most prevalent are those related to refractive errors. For example, Vitale et al. [10] estimated that in the US alone, about half of the population 20 years or older suffers from a clinically important refractive error. Generally, a refractive error means the eye cannot form a sharp image onto the retina when set for a certain focal distance because its optical power is either too strong,

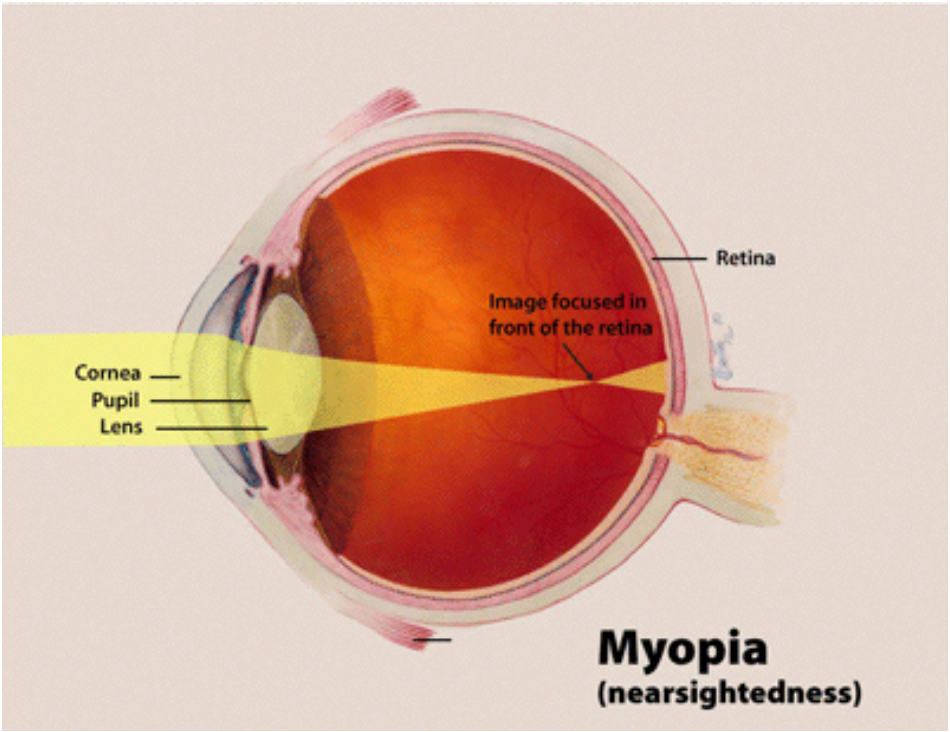

Figure 1.6: A myopic eye focuses the image before the retina.

causing short-sightedness or myopia (see Figure 1.6), or too weak, causing long-sightedness or hyperopia (see Figure 1.7).

An additional refractive disorder that might concur with myopia or hyperopia is astigmatism, meaning that because of an irregular, non-spherical shape of either the cornea or the intraocular lens the eye is unable to create a sharply focused image in a single focal plane [5]. This can be further subdivided in irregular or regular astigmatism, where the irregular type is often caused by corneal scarring of scattering in the intraocular lens, hence leading to a blurred image on the retina. Regular astigmatism is caused by the cornea or the intraocular lens having a toric shape, resulting in the light rays being focused on two different focal points and thus also leading to a blurred image.

Finally, as people grow older they start to loose their accommodative power, making it more difficult to focus on objects close to the eye. Generally, this

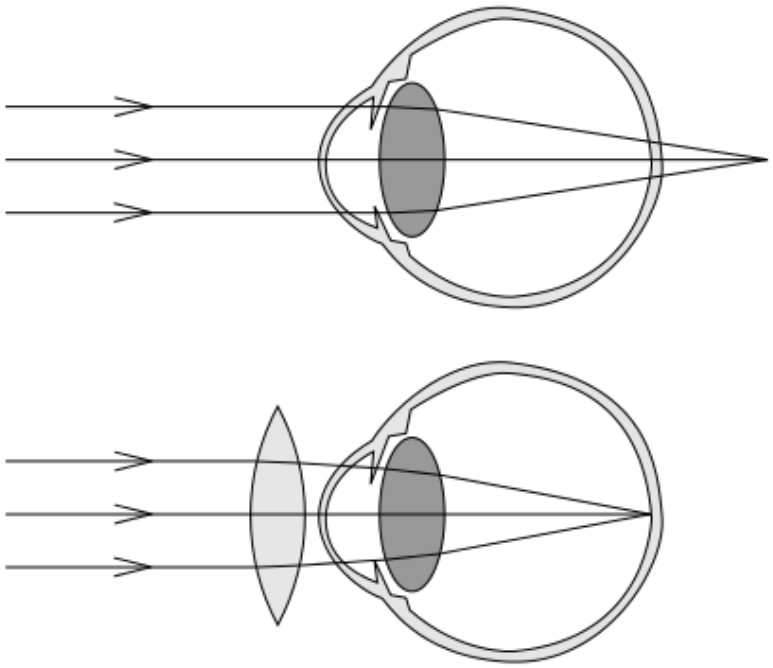

Figure 1.7: Top: in a hyperopic eye the optical system is too weak and as a result the image is focused at a point behind the retina. Bottom: by placing an additional optically active element in front of the eye refractive disorders such as hyperopia can be corrected.

decrease only becomes obvious between the age of 40 and 50 and unsurprisingly the name of this disorder, presbyopia, is derived from the greek word for 'old man' [11]. At a certain point, when the minimum accommodation distance becomes too large, people cannot read a text even held at arm's length any more, only then making it a real problematic disorder. Although a variety of factors might underlie this reduced accommodative power, it is believed that the increase in stiffness of

the intraocular lens over time is the major contributing factor [5, 12]. Optically, a presbyopic eye focused at a near object is similar to a hyperopic eye, but is solely resulting from a reduced accommodative power and not an inherent refractive error. Next to this, complex combinations such as presbyopia and hyperopia or presbyopia and myopia can exist, regularly even concurring with astigmatism.

Glasses as a solution to accommodation disorders

Most refractive disorders can be corrected by placing an optically active element such as a lens in front of the eye (see Figure 1.7). By counteracting the refractive error with an opposing refraction a clear image can thus be formed on the retina. Historic evidence indicates this principle was discovered as early as 1286, placing the invention of eyeglasses most probable for correcting presbyopia around that time [13]. These reading glasses required a set of convex lenses and could also be used to correct hyperopia. Of course eventually concave glasses were used to correct myopia, but the problem with these single focus glasses is that they do not provide a solution for people having more complex combination of visual disorders (e.g. myopia combined with presbyopia). This need was addressed in the 18th century [14] with the invention of bifocals in which lenses with two different focal points were combined in a single spectacle frame (see Figure 1.8). Most modern glasses now use progressive lenses, where the focal point gradually varies with the vertical viewing angle. In these glasses the lower part is used for reading, the middle part for looking at computer screens and the upper part for looking at objects located at a distance.

1.2 Contact lenses and their history

1.2.1 Birth of the contact lens

The theoretical invention of a contact lens is generally attributed to the British physician and astronomer John Frederick William Herschel. In 1827 Herschel described a procedure where a glass lens was filled with gelatin and directly put on top of the cornea to correct irregularities in its shape such as astigmatism [15]. Although his proposed lenses did not have any optical power, he was the first to propose the use of a lens placed directly on the eye to correct an ophthalmic disorder. However, there is no evidence Herschel tried to actually fabricate such a lens. For this one had to wait until 1888, when two independent efforts by Eugene Kalt [16] and Adolf Gaston Eugen Fick [17] resulted in glass scleral lenses used

Figure 1.8: A typical example of early bifocal glasses. Depending on the viewing angle, the wearer can select a lens to either read at close point or to look at objects at a distance.

to correct the corneal irregularities Herschel described. The term scleral lenses point to the fact that the lens is resting on the sclera of the eye, bridging the cornea, as illustrated in Figure 1.9. Scleral lenses still exist today, although more complex designs and forms are available.

Only one year after the birth of scleral lenses August Müller [18, 19] revealed glass blown lenses which were closely following the curvature of his (regular) cornea and correcting his own severe myopia. The main difference with Kalt's and Fick's work was that this lens was actively designed to have a prescribed power to correct a refractive error. In contrast to the early afocal scleral 'shells', Müller's lenses more closely resemble with what is currently identified as a real contact lens. Nevertheless, these inventions can be marked as the birth of contact lenses and related contact lens research. The need for research was immediately clear as the lenses could only be worn for several hours before they became too irritating to wear. This can be attributed to the use of glass as a material, as these heavy lenses put a lot of weight on the sclera, while they also prevented oxygenation of the cornea. Some minor improvements where achieved due to better designs and additional features such as drilling small holes (fenestrations) in the lenses [20],

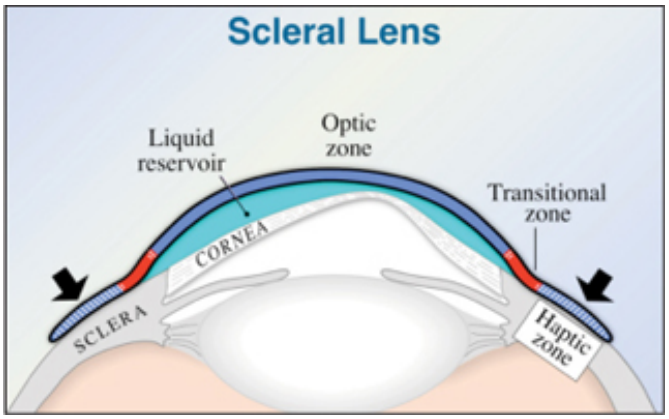

Figure 1.9: The first contact lenses where glass made scleral lenses. These lenses bridge the cornea and are used to correct corneal irregularities. The liquid reservoir between the lens and the cornea nullifies the optical aberrations created by the cornea's irregular shape. Image from [23].

but the lack of comfort prevented glass lenses to become successful. For instance, between 1935 and 1939 only about 10000 glass lenses were sold in the US [21], which is a negligible quantity when compared to the 583 million lenses sold in the UK alone in 2011 [22].

1.2.2 The first revolution: introduction of plastic materials

The main disadvantages of glass contact lenses are their weight and their oxygen intransmissibility, both leading to discomfort for the contact lens wearer. The first disadvantage was tackled in 1937, when Istvan Györffy introduced poly methyl methacrylate (PMMA) as a new material for contact lenses [24]. This lightweight, biocompatible polymer has good thermoforming properties and Györffy used it to make scleral lenses by molding PMMA sheets onto casts taken from eye impressions. This method made it much easier to fabricate lenses. Next to this, the introduction of PMMA quickly resulted in the emergence of new contact lens designs where the creation of the corneal contact lens was the most important breakthrough. In contrast to scleral lenses, which do not touch the cornea, corneal lenses only reside on the cornea and can even move freely on it. Although PMMA is oxygen intransmissible, corneal lenses improve the oxygenation of the cornea due to an improved transport by a tear mixing mechanism [25]. In this mechanism,

tears behind the lens are replenished by oxygen rich tears from other parts due to the movement of the lens. Because of this improved oxygenation and hence comfort, a large growth was seen in contact lens wearers. For instance, the number of lenses in the US rose from 50.000 in 1946 to 200.000 in 1949, primarily due to the introduction of a PMMA based corneal lens [21].

1.2.3 The second revolution: introduction of soft contact lenses

The downside of using hard materials for contact lenses such as glass or PMMA, is that a good dimensional match is needed between the lens and the cornea of the wearer, especially for corneal lenses. A mismatch will lead to discomfort and even with a good fit the sensation of having a hard object on top of the cornea requires an adaptation time of several weeks. Moreover, when debris is caught under the lens an unpleasant, stinging feeling sets in. These issues were tackled by the invention of soft contact lenses in 1961 by Otto Wichterle and Drahoslav Lim. They invented the monomer hydroxyethylmethacrylate (HEMA), which in its polymerized form can absorb a large amount of water and becomes a hydrogel [26]. Hydrogels are soft and very flexible materials which due to their hydrophilic nature can absorb up to 85 % of their weight in water [27].

Wichterle soon realized that this material could be used for contact lenses and together with Lim developed a spin casting method which allowed for a relatively easy volume production of these lenses. As illustrated in Figure 1.10, this method starts with the creation of a mould into which the unpolymerized material is deposited. When the mould is spun, the centrifugal forces push the material in a lens like shape which is then fixed permanently by a heat curing step or through ultraviolet light (UV) illumination [28]. The final shape and power of the resulting lens are due to the combination of gravity, centrifugal force, surface tension, the amount of liquid monomer in the cast and the spin speed. After the company Bausch & Lomb acquired the rights and industrialized this technology in 1971, it only took a few years time for these soft lenses to dominate the marketplace and make PMMA almost obsolete [29]. This can mainly be attributed to the easy fitting of soft lenses (since they can deform easily a good dimensional match is not needed) while they also immediately feel comfortable when inserted for the first time.

Figure 1.10: By casting some unpolymerized material in an open, spining mold, a contact lens with a spherical back surface can be created. Image from [23].

1.2.4 Modern evolutions: the quest for a high oxygen transmissibility and comfort

The introduction of soft contact lenses nearly pushed PMMA contact lenses out of the market, but this did not mean the end for rigid contact lenses. At the time of their introduction it had become increasingly clear that transport of atmospheric oxygen towards the cornea should be sufficient to prevent disorders such as corneal swelling. As a result, oxygen permeability of the contact lens material was identified as an important factor [30, 31] and a new symbol (Dk) and corresponding unit (the barrer) were introduced. A higher Dk means an increased oxygen transport and thus a better oxygenation of the cornea, but a full description of these symbols and units can be found in section 1.3.1. The discovery that contact lenses should be oxygen permeable prompted further research into new rigid contact lens materials and the birth of a new class of lenses called rigid gas permeable (RGP) contact lenses was seen. Among the first was cellulose acetate butyrate (CAB), which was introduced in 1977 as a RGP material for corneal lenses [5] and had a Dk between 4 and 8 barrer [27]. Although this would be considered a very low Dk-value at present, this was already an improvement over PMMA, which due to its oxygen blocking properties has a Dk-value of zero.

Subsequent improvements concurred with the introduction of silicone acrylates (Dk 10-60) and fluorosilicone acrylates (Dk 20-150). In 1999, a fluoro-siloxanyl styrene was introduced in the US as Menicon Z and currently has one of the largest oxygen permeabilities (Dk 189) of all contact lens materials [32, 33]. The benefits of RGP contact lenses include a very good visual correction because of their rigid shape and a high oxygen permeability, thereby reducing the chance of poor oxygenation related complications. Nevertheless, in 2012 they constituted 9 % of the fittings and refittings of contact lenses by eyecare practitioners, thus having only a minor share [34].

In contrast, a stunning 84 % of the fittings and refittings comprise soft con-

tact lenses. As mentioned in the previous section, this can be attributed to an increased comfort, reduced adaptation time and easier fitting procedures over RGP lenses [28]. After their introduction in 1971, initial efforts where focused on increasing the water content of the used hydrogels, since this leads to an increased oxygen permeability as more oxygen could dissolve and diffuse through the water contained by the gel. This was achieved by adding new copolymers such as vinyl pyrrolidone and methyl methacrylate to the original HEMA based hydrogels, leading to an increase from 38-40% to 60-85% in water content and Dk's as high as 60 barrer.

Although good progress was made for soft contact lenses in terms of oxygen permeability and comfort, a new trend in contact lens wear pushed for new developments. People wanted to wear their lenses for extended periods, ranging from several days including overnight wear to as long as a whole month of continuous wear. In 1984, Holden and Mertz [35] defined the critical oxygen level in order to avoid corneal oedema for overnight wear and it was clear that even modern hydrogels could not reach these levels. A solution came by the introduction of silicone hydrogels, which combine silicone rubber (polydimethyl siloxane, PDMS) with hydrogels monomers. Interestingly, PDMS was previously used as an alternative to hydrogels because of its extremely high oxygen permeability (up to 600 barrer), but it needs an additional surface treatment due to its inherent hydrophobicity. Even with this surface treatment, silicone contact lenses were rather unsuccessful due to their lack of comfort. Silicone hydrogels, however, combine the best of both worlds and achieve high oxygen permeabilities with very good comfort. Other than classical hydrogels, their oxygen permeability does not just increase with increasing water content and in fact, the highest permeabilities are achieved with a relatively low water content (see Figure 1.11). This can be attributed to the fact that the oxygen molecules permeate more easily through the silicone backbone than through the contained water. At present silicone hydrogels make up 64% of the contact lens fittings and refittings and are thus the prime choice for most contact lens users [34].

1.3 Important parameters for contact lenses

1.3.1 Material Parameters

The most important material properties of contact lenses are oxygen permeability and transmissibility, water content and wettability. A short description of these parameters is presented here.

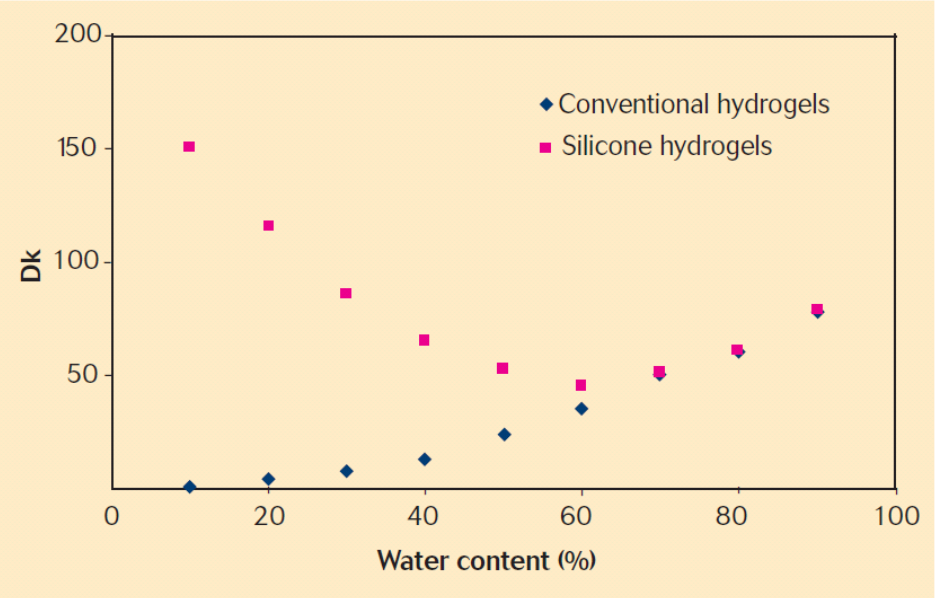

Figure 1.11: Dk versus Water Content of hydrogel and silicone hydrogel contact lenses. Other than with hydrogels the water content of silicone hydrogels does not relate directly to their oxygen permeability, since oxygen molecules permeate primarily through the silicone backbone rather than through the contained water. Image from [36].

Oxygen permeability and transmissibility

The oxygen permeability of a contact lens material is a bulk parameter and can be defined as [37]:

'The rate of oxygen flow under specified conditions through unit area of contact lens material of unit thickness when subjected to unit pressure differences.'

Generally, it is referred to using the symbol Dk, in which D corresponds to the diffusion coefficient of the oxygen molecules in the material and k is the solubility coefficient representing the number of oxygen molecules dissolved in the material. The unit issued by the ISO is 10^{-11}cm^2/s ml O_2/(ml hPa) and uses the hectopascal as its standard pressure unit. Due to historical reasons, however, Dk is often expressed in barrer, which uses mmHg as its unit of pressure: 10^{-11} cm^2/s ml O_2/(ml mmHg). Many times, barrers are called Fatt units, which is a

referral to Irvin Fatt, who introduced this quantitative measure to contact lens research. The higher the Dk value, the more oxygen can permeate through the material, leading to better oxygenation of the cornea.

Although Dk is a valuable parameter, it cannot be used straightforwardly when comparing particular contact lenses. The total amount of oxygen permeating through the lens depends on the thickness of the lens and therefore oxygen transmissibility of a contact lens is defined as the oxygen permeability divided by the lens thickness. The commonly used symbol is Dk/t, where D and k are the same as mentioned above and t is the thickness of the lens, and its unit is 10^{-9}cm/s ml O_2/(ml mmHg) (non-ISO unit).

Water content

The water content of a lens is defined as the percentage of weight of the water that has been absorbed by the lens material in comparison with the total weight:

$$\text{Water content (\%)} = \frac{\text{weight of fully hydrated lens - weight of fully dehydrated lens}}{\text{weight of fully hydrated lens}} x100$$

The water content of a contact lens can drop due to evaporation during lens wear, affecting the lens shape and tightening the fit. This can lead to an uncomfortable feeling and can be a problem especially for high water content lenses.

Wettability

Wettability is the degree to which a liquid maintains contact with a solid surface and is determined by the balance between the adhesive forces between the liquid-solid interface and the cohesive forces of the liquid. A quantitative parameter for wettability can be derived via the angle at the intersection of the liquid-solid interface and the liquid-air interface of a drop of liquid resting on a surface (see Figure 1.12). This angle is called the contact angle and when its value is below 90° the liquid preferentially adheres to the surface. When considering water, such a surface is coined hydrophilic. In the opposite case, when the contact angle is above 90°, the surface is called hydrophobic. Wettability is an important parameter for contact lenses as poor wetting means it is difficult to establish a smooth tear film between the contact lens and the cornea. As a result, lenses with a low wettability tend to be less comfortable to wear, which is also made clear in Figure 1.12, where good wettability is used as a marketing tool.

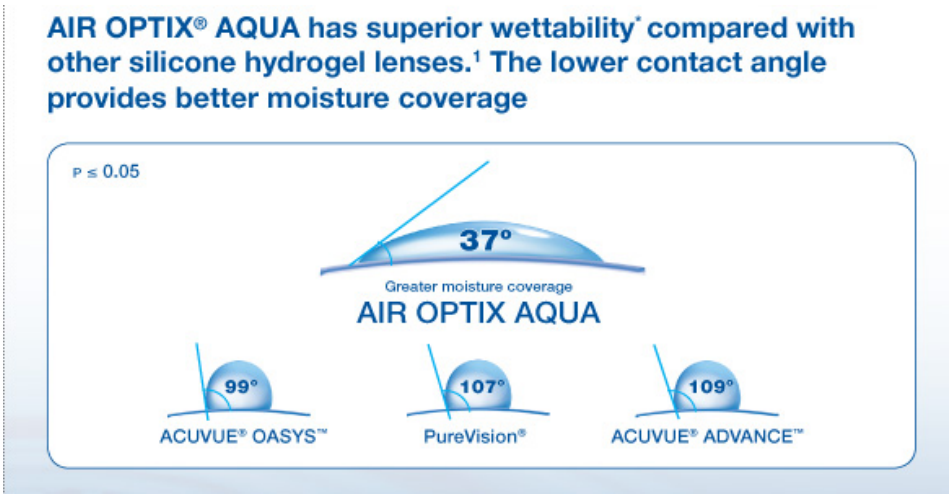

Figure 1.12: By measuring the contact angle of a liquid drop on a surface a measure for wettability can be derived. Good wettability concurs with low contact angles and generally leads to an improved comfort when considering contact lenses. Image from [38]

1.3.2 Design Parameters

The design of a contact lens is very important for comfort and even pioneers such as Adolf Fick and August Müller recognized this from early on. Simply stated, a contact lens is a lens in direct contact with the naked eye and due to the spherical shape of the cornea it should thus have a meniscus shape. In practice, such a meniscus shape only holds for the central part of the contact lens that is used for refracting the incoming light. Towards the edge the lens should flatten to account for the change in curvature when passing to the sclera or, for smaller lenses, to allow for a sufficient tear exchange and avoid lens adhesion to the cornea [27]. Like contact lens materials, designs also evolved, especially with the advent of modern manufacturing techniques. Gradually a comprehensive terminology has been developed of which we will highlight the most important concepts. As illustrated in Figure 1.13, the central part of a contact lens used for light refraction is named the optic zone and is defined by its back optic zone radius (BOZR), its back vertex power (BVP) and its thickness. The BOZR should be closely matched with the wearer's corneal radius to avoid either excessive lens movement and detachment in case of an oversized radius, or painful lens

adhesion in case of a too small radius. The thickness of the lens is determined by the refractive error which it needs to correct and is therefore directly linked to the desired back vertex power of the lens. Next to this, it is also influenced by the strength of the used material and its refractive index. Generally, the thickness is kept as low as possible to ensure sufficient oxygen permeability. Typical values for RGP lenses range between 100 and 160 µm, with a recommended minimum thickness of 140 µm for most modern materials [27]. Standard soft lenses fall in the same range, but thin and ultrathin lenses also exist, having thicknesses from 100 down to 50 µm. The optical zone is delineated by the back optic zone diameter (BOZD) after which, depending on the design, one or more peripheral curves are present. Since a flatter edge is desired, these curves have larger radii than the BOZR. They are also associated with their own back peripheral zone diameters (BPZD), while the diameter of the final curve is called the total diameter of the lens. The edge itself is generally tapered and has a smooth finish, which is required for comfort, especially while blinking.

1.4 Manufacturing Techniques

To complete this introduction, a succinct overview will be given of the most prevalent contact lens manufacturing techniques. Each technique has its advantages and disadvantages and their usage depends on the desired properties and modality of the produced contact lens [28].

1.4.1 Lathe cutting

When striving for the best visual acuity, lathe cutting is the preferred method. The process starts with the bulk fabrication of polymerized cylinders called buttons, which are completely dry before lathing. These buttons are mounted on a computer numerically controlled (CNC) lathe, a fully automated and very precise equipment. When the buttons are spun at high speed, a diamond tool cuts away excessive material, thereby closely following the desired shape of the lens. After cutting of the back surface, the lens is mounted on a new holder and is finished by cutting the front surface in a similar manner. Currently, all RGP contact lenses are made by lathe cutting, while some high precision, low volume soft contact lenses are also made with this process, with the addition of a hydration step. Although the best optical quality and variety of shapes can be achieved, the process is labour intensive and thus costly.

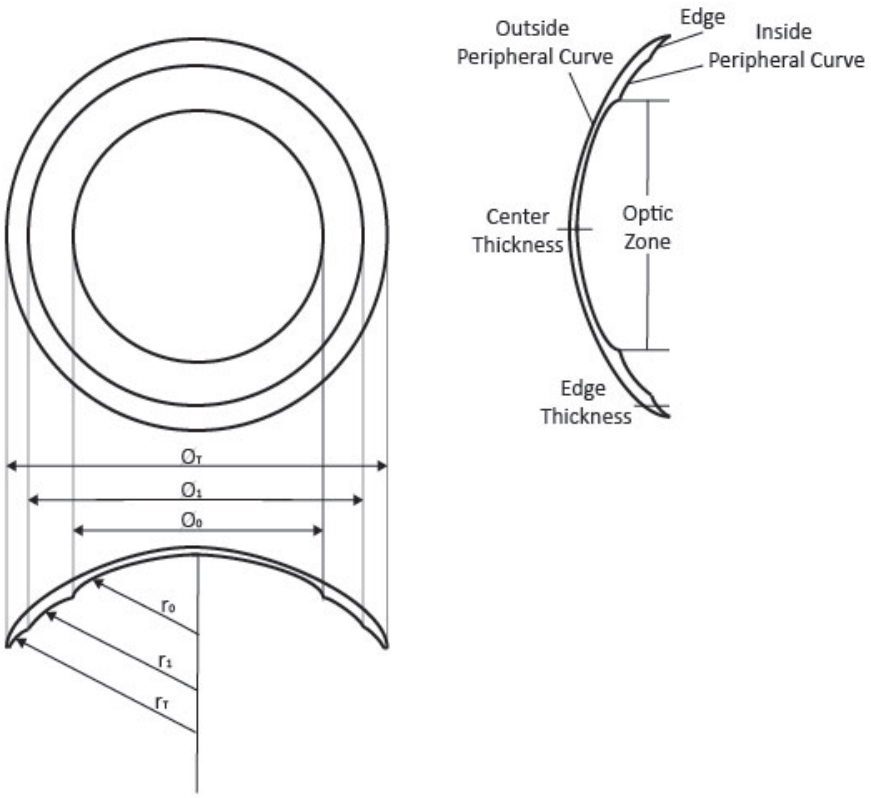

Figure 1.13: Overview of lens design terminology. r_0: back optic zone radius, r_1: first back peripheral radius, r_2: second back peripheral radius, O_0: back optic zone diameter, O_1: first back peripheral diameter, O_T: total diameter

1.4.2 Spin casting

As mentioned in section 1.2.2, spin casting was the first method used to fabricate soft contact lenses. In this method, liquid monomer is deposited in a cast having the desired front shape of the contact lens. The cast is then spun and due to the combination of gravity, centrifugal force, surface tension, the amount of monomer and the spin speed, the final shape of the lens can be fixed as the monomer is polymerized during spinning. The back surface is aspherical and its

BVP is mainly determined by the spin speed, while the dose of liquid monomer mainly determines the central thickness. Sometimes an additional lathing step is used for the front or back surface to obtain a desired profile. After processing, the lens is hydrated in deionised water, a saline solution or sodium bicarbonate, according to the used material. Spin casting is a much faster process than lathe cutting, but has a diminished variety in back surface forms. The back surfaces themselves do have a very smooth finish since they are formed without any contact with a mold, which is better for comfort.

1.4.3 Cast moulding

Although soft contact lenses have a high oxygen transmissibility, the constituent hydrogels are more prone to contamination and degradation, which favours a more frequent replacement of the lenses. As a result, several cast moulding techniques have been developed to fabricate soft contact lenses at low cost and high volume, currently forming the most important class of manufacturing techniques. Basically, this involves the creation of a male and female cast, in between which an unpolymerized solution is inserted. After polymerization in the closed casts, the lenses are removed from the casts and are hydrated and packaged. Although this method allows for a high volume production, the quality of the lenses is highly dependent on the quality of the casts, which are prone to defects. Therefore, contact lenses made by cast moulding generally have a lower optical quality, but constitute a large market of low cost, disposable lenses [34].

References

[1] D. Nilsson and P. S., "A pessimistic estimate of the time required for an eye to evolve", *Proceedings: Biological Sciences*, vol. 256, no. 1345, pp. 53–58, 1994.

[2] Wikipedia, 2013. [Online]. Available: http://en.wikipedia.org/wiki/File:Schematic_diagram_of_the_human_eye_en.svg.

[3] P. Riordan-Eva and E. Cunningham, *Vaughan & Asbury's General Ophthalmology*. McGraw-Hill Medical, 2011.

[4] M. Hom and A. Bruce, *Manual of Contact Lens Prescribing and Fitting, 3rd ed.* Elsevier Health Sciences, 2006.

[5] F. Goes, *The Eye in History*. Jaypee Brothers Medical Publishers, 2013.

[6] H. Okawa and A. Sampath, "Optimization of single-photon response transmission at the rod-to-rod bipolar synapsee", *Physiology*, vol. 22, no. 4, pp. 279–286, 2007.

[7] Webvision, 2013. [Online]. Available: http://webvision.med.utah.edu/.

[8] Originally from Webvision, 2013. [Online]. Available: http://webvision.med.utah.edu/.

[9] H. Von Helmholtz, *Treatise in Physiological Optics, English Translation*. George Banta Publishing Company, 1924.

[10] S. Vitale, L. Ellwein, M. Cotch, F. Ferris, and R. Sperduto, "Prevalence of refractive error in the united states, 1999-2004", *Arch Ophthalmol*, vol. 126, no. 8, pp. 1111–1119, 2008.

[11] Merriam-Webster Online Dictionary, retrieved on the 1st of April 2013. [Online]. Available: http://www.merriam-webster.com/dictionary/presbyopia.

[12] K. Heys, S. Cram, and R. Truscott, "Massive increase in the stiffness of the human lens nucleus with age: the basis for presbyopia?", *Molecular Vision*, vol. 10, pp. 956–963, 2004.

[13] V. Ilardi, *Renaissance vision from spectacles to telescopes*. American Philosophical Society, 2007.

[14] C. Letocha, "The invention and early manufacture of bifocals", *Survey of Ophthalmology*, vol. 35, no. 3, pp. 226–235, 1990.

[15] J. Herschel, "Light (1827), republished as section xii 'of the structures of the eye and of vision'", *Encyclopaedia Metropolitana*, vol. 4, pp. 396–404, 1845.

[16] R. Pearson, "Kalt, keratoconus, and the contact lens", *Optometry & Vision Science*, vol. 66, no. 9, pp. 643–646, Sep 1989.

[17] F. A.G.E., "Eine contactbrille", *Archiv für Augenheilkunde*, 1888.

[18] A. Müller, *Brillenglaser und Hornhautlinsen, Inaugural dissertation*. University of Kiel, 1889.

[19] R. Pearson and N. Efron, "Hundredth anniversary of august müller's dissertation on contact lenses", *Survery of Opthalmology*, vol. 34, no. 2, pp. 133–141, Sep 1989.

[20] A. Sabell, "Dr joseph dallos - an appreciation", *Contact Lens Journal*, vol. 8, pp. 16–18, 1979.

[21] History of the Cornea & Contact Lens Section , D.M. Kuwabara (22 Dec 2008), retrieved on the 18th of April 2013 from the American Academy of Optometry website. [Online]. Available: http://www.aaopt.org/content/docs/HISTORY%20OF%20THE%20SECTION%20ON%20CORNEA.doc.

[22] ACLM statistic on the British Contact Lens Association website, retrieved on the 18th of April 2013. [Online]. Available: http://www.bcla.org.uk/en/consumers/consumer-guide-to-contact-lenses/facts-and-stats-on-the-uk-len-market.cfm.

[23] Contact Lens Spectrum: Evolution of an Ocular Surface Prosthesis (2009), retrieved on the 10th of April 2013. [Online]. Available: http://www.clspectrum.com/articleviewer.aspx?articleid=103704.

[24] I. Györffy, "The history of the molded all-plastic lens", *British Journal of Physiological Optics*, vol. 21, p. 291, 1964.

[25] R. Berger, "Effect of contact lens motion on the oxygen tension distribution under the lens.", *Am J Optom Physiol Opt*, vol. 51, no. 7, pp. 441–456, 1974.

[26] O. Wichterle and D. Lim, "Hydrophilic gels for biological use", *Nature*, vol. 185, pp. 117–118, 1960.

[27] A. Gasson and J. Morris, *The Contact Lens Manual: A Practical Guide To Fitting, 4th edition*. Elsevier, 2010.

[28] C. Maldonado-Codina and N. Efron, "Hydrogel lenses – materials and manufacture: a review", *Optometry in Practice*, vol. 4, pp. 101–115, 2003.

[29] J. Schaeffer and J. Beiting, "The early history of contact lenses", in *Review of Optometry*, Jobson Medical Information, 2009.

[30] G. Smelszer and V. Ozanics, "Importance of atmospheric oxygen for maintenance of the optical properties of the human cornea", *Science*, vol. 115, p. 140, 1952.

[31] K. Polse and R. Mandell, "Critical oxygen tension at the corneal surface", *Archives of Ophthalmology*, vol. 84, pp. 505–508, 1970.

[32] Oxygen permeability of Menicon Z, retrieved on 1 May 2013. [Online]. Available: http://www.menicon.com/pro/gas-permeable/menicon-z-material/oxygen-permeability.

[33] C. Schnyder, "A primer on contact lens materials", in *Contact Lens Spectrum*, PentaVision, 2004.

[34] J. Nichols, "Contact lenses 2012 - annual report", in *Contact Lens Spectrum*, PentaVision, 2013.

[35] B. Holden and G. Mertz, "Critical oxygen levels to avoid corneal edema for daily and extended wear contact lenses", *Investigative ophthalmology & visual science*, vol. 25, no. 10, pp. 1161–1167, 1984.

[36] K. French, "Contact lens material properties, part 3: oxygen performance", *Optician*, vol. 230, no. 6030, pp. 16–21, 2005.

[37] I. Fatt and R. St Helen, "Oxygen tension under an oxygen permeable contact lens", *American Journal of Optometry*, vol. 48, no. 7, pp. 545–555, 1971.

[38] Wettability comparison of CibaVision's Air Optix Aqua contact lens with competitor's lenses, retrieved on 24th of May 2013. [Online]. Available: https://www.airoptix.com/ecp/aqua/AQUA_Wettability.shtml.

2 The Smart Contact Lens

"The only thing worse than being blind is having sight but no vision."

—Helen Keller

2.1 Early History

Regular, passive contact lenses have reached a mature state by now. From their inception in 1888, research efforts were focused on increasing their comfort, performance and ease of manufacturing, but their purpose rarely diverted to other applications than vision correction. However, after the second World War, when PMMA based lenses started to become popular (see section 1.2.2), a new use found its way into the lab. To the author's knowledge, the earliest documented use of a contact lens beyond vision correction was in 1950, when Ratliff & Riggs [1] integrated a small mirror in a scleral lens[1] which was then used to detect eye movement. This contact lens was in fact only a small part of an elaborate optical system (see Figure 2.1), but proved to be a significant improvement over existing methods at that time. In 1963, the first contact lens using an electrical component

[1] Although not explicitly mentioned the lens was likely made out of PMMA.

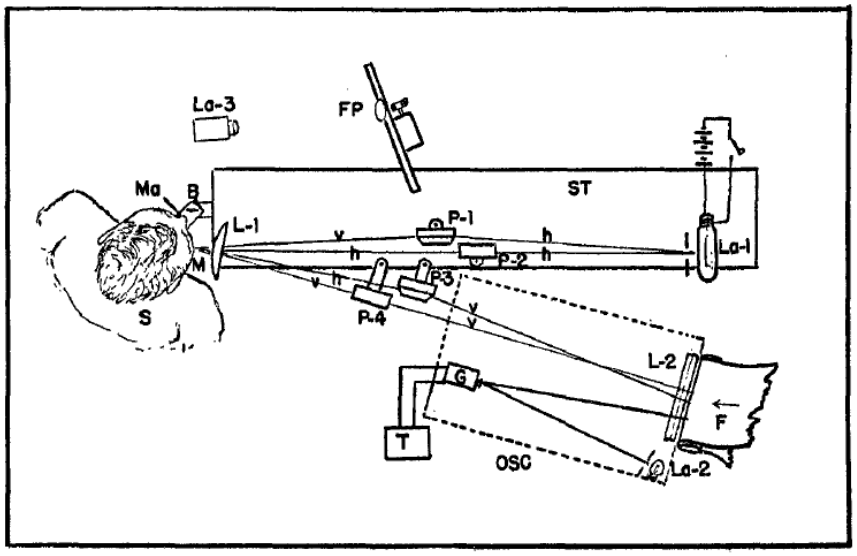

FIG. 2. Diagram of the recording apparatus. B: Biting board. F: Moving film. FP: Fixation point. G: Galvanometer. h and v: h indicates that image of the filament would be horizontal if the rays were brought to a focus at this point, v indicates that the image would be vertical. La-1: Source of light for the recording system. La-2: Oscillograph lamp. La-3: Microscope lamp. L-1: Main lens of recording system. L-2: Cylindrical camera lens. M: Mirror in contact lens. Ma: Mask covering left eye. OSC: Oscillograph. P-1 and P-3: Dove prisms rotated 45° from 'normal' position. P-2 and P-4: Dove prisms in 'normal' position. S: Subject. ST: Steel 'I' beam. T: Timing device.

Figure 2.1: Optical system used to detect eye movements in which M denotes a contact lens with an embedded mirror. Unfortunately, no detailed image is available. Image from [1].

was created by Robinson [2], who integrated an inductive coil in a contact lens again to record the eye's movement. The lens required a wired readout, but the crossover to electronics was made.

Notwithstanding this milestone already occurred 50 years ago, the ensuing decades only saw sporadic efforts in which adding new functionalities to contact lenses was investigated. For instance, a contact lens with an embedded liquid crystal cell was fabricated in 1973 to measure the corneal temperature [3] (see Figure 2.2). Due to the color dependent reflection of the embedded liquid crystal, a measure for the corneal temperature could thus be derived. In 1974, the first contact lens detecting intraocular pressure (IOP) was made [4], which triggered a

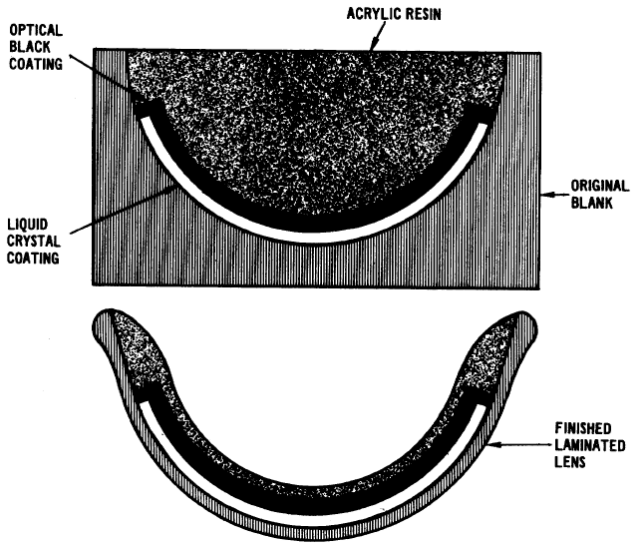

Figure 2.2: Contact lens with an embedded liquid crystal cell which measures the corneal temperature.

series of efforts by other researchers [5–7]. However, as can be seen in Figure 2.3, the state of technology at that time seemed to prevent a practical implementation. Apart from IOP, another interesting biomedical parameter to be scrutinized is glucose level. A patent by March [8] issued in 1976 suggested the use of a contact lens for monitoring the glucose level of the anterior chamber of the eye. By measuring the change in the polarization state originating from an embedded infrared laser after it crosses the anterior chamber, a measure for its glucose content can be derived. A follow-up research paper in 1982 [9] proved some principles but again, a full implementation seemed to be impossible at the time. The last noteworthy work before the turn of the century was the use of a contact lens attached to a fibre bundle which flooded the retina with both red and infrared light [10]. By carefully monitoring the reflected signal via the fibre bundle the possibility of performing pulse oximetry was investigated. However, the research seemed to have stopped after an initial study.

When analysing these pre-2000 studies one can conclude that researchers had primarily identified and used contact lenses as a new way of measuring biomedical parameters. This should come as no surprise as the eye actually reveals a lot

Figure 2.3: Complete set-up as used by Cooper et al. [7] in 1983 to detect IOP.

of information about our bodily functions and many related parameters can be measured at its surface. Since a contact lens can be unobtrusively placed on top of the eye, integrating sensors in the lens can provide for a convenient way to measure these parameters. Driven by this rationale, progress could indeed be made, but with varying success. In fact, none of these efforts resulted in a successful implementation beyond research prototyping. In retrospect, it seems the major limiting factor was a lack of adequate microfabrication technologies for constructing the micro-electronic components themselves and for successfully embedding them in a contact lens. Also the supporting structures for empowering and reading out such an electronic contact lens seemed rather bulky. However,

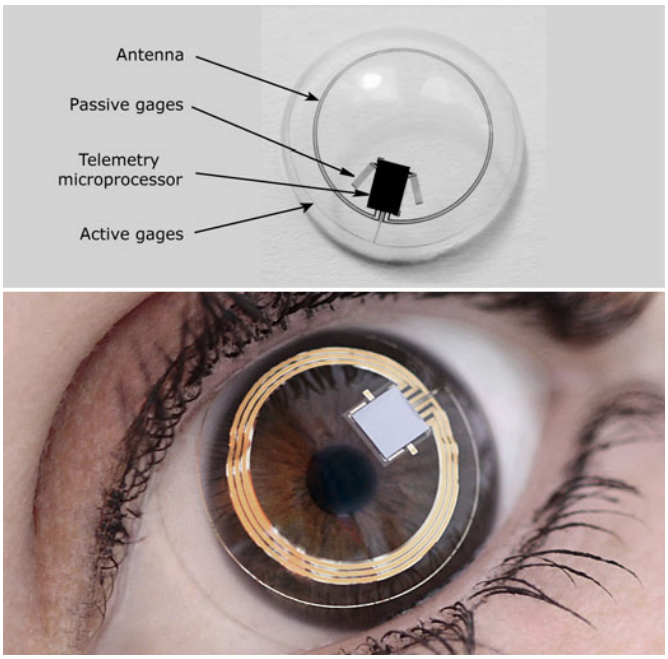

Figure 2.4: The Triggerfish by Sensimed, being a contact lens with resistive strain gauges, a telemetry microprocessor and an antenna. The lens measures and transmits the cornea's radius from which the IOP can be derived. Image from [11, 12]

around 2000 these technologies appeared to have caught up with the ideas and designs of several researchers and a new upsurge in electronic contact lens studies has since been seen.

2.2 Recent progress

2.2.1 Biomedical Sensing

IOP Sensing

After 2000, a continuation of contact lens research for biomedical monitoring can be seen, with the two most important parameters being IOP and glucose level. IOP is the fluid pressure inside the eye's anterior and posterior chambers (see Figure 1.2) and should be sufficiently large to maintain the spherical shape of the cornea. However, elevated IOP is the only biomedical parameter that can be

used to monitor glaucoma, the world's leading cause of irreversible blindness [13]. Glaucoma is a ophthalmic pathology in which the optic nerve sustains some damage and the accompanied progressive loss of visual acuity can eventually lead to total loss of vision. Since elevated IOP is the only risk factor associated with glaucoma, measuring it accurately and continuously is important to detect and potentially stop the disease from progressing. Although IOP measurement devices have been made for use in clinics and private practices, they do not allow for a practical continuous measurement over an extended period of time (e.g. 24 hours). As mentioned above, attempts have been made earlier to integrate an IOP sensor in a contact lens, as such a lens resides directly on top of the cornea and a relationship exists between IOP and the cornea's radius. Only the more recent work of Leonardi et al. [11, 14] and subsequent studies [15] resulted in a practical implementation, which combined resistive strain gauges, a telemetry microprocessor and an antenna (see Figure 2.4). A secondary coil is used to transmit energy (using a 27 MHz electromagnetic wave) to the telemetry microprocessor, as well as reading out the measured value of the strain gauges being transmitted by this microprocessor. 10 measurements are made per second and logged over a period of 24 hours by a mobile device that is worn by the patient. This technology is currently being commercialized by the Swiss company Sensimed [12], but recently the French start-up Ophtimalia [12] disclosed they are working on a competing technology based on LC-resonance, which would not require the integration of a microprocessor.

Blood Glucose Sensing

Blood glucose level is an important parameter for monitoring diabetes, a disease in which a deficiency concerning the insulin hormone prohibits the removal of excessive glucose from the blood [17]. A chronically raised blood glucose concentration is a major risk factor for microvascular complications such as atherosclerosis, coronary artery disease, stroke, and peripheral vascular disease and should thus be treated with care [18]. Although mobile 'finger prick'-tests to measure blood glucose level are prevalent today, they only provide measurements at discrete intervals and require an invasive action (albeit small). A non-invasive, continuous measurement method would therefore be beneficial and one of the potential ways would be measuring the glucose level of tears, which has a direct relationship with the glucose level of blood [19]. Despite some reports prior to 2000, detailed results involving the use of a contact lens as a measurement tool were only reported by March et al. [20] in 2004. In this work, a fluorescent

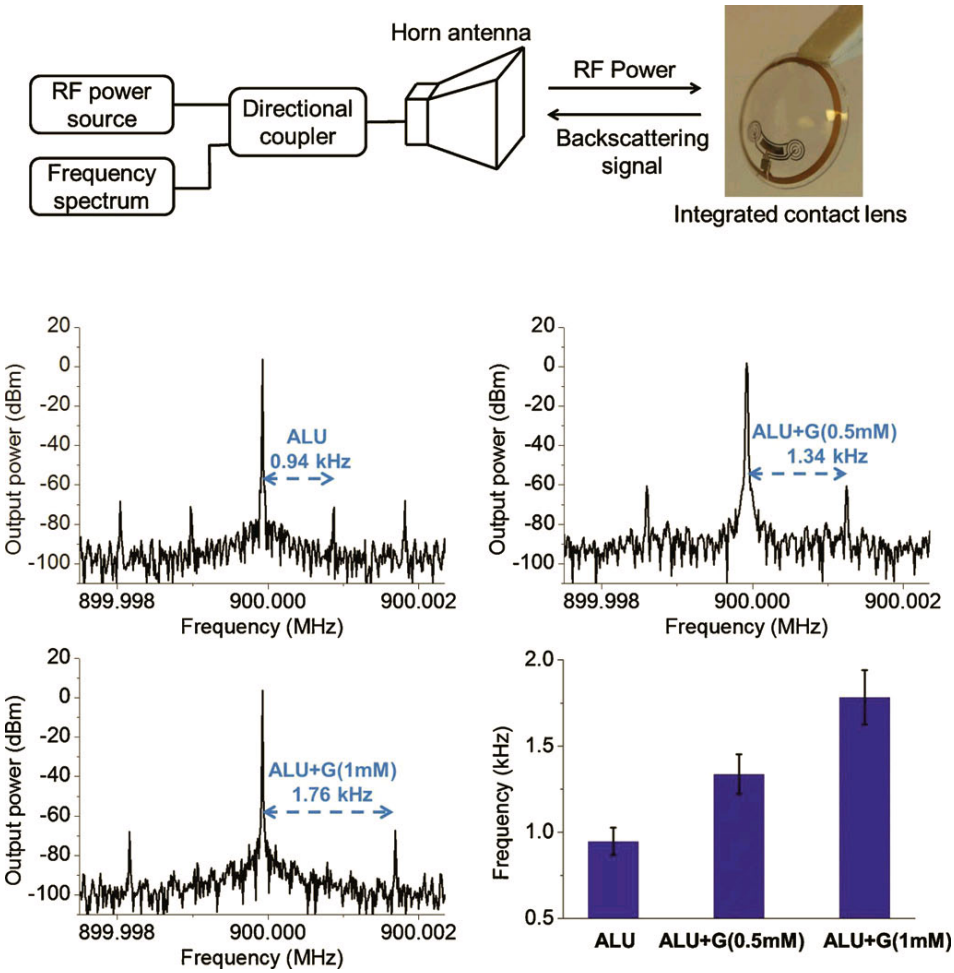

Figure 2.5: The prototype of Yao et al. containing a glucose sensor, an antenna and a communication chip which was powered by an RF-carrier wave. A frequency shifted signal from the carrier wave denotes the measured glucose level. Image from [16]

molecule was mixed in the contact lens material, which's response was dependent on the tear glucose level. By looking at the response signal invoked by an LED, a measure for the tear (and thus blood) glucose level could be derived. Despite some initial promising results, no follow-up study could be found, indicating the method probably had some severe deficiencies. Another approach is based on

an enzyme-based electrochemical reaction from which the glucose level can be derived by a potentiostat. Yao et al. [21] first showed a wired proof-of-concept demonstrator in which a sensor based on glucose oxidase was fabricated on top of a curved PET (polyethylene terephthalate) surface. In an ensuing paper [16], a fully integrated contact lens was made that contained both the sensor, an antenna and a communication chip (see Figure 2.5). The chip converted incoming radio frequency wave power to usable DC power for the sensor read-out circuit and transmitted back the sensor value by sending out a frequency deviation from the carrier wave (900 MHz). Although this is already an impressive effort, issues such as stability of the sensor over time and temperature hamper direct implementation for in-vivo studies on humans. Furthermore, other research using a similar sensor on rabbits [18] indicate a lag time of about ten minutes exists between blood glucose level and tear glucose level, which might be too long when aiming to counter dangerous glucose peaks or lows.

2.2.2 Contact Lens Display - Augmented Reality

Next to biomedical sensing, a more thought provoking and technologically challenging idea is a contact lens display for augmented reality (AR) applications. With augmented reality, a superimposed view containing virtual objects such as text and images allows a person to increase the interaction between the real world and the virtual world (also comprising all information available through the internet). A recent overview of the concept and different implementations was given by van Krevelen et al. [23], but AR generally requires a projecting display integrated in a device resembling common glasses. However, most implementations are not lightweight and might be too distracting in e.g. emergency situations faced by fire fighters or paramedics. One possible way of overcoming these hurdles is bringing the display even closer to the eye and integrating it into a contact lens. Such a contact lens display aims for a bigger coalescence of the man-machine interface and would pursue an enhancement of the real view, rather than feeling as just an add-on.

Most likely, the idea of a contact lens display has been thought of several times in the last few decades but, to the author's knowledge, the earliest documented report is in a patent application published in 1997 [24]. However, seeing that the patent application is superficially formulated and does not address several problems immediately coming to mind, it likely was just an idea not backed up by any real technological research. The possibility of a contact lens display was restated in 2008 by Ho et al. [25], who integrated microLEDs on a spherically

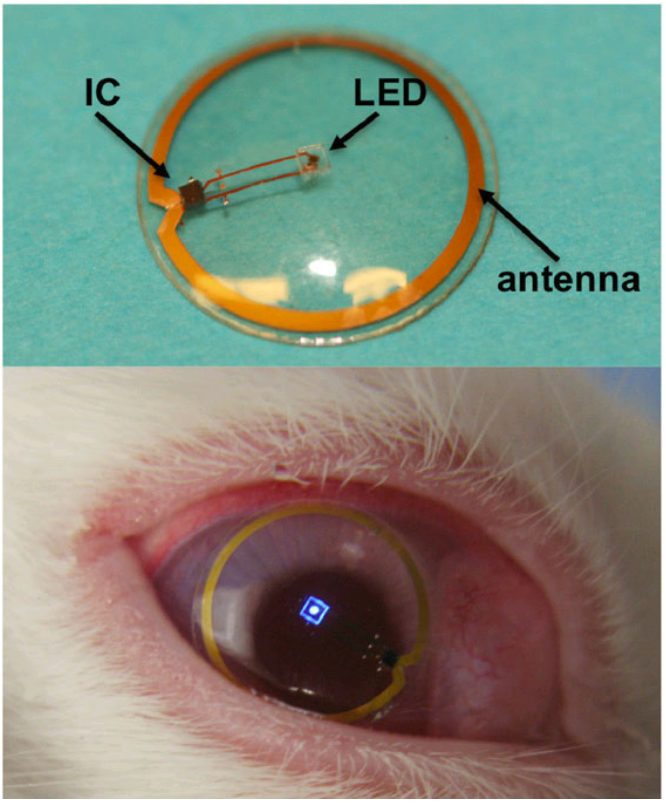

Figure 2.6: A wirelessly powered contact lens with a single embedded microLED, serving as a first step towards a contact lens display. Image from [22]

conformed PET surface with a self-assembly process. This article was followed by a more broad exploratory paper [26] written by the senior researcher, Babak Parviz, who stated the obvious requirements such as biocompatibility, successful microfabrication techniques and autonomy, but also the need for special optics to create a fully focused image on the retina. The latter requirement is a direct result of the eye not being able to focus on an object located so close to it. Ensuing efforts revealed a wirelessly powered microLED on top of a spherically conformed PET surface together with initial attempts to solve the focussing problem by integrated micro-Fresnel lenses [22, 27]. Since this research group also investigated the wireless glucose sensors in the previous section, a similar approach was used in which RF power was converted with a small chip to power the LED (See Figure

2.6). In a separate research track, the possibility of using inorganic solar cells for powering was also investigated [28].

Clearly, despite these initial results, a contact lens display for augmented reality applications will still require vast amounts of research. However, seeing the overlap in the needed supporting technologies with for instance the biomedical applications, it can serve as a long term driver whilst the more short term applications are developed en route.

2.3 The Smart Contact Lens

2.3.1 Definition

Obviously, the momentum by which the crossover between electronics and contact lenses is being made is increasing and this has prompted people to sometimes refer to them as 'smart' contact lenses. Although this generally means that some new functionality has been added beyond passive vision correction, no clear definition has been given yet to such lenses, so it might be useful to do so. An abstract, high level definition of a smart contact lens could be:

*'A **smart** contact lens is a contact lens which **actively** addresses a complex problem.'*

The keywords in this definition highlight that the lens should **actively** solve a problem. Indeed, conventional contact lenses are passive devices requiring no additional energy to function properly. However, the word active can be ambiguous when not described properly. Looking from an electronics perspective, although passive components do play a role, it is the presence of active components the lenses primarily derive their functionality from. Hence, a more specific definition is:

*'A **smart** contact lens is a contact lens that uses **active electronic components** to address a complex problem.'*

Of course, it is easy to lose oneself in semantics and even the latter definition has some drawbacks, but at this point in time it provides a fairly accurate description of what smart contact lenses are about. Anyway, a revision of this definition can be made in due time.

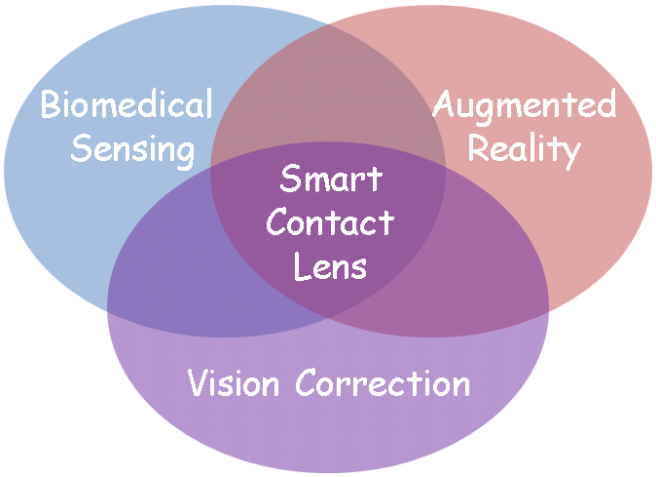

Figure 2.7: Application domains for smart contact lenses. Next to augmented reality and biomedical sensing, a large opportunity is seen in active vision correction such as an artificial iris for deficient irises and multifocal contact lenses for presbyopic patients.

2.3.2 Extending the Current Application Domains

The application domains of smart contact lenses are summarized in Figure 2.7, and have up till now been mainly constituted by biomedical sensing and augmented reality. While the added value of augmented reality is less clear at this point and certainly needs much more research, the opportunities for biomedical sensing are more obvious and are likely to expand in the coming years.

Strangely, it appears one large application domain has not been investigated yet, namely vision correction. Conventional contact lenses were specifically developed to correct ophthalmic disorders such as myopia and hyperopia, but the question emerges where smart contact lenses can outperform them in terms of vision correction. The most obvious answer is presbyopia, the disorder in which the active intraocular lens is becoming too stiff to perform its near focussing activities. Currently, presbyopia is corrected by passive solutions such as multifocal glasses or multifocal contact lenses. As mentioned in section 1.1.3, people wearing multifocal glasses have to select their desired focal distance by looking through specific parts of the glasses, which requires a significant adaptation time. Even then, undesired situations can occur such as walking down stairs with a blurred vision, as having a downwards gaze means looking through the part for

near (reading) distances. An equivalent principle has been developed for contact lenses, in which a translating movement of the lens when looking downwards results in looking through a section with a different focal length (see Figure 2.8). These translating lenses are, however, generally only bifocal and may not perform equally well for intermediate distances. Other multifocal contact lens designs use either concentric rings with alternating focal distances, aspheric designs in which the focal distance gradually changes according to the radial distance or a combination of both [29]. Although the non-translating lenses perform better across all distances, the simultaneous projection of the images coming from these multiple focal distances requires a significant adaptation, while they also result in a reduced contrast. The basic problem of multifocal glasses and contact lenses is that they are passive lenses used to correct a defective active lens, which thus will never result in an ideal solution. Therefore, a smart contact lens that can actively switch its focus would likely be a superior solution for presbyopia.

A less obvious application in the domain of vision correction is a smart lens as an artificial iris. The iris regulates the amount of light entering the eye and people having a defective iris due to trauma (e.g. iris perforation, or coloboma) or a congenital disease like aniridia [30] (in which the iris is wholly absent, see Figure 2.9) are very sensitive to light. Current solutions such as shown in Figure 2.9, are static iris implants or painted contact lenses, but due to their static nature they are only well adapted for a narrow brightness range. A full overview concerning iris deficiencies and their solutions can be found in a master dissertation which was made in the context of this research [31]. A smart contact lens with a tunable transparency could actively regulate the light transmission to the retina, achieving a vision correction that will most likely outperform the current solutions.

2.4 Introducing Non-Emitting Electro-Optic Technology to Smart Contact Lenses

As stated in the prelude, the initial idea seeding this research was to put a display in a contact lens, which was conceived independently from e.g. the recent work from the Parviz group. Of course, it was quickly realized that a fully autonomous smart contact lens providing an additional view on top of your normal view is far beyond what is feasible within a PhD - and even beyond multiple PhDs - given the current state-of-the-art. After an initial round-up of existing research and the identification of potential future applications in the domain of active vision correction, a clear starting point was found: the development of a basic

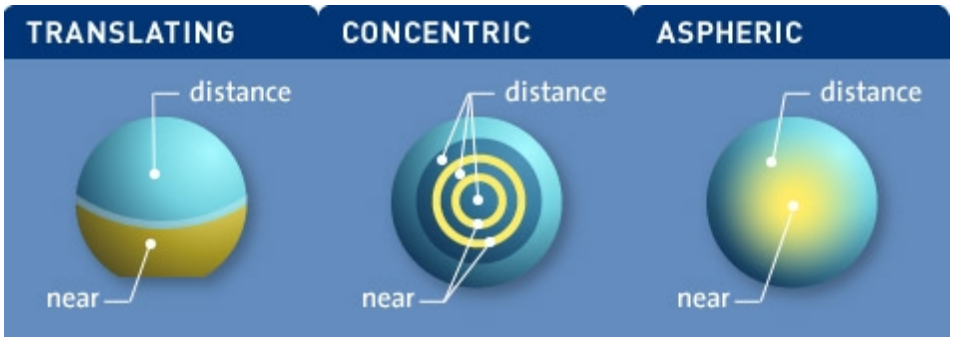

Figure 2.8: The different types of multifocal contact lenses. Image from [32]

non-emitting electro-optic technology which could be integrated into a contact lens.

Indeed, in contrast with the microLEDs from the Parviz group, an electro-optic element capable of modulating incoming light, rather than emitting new light, could be used in multiple ways. Next to their intrinsically lower power consumption, the number of pixels and their surface area can easily be changed by the patterning process of the conductive layer present in many of these electro-optic elements. This versatility allows the development of applications with a broad range of pixel counts and sizes. Once established, this technology could be altered to for instance serve as a display technology for AR applications, modulate the incoming light to act as an artificial iris or provide a solution to presbyopia by adding some multifocal functionality to the lens.

Obviously, this immediately raises the question of which electro-optic technology should be used. For this purpose, a list of desired properties was made:

- **Transparent off state**, since in case of malfunction the user's view should not be obstructed
- **High contrast**, for a sufficient optical performance
- **Fast switching time**, depending on the application this might vary between 1 and 100 ms
- **Low power consumption**, as some estimates indicate only about 20 µW will be available on the lens when using e.g. RF-power [37]
- **Low voltage**, both in terms of energy consumption as eye safety

Figure 2.9: Iris deficiencies could be a target for smart contact lenses. Top Left: Iris coloboma in which a part of the iris is missing. Top Right: person with congenital aniridia, lacking the whole iris. Bottom Left: Iris implants constitute a permanent but static solution for iris deficiencies. Bottom Right: contact lenses with a tinted ring form a non-permanent but again static solution. Images from [33–36]

- **Low thickness**, preferably below the thickness of a standard contact lens (140 µm)

Table 2.1 compares these requirements between the most feasible non-emitting displays technologies such as Liquid Crystal Displays (LCD), electrochromic displays (ECD), electrowetting displays (EWD) and electrokinetic displays (EKD). The values in this list are more or less tentative, as many of these technologies are still under development and are likely to improve. In this list LCD technology is the most mature and is currently also the dominant display technology on the market. When comparing these technologies one can see electrochromic displays have a low contrast and poor switching time, while electrowetting display require a high driving voltage and a rather thick cell. Electrokinetic displays have a poor switching time and also require a rather thick cell. Liquid crystal displays generally have similar or better values for all properties and it was thus decided

Table 2.1: Comparison of display technologies

	LCD	ECD	EWD	EKD
Transparent off state	yes	yes	yes	yes
Contrast ratio	1000:1	5:1	10-15:1	30:1
Switching time (msec)	<10	100-1000	3-10	500
Power consumption ($\mu W/cm^2$)	0.1-1	1-10	4-5	1
Driving voltage (V)	5-10	0.25-20	20-25	5
Thickness (µm, excluding substrates)	1-10	~5	25	20

to focus on this technology. Interestingly, most alternatives are also cell based technologies[2] and therefore, should any particular application nonetheless require one of these alternatives, some of the results are likely reusable.

Also noteworthy is the considerable amount of research which has been carried out concerning tunable liquid crystal lenses. A variety of configurations is available in which small liquid crystal based lenses can switch focus by applying an electrical field. Hence, once the basic technology has been established, specific research aiming for a liquid crystal based multifocal contact lens could draw significant prior knowledge from existing work.

2.5 Introduction to Liquid Crystals and LCD Technology

Before stating the objectives of this work, it is necessary to introduce liquid crystals and their implementation in displays. Liquid crystals exhibit special phase transitions beyond the classical solid-liquid-gas transitions and were first discovered by Reinitzer [38] in 1888[3]. A vast amount of scientific research has been performed concerning liquid crystals, leading to many technological successes. Since a broad review is beyond the scope of this work, we refer to the excellent overviews that have been made by Yang & Wu [39] and Lueder [40] for a more thorough introduction.

[2] A cell based technology generally comprises a sandwich of two solid substrates separated by a fixed distance filled with a liquid.

[3] Coincidentally, the same year the first contact lenses were made.

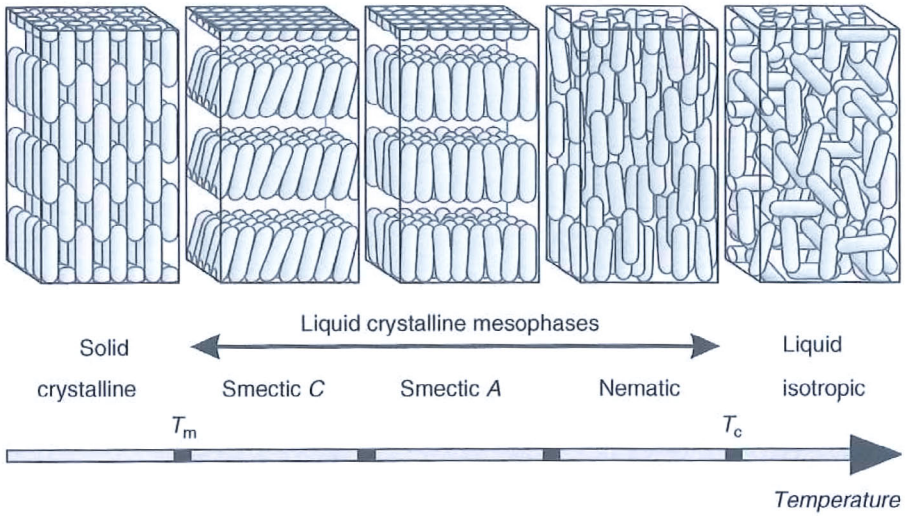

Figure 2.10: LC molecules (calamitic molecules are shown here) go through a series of phase transitions when heated from their solid state to their isotropic liquid state. Image from [40]

2.5.1 Liquid crystals

Liquid crystal molecules and phases

Liquid crystal molecules are anisotropically shaped molecules which generally have a rod-like composition (calamitic LCs), but disc-like (discotic LCs) and lath-like (sanidic LCs) also exist. A vector can be appointed to the direction of the long axis of such a molecule and is called the *director*. As illustrated in Figure 2.10, LCs differ from classical materials because, rather than exhibiting one phase transition between the solid and the liquid state, they go through a series of phases when heated from the solid state to the isotropic liquid state, in which the orientational and positional order of the molecules decreases stepwise. Smectic C is generally the first liquid phase emerging after the solid crystalline phase and is characterized by, despite its liquid state, a large ordering of the molecules in different planes. In each plane the mean orientation of the director is tilted away from the perpendicular orientation of the planes. In the smectic A phase this tilt disappears, but the planar ordering remains. The nematic phase is translational invariant with the director still having a preferred orientation and is the most

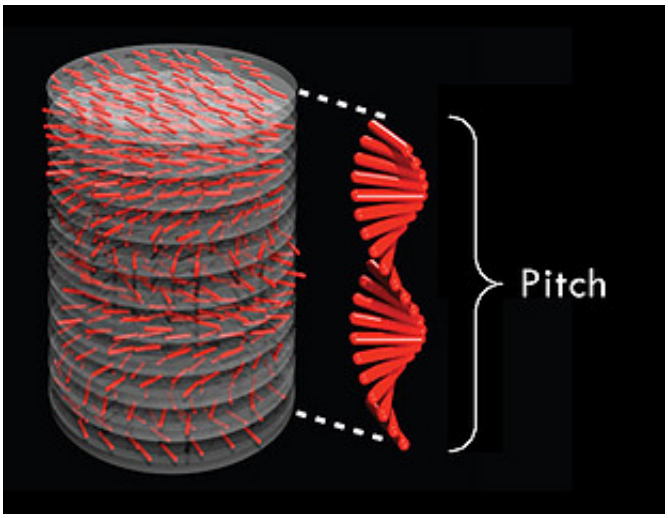

Figure 2.11: A chiral nematic liquid crystal exhibits a helical twist and is characterized by a pitch p, denoting the distance over which a 360° turn is established. Image from [41].

widely known and used phase. Finally, in the isotropic state the thermal energy of the molecules is so high the anisotropy does not manifest itself any more. Another interesting effect is observed when chiral compounds are present in the liquid crystal mixture. In the nematic phase the director then exhibits a helical twist, which is characterized by a pitch p, denoting the distance over which a 360° turn is established (see Figure 2.11).

Properties

The anisotropy in the shape of LC molecules also translates to anisotropy in their material properties. The relative dielectric constant is a tensor, which for rod-shaped molecules is as follows when the director is aligned according to the z-axis:

$$\bar{\bar{\varepsilon}} = \begin{bmatrix} \varepsilon_{\perp} & 0 & 0 \\ 0 & \varepsilon_{\perp} & 0 \\ 0 & 0 & \varepsilon_{||} \end{bmatrix} \tag{2.1}$$

The uniaxial dielectric anisotropy thus can be defined as:

$$\triangle\varepsilon = \varepsilon_{||} - \varepsilon_{\perp} \tag{2.2}$$

Liquid crystals with $\triangle\varepsilon$ >0 are called positive dielectric LCs and those with $\triangle\varepsilon$ <0 negative dielectric LCs. When the molecules are subjected to an external electrical field, they align themselves in such a way that the orientation with the largest dielectric value becomes parallel with the field. This means that in positive dielectric LCs the director aligns parallel to the electric field, while in negative dielectric LCs the director aligns perpendicular to the electric field.

For the refractive index a similar anisotropy holds true and (director aligned according to the z-axis):

$$\bar{\bar{n}} = \begin{bmatrix} n_{\perp} & 0 & 0 \\ 0 & n\perp & 0 \\ 0 & 0 & n_{||} \end{bmatrix} \tag{2.3}$$

The optical anisotropy is defined as:

$$\triangle n = n_{||} - n_{\perp} \tag{2.4}$$

LCs are thus birefringent. For optical frequencies the dielectric anisotropy and the optical anisotropy are related through:

$$\varepsilon_{||} = {n_{||}}^2 \tag{2.5}$$

$$\varepsilon_{\perp} = {n_{\perp}}^2 \tag{2.6}$$

$$\triangle\varepsilon = {n_{||}}^2 - {n_{\perp}}^2 \tag{2.7}$$

Due to the optical anisotropy, the polarization of light propagating through the liquid crystal may change. This is because the speed of light depends on the refractive index and thus varies according to the orientation of the electric field vector with the molecules. When this vector is parallel with the long axis of the molecules the speed becomes:

$$v_{||} = c/n_{||} \tag{2.8}$$

with c the speed of light in vacuum. In the case of perpendicular incidence on the molecules it becomes:

$$v_{\perp} = c/n_{\perp} \tag{2.9}$$

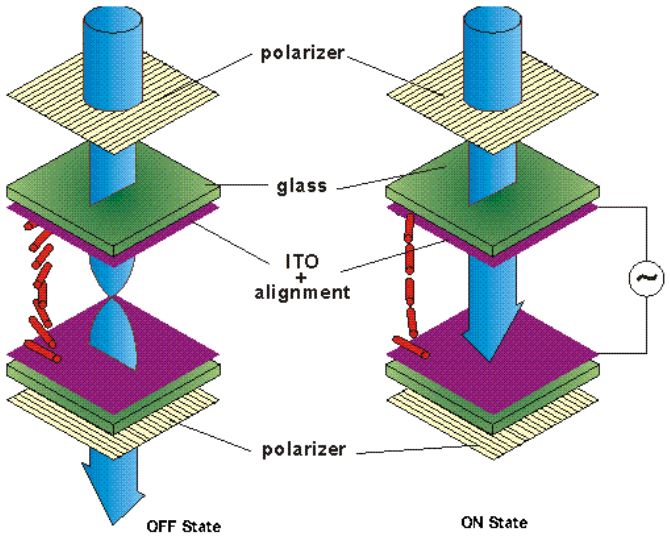

Figure 2.12: Working principle of a twisted nematic LCD. Left: When no voltage is applied the linearly polarized state is twisted over a 90° angle and goes through the second polarizer unchanged. Right: When a voltage is applied, the light only experiences the LC molecules' perpendicular refractive index and the polarization state is unaffected, meaning the light will be fully absorbed by the second polarizer.

Since any polarization state can be decomposed into base vectors along these directions, the phase difference between these becomes a function of distance and leads to a changing polarization state.

2.5.2 Liquid Crystal Displays

Liquid crystals' main properties, birefringence and reorientation under an external electric field, make them an interesting and versatile tool to fabricate electro-optic actuators, of which the most famous one is of course the Liquid Crystal Display. Although a plethora of LC modes and configurations has been used in LCDs we will only highlight the classic, most widely used configuration, the Twisted Nematic LCD, and a variant which is relevant for this work, the Guest-Host LCD.

Twisted Nematic LCD

The basic configuration of a twisted nematic (TN) LCD involves two transparent substrates (usually glass) which form a cell in between which the LC is put. At the inner sides of the substrates a transparent conductive layer resides (usually an Indium Tin Oxide (ITO) layer) which can act as a capacitor when a voltage is applied across these layers. On top of the ITO an alignment layer is applied, providing a boundary condition for the LC molecules and forcing the molecules at the interface in a particular orientation. For a TN LCD a planar alignment is used at both sides of the cell, but they are placed under a 90° angle, resulting in a gradually changing twist of 90° for the LC molecules (having a positive dielectric anisotropy). Configurations with larger angles exist, but they require the addition of a chiral dopant, which is not needed here if the cell is sufficiently thin. Two polarizers are also attached to the outer sides of the cell, in the same direction as the alignment layers. When unpolarized light hits the cell, it thus gets linearly polarized before entering the LC layer.

In the case no voltage is applied, the light's linearly polarized state is altered when propagating through the liquid crystal and the cell is tuned in such a way that a new linearly polarized state twisted over a 90° angle is formed when it exits the liquid crystal layer. Contrary to how this is frequently pictured (see Figure 2.12), the linearly polarized light does not just turn along with the LC director, as this is only true for thick TN LCD cells (the so-called Mauguin regime). In most cases the light goes through a series of elliptic and circular polarization states before forming a new linearly polarized state rotated over a 90° angle, which does require careful tuning of the LCD's parameters. Nevertheless, when the light exits the cell it propagates unaffected through the second polarizer (being parallel with it) and the display appears bright.

In case a sufficiently high voltage is applied, the LC molecules reorient themselves parallel with the electric field. In this orientation the linearly polarized light entering the LC layer only experiences one refractive index ($n_\perp$) and the polarization state thus remains unaffected throughout the whole layer. This means the light gets absorbed fully by the second polarizer and the display appears dark. Intermediate grey levels can be achieved by using lower voltages as the LC molecules will then not reorient themselves completely and not all light will be absorbed.

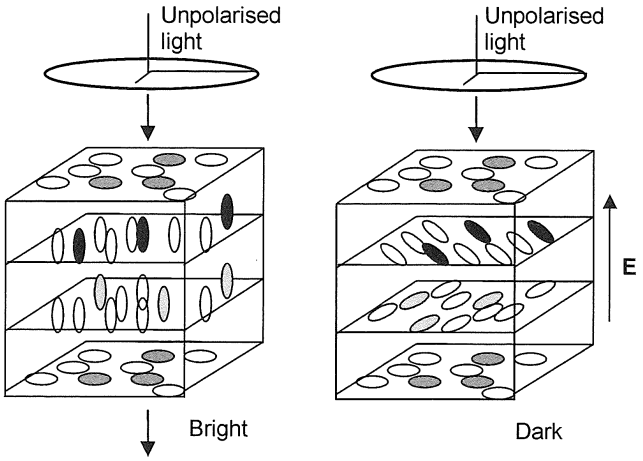

Figure 2.13: Working principle of a White Taylor Guest-Host LCD using a negative dielectric LC. Left: a bright voltage off state is created since all dye molecules are oriented perpendicularly to the electric field vectors of the incoming unpolarized light. Right: a dark voltage on state is created as the helix unwinds and the dye molecules' long axis is oriented towards the electric field vectors of the incoming unpolarized light.

Guest-Host LCD

Although most LCDs use polarizers, some polarizer-free variants also exist. Guest-Host LCD is such a variant and is based on voltage dependent light absorption [42]. In a Guest-Host LCD, a non-absorbing LC host is mixed with an anisotropically absorbing guest dye (about 1-5% dye). These dichroic dye molecules are generally rod-like molecules and their absorption depends on the polarization of the incoming light. When the polarization is parallel with the molecules' long axis it has a higher absorption than when it is aligned perpendicular to this axis. Since they align themselves with the LC molecules an electrically tunable absorption effect can be created.

Even within Guest-Host LCDs there exist many configurations, but one of the most commonly employed is the White-Taylor cell [43] (see Figure 2.13), which can be made with both positive as negative dielectric LCs [44]. In the White-Taylor cell a chiral nematic liquid crystal mixture is mixed with a dye and inserted in a LCD cell without polarizers. When using a negative dielectric LC and a homeotropic alignment (LC molecules perpendicularly oriented at the substrate

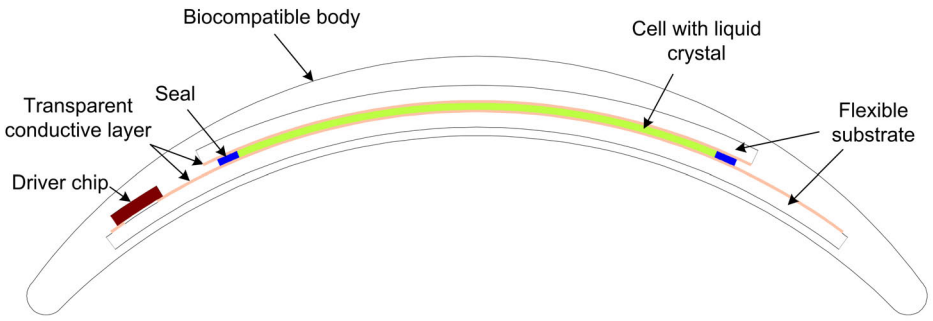

Figure 2.14: The envisioned smart contact lens with active electro-optical capabilities

interface), a bright voltage off state is created since all dye molecules are oriented perpendicularly to the electric field vectors of the incoming unpolarized light. When a voltage is applied, the LC molecules start to tilt and the helix starts to unwind, orienting the dye molecules' long axis towards the electric field vectors and thereby increasing the absorption. The total twist angle is determined by the concentration of the chiral dopant and the cell gap, but generally lies between 0° and 240°. With a 0° angle only half of the light can be absorbed since one polarization state will propagate through the cell (almost) unhampered, thus leading to a maximum contrast of 2:1. With an increasing twist angle more states will be absorbed and the total contrast will increase. However, no contrast larger than 10:1 is generally achieved.

2.6 Objectives of this Work

As mentioned above, this work strives to introduce a non-emitting electro-optic technology to smart contact lenses. After an initial survey of existing display technologies, we found that LCD technology provides the best fit with the desired properties for integration into a contact lens (see section 2.4). However, it was recognized from early on that conventional polarizers are generally too thick for contact lens embedding (most polarizers are thicker than 120 µm), suggesting a polarizer-free LCD technology should be investigated first. Since other polarizers-free modes using cholesteric liquid crystals or polymer dispersed liquid crystals are wavelength dependent and/or exhibit a scattering state [45], guest-host liquid crystal displays are deemed to be the best choice. This choice is still complemen-

tary with future research concerning the integration of polarizers and in fact, in Chapter 5 we explore the possibilities to improve the display characteristics by including polarizers anyway.

The goal of embedding guest-host LCD technology in a contact lens thus means a cell with liquid crystal should be made that is sufficiently thin and can fit in the spherical outline of a contact lens. The main objective of this work is therefore to **set up a fabrication process** to create a **thin, spherically conformed LC cell**. The cell itself should be made from flexible substrates as it will need to maintain a certain flexibility after embedding in the contact lens. Next to this, the **layers needed to align and switch the liquid crystals in a patterned way** will have to be incorporated. Once the fabrication process has been established, the cell's **basic properties will be characterized** and **potential applications can be explored**. This objective is part of a long term strategy where the LC cell can be combined with other electronic components (such as for instance a driver chip) after which the whole electronic core is embedded in a biocompatible body, thereby constituting a smart contact lens with active electro-optical capabilities. An example of such an envisioned smart lens is illustrated in Figure 2.14.

References

[1] F. Ratliff and L. Riggs, "Involuntary motions of the eye during monocular fixation", *Journal of Experimental Psychology*, vol. 40, no. 6, pp. 687–701, 1950.

[2] D. Robinson, "A method of measuring eye movemnent using a scieral search coil in a magnetic field", *IEEE Transactions on Bio-Medical Electronics*, vol. 10, no. 4, pp. 137–145, 1963.

[3] J. Kinn and R. Tell, "A liquid-crystal contact-lens device for measurement of corneal temperature", *IEEE Transactions on Biomedical Engineering*, vol. 20, no. 5, pp. 387–388, 1973.

[4] M. Greene and B. Gilman, "Intraocular pressure measurement with instrumented contact lenses", *Investigative Ophthalmology*, vol. 13, no. 4, pp. 299–302, 1974.

[5] R. Cooper and D. Beale, "Radio telemetry of intraocular pressure in vitro", *Investigative Ophthalmology & Visual Science*, vol. 16, no. 3, pp. 168–171, 1977.

[6] R. Cooper and D. Beale, "Passive radiotelemetry of intraocular pressure in vivo: calibration and validation of continual scleral guard-ring applanation transensors in the dog and rabbit", *Investigative Ophthalmology & Visual Science*, vol. 18, no. 9, pp. 930–938, 1979.

[7] R. Cooper, G. Grose, P. Wasser, and I. Constable, "Progress in continual eye pressure monitoring", *Australian Journal of Ophthalmology*, vol. 11, no. 3, pp. 143–148, 1983.

[8] W. March, *Us patent 3,958,560: non-invasive automatic glucose sensor system*, 1975.

[9] B. Rabinovitch, W. March, and A. R.L., "Noninvasive glucose monitoring of the aqueous humor of the eye: part i & ii", *Diabetes Care*, vol. 5, no. 3, pp. 254–265, 1982.

[10] V. Scott, L. Tarassenko, C. Glynn, and A. Hill, "Contact lens pulse oximetry : a valid concept?", *IEE Colloquium on Pulse Oximetry: A Critical Appraisal*, pp. 3/1–3/3, 1996.

[11] M. Leonardi, E. Pitchon, A. Bertsch, P. Renaud, and A. Mermoud, "Wireless contact lens sensor for intraocular pressure monitoring: assessment on enucleated pig eyes", *Acta Ophtalmologica*, vol. 87, pp. 433–437, 2009.

[12] Sensimed's Triggerfish continuously monitors intraocular pressure. [Online]. Available: http://www.sensimed.ch.

[13] R. Casson, G. Chidlow, J. Wood, J. Crowston, and I. Goldberg, "Definition of glaucoma: clinical and experimental concepts", *Clinical & Experimental Ophthalmology*, vol. 40, 341–349, 2012.

[14] M. Leonardi, P. Leuenberger, D. Bertrand, A. Bertsch, and P. Renaud, "First steps toward noninvasive intraocular pressure monitoring with a sensing contact lens", *Investigative Ophthalmology & Visual Science*, vol. 45, no. 9, pp. 3113–3117, 2004.

[15] K. Mansouri and T. Shaarawy, "Continuous intraocular pressure monitoring with a wireless ocular telemetry sensor: initial clinical experience in patients with open angle glaucoma", *British Journal of Ophthalmology*, vol. 95, pp. 627–629, 2011.

[16] H. Yao, Y. Liao, A. Lingley, A. Afanasiev, I. Lähdesmäki, B. Otis, and B. Parviz, "A contact lens with integrated telecommunication circuit and sensors for wireless and continuous tear glucose monitoring", *Journal of Micromechanics and Microengineering*, vol. 22, no. 7, p. 075 007, 2012.

[17] *Greenspan's Basic & Clinical Endocrinology, 9th edition*. McGraw-Hill Companies, 2011.

[18] M. X. Chu, K. Miyajima, D. Takahashi, T. Arakawa, K. Sano, S.-i. Sawada, H. Kudo, Y. Iwasaki, K. Akiyoshi, M. Mochizuki, and K. Mitsubayashi, "Soft contact lens biosensor for in situ monitoring of tear glucose as non-invasive blood sugar assessment", *Talanta*, vol. 83, no. 3, pp. 960–965, 2011.

[19] A. Gasset, L. Braverman, M. Fleming, R. Arky, and B. Alter, "Tear glucose detection of hyperglycemia", *American Journal of Ophthalmology*, vol. 65, no. 3, pp. 414–420, 1968.

[20] W. March, A. Mueller, and P. Herbrechtsmeier, "Clinical trial of a noninvasive contact lens glucose sensor", *Diabetes technology & therapeutics*, vol. 6, no. 6, pp. 782–789, 2004.

[21] H. Yao, A. J. Shum, M. Cowan, I. Lähdesmäki, and B. A. Parviz, "A contact lens with embedded sensor for monitoring tear glucose level", *Biosensors and Bioelectronics*, vol. 26, no. 7, pp. 3290–296, 2011.

[22] A. Lingley, M. Ali, Y. Liao, R. Mirjalili, M. Klonner, M. Sopanen, S. Suihkonen, T. Shen, B. Otis, H. Lipsanen, and B. Parviz, "A single-pixel wireless contact lens display", *Journal of Micromechanics and Microengineering*, vol. 21, no. 12, p. 125 014, 2011.

[23] D. van Krevelen and R. Poelman, "A survey of augmented reality technologies, applications and limitations", *The International Journal of Virtual Reality*, vol. 9, no. 2, pp. 1–20, 2010.

[24] J. Weirich, *Us patent 5,682,210: eye contact lens video display system*, 1997.

[25] H. Ho, E. Saeedi, S. Kim, T. T. Shen, and B. Parviz, "Contact lens with integrated inorganic semiconductor devices", in *Micro Electro Mechanical Systems, 2008. MEMS 2008. IEEE 21st International Conference on*, 2008, pp. 403–406.

[26] B. Parviz, "Augmented reality in a contact lens", *IEEE spectrum*, vol. 9, pp. 1–4, 2009.

[27] J. Pandey, Y.-T. Liao, A. Lingley, R. Mirjalili, B. Parviz, and B. Otis, "A fully integrated rf-powered contact lens with a single element display", *Biomedical Circuits and Systems, IEEE Transactions on*, vol. 4, no. 6, pp. 454–461, 2010.

[28] A. Lingley, B. Otis, T. Shen, and B. Parviz, "A contact lens with integrated micro solar cells", *Microsystem technologies*, vol. 18, no. 4, pp. 453–458, 2012.

[29] A. Gasson and J. Morris, *The Contact Lens Manual: A Practical Guide To Fitting, 4th edition*. Elsevier, 2010.

[30] H. Hingorani and A. Moore, Aniridia, GeneReviews, May 2003, retrieved on 31st of October 2013. [Online]. Available: http://www.ncbi.nlm.nih.gov/books/NBK1360.

[31] P. De Backer, "Design and fabrication of a tunable artificial iris", Master's thesis, Ghent Univerity, 2013.

[32] G. Heiting and M. DePaolis, Multifocal Contact Lenses, retrieved on 31st of October 2013. [Online]. Available: http://www.allaboutvision.com/over40/multifocalcls.htm.

[33] Aniridic eye, retrieved on 31st of October 2013. [Online]. Available: http://www.allaboutvision.com/over40/multifocalcls.htm.

[34] Iris coloboma, retrieved on 31st of October 2013. [Online]. Available: http://www.nei.nih.gov/health/coloboma/images/iris_coloboma.jpg.

[35] HumanOptics artificial iris implants, retrieved on 31st of October 2013. [Online]. Available: http://www.kestrelophthalmics.com/artificialiris.

[36] Soft contact lens with painted artificial iris patterns, retrieved on 31st of October 2013. [Online]. Available: http://www.aldenoptical.com/products/soft-specialty/prosthetics/hp/#products/softspecialty.

[37] Y. Liao, H. Yao, A. Lingley, B. Parviz, and B. Otis, "A 3-microwatt cmos glucose sensor for wireless contact-lens tear glucose monitoring", *Solid-State Circuits, IEEE Journal of*, vol. 47, no. 1, pp. 335–344, 2012.

[38] F. Reinitzer, "Beiträge zur kenntniss des cholesterins", *Monatshefte für Chemie*, vol. 9, no. 1, 421–441, 1888.

[39] D. Yang and S. Wu, *Fundamentals of Liquid Crystal Devices*, ser. Wiley Series in Display Technology. Wiley, 2006.

[40] E. Lueder, *Liquid crystal displays: addressing schemes and electro-optical effects, Second edition*, ser. Wiley SID series in display technology. Wiley, 2010.

[41] A chiral nematic liquid crystal, retrieved on 5/11/2013. [Online]. Available: http://www.kennislink.nl/publicaties/kruising-tussen-beeldscherm-en-papier.

[42] S. Wu and D. Yang, *Reflective Liquid Crystal Displays*, ser. Wiley SID series in display technology. Wiley, 2002.

[43] D. White and G. Taylor, "New absorptive mode reflective liquid-crystal display device", *Applied Physics Letters*, vol. 45, p. 4718, 1974.

[44] S. Kelly, *Flat Panel Displays: Advanced Organic Materials*, ser. RSC materials monographs. Royal Society of Chemistry, 2000.

[45] J. Heikenfeld, P. Drzaic, J. Yeo, and T. Koch, "Review paper: a critical review of the present and future prospects for electronic paper", *Journal of the Society for Information Display*, vol. 19, pp. 129–156, 2011.

3 Fabrication Process of a Spherically Conformed LC Cell

"You have to learn the rules of the game. And then you have to play better than anyone else."

—Albert Einstein

3.1 Design aspects and materials

One of the first and most important objectives of this work is to create a fabrication process for a thin, spherically conformed LC cell. In this chapter the focus will lie on the mechanical aspects of the cell and how they affect the different fabrication steps that were conceived. The integration of the layers needed for the electro-optic switching of the LC molecules will only be briefly mentioned here but will be thoroughly addressed in the subsequent chapter.

When creating a generic blueprint of the LC cell, there are several restrictions greatly influencing the design and fabrication methods:

- The cell should have a smooth spherical shape that afterwards can be embedded in a contact lens with the desired dimensions
- The overall cell thickness should be as small as possible, but preferably below 140 µm
- The cell should be biocompatible

The LC cell should be designed for integration into the central part of the contact lens, primarily constituted by the optic zone of the lens. This zone has only one back radius and the LC cell should thus preferably have a spherical shape concentrically matching this back optical zone radius (see Figure 1.13). Although some small deviations could be corrected by the embedding process, a smooth shape is a *conditio sine qua non* for good encapsulation in the biocompatible body. Indeed, large deviations could potentially lead to protrusions in the lens or could only be corrected by embedding the cell in a thick lens. Both cases would anyway lead to a significant discomfort for the contact lens wearer and are thus unacceptable. Next to this, the aim is to create a generic LC cell with the possibility of embedding it in both an RGP and a soft contact lens. During the creation of our fabrication process the diameter of the cell was always set at 8 mm, which meant the cell could fit in the optic zone of both RGP as well as soft contact lenses. Depending on the final application and the preferred embodiment, this dimension can of course be altered, but should only require little effort once a reproducible process flow has been established.

Another important parameter is contact lens thickness which, as mentioned in section 1.3.2, is influenced by the desired back vertex power of the lens, the strength and refractive index of the used material and a desire to keep it as minimal as possible to increase biocompatibility and comfort. To concur with existing lens designs, the LC cell itself should also be as thin as possible to ensure successful embedding in these designs. Although it is difficult to exactly quantify this parameter at this stage, a target thickness of less than 140 µm was set, as this will lead to contact lenses with a thickness that still complies with most modern standards. Thin and ultrathin soft contact lenses are likely excluded because of their extreme size.

Finally, the cell should be biocompatible, meaning it should not invoke any negative biological response of the eye. Since the cell itself should be embedded in a contact lens made of materials that have already been deemed as biocompatible, the conditions seem less stringent because there is no direct contact between the cell and the ocular surface. Although beyond the scope of this work, encapsulation

approaches using materials such as parylene C [1–3] could be used to ensure no transfer of species occurs between the eye and the interior of the contact lens. In our context, however, one should not overlook the required oxygen permeability of the contact lens since integration of the LC cell will undoubtedly influence this permeability. To make matters even more complex, oxygen transmissibility rates for LCD substrates are recommended to be below 0.1 $cm^3/(m^2$ 24h atm)(Dk/t of 0.00365 in Fatt units) to avoid long term degradation of the cell [4], four to five orders of magnitude smaller than transmissibility rates of modern contact lenses. It seems highly likely that any final application and its constituent materials and design will be the result of a trade-off between comfort, biological safety and lifetime.

Choosing an appropriate material to create and study the fabrication process was therefore a difficult task, but eventually resulted in the selection of polyethylene terephthalate (PET). PET is a flexible and transparent polymer, primarily known for its use in carbonated beverage bottles [5]. It has decent strength and good chemical resistivity, making it easy to handle while processing it with existing microfabrication techniques. Furthermore, biocompatible variants are also available [6]. The main disadvantage of PET is that it has zero Dk [7] and would thus lead to a reduced comfort as oxygenation of the cornea can only occur through the tear mixing mechanism. Still, PET was deemed an interesting choice because, besides its primarily advantageous properties, it was also used by other researchers [8–10], and could thus be benchmarked to existing work.

3.2 Creating a Fabrication Strategy

3.2.1 Learning from Flexible Displays

Our envisioned spherically conformed LC cell is actually a special kind of flexible display. As a result, similar processing techniques to fabricate flexible displays can be used to construct our cell. Since it is beyond the scope of this work to give a full overview of all existing flexible displays and their related manufacturing techniques, only the most relevant items will be described below. An excellent overview can, however, be found in reference [12] and references therein. The foremost difference between classic LCDs and their flexible counterparts is the use of transparent flexible polymers instead of glass. Glass is a stiff, inorganic material that can withstand high temperatures (easily up to 600°C) and exhibits good barrier properties against water vapour and oxygen. This makes it a good substrate to construct an LC cell as high temperature processes (between 300 and 400°C) like

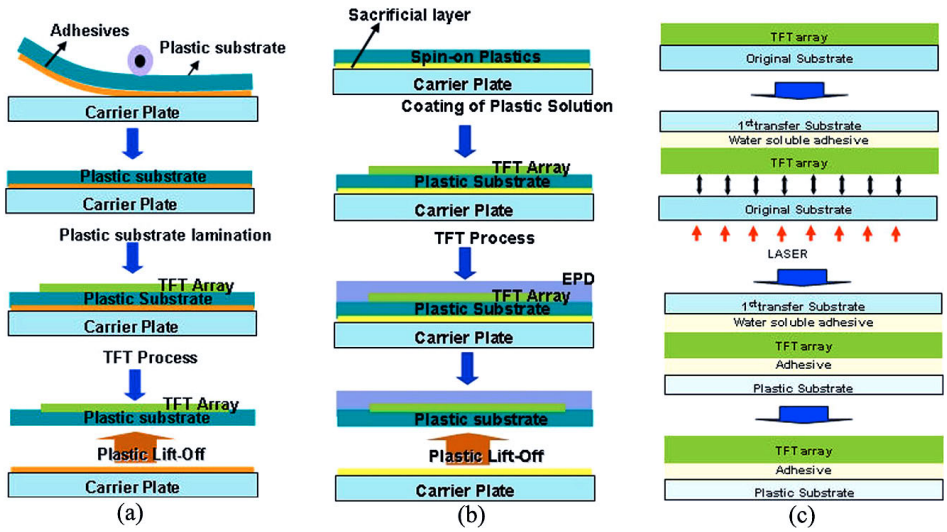

Figure 3.1: The three main methods to handle the plastic substrates in flexible displays. (a) the lamination-delamination method, (b) coating plastic method (c) transfer method. Image from [11]

Plasma Enhanced Chemical Vapour Deposition (PECVD) are required for reliable fabrication of the Thin Film Transistors (TFT). The downsides of glass are its weight and brittleness, leading to a quite heavy device which can easily break when submitted to a shock or a fall. By replacing the glass with flexible, polymer based substrates, a more durable and lightweight display can be fabricated. The biggest problem herein is the mismatch between the upper working temperature of the polymer substrates and the high temperatures generally needed during the manufacturing processes. The dimensional instabilities of the polymer films at elevated temperatures lead to unsatisfactory results and low yield for both the individual components as the display as a whole. Besides this, handling of the thin, flexible substrates themselves is also an issue. Many process steps require flat substrates and a good alignment between different steps. To tackle these problems, several strategies have been investigated and are summarized in Figure 3.1. A first approach uses a low temperature resistant plastic film which is laminated onto a hard carrier (usually glass or silicon) with a temporary adhesive, followed by specially developed low temperature processes. In the final step the plastic film is delaminated and the display is finished. In a second approach an unpolymerized monomer is spin coated on a carrier with a sacrificial

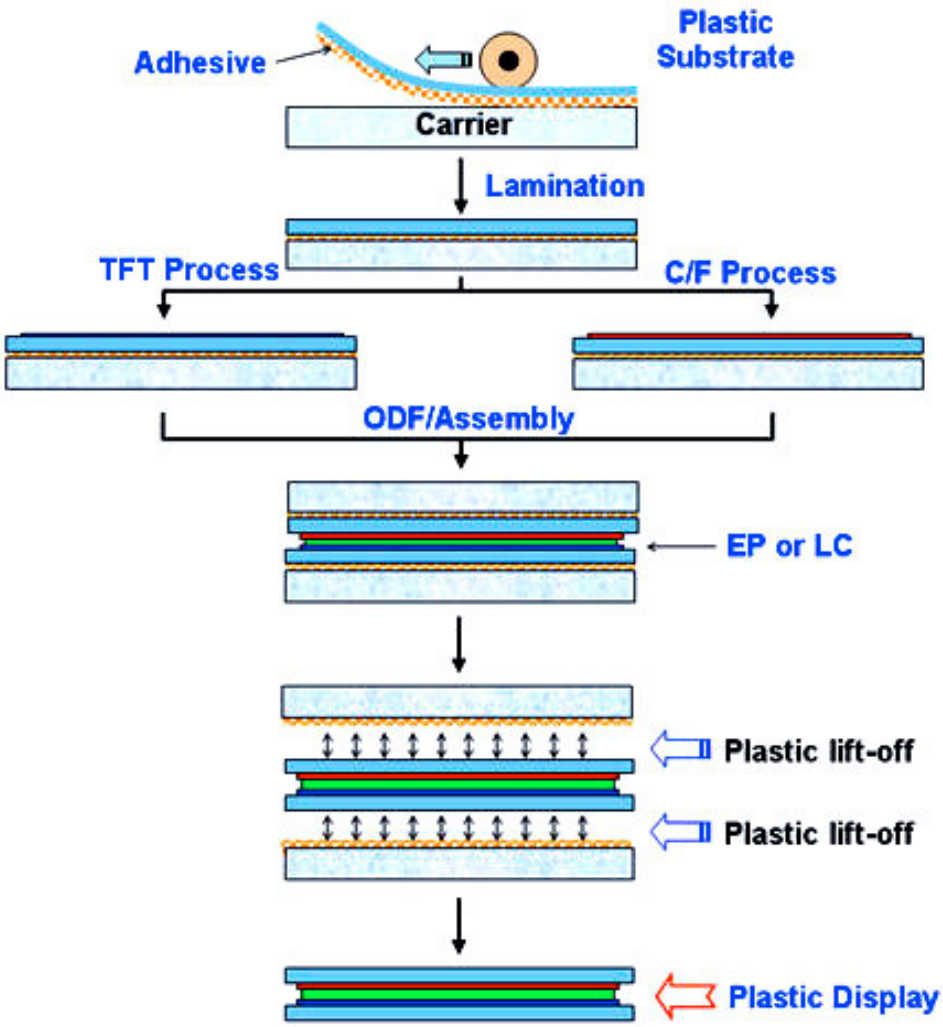

Figure 3.2: Plastic-handling process by Samsung's lamination-delamination method used for flexible LCDs. Image from [11]

layer, followed by a heating step to cure the film. Usually, these films have a higher upper working temperature, allowing for more standard manufacturing processes. Delamination is usually achieved by laser ablating the sacrificial layer through the carrier, requiring a carrier that is transparent for the wavelength

of the used laser. Alternatively, the sacrificial layer can be a material that only weakly bonds to the polymerized plastic and is applied everywhere but on the edges of the carrier. After processing, the display can be released by cutting through the film from above with a laser and subsequently peeling off the display [13]. The third approach uses a transfer method, meaning the active components are fabricated independently with standard high temperature processes on a hard carrier and are then transferred and adhered onto a plastic substrate. In this method, delamination can also be achieved by laser ablating the sacrificial layer through the carrier. Most approaches can be used for different display technologies and the ultimate choice depends on factors such as yield, cost and performance. When considering flexible LCDs, an industry giant such as Samsung seems to prefer the first approach [11] (see Figure 3.2) and for various reasons we too assessed this was the most interesting fabrication strategy for our research. First and foremost, this avoids the need for special glass carriers and a dedicated laser set-up, which would require a significant amount of resources since no such system was present in our lab. Also, questions about reliability and scalability of this approach remain unanswered. Secondly and perhaps counterintuitively, the use of spin-on plastics such as polyimides is less interesting as they tend to have a high glass transition temperature (up to 350°C). This glass transition temperature (T_g) is the temperature around which a polymer changes from being a glass-like (and to some extend thus brittle) material to a rubbery-like state [14] and is an important parameter when aiming to thermoform the material. Indeed, it was quickly realized that at least one thermoforming step was necessary to fabricate our spherically conformed LC cell and a high T_g means an impractical high temperature deformation step. A more detailed explanation will be given in the ensuing section.

3.2.2 Fabrication Strategy of the LC Cell

After our study of existing flexible display fabrication strategies, a new strategy for the spherically conformed LC cell could be proposed, similar to what is illustrated in Figure 3.3. The process flow should be more or less as follows:

- Laminate a polymer film (PET) onto a glass carrier with a temporary adhesive
- Deposit the active layers needed for the electro-optic switching, apply the spacers and circular glue joints

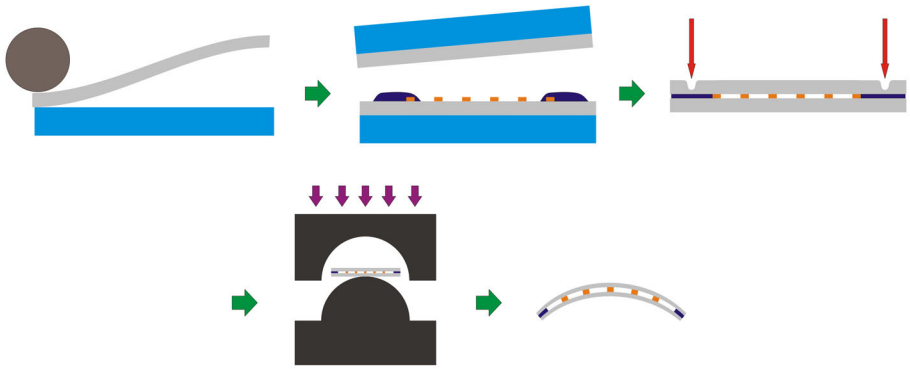

Figure 3.3: General fabrication strategy. 1: lamination of polymer film on glass carrier 2: deposition of the active layers, spacers and circular glue joints. Application of second carrier bearing a similar film, illumination with UV light 3: removal of carriers, laser cutting of circular cells through the glue joint 4: conformal shaping with a heated mold 5: filling with LC and sealing

- Put a second carrier bearing a similar film on top, press together the whole stack and illuminate with UV light to cure the glue
- Remove the carriers and cut out circular (flat) LC cells through the glue joint with a laser
- Conform the cells into a spherical shape with a mold, complete the process by filling and sealing the cells

Based on this envisioned strategy a detailed approach could be investigated. The general strategy was decomposed in single steps which were implemented using known methods from either classic or flexible LCD fabrication, leading to a first prototype.

3.3 First Prototype

The different steps and the related problems in the first prototype are described in detail below, while the total process flow is summarized in table 3.1.

3.3.1 Temporary Lamination and Delamination Process

Throughout this work, a 2 inch (5.08 cm) square glass carrier (0.7 mm thick white float glass from Präzisions Glas & Optik GmbH) was consistently used, which was found to be a good trade off between practicality and scale. Since one cell has a diameter of only 8 mm, multiple cells can be fabricated simultaneously on one carrier. Each time, a 3-by-3 matrix of nine cells was thus fabricated, allowing to differ more than one parameter at a time during testing (see Figure 3.18). According to the lamination-delamination method of flexible displays, the first step involves the lamination of a polymer film on top of this carrier with a temporary adhesive. For the polymer film we selected an optically clear, biaxially oriented PET film (Melinex 401, DuPont-Teijin) of 50 µm, which is consistent with the requirements listed in section 3.1, as this would lead to a transparent cell with a total thickness of 110 µm (cell gap included). The biggest challenge in this step was the selection of an appropriate temporary adhesive. Although the lamination-delamination method has been described in literature, most researchers do not disclose the exact composition of the adhesive, nor give a detailed description of how the delamination method is performed, preferring to keep this as in-house knowledge. For a first attempt, benzocyclobutene (BCB), a widely used adhesive in microelectronic processing [15], was selected since it is a spin coatable glue that liquefies at 150 °C. This is only a temporary effect as BCB also starts curing at this temperature. Our strategy herein was to spin coat the BCB and laminate the PET on top of the carrier and do a plastic lift-off (as illustrated in Figure 3.2) by liquefying the BCB and gently pushing off the carrier laterally via manual application of a shear force.

3.3.2 Active Layers, Spacer Balls and Glue Deposition

After lamination of the PET film on top of a glass carrier, the active layers needed for the electro-optic switching of the LC-molecules should be applied. Since these layers will be described thoroughly in the next chapter, they will only be mentioned briefly here. There are two active layers needed and the first one is the transparent conductive ITO, which is also the industry's standard material. The second layer is the alignment layer, which forces the LC-molecules in a predefined orientation. For this, obliquely evaporated SiO_2 was selected, leading to a vertical alignment of the LC-molecules.

After deposition of both layers, standard LCD manufacturing prescribes the application of ball spacers, small spherically shaped particles that are designed to keep the cell gap uniform. 10 µm spacers (Micropearl, Sekisui) were applied on

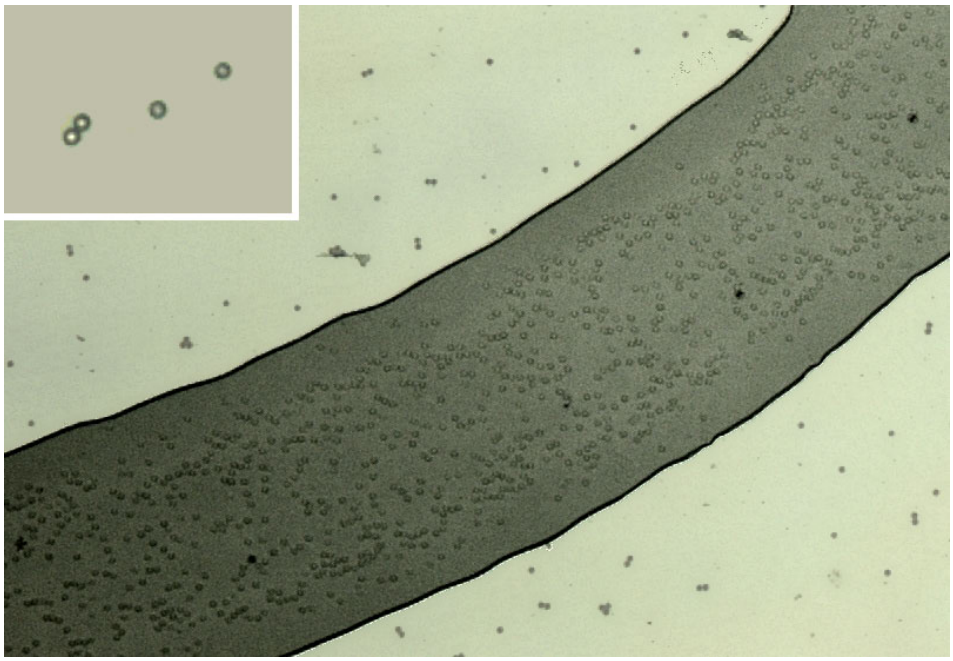

Figure 3.4: Ball spacers are used to keep the cell gap uniform and are both randomly dispersed on top of the active layers (bright areas) and present in a high concentration in the glue joint (dark band). A close-up of some spacers can be seen in the inset.

top of the active layers by spin coating them in a suspension of methanol, leaving them in a randomly dispersed pattern. Since the goal is to create circular cells (before deformation), a UV-curable glue containing the same spacers is dispensed on top of the substrate in a circular pattern with a small interruption through which the cell will be filled (see Figure 3.4 & 3.5).

The choice of the glue is important as previous research [16] has found that many glues tend to affect the long term stability of the alignment layer. Some of the known stable glues were tested and eventually the best results were obtained with UVS 91 (Norland Products), which is a glue specifically developed for sealing LCDs and is also flexible after curing.

Once the glue has been dispensed, a similar stack containing a glass carrier, PET film and active layers is then put on top and the total stack is pressed together, ensuring a close contact as the stack is subsequently illuminated with UV light to cure the glue joint.

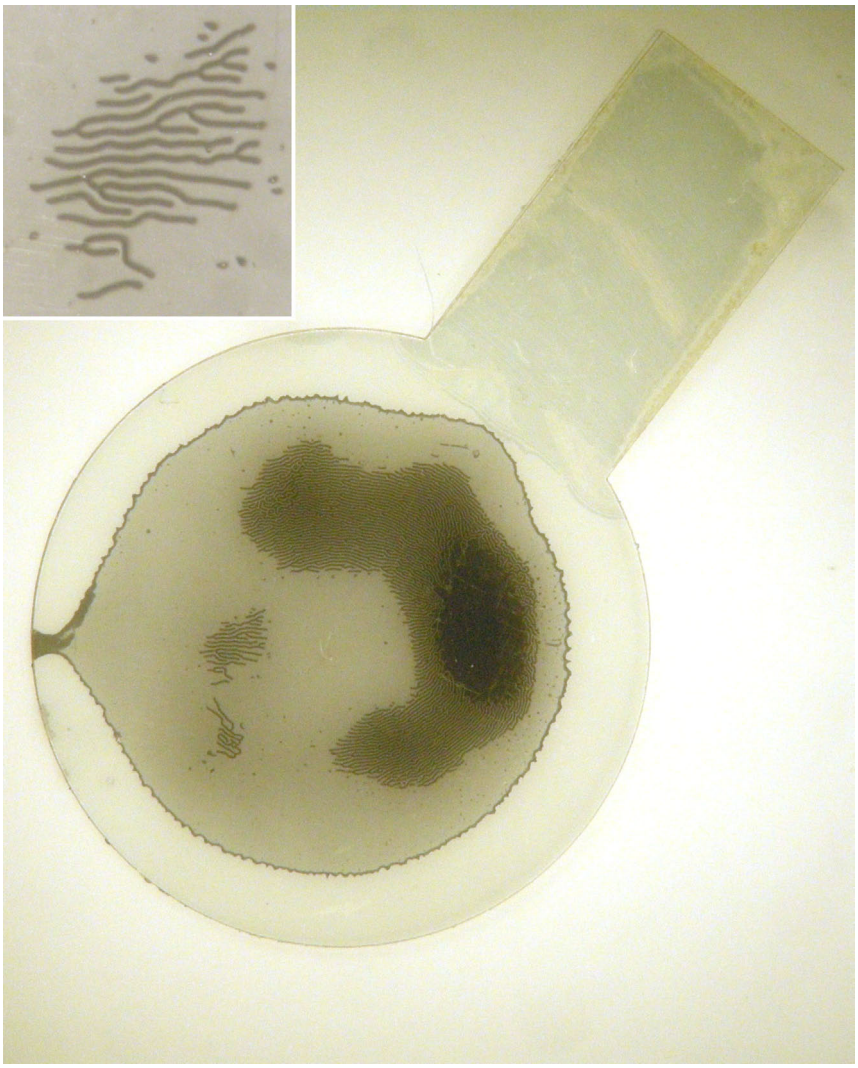

Figure 3.5: A flat, laser cut LC cell with extra rectangular contact pads. The circular glue joint has a small interruption for LC filling but tends to have an irregular shape. Cholesteric finger patterns (detailed image in inset) indicate the cell gap is locally thicker than intended.

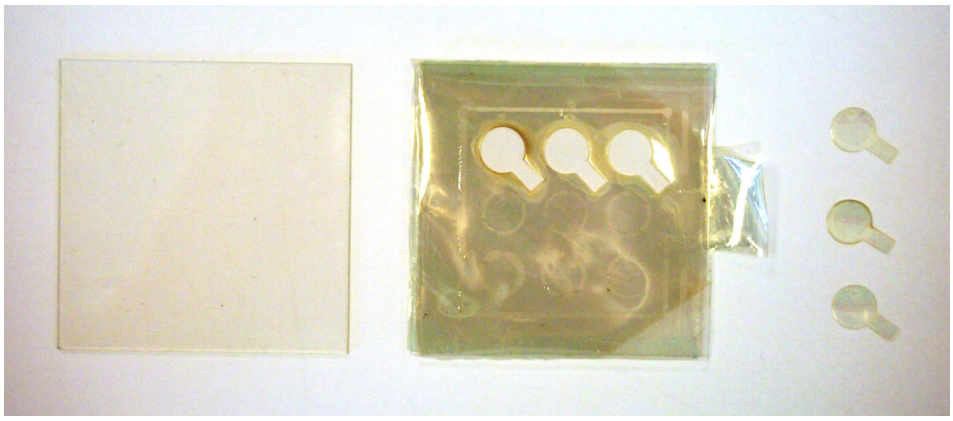

Figure 3.6: Left: 2 inch square glass carrier. Middle: delaminated PET films with active layers. A small additional rectangular area was foreseen at the side of the films to immobilize them during delamination of the carriers. Right: laser cut LC cells with additional rectangular contact pads.

3.3.3 Delamination and Laser Cutting

When the glue joints have been solidified by the UV-light, the challenging task follows of removing the glass carriers without damaging the joints nor the film. As mentioned in section 3.3.1, this is achieved by liquefying the BCB by heat and gently pushing off the carrier. The total stack was thus placed on top of a hot plate set at 155 °C, slightly above the liquefying temperature to account for thermal losses. To immobilize the bottom substrate and the glued films, a small additional rectangular area was foreseen in both films onto which manual pressure was given (see Figure 3.6), perpendicular to the substrate. The top carrier can then be pushed of by concurrently applying a force to the side of this substrate. After the top carrier is removed, the glued films can either be peeled off gently or the stack can be flipped and the process can be repeated to remove the bottom carrier, both resulting in free standing film. To free the circular LC cells from the glued films, the parameters of a CO_2-laser (10600 nm wavelength, 80 ns FWHM pulse width) were tuned so a narrow cut through the films and the glue joints could be obtained. As shown in figure 3.5, additional rectangular contact pads were foreseen at the side of the cell through which a supply voltage can be applied.

Figure 3.7: Mold comprising 2 parts: a male, convex side and a female, concave side. Both are made of aluminium and have a radius of 7.8 mm. 4 guiding pins are foreseen to ensure a correct placement of the two parts and prevent rotation vis-a-vis each other while the cells are being molded.

3.3.4 Molding

Changing the outline of the LC cells from a circular to a spherical shape requires a thermoforming step using a predefined mold. As can be seen in Figure 3.7, such a mold comprises of 2 parts: a male, convex side and a female, concave side, both having a spherical shape. The radius of both sides was set at 7.8 mm, concurring with the mean Back Optical Zone Radius of most contact lenses. Aluminium was chosen as a material for the mold since it has a high thermal conductivity, allowing it to be heated and cooled quickly, while also having a good resistance against corrosion. Fabrication of the mold was done in-house and started by coarsely shaping pre-manufactured aluminium rods (39 mm diameter) with an automated milling tool. Afterwards, the surface of the mold was polished in several steps using a Dremel tool and diamond pastes with decreasing particle size. Additionally, 4 guiding pins were foreseen to ensure a correct placement of

the two parts and prevent rotation vis-a-vis each other while the cells are being molded.

The molding process itself starts with putting the whole mold on a hot plate with a temperature of 175 °C, well above the glass transition temperature of PET (75 °C). When the mold reached this temperature, the flat LC cells were placed onto the bottom part of the mold and a soaking time of several minutes was applied. Afterwards, the upper part of the mold along with a weight of 1.2 kg was placed on top and the total ensemble was allowed to gently cool down. When the temperature of the mold was again well below the glass transition temperature of PET the now spherically shaped cells were removed from the mold. With this heating cycle, the introduction of strain and stresses into the cells was reduced.

3.3.5 Filling and Sealing

Filling the cell with liquid crystal is performed via a vacuum method requiring a vacuum bell, an actuated lever and a small cup containing the liquid crystal mixture (see Figure 3.8). The spherically shaped cell is first attached to the lever with its opening facing downwards, towards the small cup with the LC. The bell is then closed and a low pressure atmosphere (0.05 mbar) is created. In this low pressure atmosphere, the lever lowers the LC cell until the opening is submerged in the LC mixture, after which the vacuum is released. Since a pressure difference is created between the surroundings and the LC cell's interior, the liquid LC mixture is drawn into the cell. This process is continued until the cell is completely filled and and it can be retracted. After the filling procedure the cell is sealed by applying a small drop of UV-glue near the filling opening and curing the glue.

3.3.6 Problem Analysis

Out of the many runs using the first implementation of our proposed fabrication strategy, only a few prototypes could be derived, constituting a yield of no more than 20 %[1]. Furthermore, close-up pictures of such a prototype (see Figure 3.9) immediately reveal a variety of problems like a non-uniform transmission and a non-spherical shape due to the appearance of 'wrinkles'. An in-depth analysis of these problems was made and is described below.

[1] Based on approximately 10 runs

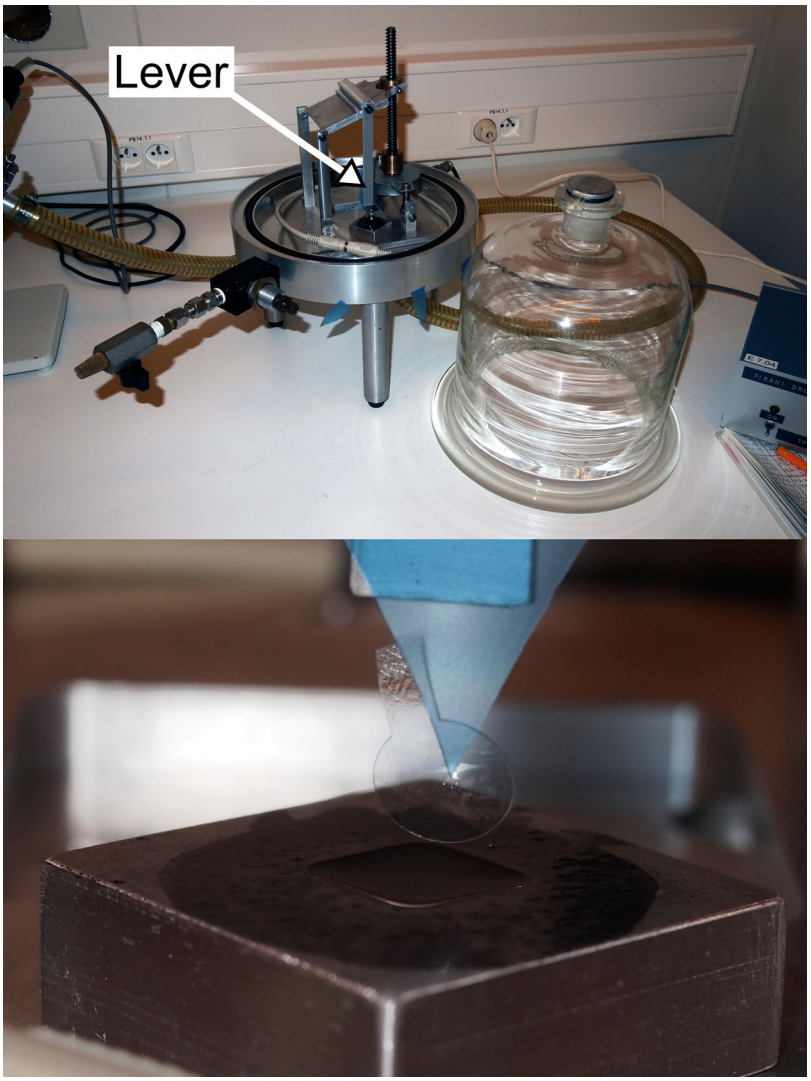

Figure 3.8: Top: Vacuum bell with an actuated lever hanging above a small cup containing the liquid crystal mixture. Bottom: close-up of the cup with an empty spherically shaped LC cell positioned above the cup.

Lamination-Delamination Method

The yield of this process was below 20%, a figure which could be mainly attributed to the lamination-delamination method. During the removal of the first glass

Table 3.1: Process flow of first prototype

Step	Description	Details
1	Clean glass substrates	RBS overnight
2	Clean PET substrates	N_2 blow, DI rinse, 5 min acetone USA, DI rinse, blow dry with N_2
3	Lamination of PET - Spin BCB - Postbake - Laminate PET	 3000 rpm, 30s hotplate, 1 min @ 95°C manual lamination
4	Sputter ITO	100 nm, 50 ohm/□
5	Evaporate SiO_2 alignment layer	6 nm, oblique evaporation
6	Spin spacers	10 µm spacer dissolved in methanol, 4000 rpm, 25 drops (1 drop/cm^2)
7	Glueing of stack - Dispense glue - UV curing	 UVS91, 250 µm needle, 1.3 mm/s 100 mW/cm^2, 2 min per corner
8	Release	directly on hotplate @ 150°C
9	Laser cutting	CO_2-laser, 97.5 % overlap (40 pulses per location), 1.1 J/cm^2
10	Molding	hotplate at @ 175°C
11	Filling	vacuum filling
12	Sealing	apply drop of UVS91 at entrance, illuminate with 100 mW/cm^2 for 1 min

carrier, about half of the samples separated prematurely, leading to rupture of the glue joints between the PET-films, thereby effectively destroying the LC cells. One of the reasons was that the delamination process was primarily manual, and therefore no well directed shear force could be applied to the carriers. This was further aggravated by the easy movement of the sample during delamination. Since the adhesive force between the PET-films and the carriers is much larger than the adhesive force between the PET-films themselves (mainly because of the large difference in area covered by the UV-glue and the BCB), any diverging force will indeed cause damage to the glue joints. Next to this, because of its high liquefying temperature and permanent curing, BCB was not an ideal choice as a temporary adhesive. The high temperature during delamination is unpractical, while it can cause additional thermal damage to the PET films. Clearly, to improve yield a more controlled delamination process and a more appropriate temporary adhesive are needed.

Figure 3.9: First prototype, showing several issues. Top: Most of these cells could not be electro-optically activated as the cells were shorted, which is likely due to a point of contact between the two opposing ITO layers at the bright areas in the LC cells (indicated by the white arrow), which in turn is due to the poor performance of the ball spacers. The deformed reflection of the ring shaped light source of the microscope reveals the presence of 'wrinkles', large deformations in the spherical surface of the cell. Bottom: the wrinkles can be clearly observed from the side of the cells.

Ineffective Spacers

Although ball spacers are standard for rigid LCDs, their use in flexible displays and certainly spherically conformed LC cells seem less appropriate. The first

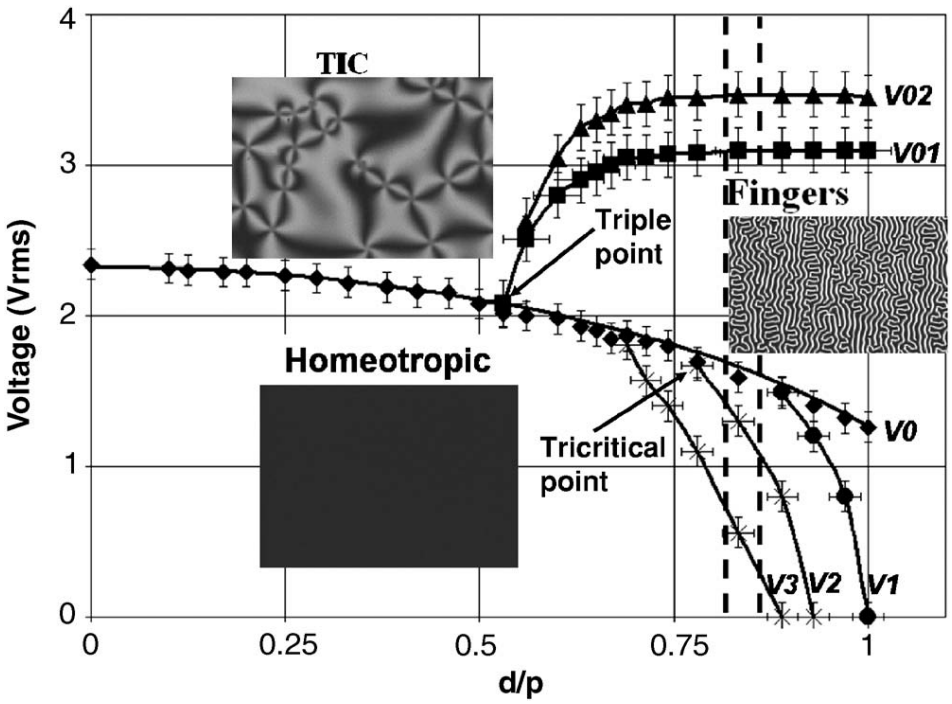

Figure 3.10: Phase diagram of a homeotropically aligned cholesteric mixture, showing the range of voltages and cholesteric pitch in which cholesteric fingers can be observed.

hint of this assertion was made clear when some flat LC cells were filled before the molding step to make an intermediate assessment of the cells' alignment layers. As can be seen in Figure 3.5, the flat LC cells contain dark spots which, when closely examined, can be identified as cholesteric finger patterns. Such patterns are manifestations of a complex director profile throughout the cell and their appearance depends on both the ratio of the cell gap (d) to the helical pitch (p) as the applied voltage. These complex profiles are well understood but an in-depth description is beyond the scope of this work. Excellent descriptions can, however, be found in references [17] & [18]. When characterizing cholesteric liquid crystal mixtures, complex phase diagrams are acquired, of which a typical example is given in Figure 3.10. In a mixture with a 180° twist (d/p=0.5) such as ours, the LC molecules should reorient from an unwound homeotropic state to an in-plane twisted state (denominated *translationally invariant configuration* (TIC) in the phase diagram) with increasing voltage. In fact, regardless of the

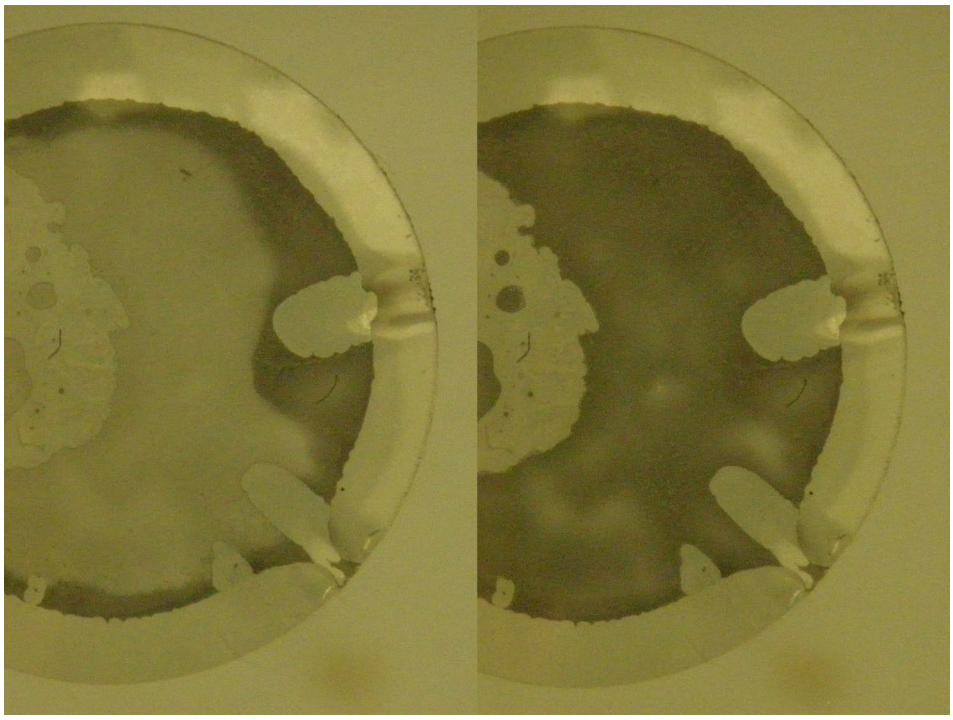

Figure 3.11: Electro-optic switching of a working first prototype. This particular cell was filled before molding, which led to the entry of air bubbles. Next to this, a large non-uniformity throughout the bulk could be observed, again revealing the poor performance of the ball spacers. Left: voltage off. Right: voltage on.

applied voltage, no cholesteric fingers should appear. Only in mixtures with higher d/p-ratio (beyond V3 in Figure 3.10) one can observe fingers in a zero voltage state, meaning that in our cells the d/p-ratio is locally diverging to higher values. Since the helical pitch p is fixed when creating the LC mixture, the cell gap is therefore thicker than intended at the areas where the cholesteric fingers can be observed. The LC cells are thus more convex than flat, which is likely resulting from the high flexibility of the PET-films and the fact that ball spacers only function well under a certain pressure and not when submitted to a pulling force.

To a certain extent, this inhomogeneity in the cell gap of the flat cells can be considered a minor concern, since only after the molding step the cells should

be homogeneous. The main consequence is that the cells should indeed be filled after molding to avoid build-up of excessive internal pressure during the molding step. Indeed, the seal of flat LC cells that were filled before the molding step broke in almost every molding attempt, leading to the entry of air bubbles (see Figure 3.11) at the point where the seal had ruptured.

However, the performance of the ball spacers after the LC cells have been spherically conformed is clearly insufficient. Every spherically shaped LC cell, of which an example is shown in Figure 3.9, contained a slightly brighter area in its bulk, indicating the cell gap is locally thinner than intended. Moreover, most of these cells could not be electro-optically activated as the cells were shorted, which is likely due to a point of contact between the two opposing ITO layers at the bright areas in the LC cells. In fact, the best switching behaviour could be observed in the cells which were filled before molding, probably because the LC acted as a buffer during the molding process. Nevertheless, also in these cells a large non-uniformity throughout the bulk could be observed.

Of course, a non-uniform and even non-functioning cell is not acceptable and an alternative for ball spacers should be investigated.

Appearance of 'Wrinkles'

From Figure 3.9 & 3.11 it should be obvious that a non-uniform transmission is not the only problem affecting our LC cells. The white ring in Figure 3.9 originates from a ring shaped light source mounted on the microscope used to capture this image. Since the lens should have a spherical shape, the light reflecting from its surface should conserve the ring shaped form of the light source, which it clearly does not. On several locations near the edge of the cells a locally inverted curvature can be observed, extending about 2 mm towards the center. These 'wrinkles' (or edge wrapping) are randomly distributed over the glue joint, but there is always one located at the entrance through which the cell is filled, indicating this is a mechanically weak spot. Furthermore, the alignment of the LC molecules seems to be affected in the wrinkled areas.

Since these wrinkles would impair good encapsulation in the biocompatible body and would cause a significant discomfort for the contact lens wearer, a deeper study on how they can be avoided is thus required.

Irregular Glue Joint

Although the UV-glue is automatically dispensed, the cured glue joint tends to have an irregular shape towards the interior of the LC cell, partly because it is

pushed together just before it is cured. For large displays this is not an issue since it can be hidden in the bezel. For our application, however, a regular glue joint is important as the irregularities cannot be hidden, while every part up until the glue joint should be usable seeing the small scale on which it will be implemented. A solution in which a regular glue joint can be achieved should therefore be foreseen.

3.3.7 Conclusions Drawn from the First Prototype

Our first prototype was the result of a straightforward application of known classic or flexible LCD fabrication techniques to our envisioned spherically conformed LC cell. This approach revealed such a transfer is not possible and a series of problems specific to our application need to be resolved. Summarized, the following action points can be formulated:

- Create a controlled delamination process using an appropriate temporary adhesive
- Find and implement an alternative for ball spacers
- Develop a method to create a well defined glue joint
- Investigate wrinkle formation in the LC cells, paying special attention to the mechanical weak spot at the entrance

How these action points were addressed is discussed in the ensuing sections.

3.4 Simple and Fast Lamination-Delamination Method

As mentioned in section 3.3.1, the envisioned strategy for the lamination-delamination was to laminate our PET-films to a glass carrier with a temporary adhesive and after processing liquefy the adhesive by a heat step and gently push off the carrier laterally via application of a shear force. Although our initial trials using BCB and the manual application of a shear force resulted in a poor yield, the strategy itself was still preferred as it had the potential of being a simple, fast and cheap method. Of course, the selection of a good temporary adhesive and the development of a controlled delamination step are indispensable. Both requirements (good adhesive & controlled delamination step) are in fact interdependent

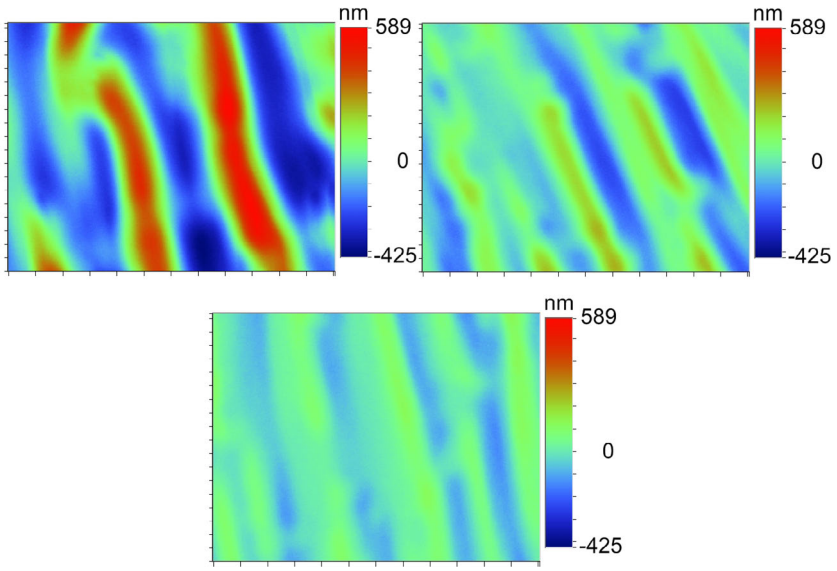

Figure 3.12: Optimization of wax parameters supported by optical profilometer measurements. Each measurement is taken about 1.5 cm off the centre of the substrate and covers 0.92 by 1.2 mm. Top Left: MW80 dissolved in acetone (3 g per 10 ml) and spincoated at 1000 rpm, showing a root-mean-squared roughness of 230 nm. Top Right: MW80 dissolved in ethanol (3 g per 10 ml) and spincoated at 1000 rpm, showing a root-mean-squared roughness of 103 nm. Bottom: optimized parameters, MW80 dissolved in ethanol (2.5 g per 10 ml) and spincoated at 1000 rpm, showing a root-mean-squared roughness of 55 nm.

and should be developed simultaneously. Nevertheless, the temporary adhesive will be discussed first before the delamination step is described in detail.

3.4.1 Wax as a Temporary Adhesive

Although there is no generally accepted definition of waxes, they form a broad class of chemical compounds with typical properties such as low melting point (generally between 50 and 90 °C), plastic behaviour and easy use as a reworkable adhesive [19]. The most well-known example is beeswax, which also plays a prominent role in the Greek mythological story of Daedalus and Icarus. Wax was quickly identified as an alternative for BCB, especially because it is widely used as a temporary adhesive, while a broad range of waxes with varying working

temperatures are available. For this work, Mounting Wax 80 (MW80, Electron Microscopy Sciences) was selected, a wax with a melting point at 80 °C. Although slightly above the T_g of PET, a melting temperature which is too low might lead to premature delamination during processing and thus 80 °C was found to be a good trade-off.

The next challenge was to apply only a thin layer of wax onto the glass carriers, since wax is a very viscous liquid above its melting point. A solution was found by dissolving the wax in a solvent followed by a spin coating step. However, a careful selection was made of the both the solvent itself as the used concentration. This is because spin coated wax shows 'striations' in its surface, a phenomenon best visualized and quantified by an optical profilometer (see Figure 3.12). For instance, wax dissolved in acetone leads to a rougher surface with more prominent 'striations', than when using wax dissolved in ethanol with the same concentration and spin coat parameters. Since evaporation rate has been identified as a largely contributing parameter for striation growth [20], the higher boiling point of ethanol (78.5 °C for ethanol versus 56.1 °C for acetone [21, 22]) and consequently lower evaporation rate leads to more uniform films.

A good uniformity is needed for the subsequent steps in the process flow and to avoid bubble entrapment between the PET-films and the glass carriers. This bubble entrapment was found to be detrimental to the quality of the cells since these bubbles either expand during vacuum steps or merge during thermal steps, leading to a non-uniform surface. Next to selecting a good solvent, spin speed also is an important parameter. Although high spin speeds reduce the amplitude of the striations, a thinner film is also formed which in term increases the shear force needed to delaminate the films. To find an optimum, different concentrations (1, 2, 2.5, 3 and 4 g/(10 ml) of wax dissolved in ethanol were made and were spin coated at various spin speeds (1000, 2000, 3000 RPM for 30 seconds). Each combination was tested for the detrimental effects of the bubble entrapment and the amount of needed shear force for the delamination step. Ultimately, a solution of 2.5 g wax per 10 ml of ethanol spin coated at 1000 RPM was found to be a good optimum.

3.4.2 Controlled Delamination Step

Apart from selecting an appropriate temporary adhesive, a more controlled delamination step was needed. Quickly, the importance was realized to immobilize both the bottom carrier as well as the glued PET-films during application of the shear force on the top carrier. For this purpose, a new sample holder was

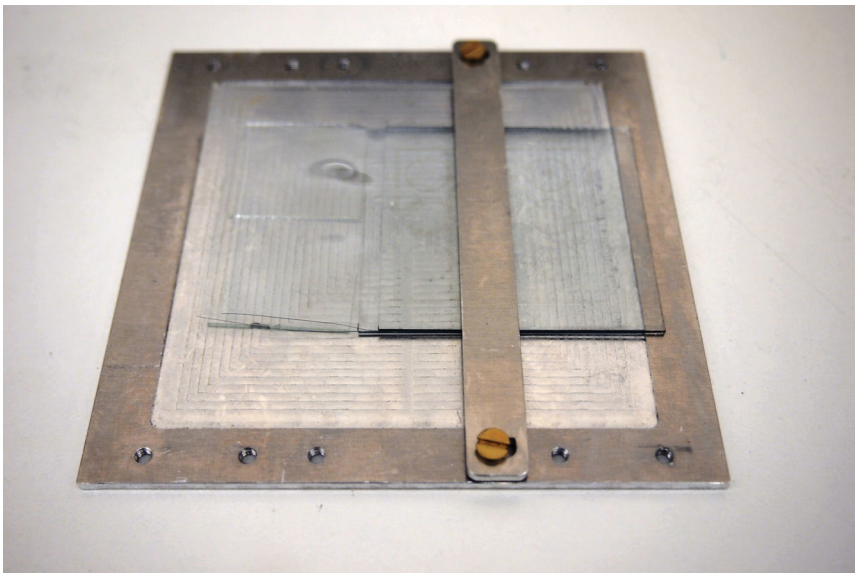

Figure 3.13: Sample holder for the delamination step. A clamping bar prevents upwards motion while the depression fixates the bottom substrate during application of the shear force.

designed and fabricated aimed at firm clamping of both the bottom substrate as the PET-films (see Figure 3.13). This sample holder was made out of a 2 mm thick square aluminium plate (10.5 cm edge) in which a depression of 0.5 mm was milled. Additionally, a clamping bar was foreseen to prevent motion in the upward direction, perpendicular to the shear force direction.

Together with this sample holder, the new method requires that during lamination, part of the PET film (about 2 cm) is extended beyond the carriers, designating an area where the PET-films can be clamped. A stack ready for delamination can be placed near the edge of the sample holder and a large clamp is then used to fixate both the stack and the sample holder onto a hot plate. A 2 by 5 cm rectangular aluminium plate is also put between the clamp and the designated area of the PET films, while 2 square 1 inch glasses are put between the PET-fims and the holder, in this way distributing the clamping force evenly and preventing rupture of the PET-films.

As should be clear from Figure 3.14, when the hotplate is heating up the total stack above the liquefying temperature of the wax, the top carrier can be pushed

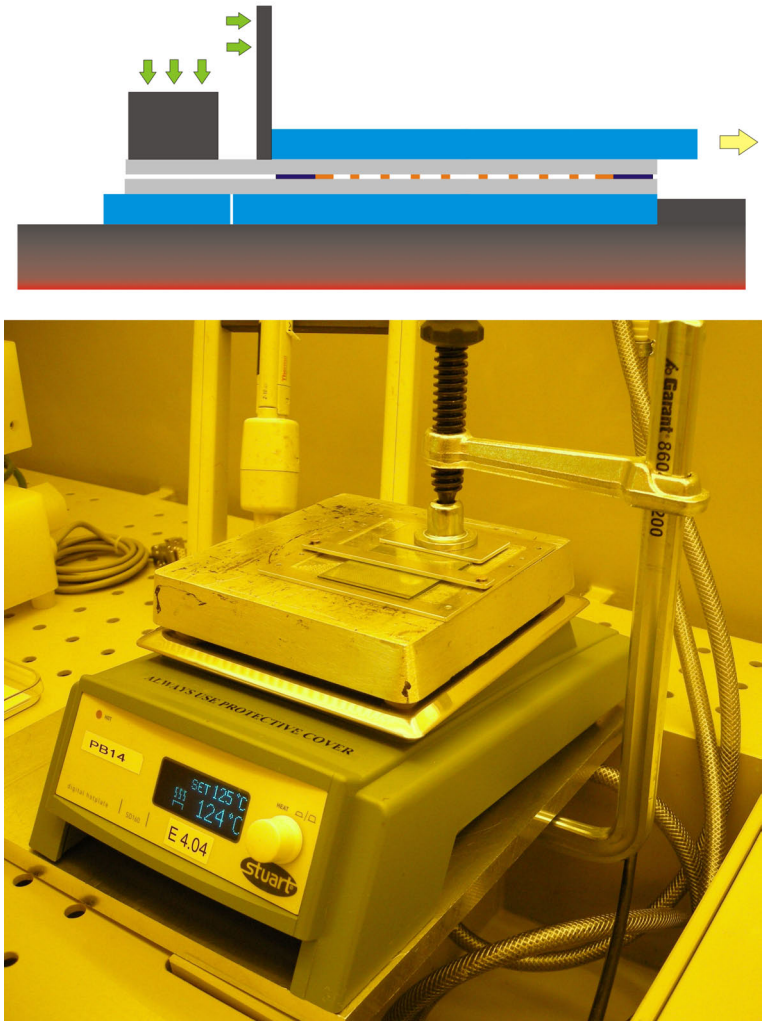

Figure 3.14: Controlled delamination step. After putting the sample holder on top of a hot plate, the sample holder, the glued PET-films and the bottom substrate are firmly fixed with an external clamp. After a short soaking time, the wax liquefies and the top substrate can be pushed off gently.

off by a shear force while the PET films and the bottom carriers cannot move. Indeed, the bottom substrate is immobilized by the edge of the depression in the sample holder while the PET-films are clamped to the bottom of the holder.

When the top carrier has been removed, the remaining stack can be taken out from the holder, flipped and clamped directly onto the hotplate, after which the second carrier (the former bottom carrier now residing on top) can be removed using a similar shear force approach. The free standing glued PET-films can then be laser cut and the process flow can be finished as foreseen in the general fabrication strategy.

3.4.3 Alternative Delamination Method: Transfer-to-Foil

As soon as both carriers have been removed, the PET-films can bend in any direction and thus the alignment of the laser needs to be repeated for each LC cell to prevent a mismatch between the laser cut and the glue pattern. Moreover, deviations are still possible due to local curving of the pre-cut cells. Alternatively, the laser cutting can be performed before removing the second carrier which, due to the firm adhesion to the carrier glass, now only needs one alignment step and can thus be done in one continuous run for all nine cells. Although this approach improves throughput, the cells are, as desired, mechanically separated from the remaining PET-films. These PET-films could be peeled off easily, but the individual cells were hard to separate from the carrier without damaging them.

Therefore, an alternative 'Transfer-to-Foil' method was created (see Figure 3.15). In the Transfer-to-Foil method the bottom carrier glass containing the laser cut cells (including the remaining glued PET-films) is flipped and put on top of a flexible foil (e.g. a 100 µm PET foil). Similar to the conventional delamination process, the stack is clamped on top of a hot plate and the bottom carrier glass is also removed by application of a shear force. The remaining films can be peeled off easily from the hot plate and the redundant part of the glued PET-films can be peeled off from the carrier foil, only leaving the LC cells behind on top of this foil. Although simple in nature, the method allows for a safe transfer of the laser cut LC cells to the new flexible carrier foil for further handling and processing. Subsequent processing steps can either involve manually picking individual cells of the flexible carrier foil or transferring the cells en masse to a new (rigid) carrier.

3.5 Integration of a Permanent Photolithographic Layer

Besides a controlled delamination method, other conclusions drawn from the first prototype suggested that its successor needed an alternative for the ball spacers, a regular glue joint and an increased mechanical strength at the filling entrance

Figure 3.15: Transfer-to-Foil Method. Top: the bottom carrier glass is removed using the conventional method after clamping the stack on top of a carrier foil. Middle: after delamination the carrier foil containing the redundant part of the glued PET-films and the laser cut LC cells can be peeled off from the hot plate. Bottom: the LC cells can be manually picked from the carrier foil or can be transferred en masse to a new rigid carrier.

of the cells. All three were tackled by integrating a permanent photolithographic layer in the LC cell, in between both PET-films. Such a layer allows for the

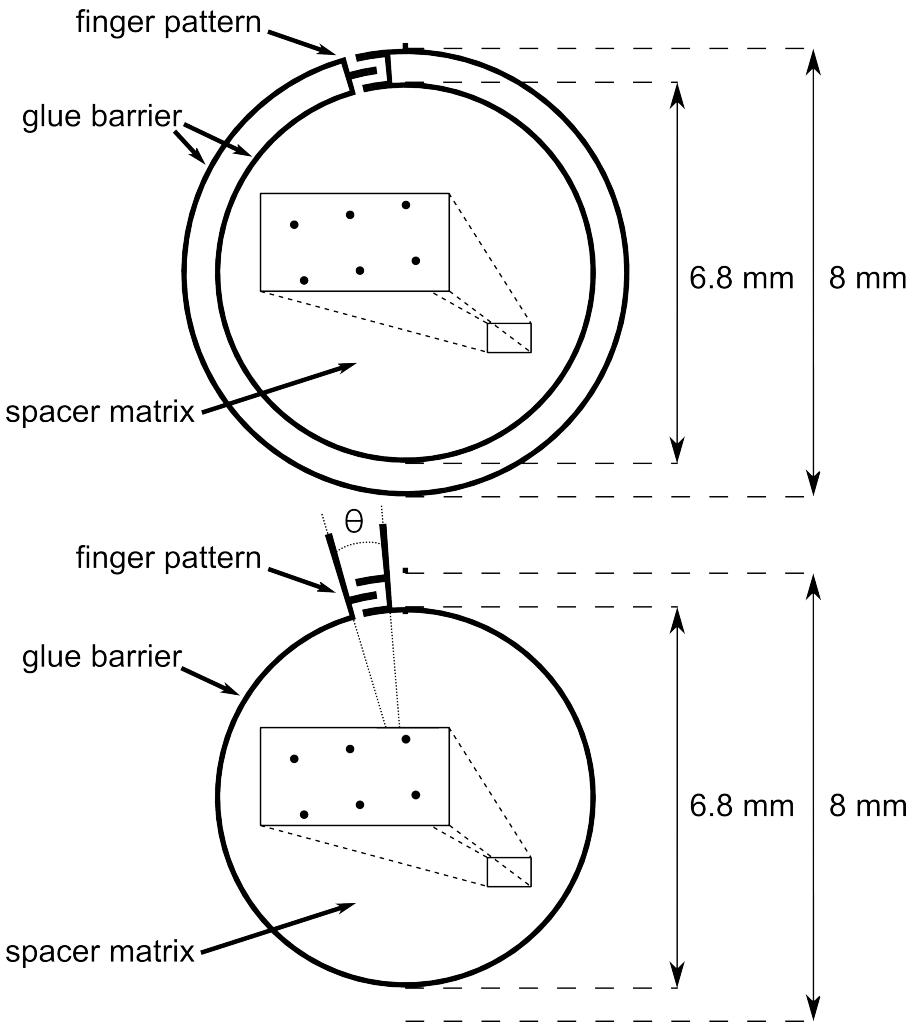

Figure 3.16: Design of the photolithographic layer of one LC cell with one (bottom) and two (top) glue barriers. The three important features are a spacer matrix, a glue barrier and a finger pattern at the filling entrance. The central angle θ delineating the finger pattern is 20°in this example.

inclusion of specifically designed features, providing a new way for solving the pending issues.

For this work SU8 3010 [23, 24] was selected, an epoxy based photoresist

designed for micromachining and other microelectronic applications and being best suited for permanent deposition. This photoresist can be spincoated which, after UV-curing and removal of the unilluminated parts, leaves behind a 10 µm thin layer, matching the intended cell gap. Our designs contained three important features tackling the aforementioned issues: a spacer matrix, a glue barrier and a finger pattern at the filling entrance (see Figure 3.16). A detailed description of these design features is given in the ensuing sections.

3.5.1 Spacer Matrix

Due to the poor performance of the ball spacers, we replaced them by a matrix of photolithographically defined, cylindrical spacers on top of one of the PET films, since their cylindrical form has been proven to be more robust when used in flexible displays [25]. The individual spacers' diameter is 20 µm and they are placed in a square matrix throughout the interior of the cell. The pitch of this matrix was set at 150 µm, 200 µm and 300 µm to test its influence on the uniformity of the cell. A large pitch increases the fill factor of the whole cell, but likely leads to a less uniform cell, while a small pitch decreases the fill factor, but is likely to increase the uniformity. For a more in-depth analysis of the influence of the spacer pitch, we refer to section 4.3.3 of Chapter 4, which handles the inclusion of the electro-optic effect in the LC cell.

3.5.2 Glue Barrier

To create a well defined glue joint, the idea of placing a glue barrier around the active area of the LC cell emerged quickly. Such a glue barrier aims to restrict the glue flow right after deposition and in later processing steps when the top substrate is placed on top and the total stack is pressed together. As can be seen in Figure 3.16, a first design contained both an inner and outer glue barrier, in between which the glue was deposited. This, however, frequently led to encapsulation of air bubbles, a likely result of irregularities in the glue deposition process and the fact air can get easily trapped between both glue barriers (see Figure 3.17). Since enclosed air bubbles act as unwanted refractive structures, their formation should be avoided.

As a result, a second design omitted the outer barrier, thereby lowering the risk of air bubble entrapment as the glue can still flow freely outwards. Although this approach can lead to irregularities in the glue joint at the outer side, these were not be visible in the final LC cell since a laser cut through the glue joint leads to a well defined edge. Additional elongated features were foreseen near the finger

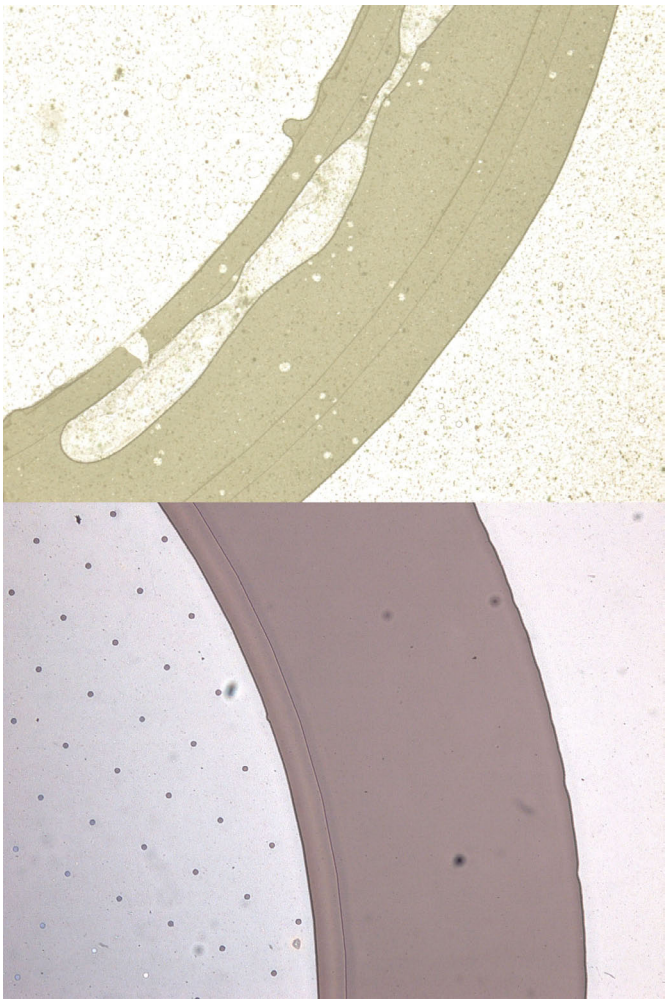

Figure 3.17: Glue barrier efficacy. Top: glue deposited between two glue barriers frequently led to air bubble encapsulation, acting as unwanted refractive structure. Bottom: with only one glue barrier at the inner side, air bubble encapsulation can be avoided and a precisely controlled interior dimension of the LC cell can be guaranteed.

patterns (see ensuing section) to prevent any excess glue from flowing towards or in these finger patterns. Like the irregularities in the glue joint, these too are cut away after the UV-curing step. The inclusion of a photolithographically defined glue barrier thus leads to a precisely controlled interior dimension of the LC cell.

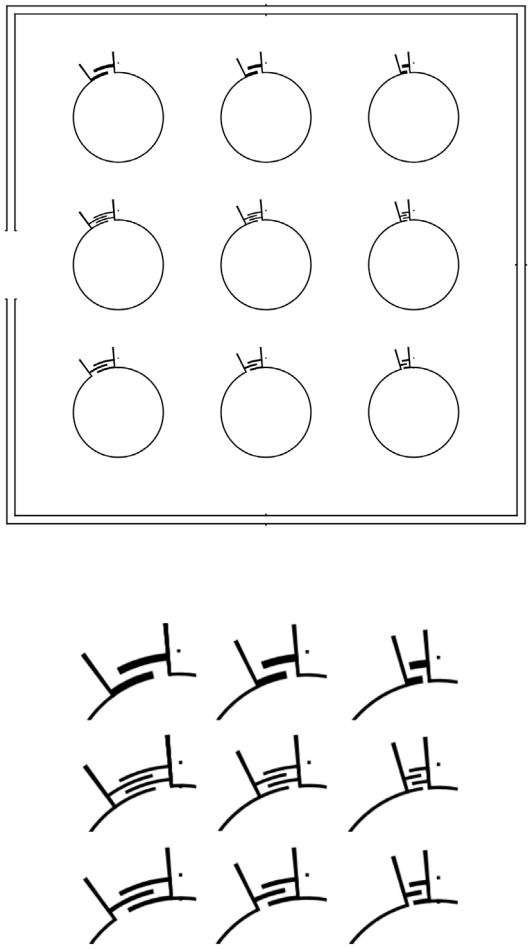

Figure 3.18: Top: Test mask for finger patterns in which the number of fingers ranged from two to four and the central angle was 20°, 30°or 40°. The outer right angles are used to align the mask with the 2 inch carrier glass. A glue gutter around the nine cells provides the final stack with additional strength during the delamination process. Bottom: Close-ups of the finger patterns.

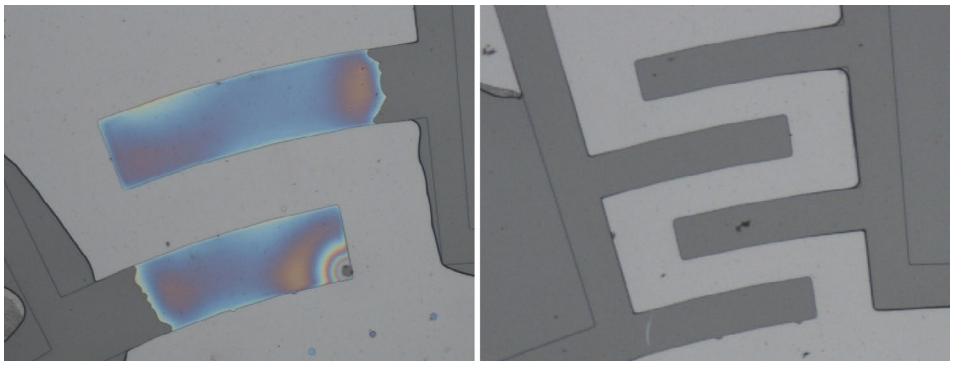

Figure 3.19: Long or thick fingers (left) had a larger tendency to no stick to the top PET-film than short, thin fingers (right), leading to a less controlled process.

3.5.3 Finger Pattern at the Filling Entrance

In the first prototype, the passage in the glue joint used for filling the LC cell was identified as a mechanical weak spot where the wrinkles easily originated. To tackle this problem, interlaced finger patterns were defined in the photolithographic layer to reinforce this passage. A variety of such patterns was created (see Figure 3.18), in which the number of fingers ranged from two to four and the central angle was 20, 30 or 40°. During the fabrication of LC cells using these patterns, it was noticed that long or thick fingers had a larger tendency to no stick to the top PET-film, leading to a less controlled process (see Figure 3.19).

This prompted the use of finger patterns with a central angle of 20° and three or four fingers, between which no significant difference could be found. However, as the filling path of the four finger pattern is longer than that of three fingers, the best trade off was thus found in the 20° central angle, three fingers pattern as shown in 3.16. The mechanical efficacy of all finger patterns was studied along with the wrinkle formation in the cells and has been described in the following section.

3.6 Creating Wrinkle-Free LC Cells

3.6.1 Influence of Film Thickness on Wrinkle formation

The appearance of wrinkles during the deformation step of our LC cells is not totally unexpected. Indeed, as a direct result from Gauss' *Theorema Egregium*

Table 3.2: Wrinkle formation dependency on film thickness. Horizontal: convex side, vertical: concave side. W: wrinkle formation, PW: partial wrinkle formation, NW: no wrinkle formation.

convex concave	36 μm	50 μm	75 μm	100 μm
36 μm	W	W	PW	PW
50 μm	W	W	PW	PW
75 μm	NW	NW	NW	NW
100 μm	NW	NW	NW	NW

[26], a flat surface cannot be deformed into a sphere without introducing some distortions. Such distortions are accompanied by certain stresses which can manifest themselves in several ways, one of which is the appearance of the wrinkles. Next to this, since polymer films are frequently made by a two-step drawing process, anisotropic shrinkage at elevated temperatures can be present [27], further facilitating the creation of the wrinkles. In the Melinex 401 films, this anisotropy is, however, rather small (0.7% vs 1% shrinkage at 150°C).

Strangely, wrinkles were not reported by other research groups [8, 9, 28], although PET was also used as material for the base substrate. Due to limited available date no comparison of anisotropic shrinkage could be made, but a closer study revealed the main difference was the thickness of the used PET-films, which in other work usually was 100 µm. This leads to the assumption that a correlation might exist between film thickness and the appearance of wrinkle formation. A thorough study of the influence of the thicknesses of the base substrates on the mechanical stability of the substrates and the formation of the local wrinkles therefore seems warranted. Out of this study a trade-off between total thickness and smoothness of the lens is then expected to present itself.

To investigate the wrinkle formation, we therefore obtained a series of PET films with decreasing thicknesses (100, 75, 50 and 36 µm), where the thinnest film was 36 µm as thinner substrates were deemed unpractical during handling. Since good optical quality of the films is primordial, the Melinex 401 PET films were chosen when possible. However, the smallest available thickness of the Melinex series is 50 µm and, therefore, the 36 µm Mylar A PET film (DuPont-Teijin) was chosen for the lower limit. Although the haze of the Mylar A series is rather high for a contact lens (22 %), this film was mainly chosen to study its mechanical properties. As each LC cell utilizes 2 PET films, the construction of the cells was

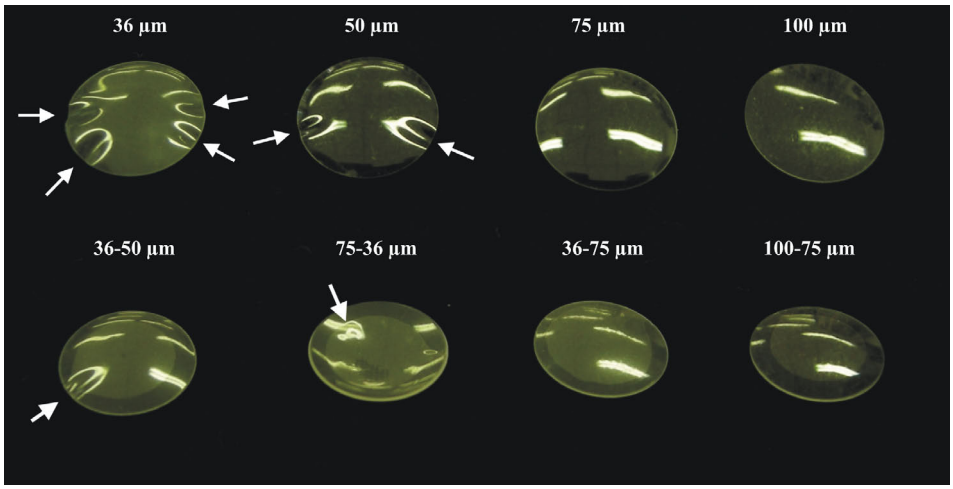

Figure 3.20: Molded single lenses and LC cells. Top: molded single layer lenses with increasing thickness. Below 75 µm, wrinkles are clearly visible (indicated by the arrows); Bottom: LC cells with various PET film combinations (convex side thickness listed first).

not limited to symmetric film thickness combinations, but was expanded to all possible thickness combinations (summarized in Table 3.2).

After fabrication, the LC cells were visually inspected under a microscope, where wrinkles were generally identified as local inversions of the curvature in the LC cell surface (see Figure 3.20). Additionally, the LC cells were examined between crossed polarizers, utilizing the birefringence of the PET layers, as the wrinkles introduce discontinuities in the fringe patterns (see Figure 3.21).

3.6.2 Single Film Lenses

In addition to the fabrication of the LC cells, single film lenses with the same thicknesses and radiuses were also cut out and deformed for comparison. As can be seen in Figure 3.20, the single lenses only exhibit wrinkles for thicknesses below 75 µm (with the 36 µm lenses showing more wrinkles than the 50 µm lenses), suggesting the existence of a threshold thickness for wrinkle formation somewhere between 50 and 75 µm. At this threshold, the mechanical stresses introduced by the molding process become too large and are relieved through the wrinkles.

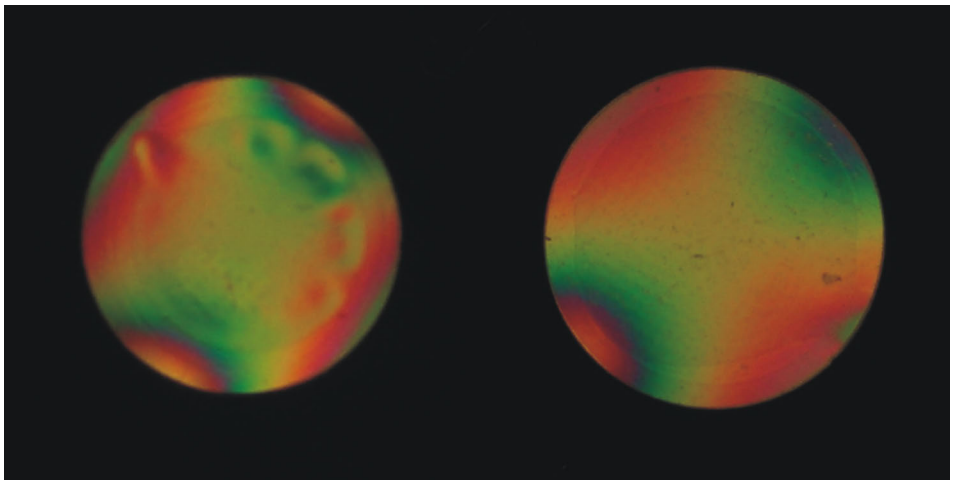

Figure 3.21: LC cells observed between crossed polarizers. Wrinkle formation can also be observed by using the birefringence of the PET layers and looking for discontinuities in the fringe patterns when placing the lenses between crossed polarizers. The 75 µm convex – 36 µm concave (left) and the 36 µm convex – 75 µm concave (right) combinations, for instance, show distinct differences in this respect, indicating the presence of wrinkles in the first

3.6.3 LC Cells

The wrinkling behavior of LC cells is more complex and can generally be categorized in three groups (summarized in Table 3.2). First, all combinations comprising only films below the threshold thickness of the single lenses (36 and 50 µm) exhibit wrinkle formation, affecting both layers simultaneously and generally extending about two millimeters from the side towards the middle of the lens (see Figure 3.20). The location of the wrinkles was randomly distributed around the glue joint and although wrinkles sometimes did appear at the filling entrance, it no longer seemed to be a preferential spot. This indicates our interlaced finger structures indeed provided a better support for the LC cell and the entrance itself was no longer a mechanical weak spot. In the large variety of finger patterns that were examined, from a mechanical point-of-view no preferential pattern could be pinpointed, but as mentioned above, the mask as shown in Figure 3.16 was deemed the best trade-off.

Secondly, when combining a thick film (75 or 100 µm) at the convex side with a thin film (36 or 50 µm) at the concave side, the LC cells are only partially

wrinkled, as is depicted in Figure 3.20 & 3.21. The inner part of the thin films was greatly deformed, while the glue joint was mostly unharmed and the thick films remained unaffected. These wrinkles were smaller when compared to the first group and were, therefore, less visible under the microscope, but could still be easily observed through the crossed polarizers. Interestingly, in the third and final group, the reverse combinations of the second group were wrinkle free, suggesting that the thick films at the concave side prevented the thin films from collapsing (see Figure 3.20 & 3.21). In addition to this, all remaining combinations with thick films exhibited no wrinkle formation, where the 100 µm convex – 75 µm concave combination is of particular interest, as it shows that the presence of a thinner film at the concave side does not automatically lead to wrinkle formation.

Seemingly, the threshold thickness for the single lenses also appears to be an important parameter for the wrinkle formation in the LC cells, as every cell made with films below this thickness exhibit wrinkles, suggesting the induced stresses are simply too large for the cells to cope with. However, the direction of these stresses also seems to play a vital role when combining films above and under this threshold. The thin films of the second group experience a more compressive stress at the concave side in contrast to their thick counterparts at the convex side, leading to the partial wrinkles. On the other hand, when these thin films are at the convex side, they experience a more tensile stress, induced by the stronger thick films at the concave side, thus preventing the wrinkle formation. Nevertheless, when only using films above the threshold thickness, the direction of the stresses no longer plays a role as is showed by the 100 µm convex – 75 µm concave combination, which does not display any wrinkles.

3.6.4 Impact

The impact of these results is twofold. First, an optimal combination of film thicknesses for contact lens integration of the LC cells can be derived. Clearly, the 36 µm convex – 75 µm concave combination is the best when only looking at the total thickness, as these exhibit no wrinkles while the total thickness is only 121 µm. Presumably, this total thickness can be further reduced by identifying the threshold value for wrinkle formation more precisely and choosing the concave film slightly above this value. In addition to this, the convex film can possibly be further reduced, although handling of such thin films might become a more difficult issue. However, since the optical quality of the films is equally important, the 50 µm convex – 75 µm concave combination has the best overall properties, having a total thickness of 135 µm, just below our target of 140 µm.

Secondly, since these results were obtained with 8 mm diameter PET based cells, the results are only valid for these cells. Depending on the application, both this dimension as the used materials might differ and a new optimization process is likely needed. A similar strategy can be used by first looking at single film lenses and subsequently fabricating a variety of LC cells, while paying special attention to the threshold thickness of the concave substrate. The final thickness can be reduced by using an asymmetric configuration with a thin layer at the convex side and a thicker but threshold dependent layer at the concave side.

3.7 Conclusion

The focus of this chapter was the design and fabrication of a spherically conformed LC cell. Since this is special kind of flexible display, existing manufacturing techniques for flexible displays were explored, resulting in a first prototype. This revealed a straightforward implementation is not possible, as application specific issues such as poor optical uniformity, lack of precise control of the dimensions and the appearance of wrinkles impede a successful integration into a contact lens. Furthermore, the yield of our process was low due to the initially used processing techniques. Therefore, new processing techniques were created to improve the yield and manufacturability while the inclusion of an additional photolithograpic layer allowed us to address other pending issues such as the optical uniformity and the need for a precisely dimensioned glue joint. A finger pattern in this layer reinforced the filling entrance while an in-depth study exposed the relationship between the thickness of the used PET-films and the formation of wrinkles. A smooth cell with a thickness of 135 µm was established by using an asymmetric configuration with a thin layer at the convex side and a thicker but threshold dependent layer at the concave side, thereby reaching our target thickness of below 140 µm. This smooth 50 µm convex – 75 µm concave configuration was therefore used as the standard configuration in the ensuing chapters.

References

[1] G. Loeb, A. Walker, S. Uematsu, and B. Konigsmark, "Histological reaction to various conductive and dielectric films chronically implanted in the subdural space", *Journal of Biomedical Materials Research*, vol. 11, no. 2, pp. 195–210, 1977.

[2] C. Hassler, R. von Metzen, P. Ruther, and T. Stieglitz, "Characterization of parylene c as an encapsulation material for implanted neural prostheses", *Journal of Biomedical Materials Research*, vol. 93B, no. 1, pp. 266–274, 2010.

[3] M. Op de Beeck, J. O'Callaghan, K. Qian, B. Morcos, A. Radisic, K. Malachowski, M. Amira, and C. Van Hoof, "Biocompatible encapsulation and interconnection technology for implantable electronic devices", *IMAPS 45th International Conference and Exhibition on Microelectronics*, 2012.

[4] E. Lueder, "Passive and active matrix liquid crystal displays with plastic substrates", *Thin-Film Transistor Technologies IV, Kuo Y., et al. (eds.) Electrochem. Soc. Proc.*, vol. 98, no. 22, pp. 336–354, 1998.

[5] M. Chanda and S. Roy, *Industrial Polymers, Speciality Polymers, and Their Applications*. 2009.

[6] H. Seitz, S. Marlovits, I. Schwendenwein, E. Müller, and V. Vécsei, "Biocompatibility of polyethylene terephthalate (trevira hochfest) augmentation device in repair of the anterior cruciate ligament.", *Biomaterials*, vol. 19, no. 1-3, pp. 189–196, 1998.

[7] G. Corporation, "Standard price list for polyethylene terephthalate, retrieved on 30th of july 2013", Goodfellow Corporation, Tech. Rep., 2013. [Online]. Available: http://www.goodfellow.com/pdf/3977_1111010.pdf.

[8] J. Pandey, Y.-T. Liao, A. Lingley, R. Mirjalili, B. Parviz, and B. Otis, "A fully integrated rf-powered contact lens with a single element display", *Biomedical Circuits and Systems, IEEE Transactions on*, vol. 4, no. 6, pp. 454–461, 2010.

[9] A. Lingley, M. Ali, Y. Liao, R. Mirjalili, M. Klonner, M. Sopanen, S. Suihkonen, T. Shen, B. Otis, H. Lipsanen, and B. Parviz, "A single-pixel wireless contact lens display", *Journal of Micromechanics and Microengineering*, vol. 21, no. 12, p. 125 014, 2011.

[10] H. Yao, A. J. Shum, M. Cowan, I. Lähdesmäki, and B. A. Parviz, "A contact lens with embedded sensor for monitoring tear glucose level", *Biosensors and Bioelectronics*, vol. 26, no. 7, pp. 3290–296, 2011.

[11] J. Souk and W. Lee, "A practical approach to processing flexible displays", *Journal of the SID*, vol. 18, no. 4, 258–265, 2010.

[12] *Flexible Flat Panel Displays*. Wiley, 2005.

[13] J. Chen, J. Ho, G. Chen, and C. Lee, "Reliability improvement of flexible amoled based on auxiliary functional film technology", *SID Symposium Digest of Technical Papers*, vol. 43, 264–267, 2012.

[14] R. Overney, C. Buenviaje, R. Luginbuhl, and F. Dinelli, "Glass and structural transitions measured at polymer surfaces at the nanoscale", *Journal of Thermal Analysis and Calorimetry*, vol. 59, pp. 205–225, 2000.

[15] S. Ying-Hung, G. P. E., I. Jang-Hi, and O. Karou, "Benzocyclobutene-based polymers for microelectronic applications", in *Polymers for Microelectronics and Nanoelectronics*, ch. 22, pp. 279–293.

[16] D. Cuypers, "Vertically aligned nematic liquid crystal microdisplays for projection applications", PhD thesis, Ghent University, 2005.

[17] P. Oswald, J. Baudry, and S. Pirkl, "Static and dynamic properties of cholesteric fingers in electric field", *Physics Reports*, vol. 337, pp. 67–96, 2000.

[18] I. I. Smalyukh, B. I. Senyuk, P. Palffy-Muhoray, O. D. Lavrentovich, H. Huang, E. C. Gartland, V. H. Bodnar, T. Kosa, and B. Taheri, "Electric-field-induced nematic-cholesteric transition and three-dimensional director structures in homeotropic cells", *Phys. Rev. E*, vol. 72, p. 061 707, 6 2005. DOI: 10.1103/PhysRevE.72.061707. [Online]. Available: http://link.aps.org/doi/10.1103/PhysRevE.72.061707.

[19] U. Wolfmeier, H. Schmidt, F. Heinrichs, G. Michalczyk, W. Payer, W. Dietsche, K. Boehlke, G. Hohner, and J. Wildgruber, "Waxes", in *Ullmann's Encyclopedia of Industrial Chemistry*. Wiley-VCH Verlag GmbH & Co. KGaA, 2000, ISBN: 9783527306732.

[20] D. Haas, "Predicting the uniformity of two-component, spin-deposited films", PhD thesis, The University of Arizona, 2006.

[21] Ethanol on PubChem Compound, retrieved on 2/9/2013. [Online]. Available: http://pubchem.ncbi.nlm.nih.gov/summary/summary.cgi?cid=702&loc=ec_rcs#x27.

[22] Acetone on PubChem Compound, retrieved on 2/9/2013. [Online]. Available: http://pubchem.ncbi.nlm.nih.gov/summary/summary.cgi?cid=180&loc=ec_rcs#x27.

[23] SU8 3000 series datasheet, retrieved on 25/9/2013. [Online]. Available: http://microchem.com/pdf/SU-8%203000%20Data%20Sheet.pdf.

[24] J. M. Shaw, J. D. Gelorme, N. C. LaBianca, W. E. Conley, and S. J. Holmes, "Negative photoresists for optical lithography", *IBM J. Res. Dev.*, vol. 41, no. 1-2, pp. 81–94, 1997.

[25] S. Jang, J. Kim, J. Bae, Y. Choi, H. Kim, S. Kim, J. Souk, and J. Kim, "Stability enhanced flexible liquid crystal display based on a micro-structure", *Molecular Crystals and Liquid Crystals*, vol. 470, no. 1, pp. 191–197, 2007.

[26] *Modern Differential Geometry of Curves and Surfaces with Mathematica, 2nd edition.* CRC Press, 1997.

[27] J. Breil, "New high-grade s-bopp and s-bopet film types produced with the linear motor stretching technology", Bruckner, Tech. Rep., 1999.

[28] H. Yao, Y. Liao, A. Lingley, A. Afanasiev, I. Lähdesmäki, B. Otis, and B. Parviz, "A contact lens with integrated telecommunication circuit and sensors for wireless and continuous tear glucose monitoring", *Journal of Micromechanics and Microengineering*, vol. 22, no. 7, p. 075 007, 2012.

4

Integration of the Electro-Optic Switching Mechanism

"The soul never thinks without a picture."

—Aristotle

4.1 Selection of Active Cell Layers

As in most Liquid Crystal Displays, an alignment layer and a transparent conductive layer need to be incorporated into the LC cell. Since we aim to use a polarizer-free guest-host configuration with a transparent voltage off state, a homeotropic alignment layer should be applied on top of the transparent conductive layer (see section 2.5.2 and Figure 2.13). Furthermore, the inclusion of these layers should be compatible with the current cell design and fabrication, in particular with the processing of the photolithographic layer. In the following paragraphs, the material selection and their integration into the existing process flow will be discussed.

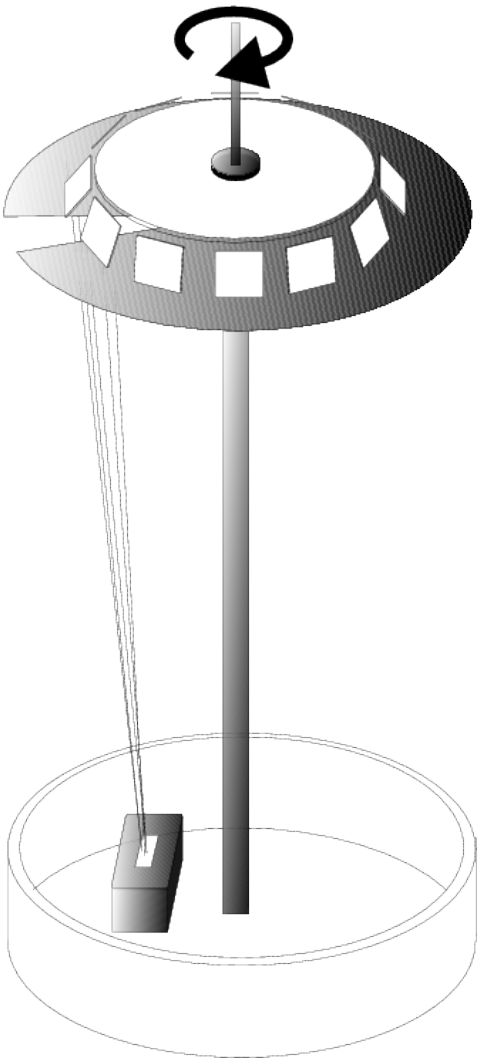

Figure 4.1: SiO_2-evaporation. A vapour stream of SiO_2-molecules hits the moving samples through a shutter plate under an oblique angle, thereby creating a homeotropic alignment layer with a small tilt angle. Image from [1].

4.1.1 Alignment Layer

Application of the homeotropic alignment layer should preferentially be contact-free, i.e. without a rubbing step, since this would likely harm the PET film surface. Moreover, since the PET films should not be heated above 150°C before molding, many known methods are excluded as they use materials which require a curing step above this temperature. Therefore, we chose oblique SiO_2-evaporation as a contact-free, low-temperature alternative, a process which was also thoroughly studied in-house in previous research [1, 2].

In this process a vapour stream of SiO_2-molecules is created in an evaporator and narrowed down using shutter plates (see Figure 4.1). Behind the shutter plates, the samples are mounted in an oblique angle (about 40°, measured with respect to the substrate normal), thereby inducing a preferential direction in the evaporated SiO_2-layer. As a result, a homeotropic alignment for the LC molecules is formed, including a small tilt angle that increases the switching speed. Normally, the spacers of an LC cell are put on top of the alignment layer, but due to the nature of the SiO_2-layer, the development process of the photolithographic spacers is likely to interfere with the quality of the alignment. Instead, the SiO_2-layer is applied after deposition and patterning of the photolithographic spacers.

4.1.2 ITO as a Conductive Layer

Indium Tin Oxide (ITO) is the standard transparent conductive layer used in rigid LCDs, but due to its brittle nature its use on flexible films is limited. Many studies about mechanical deformation of ITO layers on flexible films reveal an increase in their resistance with decreasing bending radius or increasing cyclic loading number, mainly attributed to crack formation and propagation. An overview is provided in reference [3] and references therein.

Due to the extreme deformation process and small radius of our contact lens shaped LC cells (7.8 mm), the cracking of an embedded ITO layer in these cells seemed inevitable. Nevertheless, our first prototype (see section 3.3) was fabricated with ITO since its use in conformable displays, like our LC cell, has been suggested by other authors [4]. We used a 100 nm thick ITO film which was deposited on top of our PET-films by RF sputtering and had a resistivity of 50 ohm/□ .

As can been seen in Figure 4.2, the test cells indeed revealed a cracked ITO layer, but more worrisome was the misalignment of the LCs in some areas which were delineated by crack lines. Although this suggests the ITO and/or the alignment layer delaminate during the molding step, the exact nature of this phe-

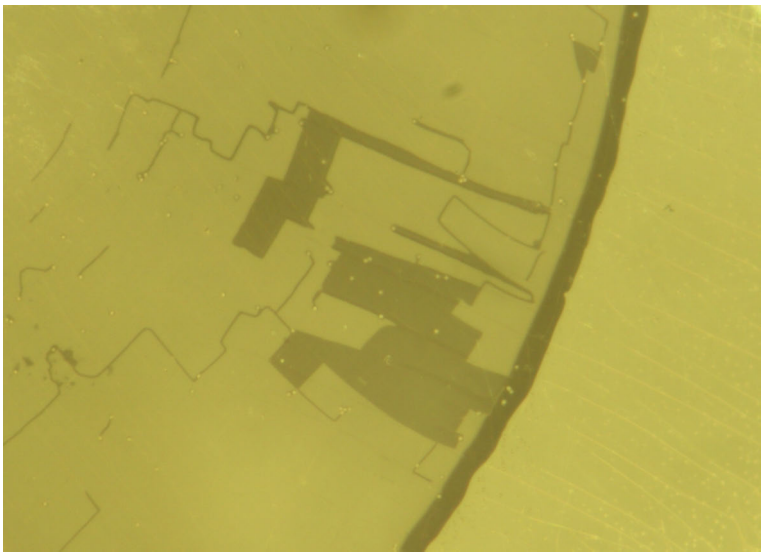

Figure 4.2: After deformation, misalignment of the LCs could be observed in some areas that were delineated by crack lines in the ITO.

Table 4.1: PEDOT:PSS optimization. Two spin coated layers on top of each other with a spin speed of 1000 rpm yielded the best results.

spin speed (rpm)	thickness (nm)	sheet resistance (ohm/□)
1000	69	431
2000	33	740
2 x 1000	110	200
2 x 2000	46	340

nomenon was not studied in detail. Nevertheless, it is clearly detrimental to the overall optical quality of the LC cell, prompting the use of other flexible conductive materials over ITO.

4.1.3 PEDOT:PSS as a Conductive Layer

As an alternative to ITO, we selected poly(3,4-ethylene-dioxy-thiophene):poly(styrene¬sulfonate) (PEDOT:PSS), a conductive polymer with a proven flexibility [5] which already received considerable attention from

the display community [3]. A commercial solution (Orgacon^{TM} S305 by AGFA) was chosen and the deposition parameters by spin coating were optimized (see Table 4.1). This was necessary because, although flexible, PEDOT:PSS has higher resistivity values than ITO. A sufficiently conducting PEDOT:PSS layer should thus be obtained while still having an acceptable quality and practical deposition process.

The optimization was done by spin coating the solution on silicon wafers at various spin speeds and measuring the sheet resistance with a 4-point probe and the thickness with an ellipsometer. Since the sheet resistance of the PEDOT:PSS was still high for single spin coated layers, double spin coated layers were also investigated. Three layers were not investigated because this starts to become unpractical, while the quality of the total stack also tends to decrease with increasing number of layers. Next to this, we found an acceptable trade off with a double spin coated layer spun at 1000 rpm, having a sheet resistance of 200 ohm/□ and a thickness of 110 nm.

4.2 Integration of PEDOT:PSS in the LC Cells

4.2.1 Adhesion of PEDOT:PSS on PET

Orgacon S305 is actually a dispersion of the PEDOT:PSS polymer in water and spin coating the dispersion directly on top of PET generally leads to an unevenly distributed coverage, with many spots having no deposited PEDOT:PSS. This is due to the largely hydrophobic nature of the PET surface, having the natural tendency to repel water. By applying a mild plasma treatment (see table 4.3) to the PET surface the wettability of the PEDOT:PSS solution can be improved and a uniform layer can be applied. Deposition of the second PEDOT:PSS layer (needed to attain a sufficiently low sheet resistance) does not require an additional plasma treatment as the wettability of solution on the first deposited layer is good.

4.2.2 Compatibility Problems

The choice for SiO_2-evaporation and PEDOT:PSS resulted in the requirement to develop the photolithographic layer on top of the PEDOT:PSS. As mentioned in section 3.5, we had selected SU8 3010 in our study of the mechanical design of our LC cell, as this is a chemically and thermally stable photoresist suitable for permanent application. However, the creation of a patterned SU8 layer directly on PEDOT:PSS is not straightforward because of two main reasons.

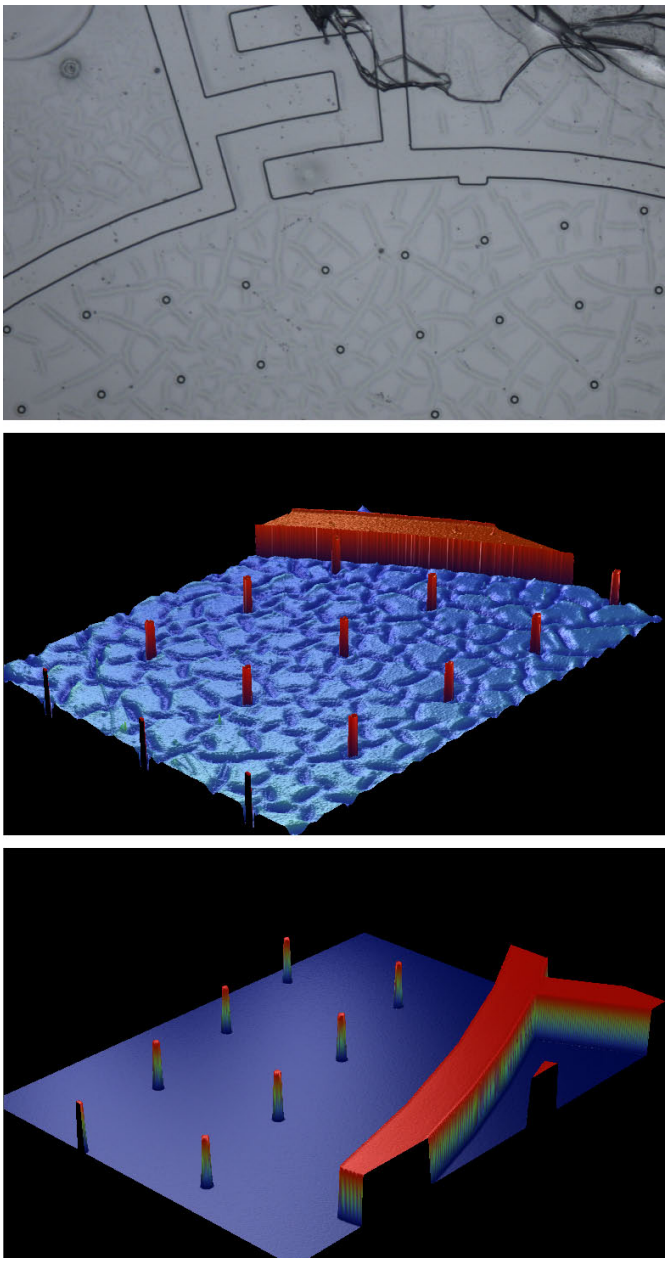

Figure 4.3: Compatibility problems between PEDOT:PSS and SU8 3010. Top: When SU8 is developed on top of PEDOT:PSS a thick residual layer of damaged unexposed SU8 remains present. Middle: Optical profilometer measurements of the poorly developed SU8 indicate a height difference of 3.6 µm exists between the exposed and unexposed area, suggesting the residual layer is about 6.4 µm thick. Down: When developed on top of a inorganic layer such as SiO_2 or directly on PET, no problems are observed.

First, PEDOT:PSS films can be damaged by aqueous solutions or certain solvents which are used as developers in conventional photolithography. Processing with these solvents should thus happen with care. Second, damage of the unexposed photoresist layer is observed when trying to process SU8 directly on top of PEDOT:PSS (see Figure 4.3). Optical profilometer measurements of the poorly developed SU8 indicate a height difference of 3.6 µm exists between the exposed and unexposed areas, suggesting a residual layer of about 6.4 µm thick remains present.

Initially, this came as a surprise as no problems were observed when the SU8 was developed on top of a inorganic layer such as SiO_2 or directly on PET. A literature survey revealed this is a common problem when a photoresist containing a photoacid generator (such as SU8) is used on top of an organic layer such as PEDOT:PSS [6, 7]. The phenomenon has been ascribed to acid diffusion and more in particular as proton diffusion from the PEDOT:PSS layer into the unexposed photoresist layer causing decomposition of the acid-labile photoresist. This affects the resolution and the overall quality of the patterned image.

Some new photoresists that are PEDOT:PSS compatible have been developed recently, but they are still in the early stages of commercialization and are also not meant for permanent application [6, 8]. Although they might be a good choice in the future, their inclusion as an SU8 replacement in the LC cells seems less appropriate at this moment.

4.2.3 SiO_2 Barrier Layer

To circumvent the compatibility problem, the (non-oblique) evaporation of an additional SiO_2 barrier layer on top of the PEDOT:PSS was proposed. Initial tests on glass indicated a thickness of 50 nm proved to be sufficient to prevent proton diffusion from the PEDOT:PSS to the SU8 3010 layer as no negative effects could be observed. Since no SU8 processing is needed at the counter side of the LC cell, a barrier layer at this side was originally not foreseen.

However, when an obliquely evaporated SiO_2 alignment layer (measuring only 6 nm) was directly applied on top of the PEDOT:PSS, the alignment of the LC molecules was not uniform throughout the LC cell, suggesting some interaction is occurring between both layers. Although the exact origin was not studied in-depth, this effect is clearly detrimental for the overall quality and a barrier layer at the counter side of the LC cell was thus also foreseen.

4.3 Fabrication of Non-Patterned LC Cells

To test and inspect the selected active layers some uniform, non-patterned LC cells were fabricated. However, during the first run it was observed that almost none of the cells could be filled via the vacuum filling method, prompting us to examine and solve this problem before the cells could be completed. Thus, prior to a detailed description of the new process flow, we will address this ineffective vacuum filling method in the ensuing paragraph.

4.3.1 Cell Reopening

Since the vacuum filling method did work when fabricating the first prototypes mentioned in section 3.3, the reason for its ineffectiveness could be narrowed down to two possible reasons: either an opening was present somewhere in the glue joint preventing creation of a vacuum, or the filling entrance was sealed off somewhere along the fabrication process. As an opening in the glue joint can be relatively easily spotted upon visual inspection and no such openings were observed, an inadvertent closing of the cell during the fabrication process was the main suspect.

Indeed, it was quickly realized that the photothermal ablation mechanism of the CO_2-laser was the main culprit, melting the PET-films locally at the laser spot, thereby joining them together at the side of the cell. To reopen the cell in a quick and easy way, a process was proposed in which an excimer laser (248 nm wavelength, 3-7 ns FWHM pulse width) makes a small (200 by 200 µm square) but precisely controlled cut at the clogged area at the filling entrance. In contrast with the CO_2-laser, excimer laser ablation predominately involves a photochemical process, allowing for a more precise cut, but coming at the cost of speed (which is the main reason the CO_2-laser is used for the general cutting of the LC cell).

To determine the optimal excimer ablation parameters, a series of experiments was performed in which a varying number of pulses (each measuring 200 by 200 µm square) with a fixed fluence (300 mJ/cm^2) was fired at a dummy PET-film. By measuring the depth of the ablation craters with an optical profilometer, a mean depth per pulse could be determined (see Table 4.2). The differences between the determined values are mainly attributed to the surface roughness of the ablated PET (see also section 4.4.2), which makes it difficult to accurately measure the depth, and the precise orientation of the laser beam according to the substrate (the laser beam should hit the PET surface at a 90° angle).

We therefore chose to apply 300 pulses, which would lead to a crater depth of

Table 4.2: To reopen the cell, a series of experiments was performed to determine the optimal excimer ablation parameters. The pulses had a fluence of 300 mJ/cm^2 and the depth was measured with an optical profilometer.

number of pulses	measured depth (µm)	depth per pulse (µm)	extrapolated depth at 300 pulses (µm)
44	10.6	0.24	72.3
48	11.2	0.23	70
52	12.3	0.24	71
88	20.8	0.24	70.9
96	22.3	0.23	69.7
104	23.7	0.23	68.4

about 70 µm. In this way, when aiming from the top, the laser would cut through the top PET film and end about 20 µm deep in the second PET-film, thereby providing a sufficient margin to assure the clogged opening at the filling entrance is freed. A typical reopening using the suggested parameters can be seen in Figure 4.4 and all successive LC cells using this method could indeed be filled via the vacuum filling method, proving its efficacy.

4.3.2 New Process Flow

The new process flow is similar to the one used to fabricate the first prototype, but for completeness the whole flow will be described. The new process flow starts with the lamination of cleaned PET films (50 and 75 µm) onto a glass carrier using a temporary adhesive (see Figure 4.5). After a plasma treatment to improve wettability, PEDOT:PSS (Orgacon S305) is spincoated on top of the PET films and a 50 nm thick buffer layer of vertically evaporated SiO_2 is applied onto the PEDOT:PSS. The 10 µm thick photoresist (SU8 3010) is spin coated and patterned on top of the 75 µm PET film, bearing the features as mentioned in section 3.5. Both PET films then receive the alignment layer by obliquely evaporating SiO_2.

A flexible glue (UVS 91) is deposited just next to the SU8 barrier with an automatic dispenser, creating a circular glue joint with a small interruption at the interlaced finger pattern. Afterwards, the 50 µm PET film is put on top and the total stack is then pressed together, ensuring a close contact as the stack is subsequently illuminated with UV light to cure the glue joint. After curing, the

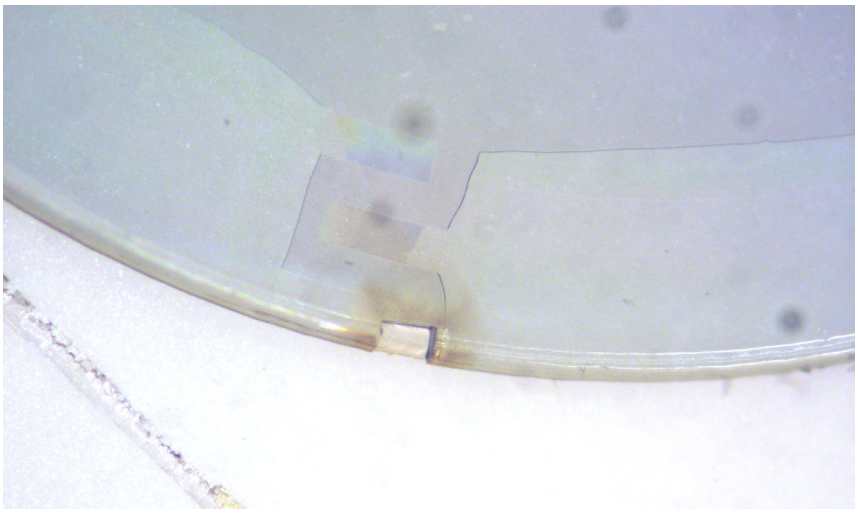

Figure 4.4: The cell was reopened by using an excimer laser to create a 200 by 200 μm square cut at the filling entrance. The laser would cut through the top PET film and end about 20 μm deep in the second PET-film, thereby providing a sufficient margin to assure the clogged opening at the filling entrance is freed.

glass carriers are removed and the LC cells are cut out through the glue joint with a CO_2-laser. Additional rectangular contact areas are provided at the side of the LC cell which, after fabrication, can be connected to a power source with a copper tape.

An excimer laser is used to make a precise cut at the filling entrance, going through the first PET film but stopping about 20 μm deep in the second film, thus reopening the LC cell entrance. The flat, cut-out lenses are then molded in an aluminum mold with a curvature radius of 7.8 mm. The molding process starts with heating the whole mold to a temperature of 175°C and, when the mold reaches this temperature, the lenses are placed onto the bottom part of the mold and a soaking time of several minutes is applied.

Afterwards, the upper part of the mold along with a weight of 1.2 kg was placed on top and the total ensemble is allowed to gently cool down until it is assured that the temperature of the mold is again well below the glass transition temperature of PET before removing the lenses from the mold. After molding, the LC cells are filled with the guest-host liquid crystal mixture with a vacuum filling method and are sealed with the same glue used for the glue joint. This

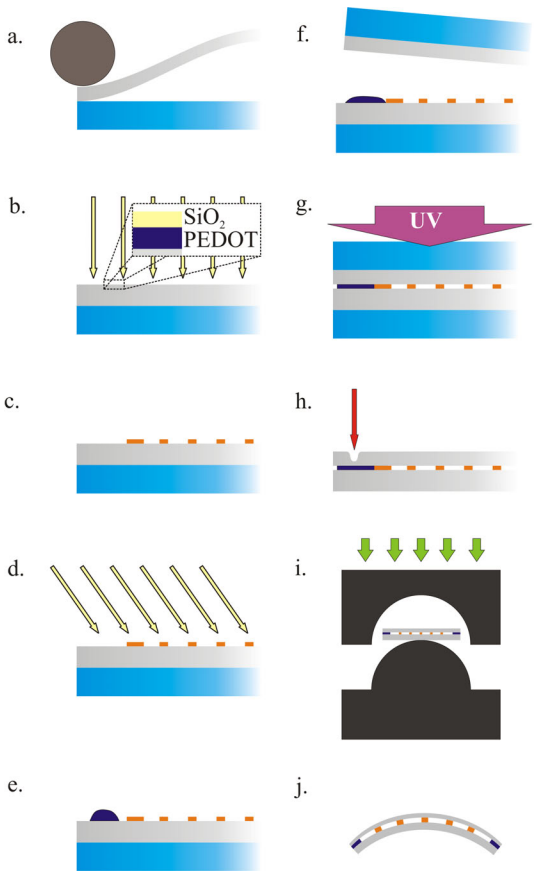

Figure 4.5: New process flow. a. the PET-films are laminated onto a glass carrier b. PEDOT:PSS is spincoated on the PET-films and the buffer layer is vertically evaporated on top c. the photolithographic layer is applied on the 75 µm PET-film d. the alignment layer is obliquely evaporated e. the glue is deposited just next to the glue barrier f. a 50 µm PET-film including the PEDOT:PSS, the buffer layer and the alignment layer is put on top g. the total stack is pressed together and illuminated with UV light h. after removal of the glass carriers, the lenses are cut out through the glue joint with a CO_2-laser and the entrance is reopened with an excimer laser i. the lenses are molded with a spherical aluminium mold j. after molding, a spherically conformed LC cell is formed, which can then be filled and sealed.

process flow is also summarized in table 4.3, but does not include step 5, which is used for patterning (described in section 4.4.2).

Table 4.3: Process flow of a spherically conformed LC cell

Step	Description	Details
1	Clean glass substrates	RBS overnight
2	Clean PET substrates	N_2 blow, DI rinse, 5 min acetone USA, DI rinse, blow dry with N_2
3	Lamination of PET - Spin wax - Postbake - Laminate PET	 1000 rpm, 30s, 2.5 g/10 ml solution hotplate, 1 min @ 95°C manual lamination
4	Apply PEDOT:PSS - Plasma treatment - Spin PEDOT:PSS - Postbake	 1 min, 150 W power (50%), 0.8 mbar in air 2*1000 rpm, 30 s spin time, 5 min @ 95°C on hot plate in between spin cycles hotplate, 5 min @ 95°C
5	Pattern PEDOT:PSS	bottom substrate, 40 µm circle mask, 125 mJ/cm^2 fluence, 50% overlap (2 pulses per location)
6	Evaporate SiO_2 barrier layer	50 nm
7	Apply photolithographic layer - Spin SU8 3010 - Illumination - Developing	 5s @ 500 rpm, 30 s @ 3000 rpm, 300 rpm/s acceleration 43 s, 5 mW/cm^2 6 min SU8 developer, 30 s in IPA
8	Evaporate SiO_2 alignment layer	6 nm, oblique evaporation
9	Glueing of stack - Dispense glue - UV curing	 UVS91, 250 µm needle, 1.3 mm/s 100 mW/cm^2, 2 min per corner
10	Release	delamination method, hotplate @ 125°C
11	Laser cutting - Cut outline - Clear filling entrance	 CO_2-laser, 97.5 % overlap (40 pulses per location), 1.1 J/cm^2 excimer laser, 300 pulses, 300 mJ/cm^2
12	Molding	hotplate at @ 175°C
13	Filling	vacuum filling
14	Sealing	apply drop of UVS91 at entrance, illuminate with 100 mW/cm^2 for 1 min

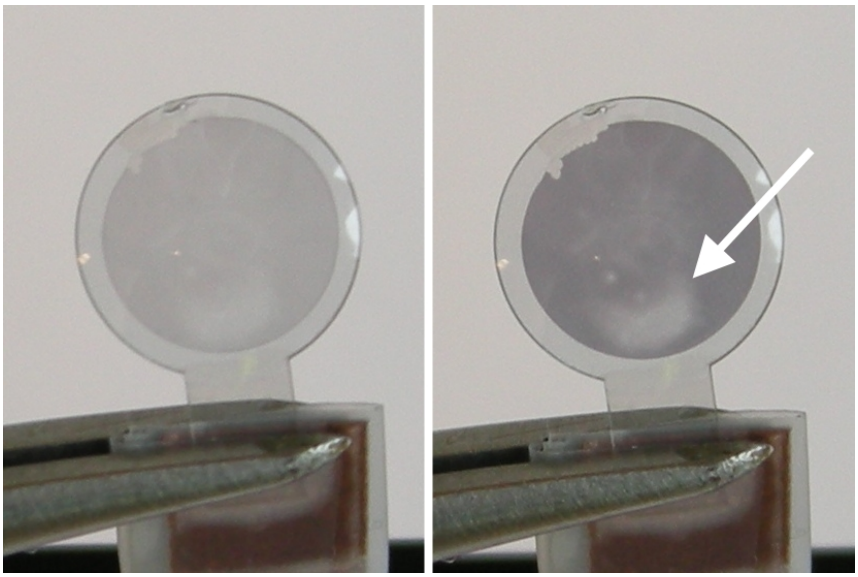

Figure 4.6: When using the first mold, most lenses showed an oblong shaped spot, which could be easily seen in the voltage on state. This oblong shaped spot was randomly located in the cells and did not appear to have a direct relationship with the spacer density, suggesting its origin was actually related to some irregularity in the used mold itself.

4.3.3 LC Cell Properties and Mold Influence

Mold Irregularity

In contrast to our first prototype, the LC cells fabricated with our new process flow did not show any wrinkles while no short circuited cells were found. The lack of wrinkles is a direct result of our study of the wrinkle formation (see section 3.6) and the choice to use the 50 µm convex – 75 µm concave combination. Seeing that all cells were able to switch electro-optically indicates the photolithographically defined spacers are indeed outperforming the conventional ball spacers. The uniformity of the cells was, however, not yet as desired.

In about seven out of nine cells from each process batch, a spot with a reduced contrast in the voltage on state could easily be observed, similar to the one in our first prototype (see Figure 3.9 & 4.6). This oblong shaped spot was randomly located in the cells and did not appear to have a direct relationship with the spacer density, suggesting its origin was actually related to some irregularity in the used

Figure 4.7: Three generations of molds. On the left the first mold used for our first prototype, in the middle a CNC fabricated mold which was deemed unpractical due to its size and on the right the third generation mold with carefully tuned dimensions.

mold itself. Such an irregularity comes to no surprise as the fabrication process of the mold was a partially manual process (especially the cascaded polishing) and was certainly prone to errors. Therefore, different molds were obtained through external partners which were fabricated with automated CNC process.

New Molds

As can be seen in Figure 4.7 the second generation mold was designed with a mantle at the concave side, forming a guiding mechanism for the convex side. Since both sides were made from the same metal, the two sides actually easily jammed when used. Next to this, although it was also made from aluminium, its large size led to large cooling down times. These issues made the mold unpractical and prevented a proper evaluation. Nevertheless, the CNC process did indeed lead to a much more precise spherical shape, showing its use is indispensable.

A third generation mold was carefully designed (see Figure 4.7 & 4.8 and fabricated in close collaboration with our external partner. The size of this mold

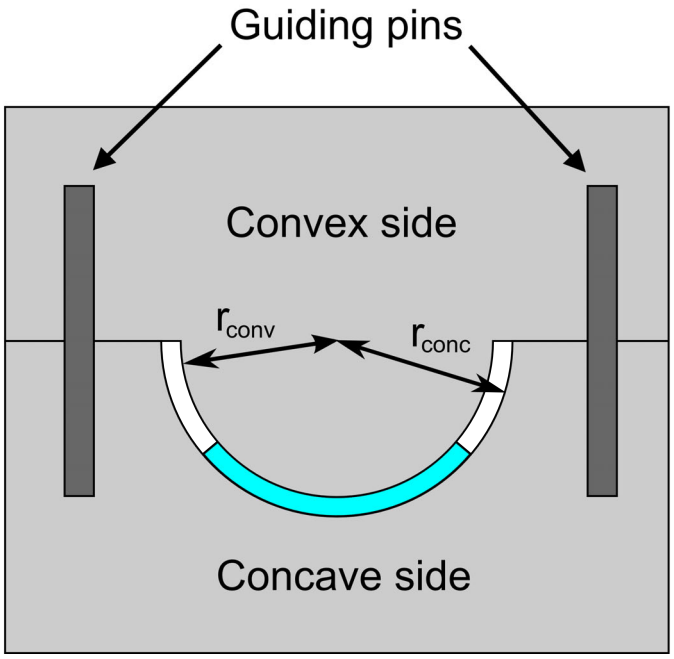

Figure 4.8: Design of the third generation mold. A constant distance of 135 µm was obtained by setting the radius of the convex side (r_{conv}) at 8 mm and the concave side (r_{conc}) at 8.135 mm and concentrically locating both sides to each other. At this location, the deformation becomes pressure independent, while lateral movements are suppressed by guiding pins. The blue shell represents the LC cell.

was kept small and the guiding pins were made of steel, providing a smooth slide in the foreseen holes of the aluminium body. As the thickness of the LC cell has been fixed at 135 µm, this was also incorporated in the mold's design. Once both sides of the mold are touching at the surrounding planes of the spherical surfaces, the distance between the surfaces is always fixed at 135 µm and will thus become pressure independent.

The constant distance was obtained by setting the radius of the convex side at 8 mm and the concave side at 8.135 mm and locating them concentrically to each other. The 8 mm radius at the convex side is slightly larger than the 7.8 mm from the first generation mold, which was mainly to take into account the offset in the BOZR after embedding in the material used for the biocompatible body. Anyway, its influence was deemed to be small in this stage of the research while a BOZR

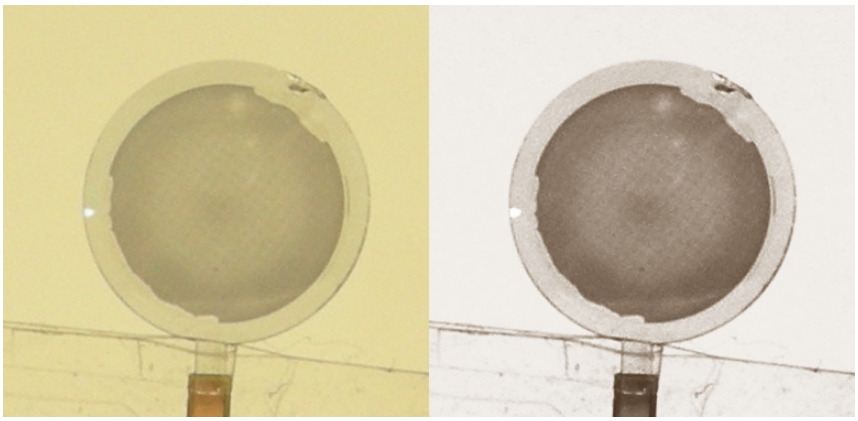

Figure 4.9: Cells molded with the 3th generation mold and having a 300 µm spacer pitch showed 3 different, more or less concentric zones with varying uniformity and contrast. Left: Original image. Right: Enhanced for clarity.

of 8 mm still fits within the bulk of used BOZRs of conventional contact lenses.

Influence Spacer Density

When the third generation mold was used, the oblong shaped spot was no longer present and uniform cells could be obtained. The accuracy of the mold (less than 5 µm of total deviation[1] and the possibility to more precisely control the processing conditions during the molding step (fixed temperature profile and pressure) clearly proved to be important. However, this did not mean all cells were uniform, but interestingly a relationship between spacer density and uniformity could be observed.

Cells with a 300 µm spacer pitch showed 3 different, more or less concentric zones with varying uniformity and contrast, while cells with a 150 µm or 200 µm pitch were uniform (see Figure 4.9 & 4.10). As could be expected, having a sufficiently high spacer density is important when aiming for uniform cells, although this comes at the expense of contrast (see ensuing section). Assessment of this trade-off should preferably be repeated for new designs or materials.

[1]Unfortunately, further information was more or less considered as in-house knowledge of the external partner

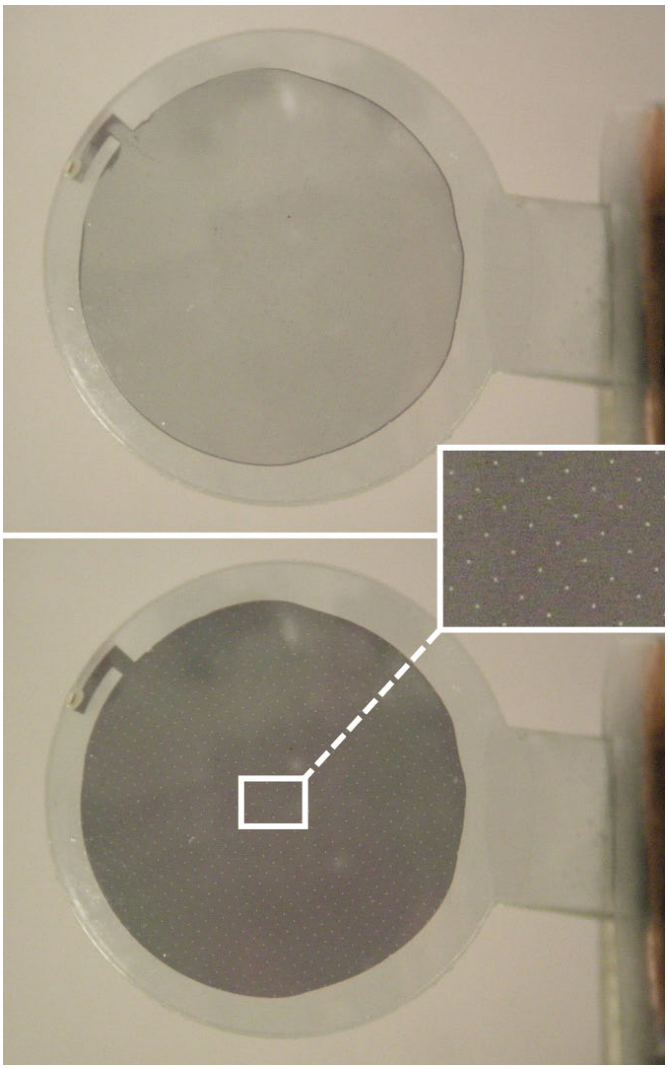

Figure 4.10: LC cells with a 150 µm or 200 µm pitch showed a clear voltage off (Top) and voltage on (Bottom) state. Inset: A microscopic image of the LC cell reveals that the photolithographic spacers can easily be distinguished in the black, voltage on state, as they are leaking more light than their surroundings.

Photolithographic Spacers

A microscopic image of the LC cell reveals that the photolithographic spacers can easily be distinguished in the black, voltage on state, as they are leaking more

light than their surroundings (see Figure 4.10). Due to their small size this poses no problems in terms of visibility as they are hardly observable by the naked eye. Furthermore, should a contact lens with an embedded LC cell reside on the cornea, these spacers would not be visible for the wearer as the eye cannot focus on an object in such a close proximity. The leakage of light through the spacers does, however, negatively affect the contrast of the display, but this could be solved by using a black photoresist, as was already explored by [9].

A closer look at the spacers in the voltage off state (see Figure 4.11) reveals that the alignment in the surroundings of the spacers is not perfect. Due to the oblique evaporation a shadow zone is present behind the spacers, as this area cannot be reached by the SiO_2-molecules and as a result, the LC molecules will not align homeotropically. The dark band observed at the front side of the spacers stems from the conflicting alignment directions imposed at the front side of the spacers and the bottom of the LC cell.

The LC molecules will align perpendicular onto the spacer wall and a transient zone can be observed until the LC molecules are again homeotropically aligned with respect to the bottom of the LC cell. The potential negative impact of this effect will depend on the application or more in particular, on the area of the affected area versus the pixel size needed for the application. However, for applications such as an artificial iris or a multifocal contact lens this should not pose any problems.

4.4 PEDOT:PSS Patterning

Although a uniformly switching LC cell has been achieved, practical applications need pixelated cells and therefore a patterning process for the PEDOT:PSS layer is required. Many patterning methods for organic materials have already been investigated, such as photolithography, embossing or inkjet printing [10], but no standard procedure has been established yet. Furthermore, not all of these techniques can be straightforwardly used on polymer based substrates. Reactive Ion Etching, for instance, can be used to etch an exposed organic layer beneath a patterned photoresist, but has little discrimination between the organic material and the polymer substrate and will likely damage the substrate. This method is therefore preferably used on inorganic substrates.

For this work, a patterning method should thus be selected and investigated that is compatible with the substrate (our PET-films). Next to this, the method should be versatile and preferably upscalable. Although we briefly investigated

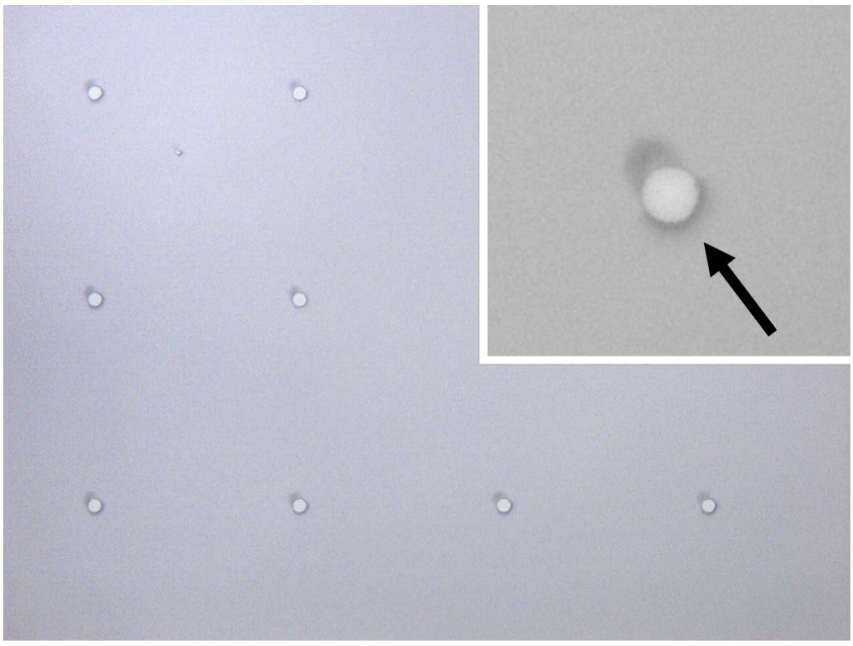

Figure 4.11: The matrix of vertical spacers after filling the cell with LC. Top Right: a close-up of such a spacer. The arrow represents the evaporation direction

a patterning method suggested by the PEDOT:PSS supplier based on chemical deactivation, we eventually selected laser ablation as our preferred means. A detailed overview of our patterning experiments is given below.

4.4.1 Chemical Deactivation

Chemical deactivation involves the extreme increase in resistivity of the PEDOT:PSS by briefly exposing it to a selected chemical. In this way, its conductive functionality is nullified while the layer remains mechanically intact on the substrate. A conductive pattern can be achieved by applying a photolithographic mask on top of the PEDOT:PSS before exposing it to the chemical. Seeing the problems with SU8, selecting a suitable photoresist was important and after some trial and error experiments with different photoresists we eventually achieved the best results with AZ 4562 (AZ Electronic Materials GmbH, Germany). Even with this resist, patterning was not straightforward.

Firstly, adhesion between the AZ 4562 and the PEDOT:PSS was poor, and

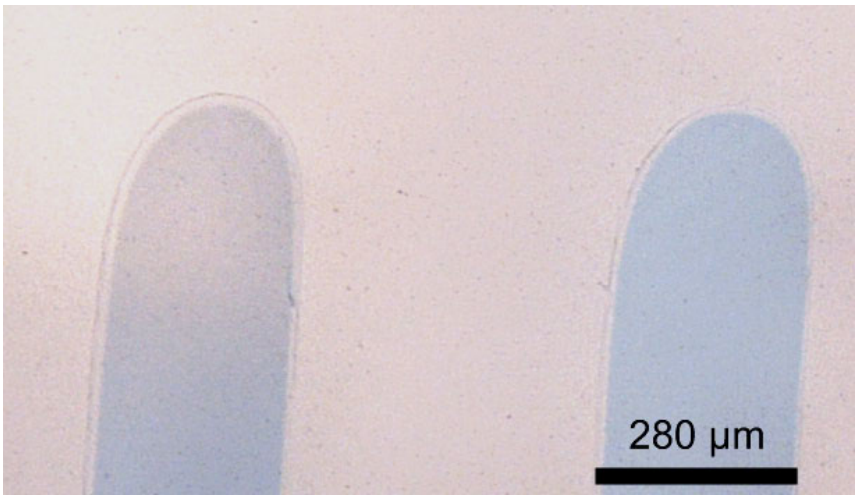

Figure 4.12: Chemical deactivation of PEDOT:PSS was accompanied by a significant underetch, limiting the resolution. White areas are deactivated and blue areas are conducting PEDOT:PSS.

a relatively strong plasma treatment with pure O_2 was needed to ensure even the finest photoresist features (about 25 µm) of our initial test mask remained attached. Secondly, when using NaOH as a chemical deactivator, no sufficiently deactivated PEDOT:PSS could be obtained without a significant underetch (see Figure 4.12), which greatly affects the resolution. LC cells in which this underetch was being avoided by minimizing the deactivation time only showed a uniform, non-patterned switching. Mainly because of this underetch this method was abandoned for laser ablation

4.4.2 Laser Ablation

When laser ablating PEDOT:PSS the goal is to partially remove material with an excimer laser, thereby creating a desired pattern. Such a method can either involve the removal of large areas of PEDOT:PSS or by just electrically isolating different areas from each other by only removing a thin line between adjacent patterns. Both methods haven been tried and investigated, but either way the challenge is to remove the PEDOT:PSS while minimizing the damage to the underlying PET.

Figure 4.13: After developing a patterned photoresist on top of the PEDOT:PSS, a laser with a 200 by 200 µm square beam shape is scanned across the surface, thereby ablating both the top layer of the photoresist as the PEDOT:PSS layer. In the middle of the picture a ablated PEDOT:PSS flake can be seen, which is washed away in a subsequent step.

Scanning Technique

When using the excimer laser for PEDOT:PSS ablation, one has to take into account the beam shape that is hitting the substrate. This beam shape is formed by a mask after it has been homogenized to assure the intensity profile is equal across the beam. In our case, a 200 by 200 µm square shape was used, which poses certain challenges when aiming to pattern large, varying designs. Firstly, since we want to pattern and thus remove large areas across the whole LC cell, the beam has to scan across the entire 8 mm diameter cell with its 200 by 200 µm square beam shape. Secondly, the square shape makes it difficult to make detailed, non-square patterns. One either has to make a pixelated looking image by only using adjacent 200 by 200 µm square pulses, or use overlapping pulses in which case the total received dose will vary across the ablated regions.

To avoid the latter problems, we proposed to scan the whole target area only

Table 4.4: Influence of fluence on PEDOT:PSS ablation on top of PET.

Fluence (mJ/cm^2)	Result
50	many flakes, incomplete PEDOT:PSS removal, almost no damage to the PET surface
75	little flakes, minor damage to PET surface
125	almost no flakes, scattering structures appear

after applying a patterned photoresist on top of the PEDOT:PSS (see Figure 4.13). In this way, the final pattern is defined by the pattern in the photoresist, while the excimer laser is only used to remove material. Of course, this means also a part of the photoresist will be removed, but since the used AZ 4562 (which was optimized during the chemical deactivation experiments) is much thicker than the PEDOT:PSS (6.2 µm versus 110 nm) this poses no problem. In a final step, the remaining photoresist is stripped, revealing an intact, patterned PEDOT:PSS layer.

The ablation of the PEDOT:PSS itself needed careful tuning as the PET was easily damaged by the excimer laser (see table 4.4). As shown in Figure 4.14, when the fluence was too high a highly scattering surface structure emerges, which has been linked to different etch rates between amorphous and semi-crystalline regions in the PET-film [11]. This highly scattering state is clearly detrimental to the optical quality of the LC cell and should be avoided. Even with a more appropriate fluence, this phenomenon can start to appear at the edges of two adjacent pulses when the inter-pulse distance is too narrow as in the overlapping zones more energy will be delivered to the substrate (see Figure 4.15).

Furthermore, the lower the fluence and larger the inter-pulse distance, the more flakes could be observed (see Figure 4.15). These flakes are partly attached PEDOT:PSS layers at the pulse intersections, which sometimes can be washed away and disappear during the stripping of the photoresist. Ultimately, a trade-off between avoiding these flakes and the PET being damaged was made by using a 75 mJ/cm^2 fluence and a 212 µm inter-pulse distance. The inter-pulse distance is slightly larger than the foreseen 200 by 200 µm square beam shape because the beam is in fact not perfectly shaped and some stray light is present at the sides. Nevertheless, even with optimized parameters, some minor craters in the

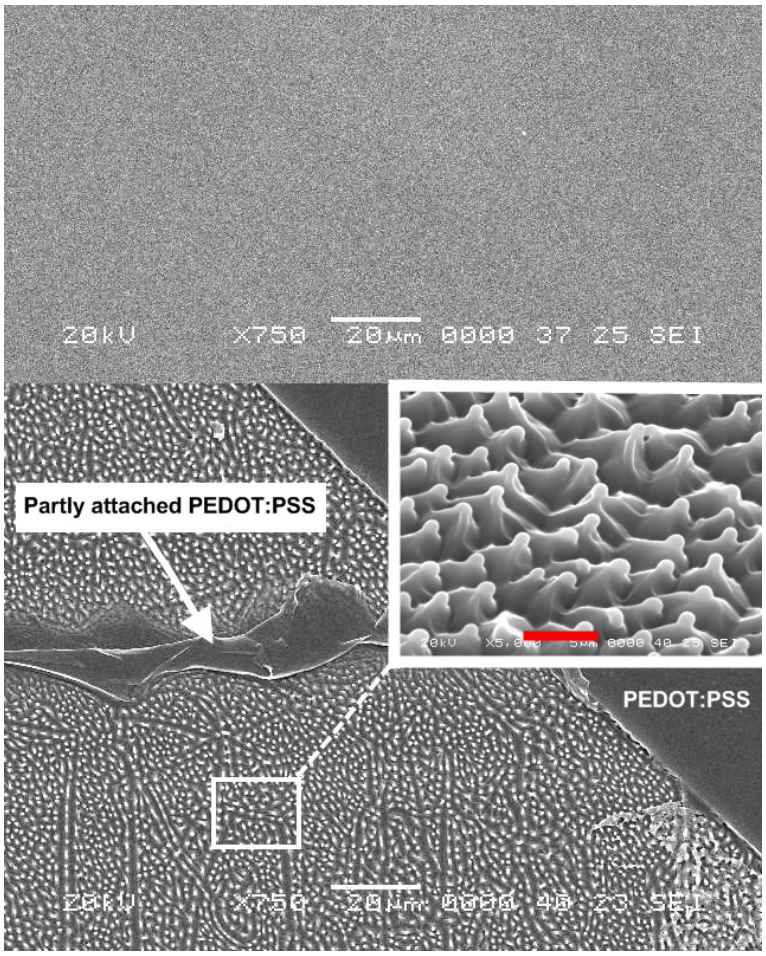

Figure 4.14: SEM images of the ablation of PEDOT:PSS on top of PET. Top: A bare PET film showing an optically clear surface. Bottom: When the laser fluence is too high the PET also gets ablated and a highly scattering surface structure emerges. The dark area at the right is PEDOT:PSS. The dark band in the middle is PET with partly attached PEDOT:PSS in between two pulses with a large inter-pulse distance. Inset: Detailed image of the scattering structures. The red scalebar is 5 µm.

PET-film away from the intersections seemed to be unavoidable.

The litmus test for using the scanning technique for the PEDOT:PSS patterning was its implementation in a working LC cell. As can be seen in Figure 4.16, this

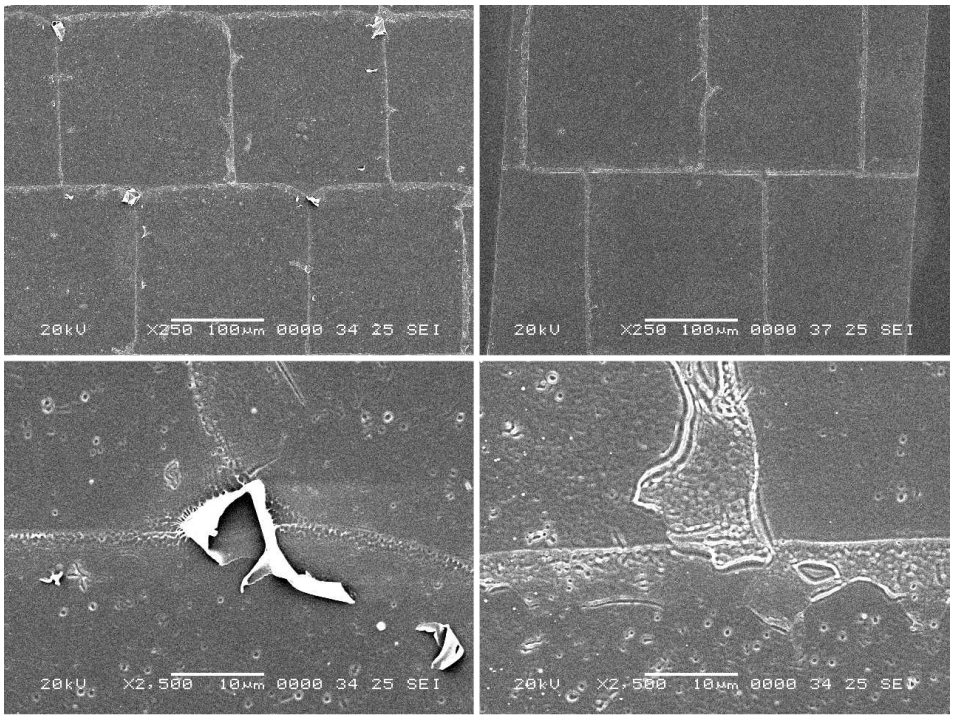

Figure 4.15: Pulse intersections. Top Left: With an appropriate fluence the damage to the PET-film can be minimized, but partly attached flakes can be present at the pulse intersections. Top Right: Flakes can sometimes be washed away and disappear during the stripping of the photoresist. Bottom Left: Close-up of a partly attached flake. Bottom Right: Even with an optimized fluence some minor damage with emerging scattering structures seemed unavoidable. Away from the intersections minor craters can also be observed.

unfortunately revealed the LC molecules did not align properly in the ablated areas and even a large non-uniformity within the ablated area is observed. Sometimes, the square mark of a single pulse could even be discriminated. Since these areas were darker than non-patterned areas, a deviation of the foreseen homeotropic alignment is suspected. The reason for this failed alignment is not entirely clear. A chemical reaction between the PET-surface and the alignment layer seems unlikely since the SiO_2-barrier layer is present between both layers.

The misalignment could, however, be a result of the topological defects introduced by the ablation process (see Figure 4.17). The molecules could still

Figure 4.16: Patterned LC cell using the scanning technique. Top: The voltage off state reveals the LC molecules did not align properly in the ablated areas and sometimes the square mark of a single pulse could even be discriminated. Bottom: When applying a voltage and thereby switching the cell it was confirmed that the PEDOT:PSS was sufficiently removed.

be homeotropically aligned onto these defects, but this would result in a non-perpendicular alignment towards the incoming light going straight through the LC cell. When applying a voltage and thereby switching the cell it was confirmed

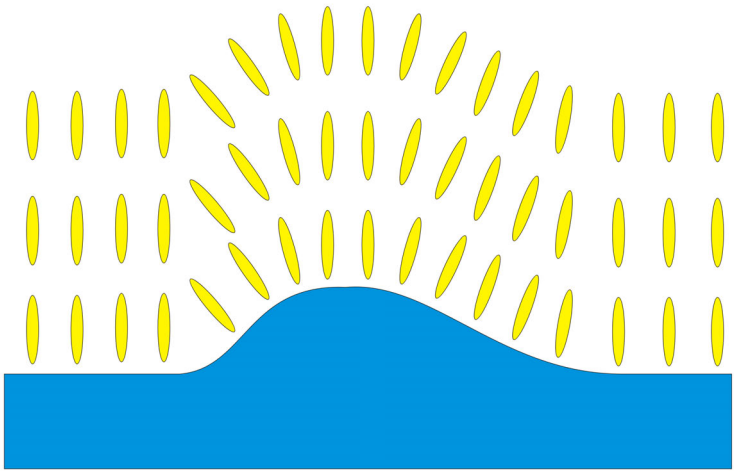

Figure 4.17: The misalignment of the LC molecules (in yellow) could be a result of the topological defects introduced by the ablation process. The molecules could still be homeotropically aligned onto these defects, but this would result in a non-perpendicular alignment towards the incoming light going straight through the LC cell.

that the PEDOT:PSS was sufficiently removed. Nevertheless, the misalignment is unacceptable when aiming for a sufficiently high optical quality of the LC cell. Therefore, this method was eventually abandoned for the isolation technique, as there only a minor fraction of the surface is ablated, resulting a better performance.

Isolation Technique

The isolation technique involves electrically isolating different areas from each other by only removing a thin line between adjacent patterns. The main reason why this method was not used initially was that after patterning, the redundant areas should either be grounded or remain present as a floating electrode. Floating electrodes can sometimes interfere with nearby active electrodes and are thus generally avoided. On the other hand, the technique is simple and straightforward and could be easily upscaled and used in roll-to-roll processing. Since the scanning technique bared unsatisfactory results, this method was subsequently investigated.

In contrast with the scanning technique, the isolation technique requires the

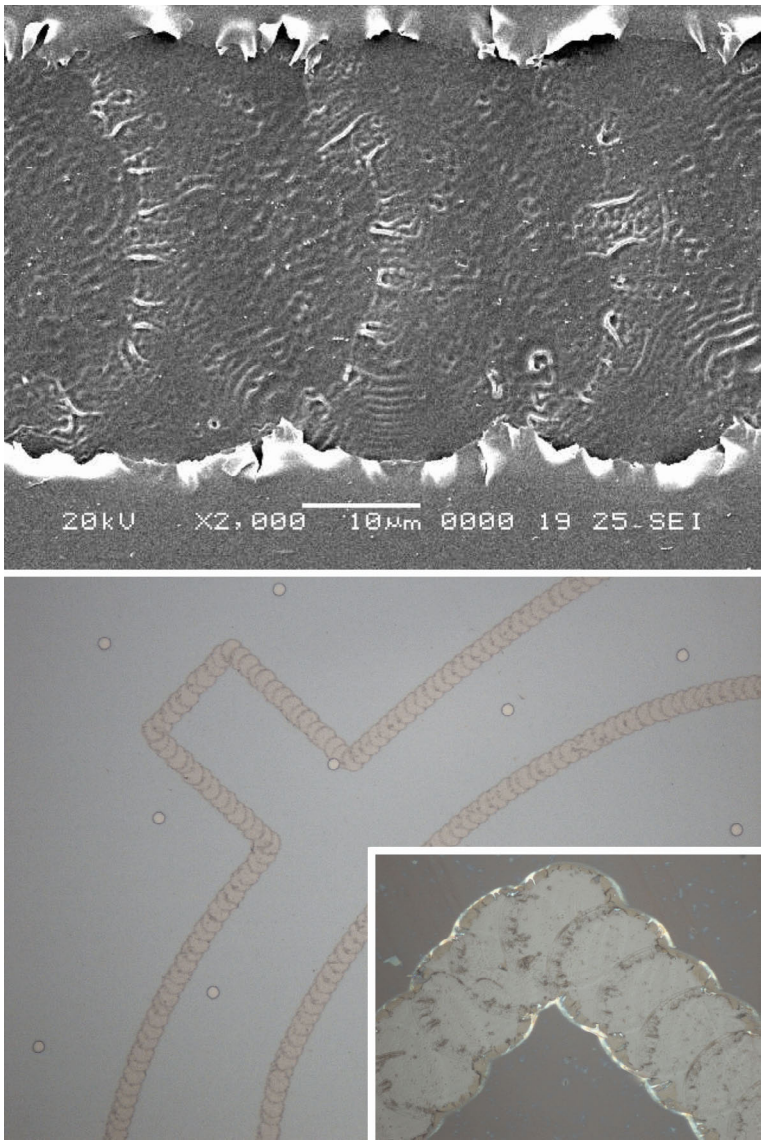

Figure 4.18: Isolation Technique. Top: Similar phenomena like in the scanning technique were observed such as partly attached flakes and emerging scattering structures. Bottom: A thin, isolating line can be made by aiming the pulses next to each other, thereby forming a pattern in the PEDOT:PSS layer. Inset: Detailed optical image of the pulses.

laser beam to be as small as possible to minimize the footprint of the isolating line and improve the achieved resolution. The smallest beam shape in our laser system was a 40 µm diameter round spot which thus became the prime patterning tool. Fortunately, the experience gained when investigating the scanning technique could be reused, expediting the development of this process. A thin, isolating line can be made by aiming the pulses next to each other with about one radius (20 µm) of inter-pulse distance. As shown in Figure 4.18, similar phenomena were observed such as partly attached flakes and emerging scattering structures. Interestingly, the same fluence used in the scanning technique (75 mJ/cm^2) was insufficient in isolating different regions and it had to be increased to 125 mJ/cm^2 for a successful ablation. No clear explanation has been found for this, but it could be related to the narrow circular beam shape, as there is an increased chance some residual conductive paths remain between adjacent areas.

After optimization of the isolation technique it was implemented in a LC cell. The cell was fabricated according to the process flow mentioned in section 4.3.2 and table 4.3, but now including a patterning step (step 5). A single pixel (a dollar sign) was patterned in the PEDOT:PSS layer of the bottom 75 µm PET-film. As can be seen in Figure 4.19, the ablated line can be faintly seen in the voltage off state. This again reflects a misalignment of the LC molecules at the ablated regions, but the extent is of course greatly diminished when compared to using the scanning technique. When an external voltage is applied to the cell, the single pixel switched clearly and uniform, while no unwanted effects could be observed concerning the floating electrode surrounding the pixel. In its current form, the isolation technique is thus a viable technique for PEDOT:PSS patterning.

Nevertheless, one could still improve the cell's optical quality by preventing the misalignment of LCs in the ablated region. An interesting approach has been reported by Naithani et al. [12], who ablated PEDOT:PSS on top of a multilayered barrier using the same laser as in our experiments. The top silicon nitride layer prevented the underlying layers from being damaged by the ablation process and allowed for a clean removal of the PEDOT:PSS. Such an approach could be investigated and transferred to this work, but would lead the addition of yet another vacuum step, making industrialization more difficult. Alternatively, one could attempt to integrate a different low temperature alignment layer which is less prone to the misalignment defects. Photoalignment [13] could potentially be such a candidate.

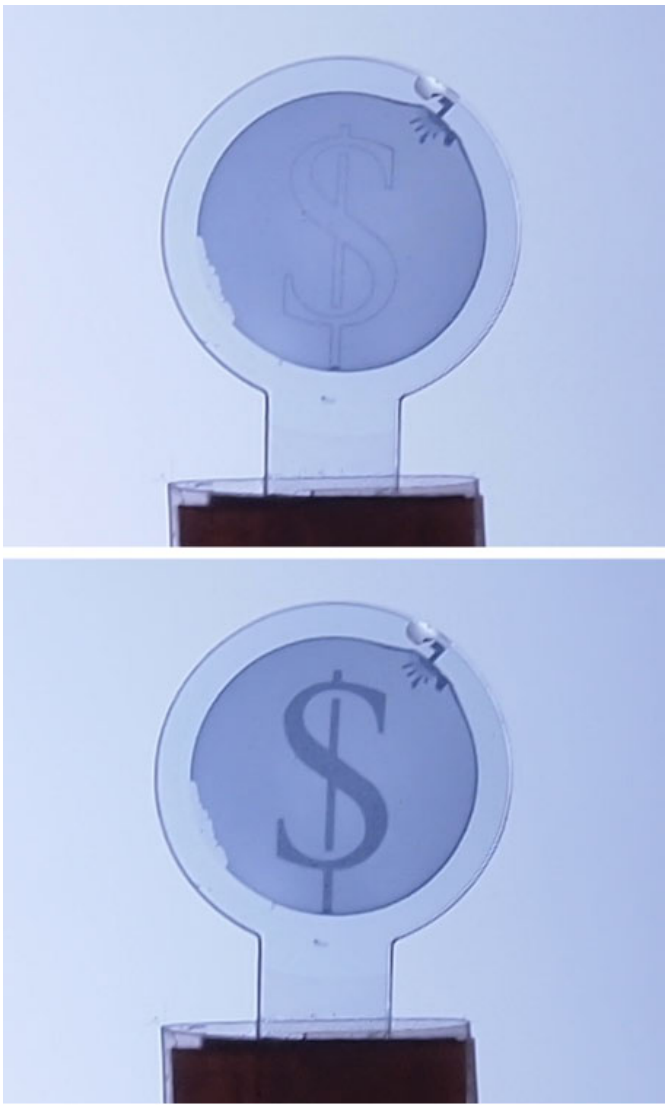

Figure 4.19: Patterned LC cell using the isolation technique. Top: The ablated line can be slightly seen in the voltage off state, reflecting the misalignment of the LC molecules at the ablated regions. Bottom: When an external voltage is applied to the cell, the single pixel switches clearly and uniform.

4.5 Manufacturability in an Industrial Environment

At this point, it is already useful to investigate if and how the whole process can be transferred to an industrial environment. Although all used tools have an industrial equivalent, scrutinizing individual steps is important to assure a sufficiently high yield and scaling up is possible. Scaling up by using larger carriers is possible as many machines use wafer size substrates and the number of LC cells made on each carrier would thus also increase. Circular glass carrier wafers with dimensions matching industrial standards such as 150 mm (6 inch) or even 300 mm could be explored.

Our lamination-delamination method is similar to existing commercial thin wafer handling solutions based on wax based adhesives and automated bonding and debonding tools [14], which have been recently introduced into high volume manufacturing for 300 mm CMOS wafers [15]. The method could therefore likely be implemented in an industrial environment, but will need careful attention concerning the wax and the debonding temperature, as to avoid thermal damage to the used films. Should future versions proof to be incompatible with this approach, alternative temporary bonding processes can be examined [14].

As mentioned above, deposition of all layers should not impede any transfer to industry as all steps have an industrial analogue. Cycle times of vacuum deposition equipment such as those needed for SiO_2-evaporation are generally long for research machines (up to 24 hours), but are on par with other manufacturing techniques for industrial versions. Nevertheless, options to eliminate one or both evaporation step can be explored. The barrier layer, for instance, is used to chemically isolate the PEDOT:PSS for the SU8 3010. One could either look for an PEDOT:PSS compatible photoresist, omitting the need for a barrier layer, or look for a compatible alignment layer that simultaneously acts as a barrier layer and is not affected by the phototlithographic process, omitting both evaporation steps.

Filling and sealing the LC cells is currently a very manual process and, although a more automated process could be developed, a revision might be useful. Preferably, such a revision should also include a way to circumvent the cell reopening with the excimer laser. Despite our negative experience with our first prototypes (see section 3.3.6), filling the cells before molding them could allow for a more industrial fabrication method. One possible method could be based upon the 'One Drop Filling' process used in LCD manufacturing. Here, the glue is first dispensed with no interruptions after which a precisely controlled amount of liquid crystal is deposited in the area inside the glue joint. The top substrate is then placed on top in vacuum, preventing encapsulation of bubbles and resulting

in a completely filled LC cell. A similar method would allow us to simultaneously fill and seal all LC cells on a single wafer, but can only be successful if the subsequent molding process does lead to a ruptured glue joint. Whether such an approach is possible under precisely controlled conditions requires further research. Anyway, the dispensing resolution will have a larger influence on our small LC cells than on large LCDs and thus requires attention.

Throughout this work the LC cells were cut out using an older CO_2-laser with a very low speed of about 0.2 mm/s, resulting in a total cutting time of about one minute for a single cell. Such a speed would be unacceptable in an industrial environment, but fortunately modern systems can reach much higher speeds. A recently installed system in CMST contains a Nd:YAG laser (532 nnm) capable of producing much shorter pulses (12 ps FWHM versus 80 ns FWHM) with a higher pulse frequency (50 kHz versus 100 Hz). With this laser a cutting speed of 20 mm/s was already tested, resulting in a total cutting time of only 0.63 seconds for a single cell, demonstrating its potential applicability in a commercial manufacturing process. The excimer laser used for pattering the PEDOT:PSS has a speed of 2 mm/s, which is still likely to be considered slow (10 to 30 seconds for pattering a cell, depending on the complexity of the pattern). Switching to lasers with shorter pulses will probably also make a transfer to industry feasible.

4.6 Conclusion

To create an active LC cell, both an alignment and a transparent conductive layer was integrated in the cell. An obliquely evaporated SiO_2-layer was selected and used as a contact-free, low-temperature alignment layer. Due to the delicate nature of the SiO_2-layer, it was applied after deposition and patterning of the photolithographic spacers, which resulted in small transient alignment zones near to the spacers. Since ITO proved to be too brittle for the molding process, the transparent conductive polymer PEDOT:PSS was chosen as an alternative. This required the addition of a barrier layer in between PEDOT:PSS and the photolithographic layer, as the development process of the photolithographic layer was disturbed by the presence of the PEDOT:PSS. With the electro-optic effect established, the quality of the mold was found to be important to achieve a good uniformity across the cell while a sufficiently high spacer density also proved to be necessary. Different patterning techniques for the PEDOT:PSS layer were investigated and were mainly based on laser ablation. Even after optimization, minor damage to the underlying PET-films could not be avoided, apparently

affecting the alignment of the LC molecules. The isolation technique, having the smallest footprint, led to good patterned cells and was thus deemed as a viable technique for PEDOT:PSS patterning.

References

[1] D. Cuypers, "Vertically aligned nematic liquid crystal microdisplays for projection applications", PhD thesis, Ghent University, 2005.

[2] K. Hiroshima, "Controlled high-tilt-angle nematic alignment compatible with glass frit sealing", *Jpn. J. Appl. Phys.*, vol. 21, no. 12, L761–L763, 1982.

[3] *Flexible Flat Panel Displays*. Wiley, 2005.

[4] D. Cairns, S. Gorkhali, S. Esmailzadeh, J. Vedrine, and G. Crawford, "Conformable displays based on polymer-dispersed liquid-crystal materials on flexible substrates", *Journal of the Society for Information Display*, vol. 11, pp. 289–295, 2003.

[5] S. Gorkhali, D. Cairns, and G. Crawford, "Reliability of transparent conducting substrates for rollable displays: a cyclic loading investigation", *Journal of the Society for Information Display*, vol. 12, pp. 45–49, 2004.

[6] P. G. Taylor, J. Lee, A. Zakhidov, M. Chatzichristidi, H. Fong, J. DeFranco, G. Malliaras, and C. Ober, "Orthogonal patterning of pedot:pss for organic electronics using hydrofluoroether solvents", *Advanced Materials*, vol. 21, 2314–2317, 2009.

[7] J.-K. Lee, M. Chatzichristidi, A. A. Zakhidov, H. S. Hwang, E. L. Schwartz, J. Sha, P. G. Taylor, H. H. Fong, J. A. DeFranco, E. Murotani, W. W. H. Wong, G. G. Malliaras, and C. K. Ober, "Acid-diffusion behaviour in organic thin films and its effect on patterning", *J. Mater. Chem.*, vol. 19, pp. 2986–2992, 19 2009.

[8] OSCoR 4000, a PEDOT:PSS compatible photoresist commercialized by Orthogonal inc., retrieved on 15/10/2013. [Online]. Available: http://www.orthogonalinc.com/.

[9] A. Shultz, J. Heikenfeld, H. Kang, and W. Cheng, "1000:1 contrast ratio transmissive electrowetting displays", *Journal of Display Technology*, vol. 7, pp. 583–585, 2011.

[10] E. Menard, M. Meitl, Y. Sun, J. Park, D. Shir, Y. Nam, S. Jeon, and J. Rogers, "Micro- and nanopatterning techniques for organic electronic and optoelectronic systems", *Chemical Reviews*, vol. 107, no. 4, pp. 1117–1160, 2007.

[11] Y. Novis, J. J. Pireaux, A. Brezini, E. Petit, R. Caudano, P. Lutgen, G. Feyder, and S. Lazare, "Structural origin of surface morphological modifications developed on poly(ethylene terephthalate) by excimer laser photoablation.", *Journal of Applied Physics*, vol. 64, no. 1, pp. 365–370, 1988.

[12] S. Naithani, D. Schaubroeck, Y. Vercammen, R. Mandamparambil, I. Yakimets, L. Van Vaeck, and G. Van Steenberge, "Excimer laser patterning of pedot:pss thin-films on flexible barrier foils: a surface analysis study", *APPLIED SURFACE SCIENCE*, vol. 280, pp. 504–511, 2013.

[13] V. Chigrinov, V. Kozenkov, and H. Kwok, *Photoalignment of Liquid Crystalline Materials: Physics and Applications*, ser. Wiley Series in Display Technology. Wiley, 2008.

[14] D. Kharas and N. Sooriar, "Cycle time and cost reduction benefits of an automated bonder and debonder system for a high volume 150 mm gaas hbt back-end process flow", in *Proceedings of CS MANTECH Conference*.

[15] Article 'Thermal Slide Off Debonding' on EVG website. [Online]. Available: http://www.evgroup.com/en/solutions/3d-ic/thin_wafer_processing/thermal_slide_off.

5

Electro-Optical Characterization of the Guest-Host LC Mixture and Transition to the Spherical LC Cell

"An experiment is a question which science poses to Nature, and a measurement is the recording of Nature's answer."

—Max Planck

5.1 Introduction

Up until now, very little detail has been given about the Guest-Host LC mixture itself as it was primarily used as a qualitative indicator. In this Chapter, a more in-depth description will be given about its exact nature and how it was assembled and examined for use in our LC cells. Although the desired specifications of the LC cell will depend on the application, an initial study of the mixture was performed to have an idea of the likely performance boundaries. After this initial

study, the spherically conformed LC cell was fully electro-optically characterized in conjunction with a study of the transition from glass substrates to the LC cell. Since this revealed only moderate contrast and switching times, progress towards the integration of polarizers is also discussed.

5.2 Guest-Host LC Mixture

The Guest-Host LC mixture in a White-Taylor configuration comprises three components: a host liquid crystal, a chiral dopant and a guest dichroic dye. Since a transparent voltage off state is desired, the molecules should be homeotropically aligned and the LC should thus have a negative dielectric anisotropy. Next to this, the birefringence should preferably be low, especially when using a twisted configuration. This can be understood by considering the ideal case when the LC has zero birefringence and absorption is the only involved mechanism. The induced twist is then used to absorb both polarization states of the incoming unpolarized light.

In the non-ideal case, however, the birefringence of the LCs will change the polarization state when the light propagates through the cell. This means one polarization will favourably rotate with the dye molecules and its total absorption will increase. The orthogonal state, however, will rotate along the dye molecules' minimal absorption axis and its total absorption will therefore decrease. The combined effect results in a decrease of the contrast ratio and should thus be avoided.

Since it was beyond the scope of this work to study a broad number of constituents, an advised choice of the basic components was therefore made. After consulting our supplier we selected MLC-6608 (Merck KGaA), a negative dielectric liquid crystal with a low $\triangle$n of 0.08.

A chiral dopant is added to the liquid crystal to induce a twist, a process governed by the following equation:

$$p = \frac{1}{\beta c} \tag{5.1}$$

with p the pitch, β the *helical twisting power* and c the concentration of the chiral dopant. The helical twisting power (HTP) is an intrinsic property of the chiral dopant and determines how strongly it can rotate the liquid crystal molecules. For a cell with a desired twist Φ and thickness d, the needed concentration of the chiral dopant thus is:

$$c = \frac{2\pi}{\Phi}\frac{1}{\beta d} \tag{5.2}$$

For this work, the chiral dopant S-811 (Merck KGaA) was selected, which has a HTP of 10.5 µm.

The most difficult component to obtain for the Guest-Host LC mixture was the dichroic dye. Only very little Guest-Host displays are currently fabricated and finding a supplier for the dyes proved to be difficult. Eventually some research quantities could be obtained under a non-disclosure agreement, limiting the information about these dyes that can be discussed freely. Over time two batches were received, of which the first was used to establish the general trends in Guest-Host LC mixtures on glass substrates. The second batch had a slightly improved performance and was used to make one mixture with optimized parameters. This mixture was then used to electro-optically characterize and to investigate the transition from glass substrates to our spherically conformed LC cell.

5.3 Influence of Dye Concentration and Twist on the Electro-Optical Response

5.3.1 Test cells

With our first batch of dye, multiple mixtures were made in which both the dye concentration as the twist was varied. Mixtures with 1% and 4% dye concentration were made and the twist was set at 0°, 90°, 180° and 270°. For the variation in twist multiples of 90° were used since this could conveniently be achieved by turning and aligning the 1 inch square glasses (see Figure 5.1) which were used in the fabrication process of the test cells. This fabrication process started by applying an ITO-layer and a obliquely evaporated SiO_2-layer on top of the 1 inch square glasses. Subsequently, ball spacers with a 10 µm diameter were spin coated on one glass plate and a UV-glue was deposited. The glass plates where then pressed together and the UV-glue was cured. Afterwards, the cells were filled with different Guest-Host LC mixtures via a capillary filling method and sealed.

5.3.2 Measurement Set-Up

The measurement set-up used to characterize the test cells is shown in Figure 5.2. A xenon arc lamp is used as an unpolarized white light source and the light emerging from this source is captured by a lens and redirected towards

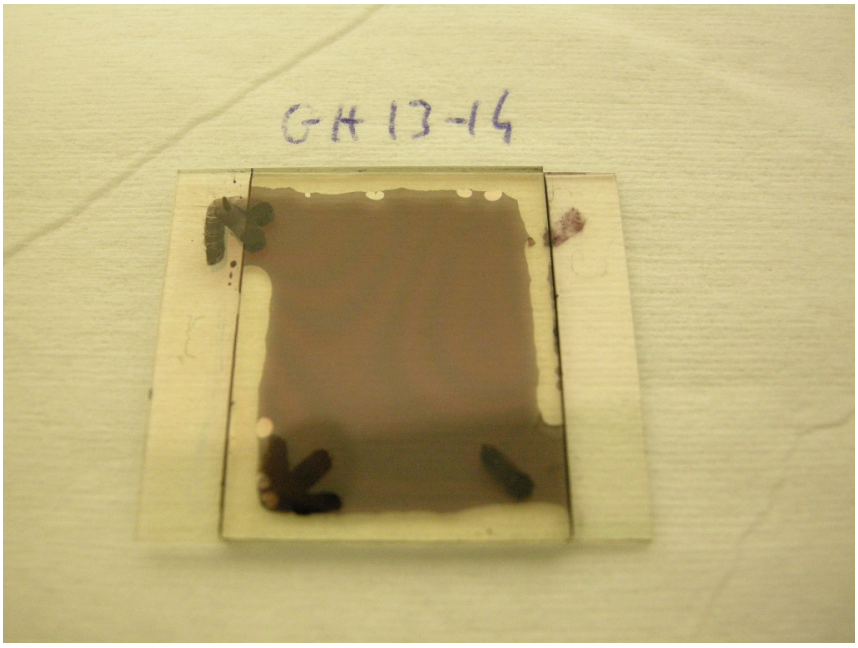

Figure 5.1: A typical test cell used for the characterization of the Guest-Host LC mixtures. The arrows indicate the evaporation direction and are used to assemble the cells according to the desired twist.

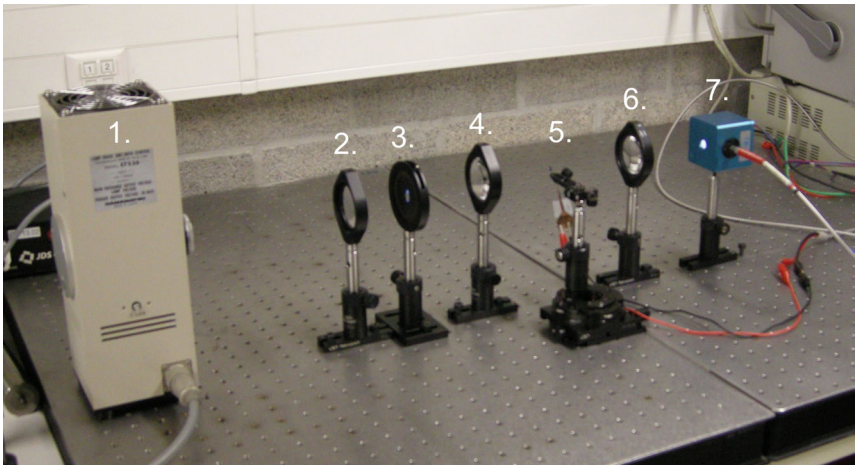

Figure 5.2: Measurement Set-Up. 1. xenon arc lamp 2. lens 3. diaphragm 4. lens 5. sample 6. lens 7. integrating sphere.

a diaphragm. This diaphragm is used to control the beam shape and remove the non-uniform outer areas. After passing through the diaphragm, the light is refocused with a second lens to make the spot as small as possible before hitting the sample, residing at the focal point of the second lens. Behind the sample a third lens is used to capture the exiting light beam from the sample and refocus it at an integrating sphere, which is connected with an OceanOptics HR 2000+ spectrometer. The f-number of this set-up is 1.72 and the the approximate spot size at the sample location is 1 mm.

The contrast ratio (CR) of a sample is derived by dividing the measured spectrum of the voltage off state (T_{max}) with the measured spectrum of the sample when its electro-optic response was fully saturated (T_{min}):

$$CR = \frac{T_{max}}{T_{min}} \tag{5.3}$$

When plotted across the visual spectrum, one can assess whether the dye is sufficiently wavelength independent (and thus appears black). However, for an easy numerical comparison, we will use the the CR's value at 555 nm, being at the peak sensitivity of a human eye. The used voltage wave form was a square wave with a frequency of 1 kHz.

5.3.3 Influence of Dye Concentration

As can be seen in Figure 5.3, the contrast of a cell increases with increasing dye concentration. The contrast at 555 nm for a Guest-Host LC mixtures with a 90° twist and 4% dye concentration is 1:2.4, while a mixture with 1% has a contrast of 1:1.9. This trend was observed independently of the amount of twist. The increased contrast comes, however, at a price. In a cell with 90° twist, the threshold voltage needed to observe any electro-optical switching rose from 2.1 V_{pp} to 3.5 V_{pp}, while the voltage at which 90% of the saturated contrast value was reached rose from 4.5 V_{pp} to 6.7 V_{pp}. The increase in threshold voltage indicated the dye has a negative effect on the dielectric anisotropy of the mixture. The dye could for instance have a positive dielectric anisotropy, thereby counteracting the LCs negative dielectric anisotropy. Next to this, it also known many dyes tend to increase the viscosity of the mixture [1]. Since no exact information about the dye was available, no conclusion about the nature of the threshold voltage increase could, however, be made. Still, since high voltages should be avoided in the lens, the maximum concentration will also be limited by this phenomenon.

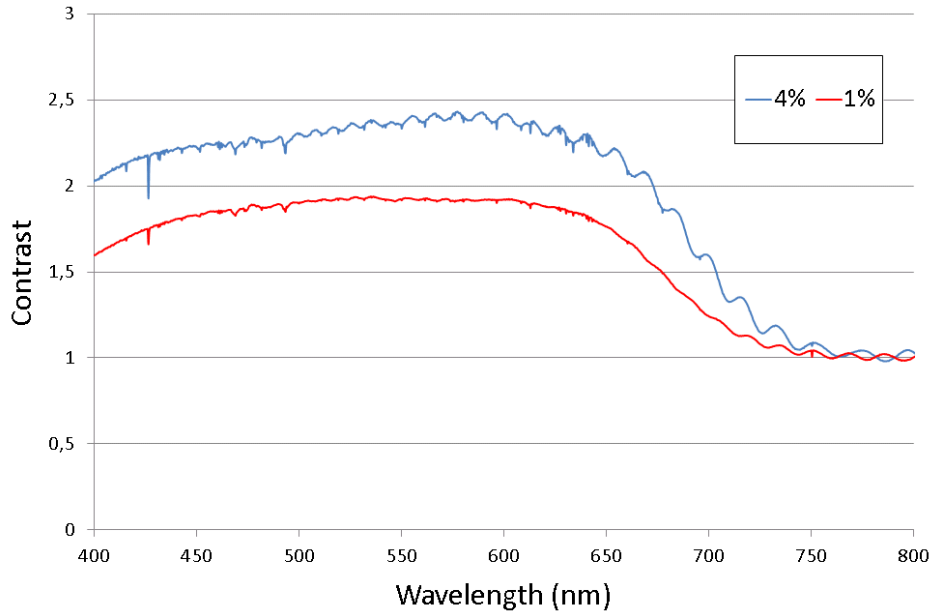

Figure 5.3: Influence of dye concentration on contrast in Guest-Host LC mixtures with a 90° twist. A higher concentration leads to a higher contrast.

5.3.4 Influence of Twist

When more chiral dopant is added to a mixture and the twist is increased, the contrast also increases. This could be observed on both the 1% (see Figure 5.4) as the 4% mixture (see Figure 5.5). The undulating appearance of the contrast ratios with respect to the wavelength is believed to originate from Fabry-Perot interference of the glass substrates. At 555 nm, the 1% percent dye mixture has a contrast ratio of 1:1.7, 1:1.9 and 1:2.1 for a respective twist angle of 0°, 90° and 180 °, while the 4% mixture has contrast ratios of 1:1.8, 1:2.4 and 1:2.7 for the same twist angles. The influence of the twist angle thus seems to increase with increasing dye concentration. As expected, the contrast ratio of mixtures with 0° twist does not exceed 1:2 (see section 2.5.2).

5.3.5 Cells with a 270° Twist

As mentioned above, mixtures were also made with a 270° twist. In the voltage off state these frequently exhibited cholesteric finger patterns (see Figure 5.6,

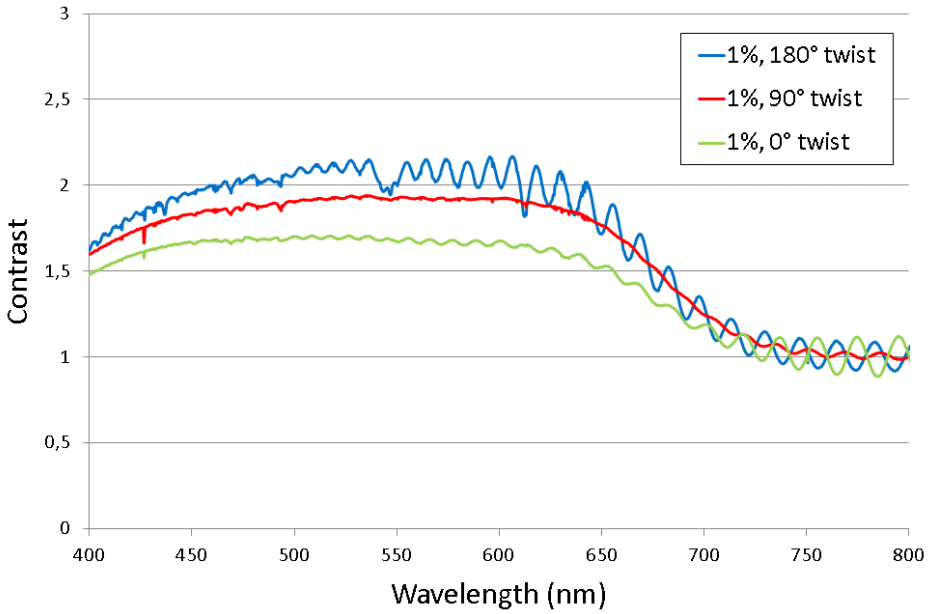

Figure 5.4: Influence of twist on contrast for a dye concentration of 1%. The undulating appearance of the contrast ratios with respect to the wavelength is believed to originate from Fabry-Perot interference of the glass substrates.

similar to the ones reported in section 3.3.6. In this case however, the cell gap should be within the correct range to avoid these cholesteric fingers and their appearance was thus likely the result of the high concentration of chiral dopant. Since these cholesteric fingers are scattering their presence is unwanted, as they would deteriorate the optical transmission through the lens. Furthermore, it has been reported that mixtures with a 270° twist are prone to hysteresis, which makes gray scale control difficult [1]. Generally, the maximum twist angle is advised to below 250°, but this requires careful alignment of the substrates with respect to each other. In our set-up and fabrication process this is difficult to achieve and thus 180° was the maximum twist angle that was investigated. Nevertheless, ensuing work could explore twist angles beyond 180°.

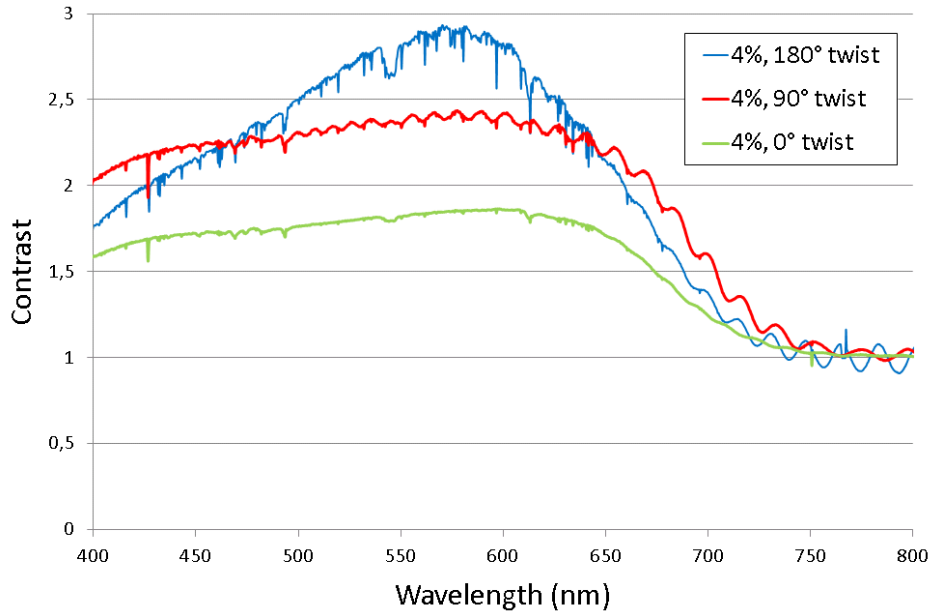

Figure 5.5: Influence of twist on contrast for a dye concentration of 4%. A higher twist leads to a higher contrast.

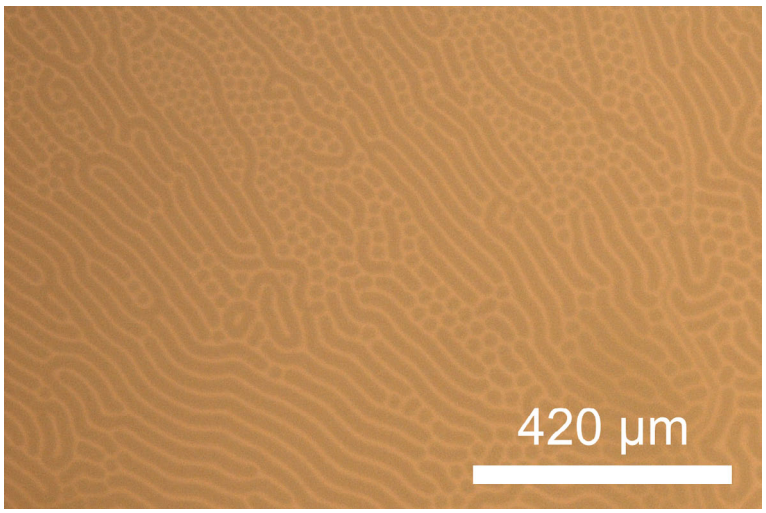

Figure 5.6: Guest-Host LC mixture with a 270° twist. In the voltage off state cholesteric finger patterns are visible, which due to their scattering nature are undesired.

5.3.6 Choosing the Optimal Parameters

The contrast measurements performed with the first batch of dye provided us with certain performance boundaries. Clearly, the best results were obtained with the 180° twist and 4% dye concentration, leading to a contrast ratio of 1:2.7. Although a twist of 180° is best suited for ensuing mixtures, one should carefully consider the influence of the dye concentration on the saturation voltage in order to limit the maximum voltage in the smart contact lens. Besides a desired maximum value of 10 V_{pp}, the saturation voltage should also preferably be below this value, as this opens up the possibility to study overdrive methods (see section 5.4.2).

Since the second batch had a better dichroic ratio (14.3), an improved but still moderate contrast of 1:3 could be achieved using a 3% mixture with a 180° twist (see Figure 5.7). The dye concentration was not further increased because with this concentration, the threshold voltage had already increased to 4 V_{pp} while 90% of the saturated contrast was reached at 6.6 V_{pp}.

5.4 Transition from Glass Cell to Spherically Conformed Cell

The optimized mixture was used to study the electro-optical properties of the LC cell and how the transition from a glass test cell to our spherically conformed LC cell affected these properties. For this purpose, both glass cells as standard (50 µm convex – 75 µm concave configuration) spherically conformed LC cells were fabricated and filled with the optimized Guest-Host LC mixture. Measurements on the LC cells were done by placing them again at the focal point of the second lens and positioning the light spot at the middle of the cell. Furthermore, the cell was oriented in such a way that the light was hitting the cell's surface at an angle of 90°.

5.4.1 Contrast Ratio & Transmission

A comparison between the contrast ratio of the glass test cells with the spherically conformed LC cell revealed the contrast drops from 1:3 to 1:2.3 at 555 nm (see Figure 5.7). To further investigate this contrast ratio drop, the transmission was also measured. As shown in Figure 5.7, the transmission in the voltage off state of a spherically conformed LC cell is about 5% lower, but in the saturated voltage on state it is about 2% higher, indeed leading to a lower contrast. Part of the reduced transmission at the voltage off state can be attributed to increased Fresnel losses

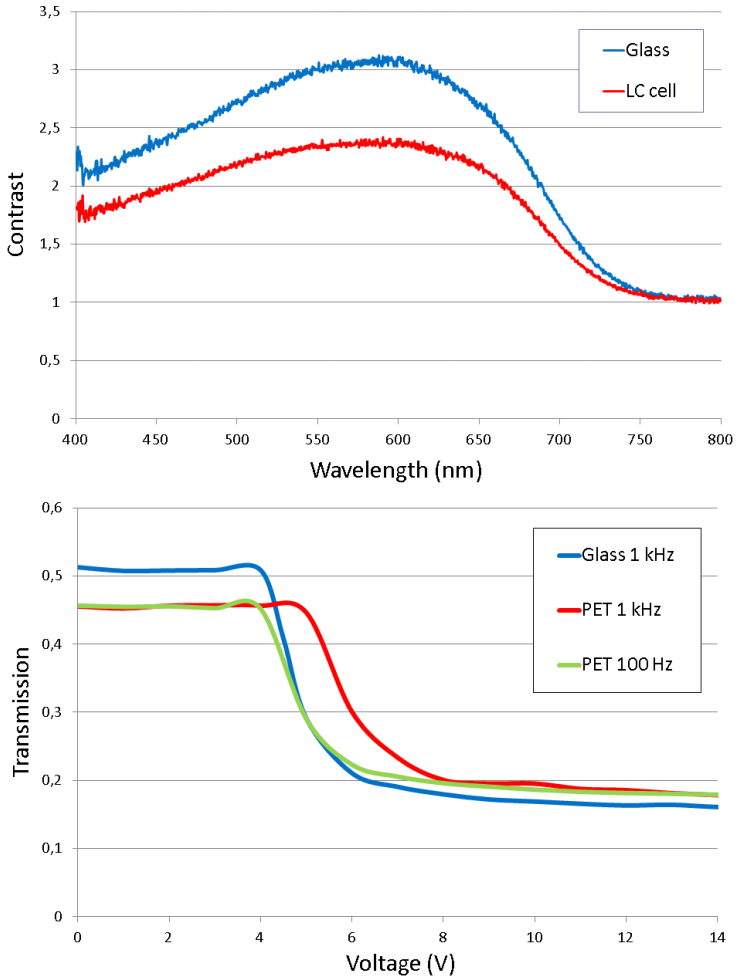

Figure 5.7: Transition from glass cell to spherically conformed cell. Top: Contrast drops from 1:3 to 1:2.3 at 555 nm when using the same Guest-Host LC mixture. Bottom: Transmission in the voltage off state of a spherically conformed LC cell is about 5% lower in comparison with a glass cell, but in the saturated voltage on state it is about 2% higher. A threshold voltage shift is observed in the spherically conformed LC cell when using a 1 kHz frequency, which is likely caused by a high series resistance.

since the refractive index of the PET is higher than that of glass (1.67 versus 1.52). The reflection coefficients of PET and glass for normal incidence are:

$$R_{PET} = \left(\frac{n_{air} - n_{PET}}{n_{air} + n_{PET}}\right)^2 = \left(\frac{1 - 1.67}{1 + 1.67}\right)^2 = 0.063 \tag{5.4}$$

$$R_{glass} = \left(\frac{n_{air} - n_{glass}}{n_{air} + n_{glass}}\right)^2 = \left(\frac{1 - 1.52}{1 + 1.52}\right)^2 = 0.043 \tag{5.5}$$

Hence, when considering our samples as plan parallel plates (and thus ignoring the LC), the total transmission for normal incidence is:

$$T_{PET} = \frac{1 - R_{PET}}{1 + R_{PET}} = \frac{1 - 0.063}{1 + 0.063} = 0.881 \tag{5.6}$$

$$T_{glass} = \frac{1 - R_{glass}}{1 + R_{glass}} = \frac{1 - 0.043}{1 + 0.043} = 0.918 \tag{5.7}$$

Therefore, Fresnel losses alone should lower the transmission from 50.9% to 48.8% in the voltage off state. As the actual value is 45.6%, other losses could be due to scattering or the spherical shape of the LC cell.

However, the higher transmission in the saturated voltage on state indicated the cell gap was smaller than intended as this would lead to a decrease in total absorption. Since a reduced cell gap generally leads to a lower switching time, switching speed measurements should substantiate such a claim, but this is discussed in the ensuing section.

Next to the contrast ratio drop, the transmission measurements also revealed a significant contact resistance existed between our LC cells and the flexible copper connectors used to deliver the voltage. When the same driving frequency was used as for the glass test cells (1 kHz), a seemingly higher threshold voltage was observed. However, this threshold voltage could be lowered and match the test cells' threshold voltage by lowering the driving frequency. This indicates the voltage shift is actually caused by a voltage drop over a resistor placed in series with our LC cell (see Figure 5.8). When the connector was clamped more firmly or was repositioned, a minor shift could be observed, confirming that the contact resistance was largely responsible for the voltage shift. An estimated value for this contact resistance can be derived as follows. Assuming all signals are in sinusoidal steady state regime, the voltage V_C over the capacitor (the LC cell) is:

$$V_C = \frac{1}{1 + j\omega RC} V_{in} \tag{5.8}$$

with ω the angular frequency (2πf), R the series resistance and C the capacity

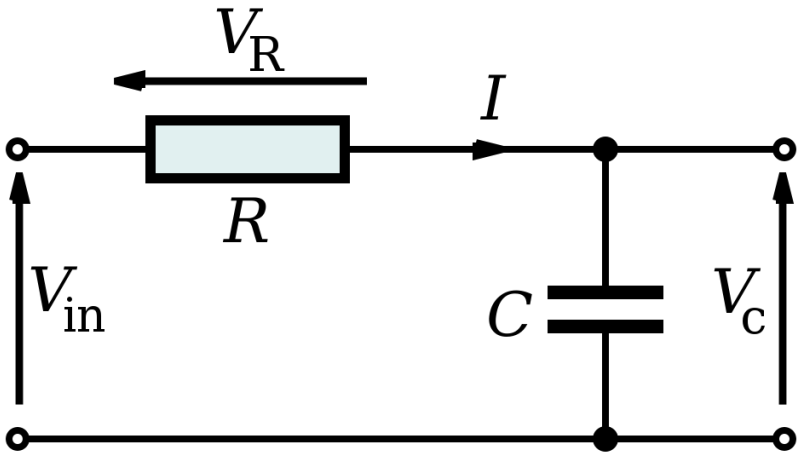

Figure 5.8: Equivalent circuit of our connected LC cell. The voltage shift in our transmission measurements (caused by the changing frequency) indicate the connected LC cell is more accurately modelled by placing a contact resistance in series with the LC cell, which can be modelled as a capacitor.

of the LC cell and V_{in} the amplitude of the input signal. A value for R can be derived by looking at how the input voltage shifts with changing frequency while choosing a certain transmission (and thus a related V_C). For a transmission of 30%, the amplitude of the input voltage shifts from 2.5 V to 3 V (5 V_{pp} to 6 V_{pp}) when the frequency increases from 100 Hz to 1 kHz. This can be written as:

$$|V_{in,100Hz}| = |V_C||1 + j(2\pi 100)RC| = 2.5 \tag{5.9}$$

$$|V_{in,1kHz}| = |V_C||1 + j(2\pi 1000)RC| = 3 \tag{5.10}$$

or also:

$$V_{in,100Hz} = V_C\sqrt{1 + ((2\pi 100)RC)^2} = 2.5 \tag{5.11}$$

$$V_{in,1kHz} = V_C\sqrt{1 + ((2\pi 1000)RC)^2} = 3 \tag{5.12}$$

When assuming the cell's capacity can be approximated as a plan parallel capacitor its value can be calculated as follows:

Table 5.1: Switching times measured on glass and on a LC cell. Both the voltage and the frequency were varied. T_{on}: switch on time, T_{off}: switch off time.

Switching time	glass 1 kHz (ms)	LC cell 1 kHz (ms)	LC cell 100 Hz (ms)
T_{on} ($8V_{pp}$)	208	222	164
T_{on} ($10V_{pp}$)	70	94	70
T_{on} ($12V_{pp}$)	34	32	30
T_{off} ($8V_{pp}$)	296	128	152
T_{off} ($10V_{pp}$)	278	138	146
T_{off} ($12V_{pp}$)	288	138	150

$$C = \varepsilon_0 \varepsilon_r \frac{\pi r^2}{d} \tag{5.13}$$

with ε_0 the vacuum permittivity, ε_r the relative permittivity of the Guest-Host LC mixture, r the radius of the active cell area and d the cell gap. Strictly speaking, ε_r depends on the orientation of the LC molecules, but for the sake of simplicity we assume it to be $\varepsilon_\perp$, being the largest value. When substituting the values of all variables (ε_0 = 8.85 10^{-12}F/m, ε_r = 7.7, r = 1 mm[1], d = 10 µm) we find a capacity of 21,4 pF. Solving equation 5.11 and 5.12 thus results in:

$$R = 4.97\ M\Omega, V_C = 2.49\ V \tag{5.14}$$

Although one could try to reduce this contact resistance by for instance applying some anisotropic conductive glue, this is of no use as in the long run the contact lens should eventually become wireless.

5.4.2 Switching speed

Measurement Set-Up

Besides contrast another interesting electro-optical parameter is the cell's switching speed. To measure the switching speed, the integrating sphere in our set-up was replaced with an avalanche photodiode which was read out with a oscilloscope. Measurements were performed on both the glass sample as the LC cell.

[1]For these particular measurements only a circular pixel of 2 mm diameter was used. It was confirmed deactivating the other pixels did not influence the transmission measurement.

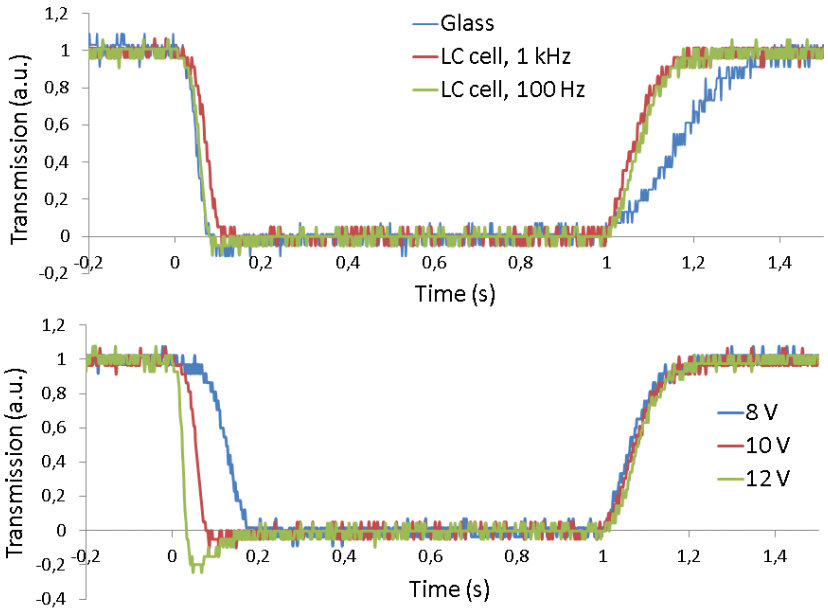

Figure 5.9: Switching time measurements. Top: When using a voltage amplitude of 10 V_{pp}, switch on times were similar, with the LC cell driven at 1 kHz having a slightly larger value. This was attributed due to the fact that the effective voltage across the cell is lower than intended because of the series resistance. The significantly larger switch off time of the glass cell indicated the LC cell has a lower cell gap. Bottom: When increasing the voltage amplitude, the switch on time for a particular configuration (LC cell driven at 100 Hz shown here) decreases dramatically, while the switch off times are unaffected.

A voltage pulse (square wave profile) of 1 second with a fixed amplitude and driving frequency was applied and the response was measured. Voltage amplitudes of 8 V_{pp}, 10 V_{pp} and 12 V_{pp} were used, since at these amplitudes the T-V measurements (see Figure 5.7) of all signals were almost saturated, allowing us to study the effects of overdriving the cell. Furthermore, the voltage off transmission was equalized with one and the saturated voltage on transmission was equalized with zero, as this allowed for a clearer comparison between the glass cell and LC cell. As can be seen in Figure 5.9, the switch on behavior and the switch off behavior differs when considering both the glass cell as the conformed LC cell. Especially the significantly larger decay time of the glass cell is remarkable. For a quantitative comparison the switch on and switch off times were measured.

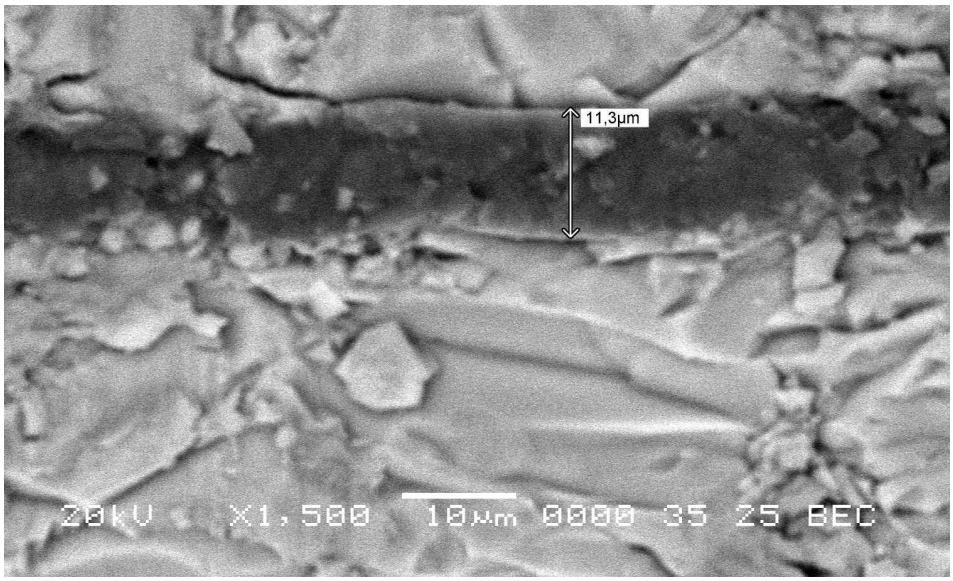

Figure 5.10: The cell gap at the location of the electro-optical measurements in the glass cell was determined by a linear interpolation between the measured cell gaps (example shown here) at both sides of the cell. This method resulted from the difficulty to obtain a trustworthy value at the electro-optical measurements' location because of the large surface roughness and tiny broken off glass chips.

The switch on time was defined as the time between the start of the pulse and the moment the optical response had reached 90% of the saturated level (or the time between 100% and 10% of the normalized transmission). The switch off time is defined as the time between the end of the pulse and the moment the optical response again reached 90% of the voltage off value (or the time between 0% and 90% of the normalized transmission). The switch on and switch off times are summarized in Table 5.1.

Switch Off Time and Spacer Influence

Regardless of the applied voltage, the switch off times of the glass cell are indeed significantly larger than those of the LC cell (about 287 ms versus about 142 ms). The switch off process is driven by the relaxation of the LC molecules and its relaxation time is generally governed by the following, voltage independent equation [2]:

$$T_{relaxation} = \frac{\gamma}{K}\left(\frac{d}{\pi}\right)^2 \tag{5.15}$$

with γ the rotational viscosity of the liquid crystal, K a parameter based on the elastic constants of the liquid crystal and d the cell gap. Since the same liquid crystal mixture is used for all cells, the large difference in relaxation time (here thus the switch off time) again points to a difference in cell gap between the glass cell and the LC cell. To further investigate this assertion the cell gap of of both cells was measured. The glass cell was first cut with a automated diamond saw through the spot where the measurements had occurred. Initially, the intention was to directly measure the cell gap with a SEM, but it proved to be difficult to obtain a trustworthy value at the location of the electro-optical measurements because of the large surface roughness and tiny broken off glass chips. Since a more accurate value could be derived from the sides of the cell where the glue was still present (see Figure 5.10), the cell gap was determined by a linear interpolation between the measured cell gaps at both sides of the cell. In this way, the cell gap at the location of the electro-optical measurements was found to be 9.95 µm, very close to its intended value.

To measure the cell gap of our spherically conformed LC cell, the cell was carefully split by pulling it apart at the rectangular contact areas. The photolithographic spacers still resided at the bottom, concave side and could be measured with an optical profilometer (see Figure 5.11). By averaging out the height several spacers at both the middle of the cell and at 1 mm radially from the center, the cell gap was found to be 8.4 µm. One should note that the cell gap and the height of the spacers can only be equated if the spacers are not pressed into the PET-films. Such an impression could not, however, be detected with the profilometer and additional SEM images also did not reveal any deviation (see Figure 5.12). Also the opposing convex side showed no indentations while the SEM images revealed only the PEDOT:PSS layer was generally ruptured at the location where a spacer was touching the surface (see Figure 5.12).

The cell gap measurements thus did reveal a difference exists between the glass cells and the LC cells and mainly showed the LC cells had a deviating value. Despite having followed the predefined spin coat parameters for achieving a 10 µm layer thickness, it appears these parameters should be carefully monitored when aiming to replicate the same electro-optic response measured on glass cells. In-house experience also suggests sometimes SU8 mixtures tend to have decreased thicknesses after being in use for a considerable amount of time. Normally, these deviations can be avoided in an industrial environment and a similar electro-

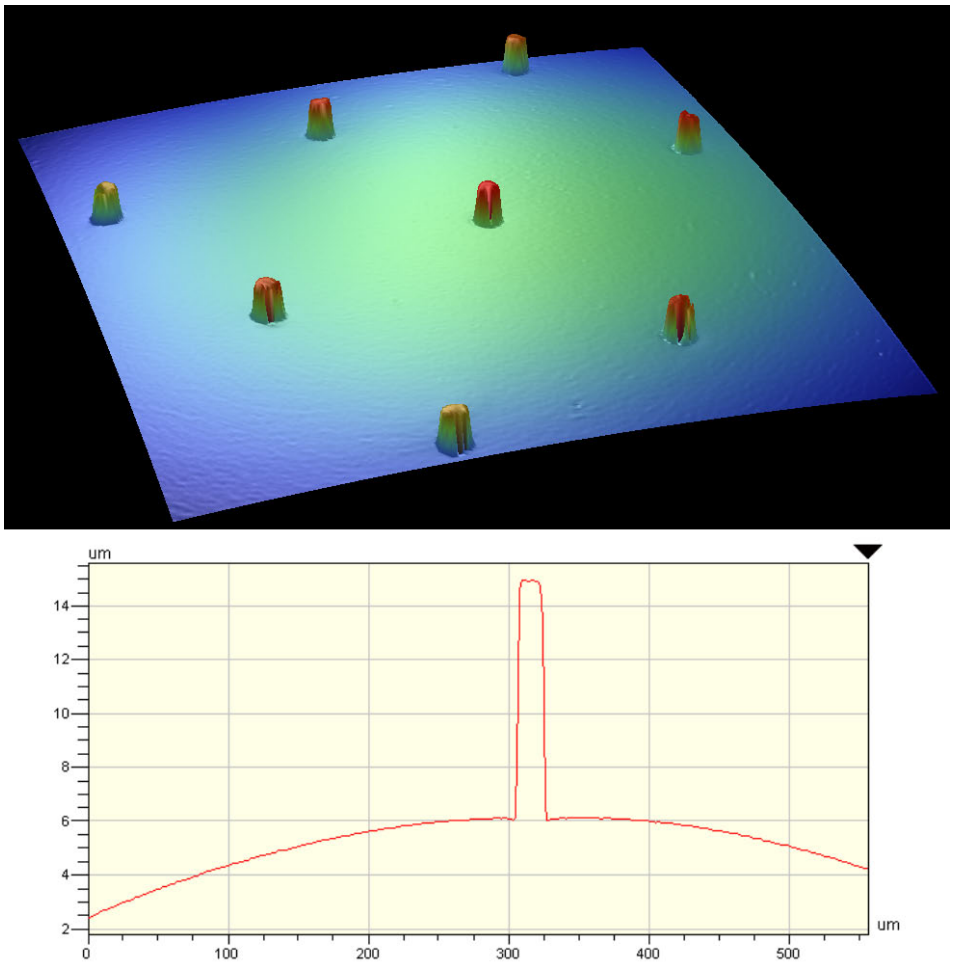

Figure 5.11: The cell gap in the LC cell was obtained by carefully splitting the LC cell at the rectangular contact areas and measuring the photolithographic spacers with an optical profilometer. Top: 3D view of an array of spacers. Bottom: 2D cut revealing the curvature of the cell and the height of a single spacer. The spacers showed no significant indentation into the underlying PET-film.

optical response between a glass cell and a spherically conformed LC cell is expected.

Because the smaller cell gap of the LC cell also means that the total absorbing layer is thinner in the voltage on state, this explains why the transmission of the

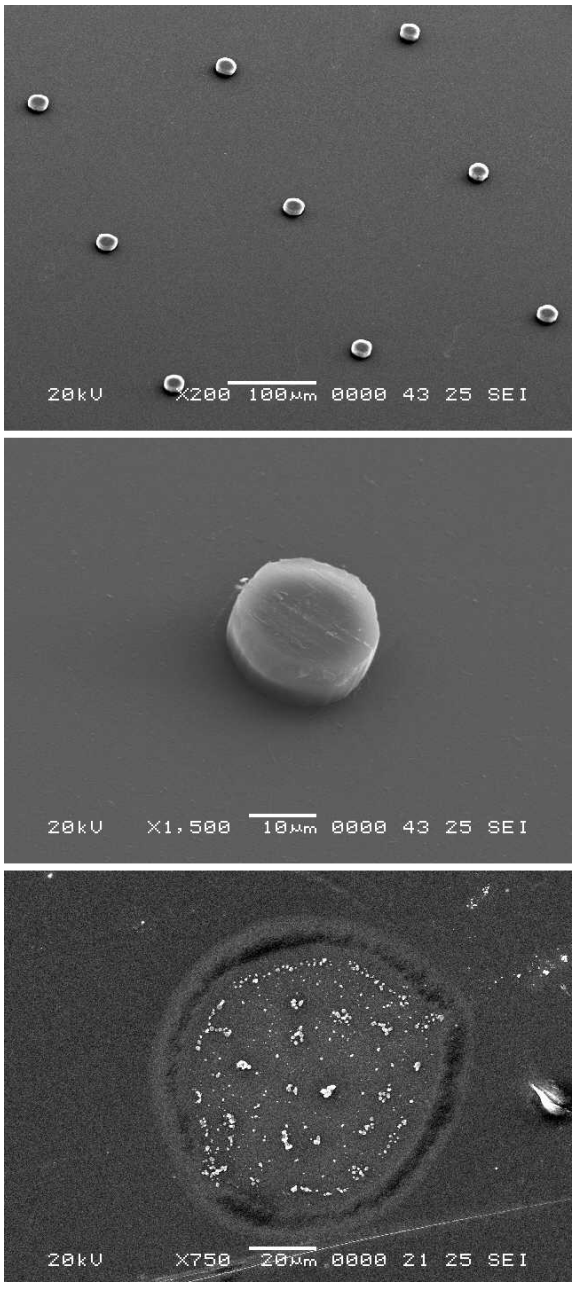

Figure 5.12: SEM images from the interior of a split LC cell. Top: Array of spacers. Middle: Close-up of a single spacer. Bottom: The convex side also showed no indentations but the PEDOT:PSS layer was generally ruptured at the location where a spacer was touching the surface.

LC cell in the voltage on state is higher when compared to the glass test cells (see Figure 5.7).

When considering formula 5.15, a switch off time of 278 ms for cell of 10 µm thickness (glass cell at 10 V_{pp}) should result in a switch off time of about 206 ms for for a cell 8.4 µm thickness. Although our measured value of 138 ms (LC cell at 10 V_{pp}) is indeed following a downwards trend, there is still a large difference with the theoretical value, of which the origin is unclear.

Nevertheless, when considering the absolute values of the switch off times, these are still rather large and displaying video images would, for instance, not be possible. Further improvements can be obtained by decreasing the cell gap (at the expense of the already moderate contrast) or by using another liquid crystal mixture.

Voltage Dependent Switch On Time

No difference was found between the switch on time of the glass cell driven at 1 kHz and the LC cell driven at 100 Hz (T_{on}= 70 ms). A slight increase was found when the LC cell was driven at 1 kHz, which is likely due to the fact that the effective voltage across the cell is lower than intended because of the series resistance. The switch on time is largely affected by the driving voltage, as for instance the switch on time of the LC cell decreases from 164 ms to 30 ms when the voltage is increased from 8 to 12 V_{pp} with a 100 Hz driving frequency (see Figure 5.9 and Table 5.1). Depending on the desired switch on time, an appropriate voltage amplitude could thus be selected. One does have to consider what a safe voltage amplitude in a smart contact lens is and how this affects the power consumption of the LC cell. The latter is explored more in-depth in the ensuing section.

5.4.3 Reducing the Power Consumption of the LC Cell

Although the initial reason for decreasing the driving frequency was reducing the effect of the contact resistance, it is useful to consider its influence on power consumption. Since the LC cell is basically a capacitor which constantly needs to be charged and discharged during operation, the power consumption of its driving electronics is given by [2]:

[2] Note that although theoretically a capacitor does not require any real power, any practical implementation would result in real power consumption in the driving electronics.

$$P = \frac{1}{2} C V^2 f \tag{5.16}$$

With C the capacitance of the LC cell, V the driving voltage and f the driving frequency. When assuming the cell can be approximated by a parallel-plate model, this translates to:

$$P = \frac{1}{2} \varepsilon_0 \varepsilon_r \frac{\pi r^2}{d} V^2 f \tag{5.17}$$

with ε_0 the vacuum permittivity, ε_r the relative permittivity of the Guest-Host LC mixture, r the radius of the active cell area and d the cell gap. As in section 5.4.1, we also assume $\varepsilon_r = \varepsilon_\perp$. When substituting the values of all variables and assuming a driving voltage of 10 V_{pp} at 1 kHz (ε_0 = 8.85 10^{-12}F/m, ε_r = 7.7, r = 3,4 mm, d = 10 µm, V = 5 V, f = 1 kHz), the power consumption of the LC cell amounts to:

$$P = 3.1\ \mu W \tag{5.18}$$

When aiming to lower the power consumption of the LC cell without physically changing it, one can either tune the driving voltage or the driving frequency. Since lowering the driving voltage would significantly influence the switching times, lowering the frequency seems the most interesting route. Indeed, lowering the driving frequency to 100 Hz leads to a 10-fold decrease in power consumption, namely 0.31 µW. Such a low power consumption opens up the possibility to directly power the whole LC cell with a photovoltaic cell. The output power of such a photovoltaic cell is given by:

$$P = I \eta A \tag{5.19}$$

with I the incident light intensity, η the cell's efficiency and A the surface area. When considering office lighting (5 W/m^2) and a typical organic solar cell[3] efficiency of 5% [3], a solar cell of 2 mm^2 could already generate sufficient power (0.5 µW) to drive the whole LC cell.

[3] Organic solar cells are used as an example here as they are inherently flexible and thin, thus making them a likely candidate for powering smart contact lenses.

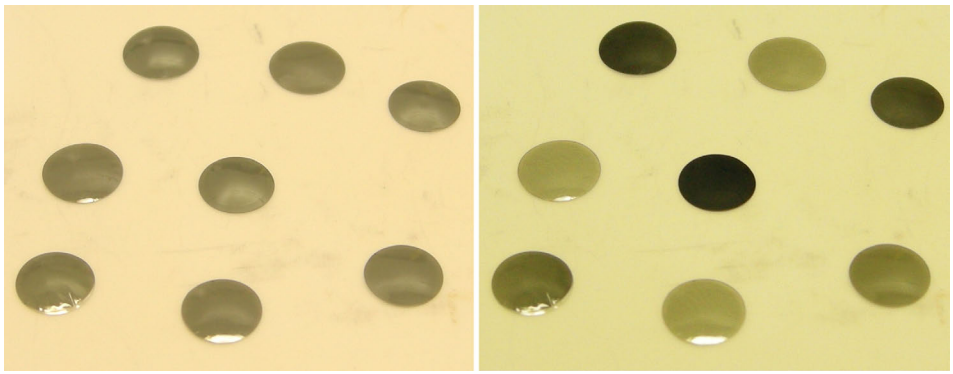

Figure 5.13: LC cells with a 40 µm PVA-film as top layer and a 75 µm PET-film as bottom layer. Left: Randomly placed cells observed with unpolarized light. Right: When observed through a linear polarizer the appearance of the cells depends on the polarizing axis of the top PVA-film. The darker the appearance, the more its axis is perpendicularly oriented with respect to the axis of the polarizer.

5.5 Progress Towards the Integration of Polarizers

Although the contrast of our LC cell has not been fully optimized, the current value is only moderate. One could consider improving the contrast by further increasing the twist or the cell gap or choosing a dye with an better dichroic ratio. Even after such an optimization, a contrast larger than 1:10 is not expected. Furthermore, any increase in contrast will likely lead to a dramatic increase in switching time or threshold and saturation voltage.

Further improvement of the electro-optic response of the LC cell without negatively affecting other important characteristics cannot likely happen without the inclusion of polarizers. As stated in section 2.6 these, however, are generally too thick to be integrated in the lens. Since it is expected that some applications will need a better performing LC cell, we investigated how polarizers could anyway be integrated.

5.5.1 Polyvinyl Alcohol Polarizers

Conventional LCD polarizers are based on Polyvinyl Alcohol (PVA) doped with iodine. During the fabrication process the PVA is stretched along one direction, aligning the polymeric chains of the PVA along the stretching direction. The iodine attaches to the PVA chains, thereby also forming long conducting chains which

primarily absorb the light along the stretching direction. When unpolarized light propagates through such a polarizer, the transmitted light is linearly polarized perpendicular to the stretching direction [4]. Most modern polarizers contain a PVA layer of about 15 to 30 µm thick which laminated between two protecting non-birefringent films, since the bare PVA-film is rather brittle and easily damaged. It are thus mainly the protective films that account for the thickness of the polarizers, easily leading up to 200 µm. Since the total thickness of the lens should be as small as possible, acquiring sufficiently thin polarizing films is important, but proved to be difficult.

Eventually, we were able to obtain a 40 µm polarizing PVA-film having no protective outer films (Onbitt Co., Ltd.). To investigate the use of these films, LC cells were made using the 40 µm PVA-film as the top layer and a 75 µm PET-film as the bottom layer. Originally it was planned to use a similar fabrication process as in section 4.3.2, but without the active layers and the filling step. However, the PVA-film proved to be thermally unstable and tended to shrink dramatically upon heating. Each thermal step needed to be retuned and monitored carefully during the fabrication process. The temperature of the delamination step needed to be tuned down from 125 °C to 105 °C while the PVA-film needed to be clamped after removing the glass carrier since as long as it was submitted to a high temperature it would otherwise curl up. Furthermore, the molding temperature was also an issue. When a circularly cut LC cell was placed on a mold having a temperature above the glass transition temperature of PVA (85 °C), the top PVA-film curled up and fully detached from the bottom PET-film even before closing the mold. Only by carefully steering and monitoring the temperature to 80°C (just in between the T_g of PET and PVA) spherically conformed LC cells could be made (see Figure 5.13). Initial inspection of the cells through a linear polarizer indicate the polarizing abilities of the top PVA-film largely remained intact.

However, closer inspection revealed about 70% of the cells had partially detached glue joints and that the detachments mainly were located along the stretching direction of the top PVA-film (see Figure 5.14). This indicates that despite the lowered molding temperature, the inherent stresses in the PVA-films are so high any further attempt to increase the yield will be very difficult. Notwithstanding the low yield, fabrication of some active cells was also pursued. Although the PEDOT:PSS deposition was successful, the PVA-films split along their stretching direction during any vacuum process (i.e. SiO_2-evaporation). The reason for this was not entirely clear, but it was suspected small air bubbles trapped between the carrier and the PVA-film were to blame, since their inflation during the vacuum step could cause the PVA-film to rupture. Anyway, it was concluded that *bare*

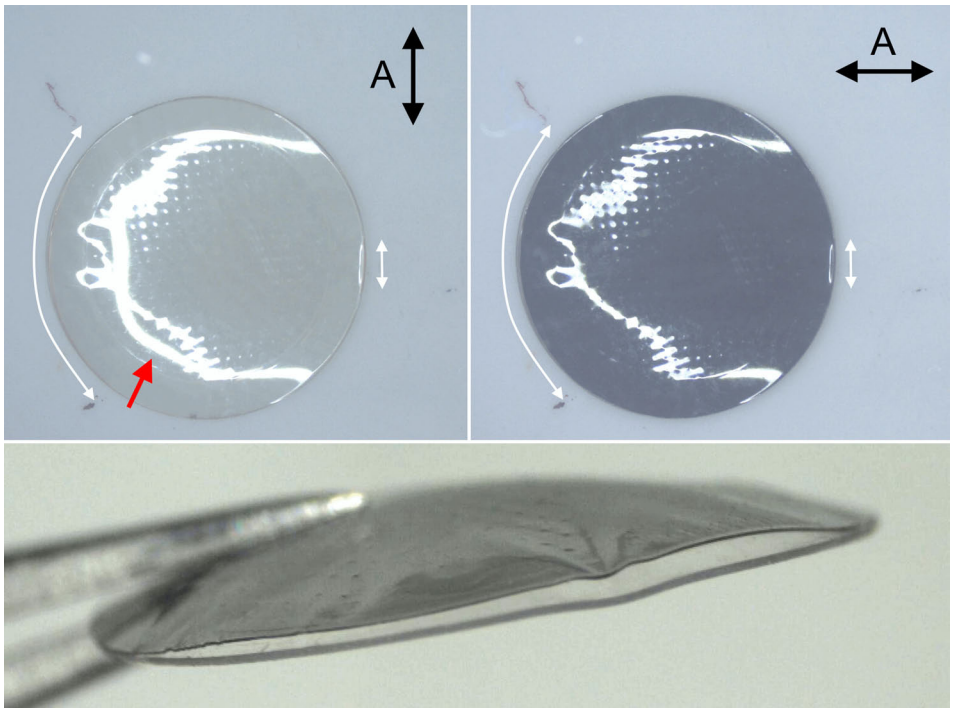

Figure 5.14: Partially detached glue joints observed in the cells with an integrated PVA-polarizer were located along the stretching direction of the film. The black arrow indicates the polarization axis of the analyser placed before the camera. The white arrows indicate the detached areas. Left: A clear cell is observed when the analyser is parallel with the polarization axis of the LC cell's PVA-film (and thus perpendicular with the film's stretching direction). The red arrow indicates the reflection from the PET-film, behind the PVA-film. Right: A dark cell is observed when the analyser is perpendicular with the polarization axis of the LC cell's PVA-film (and thus parallel with the film's stretching direction). Note that the reflection from the PET-film behind the PVA-film has disappeared. Bottom: Side view of a partially detached glue joint.

PVA-based polarizers possess too much internal stresses and are mechanically too weak to be included in a spherically conformed LC-cell.

Since a bare PVA-film proved to be rather unstable an additional experiment was set up to investigate whether a PVA-film glued to a thin supportive film could alleviate the observed problems. For this purpose a conventional polarizer with protective films made of cellulose acetate butyrate (CAB) was used. The

polarizer was first laminated onto a temporary carrier and the top CAB layer was stripped in an acetone bath. When the top CAB layer was removed, a 23 μm PET-film (Goodfellow) was glued on top of the exposed PVA-film with a flexible, two-component glue (301-2FL, Epoxy Technology). The total stack was then delaminated, flipped and rebonded with a new temporary carrier, after which the second CAB layer was stripped. Ultimately, a thin, flexible polarizer was obtained, consisting of the PET as supportive film and the PVA as polarizing film, having total thickness of only about 50 to 60 μm.

One batch of LC cells using this new film was made, where the film was put at the convex side with the PVA facing inwards. Using the same adapted fabrication process as mentioned above, no ruptures in the glue joints were observed, indicating the PET-film seems to counteract the stress release in the PVA-film at elevated temperatures. However, since the creation of this thin laminated polarizer was very cumbersome and had low yield, this route was not pursued any further, as it would have taken up too many resources for further investigation.

Rather, our attention was turned towards other thin film polarizers, which seemed to have better intrinsic properties.

5.5.2 Thin Film Polarizers

As mentioned above, conventional polarizers are based on stretched PVA-films impregnated with iodine. More recently, new polarizers have emerged in which the polarizing layer is applied *on top* of a polymer film. This polarizing layer itself also tends to be very thin, generally having thicknesses below 1 μm. Such an approach allows for a more versatile use of substrates and, combined with the limited thickness, is therefore more suitable for integration in a contact lens. Usually, fabrication of these thin film polarizers involves the deposition of a mixture of dichroic dyes in a solvent and aligning the molecules along one preferential axis. Alignment can be obtained by shear flow induced by a rod propagating across the substrate [5, 7] or by spin coating the mixture on a predeposited alignment layer [6, 8](see Figure 5.15). Variants also exist where the alignment is induced by illumination of linearly polarized UV-light [9].

Alternatively, one could consider using a wire grid polarizer, which uses extremely thin parallel metallic wires to linearly polarize light. When the pitch of these wires is sufficiently low (below half of the targeted wavelength), it can also be used for the visual spectrum. Because of their good optical performance and thermal stability, they are frequently used in LCOS (Liquid Crystal On Silicon)

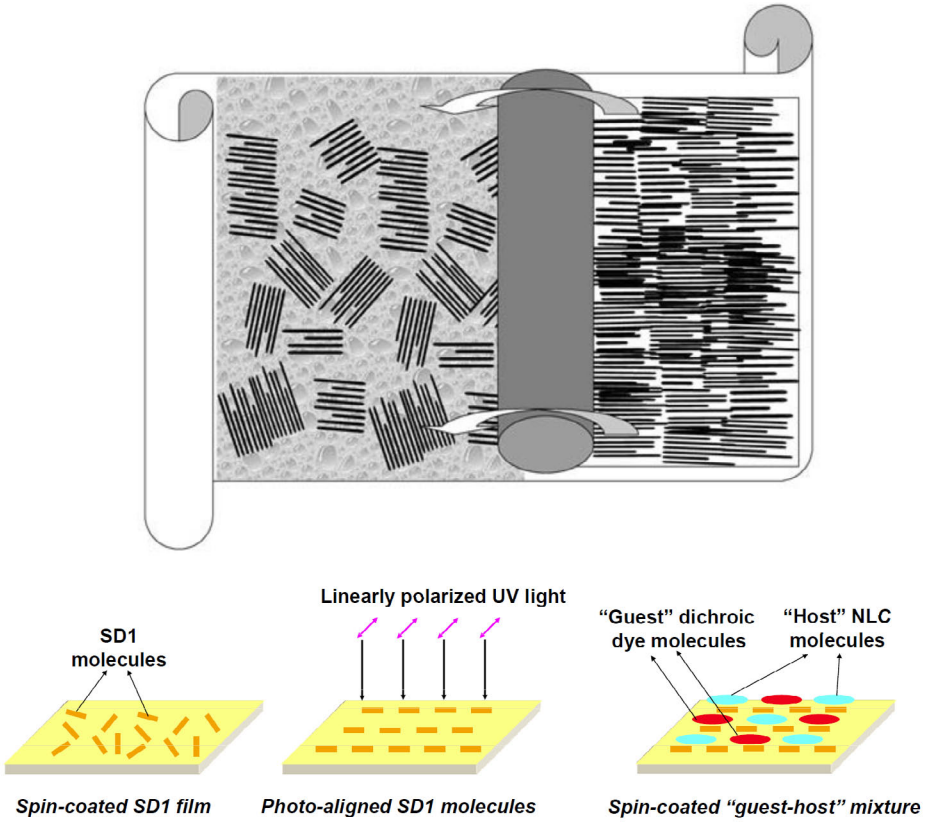

Figure 5.15: Different fabrication steps for thin film polarizers. Top: After deposition, the dichroic dye molecules can be aligned by shear flow induced by a rod propagating across the substrate. Image from [5]. Bottom: Other methods first apply an alignment layer, after which a mixture containing dye molecules is spin coated on top. Image from [6].

projectors [10]. Interestingly, during this work a wire grid polarizer embedded in PDMS for use in a contact lens was reported by Hollowell et al. [11]. However, due to the fine pitch (180 nm) this approach could not be replicated in our laboratory, while the needed multitude of vacuum processes seems to hamper a successful implementation beyond the research stage.

Therefore, it was decided to start some exploratory work concerning the fabrication of thin film polarizers using dichroic dyes. This again proved to be

difficult as none of the approaches mentioned above has been industrialized and no direct supplier of appropriate dye mixtures exists. A sample of AD-1 dye was directly obtained from the research group the which had originally developed a thin film polarizer based on this dye [9], but attempts to recreate this polarizer were unsuccessful due to a lack of support and appropriate available tools. Next to this, initial experiments based on the polymerization of a Guest-Host LC dye mixture (similar as reported in [12]) were also performed in collaboration with the Liquid Crystal and Photonics Group of Ghent University, but due to lack of time and resources no successful implementation in a spherically conformed LC cell could be obtained.

Nevertheless, despite our unsuccessful exploratory experiments, thin film polarizers are believed to be a good alternative for PVA based polarizers. Mainly because of their reduced thickness and thermal stability [7], their integration in a smart contact lens should be a topic of future research. Integration in a smart contact lens could prove both an enabling step for the lens as a viable niche market for thin film polarizers themselves.

5.6 Conclusion

To investigate the performance boundaries of the Guest-Host technology, an in-depth study was performed on the influence of the twist and the dye concentration on the electro-optical response of the LC cell. This revealed a 180° twist results in the best contrast while still being practically implementable. Although increasing the dye concentration does indeed lead to an improved contrast, this also increases the threshold voltage and the saturation voltage and a trade-off should thus be considered. With an optimized mixture, the LC cell was fully characterized, giving special attention to the transition between glass test cells and the LC cell. Transmission-voltage measurements and switching speed measurements indicated the cell gap of the LC cell was lower than intended, which was confirmed by cell gap measurements. This indicated the height of the photolithographic spacer should be carefully monitored during fabrication. Even then, contrast and switching speed were only moderate, which might hamper use of the LC cell for some applications. An initial study concerning the integration of polarizers revealed PVA based polarizers are likely too thermally unstable to be integrated into contact lenses. Thin film polarizers seem to be a good alternative and should be the subject of future research.

References

[1] S. Wu and D. Yang, *Reflective Liquid Crystal Displays*, ser. Wiley SID series in display technology. Wiley, 2002.

[2] E. Lueder, *Liquid crystal displays: addressing schemes and electro-optical effects, Second edition*, ser. Wiley SID series in display technology. Wiley, 2010.

[3] Private communications with imec's Organic Photovoltaics Group, 5 November 2012.

[4] E. Land, "Some aspects of the development of sheet polarizers", *J. Opt. Soc. Am.*, vol. 41, no. 12, pp. 957–962, 1951.

[5] *Optical Applications of Liquid Crystals*. Taylor & Francis, 2003.

[6] X. Zhao, F. Boussaid, A. Bermak, and C. V.G., "High-resolution thin guest-host micropolarizer arrays for visible imaging polarimetry", *Opt. Express*, vol. 19, no. 6, pp. 5565–5573, 2011.

[7] Y. Bobrov, L. Blinov, L. Ignatov, G. King, P. Lazarev, V. Nazarov, N. Ovchinnikova, and S. Remizov, "Environmental and optical testing of thin crystal film™ polarizers", *Journal of the Society for Information Display*, vol. 11, no. 1, pp. 63–70, 2003.

[8] W. Yip, H. Kwok, V. Kozenkov, and V. Chigrinov, "Photo-patterned e-wave polarizer", *Displays*, vol. 22, no. 1, pp. 27–32, 2001.

[9] X. Zhao, F. Boussaid, A. Bermak, and V. Chigrinov, "Thin photo-patterned micropolarizer array for cmos image sensors", *Photonics Technology Letters, IEEE*, vol. 21, no. 12, pp. 805–807, 2009.

[10] M. Pate, J. Meyer, J. Shiefman, and D. Hansen, "Wire-grid polarizers in modern lcos light-engine configurations", *Journal of the Society for Information Display*, vol. 14, no. 3, pp. 275–283, 2006.

[11] A. E. Hollowell and L. J. Guo, "Nanowire grid polarizers integrated into flexible, gas permeable, biocompatible materials and contact lenses", *Advanced Optical Materials*, vol. 1, no. 4, pp. 343–348, 2013.

[12] E. Peeters, J. Lub, J. Steenbakkers, and D. Broer, "High-contrast thin-film polarizers by photo-crosslinking of smectic guest–host systems", *Advanced Materials*, vol. 18, no. 18, pp. 2412–2417, 2006.

6 Applications

"Il n'existe pas de sciences appliquées, mais seulement des applications de la science"

—Louis Pasteur

6.1 Artificial Iris

6.1.1 Design & New Features

As mentioned in section 2.3.2, our spherically conformed LC cell could be used as the electro-optic actuator in a tunable artificial iris. This concept was studied in-depth in two separate master dissertations which were made in the context of this research [1, 2]. The most important results will be highlighted in this section. It was not the intention to create an already fully deployable tunable artificial iris, but rather to obtain a first proof-of-concept, providing us with insights in where and how our fabrication process should be altered.

The basic idea is to divide our spherically conformed LC cell in concentric, ring-shaped pixels and sequentially activate them from outwards to inwards to

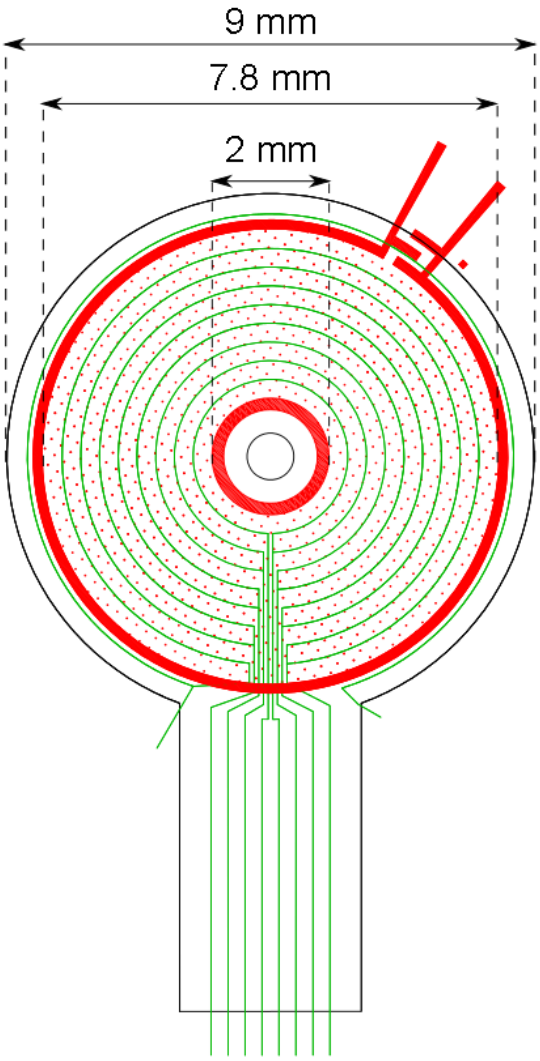

Figure 6.1: Design of our LC cell for use as an artificial iris. The black lines are the outline of our LC cell cut by a CO_2-laser, the red features are the SU8 patterns and the green lines are the isolation lines cut in the PEDOT:PSS by an excimer laser. The LC cell has a central hole and contains 9 pixels.

mimic a contracting iris, or from inwards to outwards to mimic a relaxing iris. The dimensions of the LC cell were, however, slightly altered to more closely

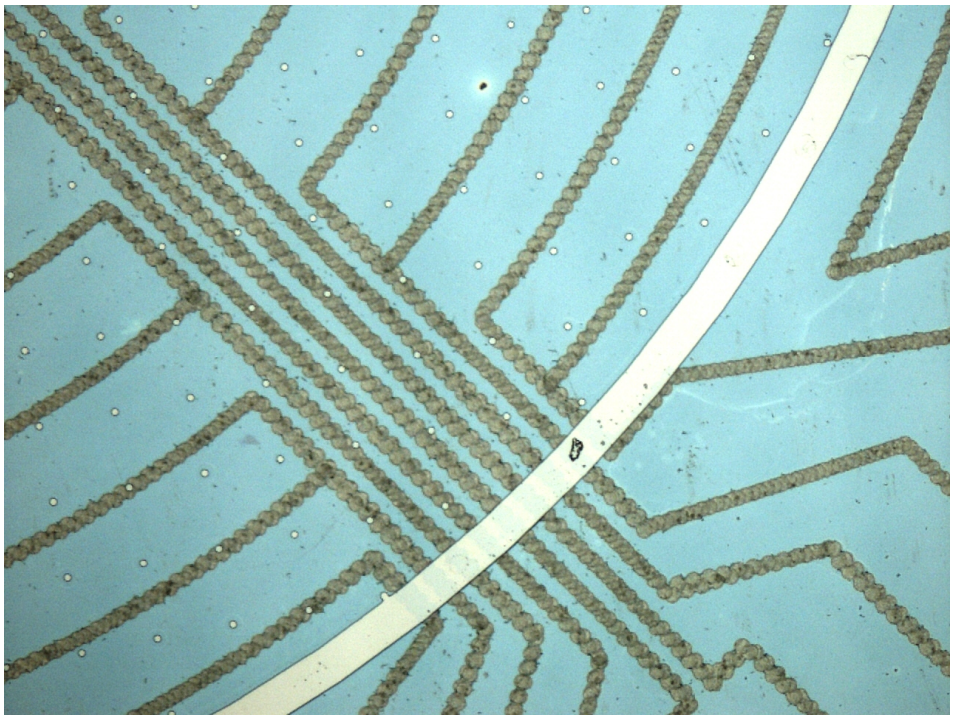

Figure 6.2: Since the excimer spot had a diameter of 40 µm, the minimum pitch of the feeding lines in the PEDOT:PSS was set 80 µm, already occupying a significant amount of area near the border of the active switching zone when using 9 pixels.

match anatomic dimensions of typical irises. The inner diameter of an actual iris, defining the outline of the centrally located pupil, generally varies between 2 mm in very bright lighting conditions and 8 mm in very dim conditions, with 3 mm being the dimension with the best overall performance [3]. Therefore, the outer diameter of our LC cell was increased to 9 mm and an active pixelated switching zone was foreseen to extend from 2 mm to 7.8 mm (see Figure 6.1). Although it is still unclear what an optimal amount of pixels is, demonstrators with as much as 9 pixels were fabricated. The main limiting factor for the number of pixels is the resolution of the PEDOT:PSS ablation and the increasing amount of feeding lines that can practically be driven via the flexible connector (see section 6.1.2). Since the excimer spot had a diameter of 40 µm, the minimum pitch of the feeding lines in the PEDOT:PSS was set 80 µm, already occupying a significant amount of

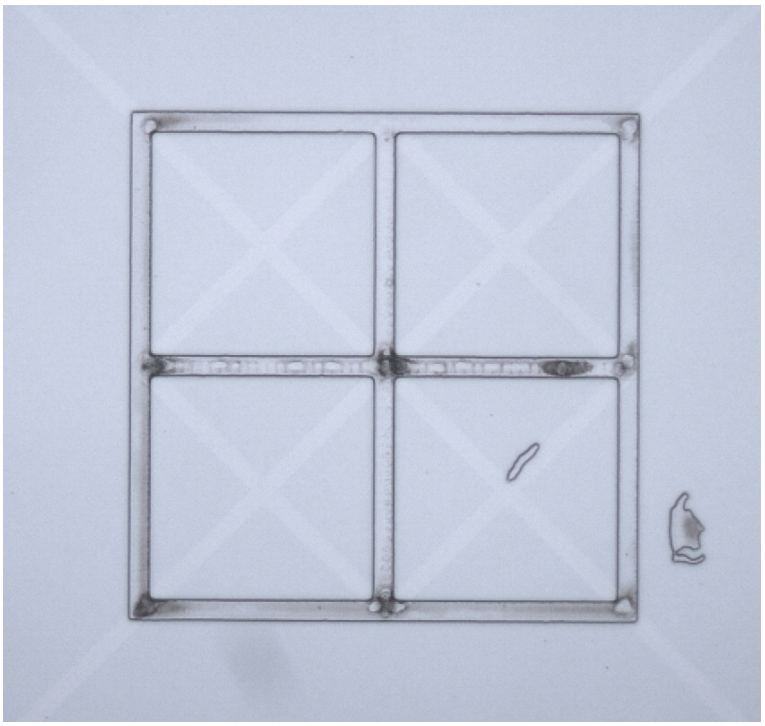

Figure 6.3: Additional alignment markers were foreseen in both the PEDOT:PSS layer (crosses) and the SU8 layer (squares). Alignment could be obtained with an accuracy of about 10 µm.

area near the border of the active switching zone when using 9 pixels (see Figure 6.2 & 6.7). Because of the decreasing pixel sizes, the alignment of the SU8 layer with respect to the PEDOT:PSS layer was also important. Additional alignment markers were foreseen in both layers and alignment could be obtained with an accuracy of about 10 µm (see Figure 6.3).

Since it is expected that the LC cell will severely block the oxygen flow through the contact lens, a central hole could partly alleviate this problem, especially because the oxygen need is the highest in the middle of the cornea (see Figure 6.4). For this purpose, another glue barrier layer at the inner side of the active switching zone was foreseen in the SU8 layer (see Figure 6.1). The diameter of the glue barrier was set at 2 mm to concur with the diameter with a maximally constricted iris. At the central hole, the cell is sealed by depositing glue at the

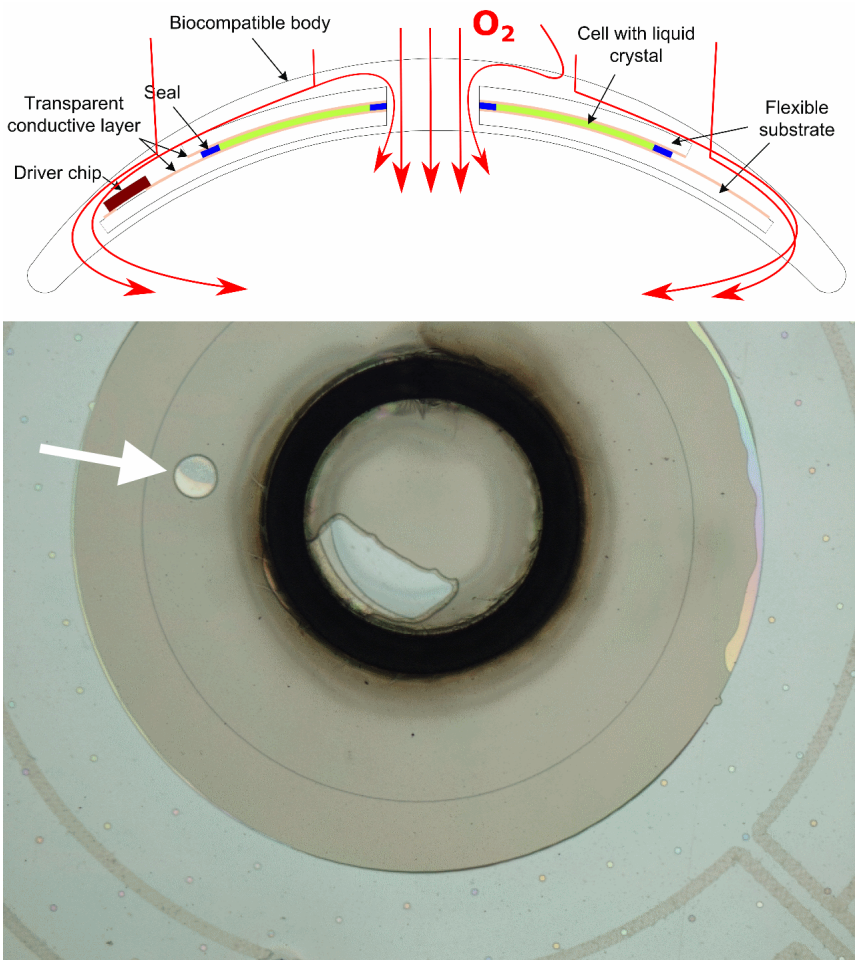

Figure 6.4: Central hole in the LC cell. Top: Since it is expected that the electronic core of the LC cell will severely block the oxygen flow through the contact lens, a central hole could partly alleviate this problem. Bottom: The hole was cut simultaneously with the CO_2-laser cutting of the LC cells (black circle) and generally had a diameter of 0.8 mm. Air bubbles (white arrow) were frequently encapsulated in the interior glue joint.

inside of the inner glue barrier, but this frequently led to the encapsulation of air bubbles in this interior glue joint (see Figure 6.4). This is because the glue barrier effectively encloses the deposited glue and air can get entrapped more easily. Although these air bubbles showed no detrimental effect on the functioning of the

artificial iris, their scattering nature can cause blur and should thus be avoided in future work. The hole was cut simultaneously with the CO_2-laser cutting of the LC cells and generally had a diameter of 0.8 mm, but larger diameters are also possible (see Figure 6.4).

6.1.2 New Flexible Connector

To apply a voltage to LC cells with a simple pattern such as in Figure 4.19, a simple copper tape was cut into several pieces and taped back to back before it was inserted in between the foreseen rectangular contact areas. When confronted with an artificial iris having nine pixels, such an approach does not suffice. A more advanced flexible connector was made based on a commercial copper clad laminate (UPILEX-N, UBE Industries, Ltd.). This laminate consists of a 25 µm thick polyimide film with a 9 µm copper film residing at both sides of the film. Intricate patterns can be made by applying a photoresist on top of the copper and etching the exposed areas. This process can be performed on both sides, allowing the creation of an advanced double-sided connector (see Figure 6.5). A multitude of connectors was designed and usually comprised a long narrow rectangular part and a fan-out. After the connectors are cut out of the patterned films with an Nd:YAG laser, they are inserted and carefully aligned with the PEDOT:PSS tracks at the rectangular contact areas of the LC cell. Generally, a standard transparent adhesive tape is used to fix the connector with the LC cell, pressing the copper tracks onto the PEDOT:PSS tracks.

6.1.3 Implementation

A prototype having nine pixels and a central hole is shown in Figure 6.6. By consecutively switching on the pixels from outside to inside, the iris constriction can indeed be mimicked. A close-up (see Figure 6.7) reveals the isolation lines in the PEDOT:PSS are clearly visible when all pixels have been switched on and especially take up a considerable amount of area at the side where they are guided towards the flexible connector. It remains to be seen whether this might influence the sight of the potential user but their influence could be reduced by further improving the resolution of the PEDOT:PSS patterning. At some areas misalignment of the LC molecules at the isolation lines could be observed, but this was not present throughout the whole LC cell. What makes some lines more prone to the misalignment is unclear, but it should preferably be avoided in a real implementation.

Figure 6.5: New flexible connector. Top: Copper clad laminate patterned on both sides. Yellow areas is polyimide, orange areas is copper at the top surface, dark areas is visible copper at the backside. A multitude of connectors was designed and usually comprised a long narrow rectangular part and a fan-out. Bottom: Close-up of a connector that was inserted and carefully aligned with the PEDOT:PSS tracks at the rectangular contact areas of the LC cell.

When considering the current switching speed and contrast of our LC cell, switching speed should definitely be sufficient in an application such as the

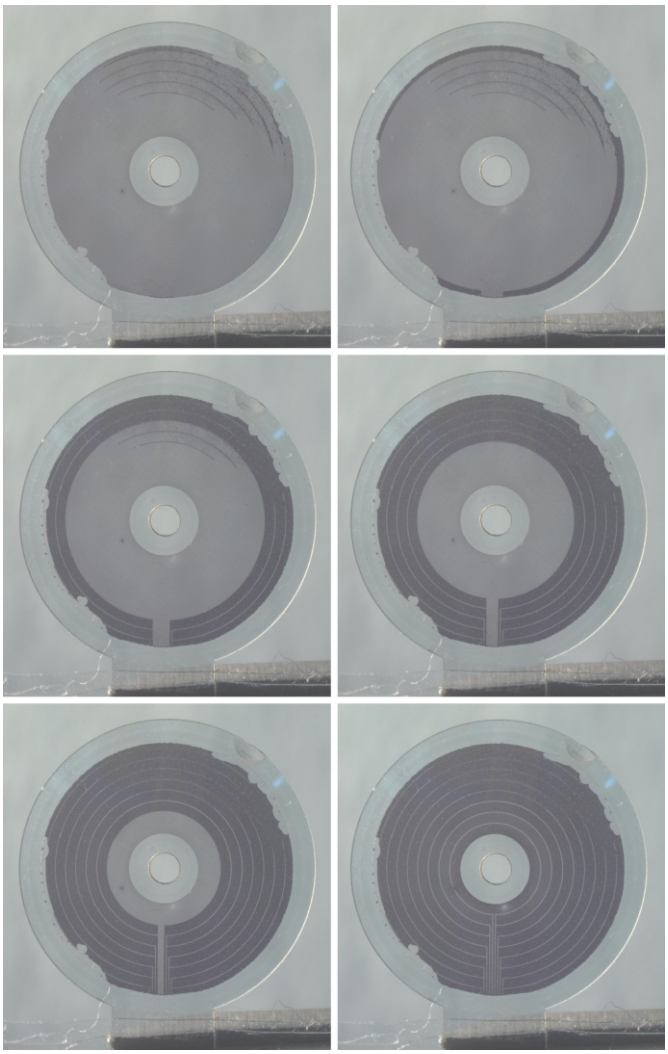

Figure 6.6: LC cell showing 0, 1, 3, 5, 7 and 9 pixels switched on. By consecutively switching on the pixels from outside to inside, the iris constriction can indeed be mimicked.

artificial iris. The maximum constriction velocity of an iris of some people can be as high as 7 mm/s [4], meaning that the time needed for an iris to constrict from a maximal dilated state (8 mm) to a minimal constricted state (2 mm) would be

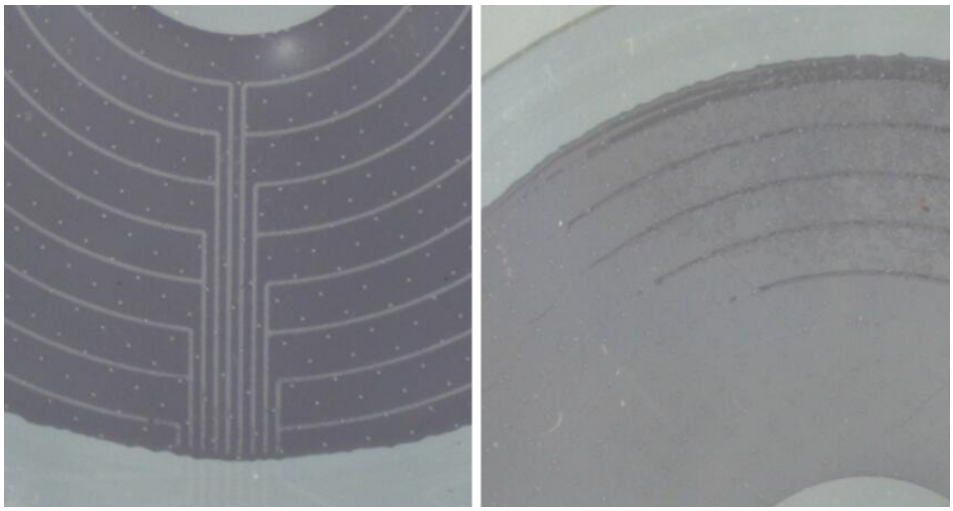

Figure 6.7: Left: When all pixels are switched on, the isolation lines in the PEDOT:PSS are clearly visible. Right: At some areas misalignment of the LC molecules at the isolation lines could be observed, but this was not present throughout the whole LC cell.

about 0.86 seconds. This time is in reality even larger as there is a latency period before the eye reacts to a light stimulus (at least 0.22 seconds). Although there will likely also be a latency time in a real implementation of the artificial iris, our LC cell could dim as a whole in 0.07 seconds (when driven at 10 V, see Table 5.1), clearly outperforming a normal iris.

The main problem could be the contrast of the LC cell. A normal iris practically blocks all incoming light (especially when compared to the clear pupil) while our minimum transmission is about 19%. Although this is already a significant reduction of the incoming light, it is unclear whether this is sufficient to alleviate excessive light conditions perceived by patients. An improved contrast with a darker voltage on state would be preferable and might be achieved at the expense of switching time. Likely, an implementation using polarizers would reach a minimal transmission that is comparable with a normal iris.

6.1.4 Crossover Technology

An important feature of the LC cell, especially when considering its long term development, is the inclusion of a crossover. A crossover is a well-defined conductive path that connects the conductive layer from one side of the cell (usually the

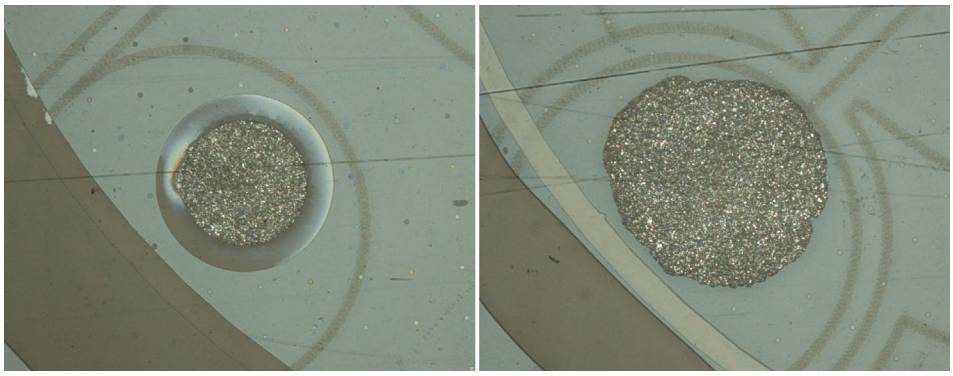

Figure 6.8: For the crossover, a cylindrical structure (500 µm inner diameter) was added in the photolithographic mask near the side of the cell which was filled with a flexible conductive adhesive (left). Dispensing the adhesive was, however, not straightforward and frequently led to an overflow of the cylinder (right).

ground plane) with the opposing pixelated side. In this way, all driving voltages for the LC cell can be applied to the cell through a single-sided connection. In a smart contact lens application such as the artificial iris this could be for instance the connection between an integrated driver chip and the embedded LC cell.

In conventional LCDs a crossover is generally established by putting a drop of conducting adhesive at the edge of the cell, but like the deposition of the glue barrier, a more dimensionally controlled deposition is preferred. Furthermore, the crossover should be rather flexible and able to withstand the molding process.

For this purpose, we proposed to add a cylindrical structure (500 µm inner diameter) in the photolithographic mask near the side of the cell and fill it with a flexible conductive adhesive (FCA, see Figure 6.8) before closing the cell. For our application, the 102-32 adhesive (Creative Materials, Inc) was recommended as it is a thermally curing flexible conductive adhesive which can be applied to a variety of substrates. Deposition of the adhesive was, however, not straightforward because of its paste-like consistency. When dispensing it with a syringe, the adhesive did not flow easily and usually clung to the needle while accumulating as one big drop. This meant creating the correct dose was very difficult and many times an overdose was dispensed, leading to an overflow of the cylinder. Dispensing was ameliorated by diluting the paste with a small amount of toluene (10 weight percent) but still resulted in a considerable variety in the dispensed quantity (see Figure 6.8).

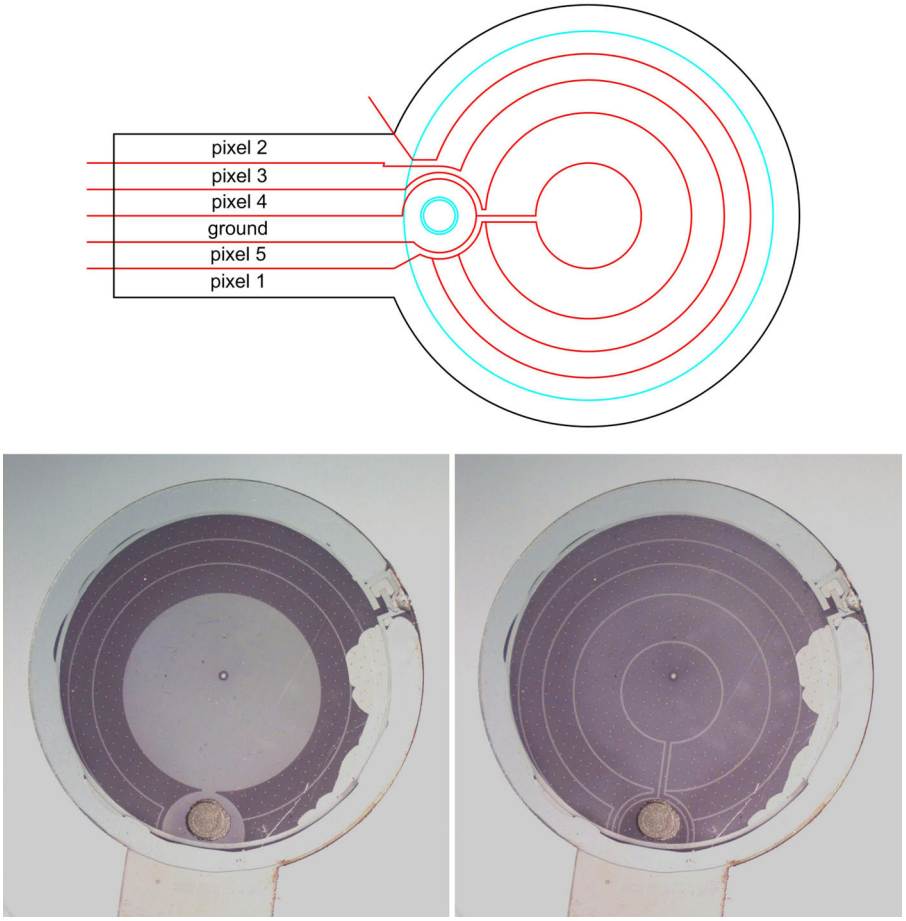

Figure 6.9: Artificial iris with 5 pixels and a crossover. Top: Design of the artificial iris showing the outline of the cell (black lines), the isolation lines for the PEDOT:PSS patterning (red lines) and the glue barrier and cylindrical structure for the crossover in the SU8 layer (blue lines). Left: When the outer three pixels are driven (pixel 1-3), they function as desired, showing the crossover works in principle. Right: When one or both of the inner pixels (pixels 4-5) are driven, the total contrast drops, which is likely due to overflow in the crossover towards these pixels.

To test the crossover an artificial iris with 5 pixels was designed (see Figure 6.9). While the 5 pixels at one side were directly driven via the new flexible connector, the opposing side serving as the common ground was first brought to

the same side using the crossover. Around the crossover a clearance zone was foreseen to contain any potential overflow. An example of this artificial iris is shown in Figure 6.9, demonstrating the LC cell could be driven and the crossover functions. However, in this particular example functionality was only as desired when the three outer pixels were activated. When one or both of the remaining pixels was activated, the total contrast of all the pixels decreased slightly. Closer inspection of the crossover (see Figure 6.8, right) reveals that, despite the clearance zone, the overflow's edge still ends in the isolation line between the crossover and the two inner pixels. The two inner pixels are thus likely connected to the ground with a highly resistive path, thereby affecting the total contrast when one of these pixels is activated.

This again demonstrates a better dispensing method is needed to successfully implement a crossover with the proposed principle in new designs. One such method could be screen printing, as this allows for a well defined patterned deposition and is suitable for an industrial environment. Not only could this diminish the chance of overflow, but also likely reduce the total footprint of the crossover. Next to this, the rheology of the flexible conductive adhesive could also be optimized for an improved deposition.

6.2 From Artificial Iris to Presbyopia

As mentioned in section 2.3.2, besides an artificial iris, we believe smart contact lenses could also provide a better solution for presbyopia. This would require an electro-optic actuator providing the lens with some multifocal capabilities. Although many physical properties could be exploited for this purpose, it was also stated such a feature could be accomplished by liquid crystal based technology. During this work several ideas have risen on how our technology can be used to realize this multifocal capability, but these are currently the subject of a patent application. Therefore, the exact working principles cannot be disclosed at this moment.

6.3 A Contact Lens Display

As stated in the prelude, this work was created out of the idea of integrating a display in a contact lens that could be seen by its user. Now that we have established an LCD based technology that indeed can be integrated into a contact lens, the question arises whether this technology can be used in this way (see

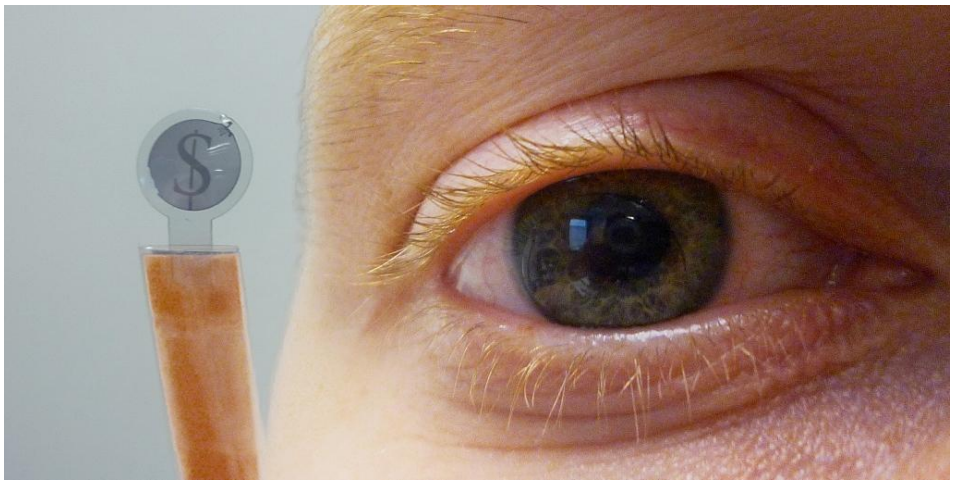

Figure 6.10: Prototype with a dollar sign held next to a human eye. Although we have established an LCD based technology that indeed can be integrated into a contact lens, pixels on this lens cannot be seen clearly by a potential user as they are beyond the eye's minimal focussing distance.

Figure 6.10). The first problem that immediately comes to mind is how to create a focussed image on the retina. Indeed, pixels residing just in front of the cornea cannot be seen clearly as they are beyond the eye's minimal focussing limit.

One could consider having an additional optical structure that refocuses the incident light onto the retina. This idea was also put forward by the Parviz group which investigated the use of micro Fresnel zone plates to refocus the light of individual microLEDs [5]. Their work did, however, lack a more detailed study of what could be optically achieved with this principle and, for instance, what the pixel distribution across the retina could be.

Some exploratory simulations were therefore performed in a separate master dissertation [6, 7] using Zemax [8] as the optical simulation tool (see Figure 6.11). A contact lens was put in front of an eye model and contained small light sources and additional (ideal) microlenses. The light sources were in fact small circular pinholes placed in front of light emitting planes. The best results were obtained with 1 µm pinholes placed at 100 µm distance behind a 60 µm diameter microlens, leading to a light spot of 0.4 mm on the retina. More complex patterns could be obtained by placing several pinholes next to each other with a 100 µm spacing.

Several concerns should be raised when evaluating these first results. First of

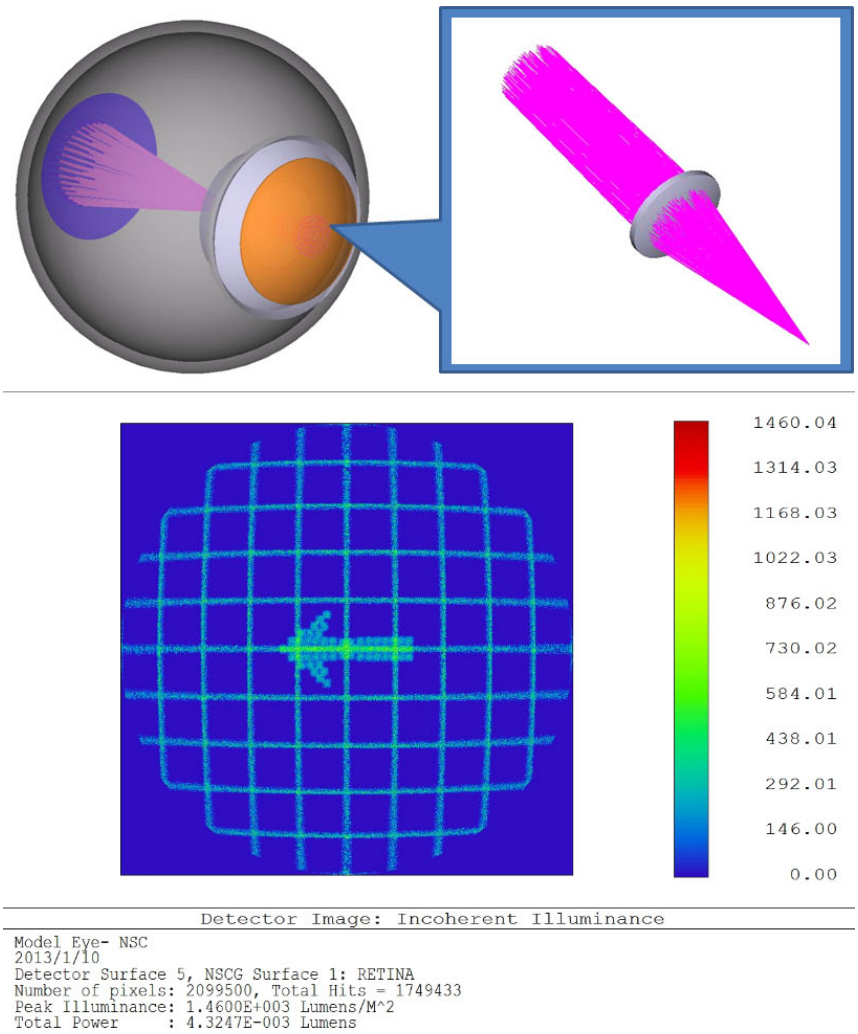

Figure 6.11: Exploratory simulations in Zemax were performed to investigate whether a small light source combined with a microlens could lead to a focused spots on the retina. It was found 1 µm pinholes placed at 100 µm distance behind a 60 µm diameter microlens, led to a light spots of 0.4 mm on the retina. More complex patterns could be obtained by placing several pinholes next to each other with a 100 µm spacing.

all, 1 µm light sources are extremely small and it is questionable whether such sources could be fabricated with the current state-of-the-art microfabrication

techniques. Secondly, and perhaps more importantly, a spot size of 0.4 mm on the retina is actually still significantly large. For a high acuity visual task such as for instance reading text, only the centrally located fovea is used (see section 1.1.2). The fovea generally has a size of only 1.5 mm [9] while its innermost centre, the foveola, only has a diameter of 0.35 mm. Even if we could thus manufacture the set-up as investigated in our simulations, this would mean only about 4 by 4 pixels could be projected in the region with highest acuity, allowing the projection of only very simple patterns.

It seems before any display technology should be further investigated for application as a contact lens display, a more in-depth study is needed on how a highly detailed image can be projected onto the fovea. Since our simulations indicate a classical optical approach will not suffice, more advanced techniques such as for instance holography will be likely needed. It remains to be seen whether LCD technology can be used for this purpose as it is the proven optical concept which will probably dictate for which technology one should opt.

6.4 Conclusion

With the basic technology established and characterized, the first applications could be explored. For use as an artificial iris, the LC cell was adapted and new features such as a central hole for increased biocompatibility were added. Alignment markers were added as the high number of pixels - up to nine in our prototypes - required careful alignment. A new flexible connector based on commercial copper clad laminates was developed to drive the different pixels. By consecutively switching on and off the concentric pixels, iris constriction and dilation could be successfully mimicked. A crossover was also implemented as this allows to bring all necessary connections to one side of the substrates. The deposition process of the flexible conductive glue was, however, not well controlled and could lead to unwanted connections deteriorating the contrast of the pixels. Although further work should address this problem, the artificial iris seems well suited as a first application for this newly developed technology.

Another application in the vision correction domain is a smart contact lens for presbyopia. Therefore, its use in a smart contact lens with multifocal functionality was studied, but since this is currently the subject of a patent application, no more information can be disclosed here.

For the final application, a contact lens display for augmented reality, it was quickly realized that pixels residing just in front of the cornea cannot be

seen clearly as they are beyond the eye's minimal focussing limit. Exploratory simulations indicate that even under ideal circumstances a classical approach using integrated microlenses could likely lead to projected spot sizes as large as 0.4 mm. This would mean only about 4 by 4 pixels could be projected in the region with highest acuity, allowing the projection of only very simple patterns. Therefore, it seems before any display technology should be further investigated for application as a contact lens display, a more in-depth study is needed on how a highly detailed image can be projected onto the fovea. It remains to be seen whether LCD technology can be used for this purpose as it is the proven optical concept which will probably dictate which technology one should opt for.

References

[1] P. De Backer, "Design and fabrication of a tunable artificial iris", Master's thesis, Ghent Univerity, 2013.

[2] E. Islamaj, "Biocompatibility study of an artificial switchable iris", Master's thesis, Ghent Univerity, 2013.

[3] A. Watson and J. Watson, "A unified formula for light-adapted pupil size", *J Vis.*, vol. 12, no. 10, p. 12, 2012.

[4] C. Ellis, "The pupillary light reflex in normal subjects.", *Br J Ophthalmol.*, vol. 65, no. 11, pp. 754–759, 1981.

[5] A. Lingley, M. Ali, Y. Liao, R. Mirjalili, M. Klonner, M. Sopanen, S. Suihkonen, T. Shen, B. Otis, H. Lipsanen, and B. Parviz, "A single-pixel wireless contact lens display", *Journal of Micromechanics and Microengineering*, vol. 21, no. 12, p. 125 014, 2011.

[6] C.-P. Weng, "Computer simulation on an image projection system within a contact lens", Unpublished report.

[7] H. De Smet, J. De Smet, D. Cuypers, C. Weng, and P. Joshi, "A contact lens with built-in display: science fiction or not?", *SID Symposium Digest of Technical Papers*, vol. 44, pp. 8–11, 2013, ISSN: 2168-0159.

[8] Radiant Zemax. [Online]. Available: https://www.radiantzemax.com/en.

[9] *The Retina*. The University of Chicago Press, Illinois, 1941.

7 Conclusion and Outlook

"Once a new technology starts rolling,
if you're not part of the steamroller,
you're part of the road."

—Stewart Brand

7.1 Main Achievements

The main objective of this work was to set up a fabrication process to create a thin, spherically conformed LC cell which can be integrated into a contact lens. Inspired by existing flexible display manufacturing techniques a new process was proposed and investigated. Handling the thin PET-films which were used as substrates proved to be challenging and the creation of a new lamination-delamination method was crucial. Using wax as a temporary adhesive and a dedicated substrate holder, the glass carriers could be removed without damaging the LC cells. Because it was discovered ball spacers performed poorly after the deformation process, a photolithographic layer was added and comprised both cylindrical spacers as additional features such a glue barrier and a finger pattern

at the filling entrance.

While the glue barrier allowed us to carefully dimension the LC cell, the finger pattern was needed to avoid wrinkle formation at the filling entrance. It was discovered these wrinkles are mainly related to the thickness of the used PET-films and a smooth cell with a total thickness of 135 µm was established by using an asymmetric configuration with a thin layer at the convex side and a thicker but threshold dependent layer at the concave side. Furthermore, the uniformity of the transmission was found to be dependent on the accuracy of the used mold and the spacer pitch. Uniform cells could be manufactured by using a CNC fabricated mold which takes the total thickness of the lens into account and having a spacer pitch of at least 200 µm.

Next to a good mechanical design, an equally important material selection was made for the active layers of the cell. The choice of a conductive polymer such as PEDOT:PSS over the classical ITO was indispensible due to the extreme deformation during the molding step. The PEDOT:PSS showed no optical defects after the molding process, while its function as a conductive layer was kept intact. However, its integration into our process flow was not trivial, since there is no standardized way of patterning PEDOT:PSS on top of PET and photolitographic patterning on top of PEDOT:PSS is not straightforward. Patterned pixels could be obtained by isolating individual pixels using laser ablation. Minor damage to the underlying PET did, however, sometimes lead to misalignment of the LC molecules. The use of a SiO_2 barrier layer also allowed to chemically separate the PEDOT:PSS from the photolitographic patterning of the SU8 layer, which would otherwise cause damage to the unexposed SU8 layer.

Careful characterization of the contrast and switching times of the spherically conformed LC cell revealed their values are only moderate and, depending on the application, would not suffice. Furthermore, the height of the photolithopgraphically defined spacers was found to sometimes deviate from the intended value and close monitoring during fabrication is thus advised. To improve the characteristics of the LC cells, initial attempts were undertaken to integrate polarizers in the cell. Classical PVA based polarizers seemed to have too much internal stresses, leading to partially detached glue joints after the molding step. Likely, alternative thin film polarizers should provide better results.

After having established the basic technology, some first applications were explored. An implementation as an artificial iris was studied and a prototype with 9 pixels and a central hole for increased biocompatibility was fabricated. Besides the central hole, other extensions to the technology included the use of alignment markers and a crossover. It was shown iris constriction and dilation

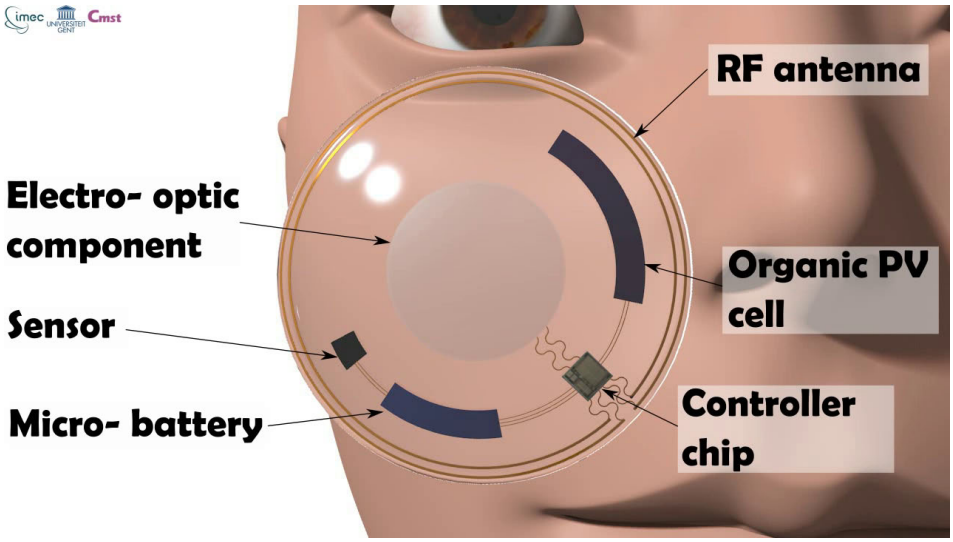

Figure 7.1: Future smart contact lenses might comprise several components providing the lens with complex functionality and autonomy.

could indeed be mimicked by consecutively switching on and of the concentric pixels from outwards to inwards and vice versa. Ideas to use the technology for a multifocal contactlens to address presbyopia were put forward and are currently the subject of a patent application. Finally, initial simulations show a solution has to be found for the focussing problem before one can consider to use this newly developed technology in a contact lens display for augmented reality.

To conclude, we have shown for the first time it is possible to create a non-emitting electro-optic technology that can be integrated into a contact lens. This milestone brings us one step closer to a new generation of contact lenses, potentially leading to breakthrough applications in biomedical and augmented reality fields.

7.2 Future Work

To bring the vision of a smart contact lens to life, a multitude of issues still needs to be addressed. First of all, the electro-optical characteristics of our LC cell should be improved and its fabrication process should be simplified. For this purpose, the integration of thin film polarizers should be investigated. Furthermore, by using

alternative alignment layers or new photolithographic materials the required barrier layer could perhaps be avoided.

To increase the biocompatiblity and optical quality other materials than PET should be studied. Regarding biocompatibility, apart from sufficient oxygenation of the cornea, diffusion of species from the LC cell to the eye or from the surroundings into the LC cell is a major concern. Potentially hazardous materials should be confined within the cell, while the cell should be protected from the detrimental effects of water and oxygen. Most likely, an approach using various barrier layers will be necessary and should be the focus of a follow-up study aiming for full biocompatibility. Interestingly, recent progress in biocompatible packaging for implantable electronic devices [1, 2] also seems applicable to smart contact lenses. Concerns regarding the influence of integrated chips, metals and passive components are similar and the proposed solutions (see Figure 7.2) can potentially be reused.

Providing autonomy to the lens is also an important issue and although it has been shown that an smart contact lens can be powered wirelessly by electromagnetic induction [3–6], the continuous need of a secondary coil does not constitute full autonomy. This approach should be combined with energy harvesters, like solar cells, and energy storage components, like microbatteries, so the lenses can be charged when not inserted in the eye, much like electronic devices such as electric toothbrushes or mobile phones (see Figure 7.1).

For the components one should also consider alternatives to the classic silicon based chips. The emerging domain of organic electronics holds promise of cheap, disposable circuits that can be fabricated on transparent, flexible foils (see Figure 7.3). Although these circuits are much slower than their silicon counterparts, other properties such as low cost and power consumption makes them interesting candidates for smart contact lens integration [7].

Of course, the complexity of the lens and the required components will depend on the application. An artificial iris would, besides the LC cell, probably only need a driver chip and a solar cell, since there exists a direct relationship between the energy need of the LC cell and the energy generation of the solar cell. In a smart contact lens with multifocal functionality such a relationship does not exist and some sort of communication or sensing capability should be introduced to know where the lens should focus. This will thus likely increase its complexity and number of embedded components.

The outer shell of smart contact lenses should not be confined to one type of material. The artificial iris, for instance, lends itself more to RGP materials. Since disorders that can be alleviated with this lens are rare diseases, the lens

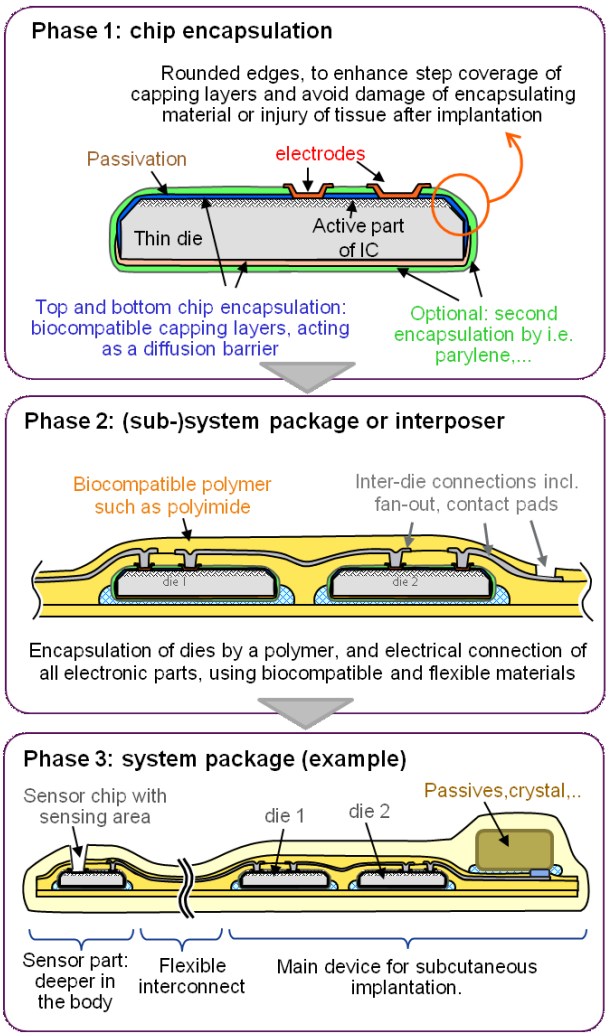

Figure 7.2: Concerns regarding the influence of integrated chips, metals and passive components for implantable electronic devices are similar to smart contact lenses and the proposed solutions can potentially be reused. Image from [2].

will likely need to be custom made and hence more expensive. Since most RGP lenses are anyway custom made and have a significant longer lifetime than soft lenses, embedding of the electronic core in an RGP material would thus be more appropriate and cost effective. A potential embedding process is shown in Figure

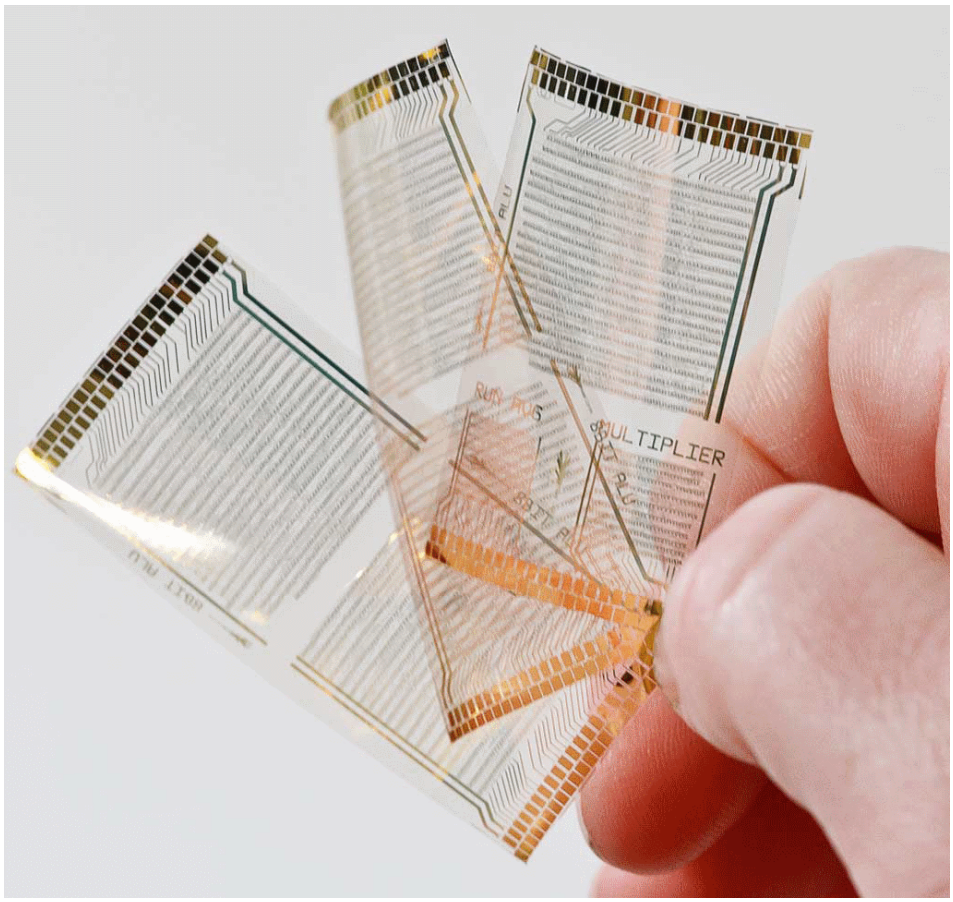

Figure 7.3: The emerging domain of organic electronics holds promise of cheap, disposable circuits that can be fabricated on transparent, flexible foils. Image from [7].

7.4, and starts from two preshaped buttons in between which the electronic core is sandwiched. After the buttons are attached to each other with for instance unpolymerized RGP material, the final lens can be lathe cut in a two step process.

Presbyopia, on the other hand, affects 1.04 billion people globally [8] and a smart contact lens with multifocal functionality would thus address a mass market. Hence, embedding of the electronic core in a soft contact lens could be favoured.

Finally, the most challenging but perhaps also the most intriguing application

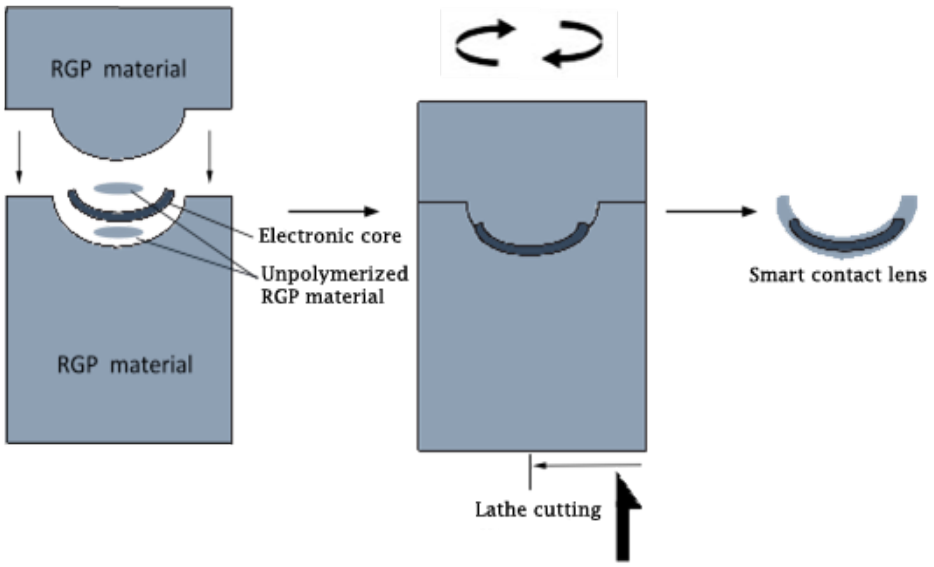

Figure 7.4: Potential embedding process of the electronic core in an RGP material.

would be a contact lens with embedded display. Here, initial efforts should be aimed at solving the focussing problem. Even if an optical solution can be found it is still unclear how such an image will perceived. Normally, the eye uses a complex series of movements when scanning a scene and has the tendency to filter out images which are static with respect to the retina. Images projected directly from a contact lens therefore might need additional methods to circumvent these potential problems. Good understanding of the human visual system will be indispensable, but perhaps a contact lens display could even extend our knowledge in this field.

Anyway, research concerning smart contact lenses has really only just begun and will remain an interesting emerging domain in the years to come.

References

[1] C. Hassler, R. von Metzen, P. Ruther, and T. Stieglitz, "Characterization of parylene c as an encapsulation material for implanted neural prostheses", *Journal of Biomedical Materials Research*, vol. 93B, no. 1, pp. 266–274, 2010.

[2] M. Op de Beeck, J. O'Callaghan, K. Qian, B. Morcos, A. Radisic, K. Malachowski, M. Amira, and C. Van Hoof, "Biocompatible encapsulation and interconnection technology for implantable electronic devices", *IMAPS 45th International Conference and Exhibition on Microelectronics*, 2012.

[3] Y. Liao, H. Yao, A. Lingley, B. Parviz, and B. Otis, "A 3-microwatt cmos glucose sensor for wireless contact-lens tear glucose monitoring", *Solid-State Circuits, IEEE Journal of*, vol. 47, no. 1, pp. 335–344, 2012.

[4] H. Yao, Y. Liao, A. Lingley, A. Afanasiev, I. Lähdesmäki, B. Otis, and B. Parviz, "A contact lens with integrated telecommunication circuit and sensors for wireless and continuous tear glucose monitoring", *Journal of Micromechanics and Microengineering*, vol. 22, no. 7, p. 075 007, 2012.

[5] J. Pandey, Y.-T. Liao, A. Lingley, R. Mirjalili, B. Parviz, and B. Otis, "A fully integrated rf-powered contact lens with a single element display", *Biomedical Circuits and Systems, IEEE Transactions on*, vol. 4, no. 6, pp. 454–461, 2010.

[6] A. Lingley, M. Ali, Y. Liao, R. Mirjalili, M. Klonner, M. Sopanen, S. Suihkonen, T. Shen, B. Otis, H. Lipsanen, and B. Parviz, "A single-pixel wireless contact lens display", *Journal of Micromechanics and Microengineering*, vol. 21, no. 12, p. 125 014, 2011.

[7] K. Myny, E. van Veenendaal, G. Gelinck, J. Genoe, W. Dehaene, and P. Heremans, "An 8-bit, 40-instructions-per-second organic microprocessor on plastic foil", *Solid-State Circuits, IEEE Journal of*, vol. 47, no. 1, pp. 284–291, 2012.

[8] B. Holden, T. Fricke, S. Ho, R. Wong, G. Schlenther, S. Cronjé, A. Burnett, E. Papas, K. Naidoo, and K. Frick, "Global vision impairment due to uncorrected presbyopia", *Archives of ophthalmology*, vol. 126, no. 12, pp. 1731–1739, 2008.